



Federal Ministry  
for Economic Affairs  
and Energy

Federal Ministry for Economic Affairs and Energy • D-11019 Berlin • Germany

International Seabed Authority  
The Secretary General  
H.E. Michael Lodge  
14 - 20 Port Royal Street  
Kingston  
Jamaica, W.I.

SWITCHBOARD +49 30 18615 0  
FAX +49 30 18615 7010  
INTERNET [www.bmwi.de](http://www.bmwi.de)  
PREPARED BY MR'in Dr. Brigitte Schwadorf-Ruckdeschel  
TEL +49 30 18615 6310  
FAX [brigitte.schwadorf-ruckdeschel@bmwi.bund.de](mailto:brigitte.schwadorf-ruckdeschel@bmwi.bund.de)  
E-MAIL [ruckdeschel@bmwi.bund.de](mailto:ruckdeschel@bmwi.bund.de)  
FILE No. VB2 - 50109/003-07  
DATE Berlin, 28 March 2018

SUBJECT Submission of an Environmental Impact Assessment for the testing of collector components in the German license area

ENCL Environmental Impact Assessment

Excellency,

As the International Seabed Authority is aware, on June 6<sup>th</sup>, 1995 the Federal Republic of Germany adopted national legislation to transpose the 1982 United Nations Convention on the Law of the Sea and the 1994 Implementation Agreement. Since then, the German Seabed Mining Act governs the prospecting and other activities conducted in the Area subject to German law.

In accordance with this Act and with guidance received from the International Seabed Authority in relation to document ISBA/19/LTC/8, the German Federal Ministry for Economic Affairs and Energy submits the enclosed Environmental Impact Assessment for the testing of collector components in the German license area, as prepared by the German Federal Institute for Geosciences and Natural Resources (*Bundesanstalt für Geowissenschaften und Rohstoffe*) and approved by the German State Authority for Mining, Energy and Geology (*Landesamt für Bergbau, Energie und Geologie*).

STREET ADDRESS Scharnhorststraße 34 - 37  
10115 Berlin

U6 UNDERGROUND LINE Station: Naturkundemuseum  
S-BAHN SURFACE LINE Berlin Hauptbahnhof  
Tram Invalidenpark

The Federal Republic of Germany avails itself of this opportunity to renew to the International Seabed Authority the assurances of its highest consideration.

Yours sincerely,



Brigitte Schwadorf-Ruckdeschel

# Umweltfachliche Stellungnahme

**zum Kollektorkomponententest im  
Rahmen des Forschungsprojektes  
"JPI-Oceans MiningImpact II"**

Antrag auf Prüfung nachträglicher  
Auflagen nach MBergG § 4 (9)

Hannover, 15. Februar 2018







Bundesanstalt für  
Geowissenschaften  
und Rohstoffe

Federal Institute for Geosciences and Natural Resources  
Stilleweg 2  
D-30655 Hannover  
Germany

International Seabed Authority  
The Secretary-General  
14 - 20 Port Royal Street  
Kingston  
Jamaica  
West Indies

## **Environmental Impact Assessment**

**for the testing of a pre-prototype manganese  
nodule collector vehicle in the Eastern German  
license area (Clarion-Clipperton Zone) in the  
framework of the European JPI-O MiningImpact  
2 research project**



# Table of contents

<b>Executive summary .....</b>	<b>7</b>
<b>1. Introduction.....</b>	<b>9</b>
1.1 Background and rationale .....	9
1.2 Project proponent and history: German license area .....	11
1.3 Objectives and structure of the proposed project .....	12
1.3.1 Biodiversity, connectivity, resilience (WP1) .....	13
1.3.2 Fate and toxicity of the sediment plume (WP2) .....	13
1.3.3 Biogeochemistry and ecosystem functioning (WP3) .....	14
1.3.4 Data and sample management (WP4) .....	14
1.3.5 Project dissemination and coordination (WP5).....	15
1.3.6 Plume monitoring and habitat/disturbance characterisation (CCT1).....	15
1.3.7 Disturbance effects in time and space (CCT2) .....	15
1.3.8 Environmental risk assessment and policy recommendations (CCT3) .....	16
1.4 This report .....	16
<b>2. Policy, legal and administrative context.....</b>	<b>18</b>
2.1 Applicable mining and environmental legislation, agreements and policies .....	18
2.2 Relevant international and regional agreements .....	19
2.3 National agreements .....	19
<b>3. Project description .....</b>	<b>20</b>
3.1 Purpose of the proposed project.....	20
3.2 Location.....	20
3.3 Mineral resource estimation .....	24
3.4 Description of the pre-prototype collector and testing design.....	26
3.4.1 General remarks and background .....	26
3.4.2 Description of the Patania II collector vehicle .....	27
3.4.2.1 Mineral collection technique .....	27
3.4.2.2 Depth of penetration into the seabed .....	32
3.4.2.3 Running gear which contacts the seabed .....	33
3.4.2.4 Methods for separation of the mineral resource and the sediment .....	33
3.4.2.5 Mineral crushing and processing methods at the seabed .....	33
3.4.2.6 Transport of material to the surface .....	33
3.4.2.7 Mineral resource separation and processing on the surface vessel.....	33
3.4.3 Collector test design .....	33
3.4.3.1 Probable duration of the test .....	33
3.4.3.2 Test plan .....	33
3.4.3.3 Spatial scale and test design .....	34

3.5	Events that could cause suspension or modification of the planned activities .....	39
<b>4.</b>	<b>Description of the existing physico-chemical environment .....</b>	<b>40</b>
4.1	Regional overview .....	40
4.2	Physico-chemical environment in and around the Eastern German license area .....	43
4.2.1	Geological setting .....	43
4.2.2	Meteorology .....	47
4.2.3	Physico-chemical oceanographic setting.....	50
4.2.3.1	Water column characteristics .....	50
4.2.3.2	Chemical composition of bottom water .....	53
4.2.3.3	Upper ocean currents.....	55
4.2.3.4	The current regime close to the seafloor.....	59
4.2.3.5	Controlling factors on abyssal currents and the significant influence of eddies on the abyssal current regime.....	65
4.2.4	Seabed substrate characteristics.....	70
4.2.4.1	Dry bulk densities; shear strengths; grain-size analyses.....	70
4.2.4.2	Particle sinking velocities and aggregation .....	75
4.2.4.3	Pore water and sediment geochemistry .....	77
4.2.4.4	Sedimentation rates .....	82
4.2.5	Natural hazards.....	82
4.2.6	Noise .....	83
<b>5.</b>	<b>Description of the existing biological environment.....</b>	<b>84</b>
5.1	Regional overview .....	84
5.2	Biological communities in and around the Eastern German license area .....	85
5.2.1	Surface.....	85
5.2.1.1	Seabirds and marine mammals.....	85
5.2.1.2	Phytoplankton .....	86
5.2.1.3	Zooplankton .....	86
5.2.2	Midwater .....	87
5.2.3	Seafloor.....	87
5.2.3.1	Megafaunal diversity .....	88
5.2.3.2	IRZ vs. PRZ: Faunal composition and population genetic analyses.....	91
5.2.3.3	Connectivity: Macrofaunal and meiofaunal comparisons between the German and French license areas.....	104
5.2.3.4	Meiofaunal communities and their dependence on abiotic parameters.....	109
5.2.3.5	Bioturbation .....	112
5.2.3.6	Microbes .....	113
5.2.3.7	Epifauna.....	116
5.2.3.8	Demersal scavengers and fish.....	118
<b>6.</b>	<b>Description of impacts on the physico-chemical environment.....</b>	<b>119</b>
6.1	Description of potential impact categories .....	119
6.2	Emissions to air .....	119

6.3	Nodule removal .....	119
6.4	Sediment disturbance and plume formation over time .....	120
6.4.1	Assessments from benthic impact experiments .....	120
6.4.2	Previous hydrodynamic plume modelling exercises .....	122
6.4.2.1	Dissolved tracer plume modelling .....	125
6.4.2.2	Particle-based plume modelling .....	126
6.4.2.3	Integration of a sediment transport model to account for aggregation .....	127
6.4.3	Hydrodynamic plume modelling of the collector test .....	130
6.5	Biogeochemical alterations .....	135
6.6	Toxic discharges .....	136
6.6.1	Metal release from the sediment .....	136
6.6.2	Potential toxicity due to hydraulic oil discharge, chemical contamination .....	138
6.7	Natural hazards .....	138
6.8	Accidental events .....	139
6.8.1	System failures and mitigation measures .....	140
6.8.2	Emergency recovery .....	140
<b>7.</b>	<b>Description of impacts on the biological environment .....</b>	<b>144</b>
7.1	Description of potential impact categories .....	144
7.2	Biological impacts at the surface .....	144
7.3	Biological impacts at midwater depths .....	145
7.4	Biological impacts at the seafloor .....	145
7.4.1	Nodule removal and effects on the epifauna .....	146
7.4.2	Faunal abundance changes related to sediment disturbance and plume deposition (blanketing) .....	146
7.4.3	Effects of plumes on epifauna, demersal scavengers and fish .....	149
7.4.4	Biogeochemical alterations, benthic ecosystem processes and microbial activities .....	150
7.4.5	Effects of toxic discharges on faunal organisms .....	151
7.4.6	Light and noise pollution .....	153
7.5	Cumulative impacts .....	154
<b>8.</b>	<b>Environmental management, monitoring and reporting .....</b>	<b>155</b>
8.1	Organisational structure and responsibilities .....	155
8.2	Environmental Monitoring Plan .....	156
8.2.1	Monitoring approach .....	159
8.2.1.1	Biodiversity, connectivity, resilience (WP1) .....	159
8.2.1.2	Fate and toxicity of the sediment plume (WP2) .....	162
8.2.1.3	Biogeochemistry and ecosystem functioning (WP3) .....	166
8.2.1.4	Plume monitoring and habitat/disturbance characterisation (CCT1) .....	170
8.2.1.5	Disturbance effects in time and space (CCT2) .....	171
8.2.2	Monitoring programme .....	173
8.3	Data management, reporting and dissemination .....	176

---

8.3.1 Data management .....	176
8.3.2 Sample management.....	177
8.3.3 Data image analysis and archiving .....	177
8.3.4 Dissemination .....	179
<b>9. Glossary and abbreviations .....</b>	<b>181</b>
<b>10. Study team .....</b>	<b>187</b>
<b>References .....</b>	<b>188</b>
<b>A Appendix 1 .....</b>	<b>204</b>

## Executive summary

In April 2019, an *in situ* technical test of a pre-prototype nodule collector vehicle (Patania-II) currently being developed by the Belgian company DEME-GSR is planned to occur in the eastern part of the German contract area for the exploration of polymetallic nodules in the Clarion-Clipperton Zone (NE Pacific). During the test, nodules will be collected from a limited ca. 100 x 900 m (~0.1 km<sup>2</sup>) area of seafloor at a water depth of ~4100 m over a time period of maximally 4 days. From a scientific point of view, the DEME-GSR pre-prototype collector trial offers unique opportunities to realistically and independently assess the environmental impact arising from a potential future nodule mining operation on the seafloor for the first time. This assessment is planned to take place in the framework of the European “Joint Programming Initiative – Oceans” project “MiningImpact 2”, which has been positively evaluated and is set to start on the 1<sup>st</sup> August 2018 for a time period of 3.5 years. The consortium of 30 partners from scientific institutions and industry, spread out through 9 European countries, and the ISA, aims at delivering new and relevant state of the art information and knowledge on future deep-sea nodule mining by (1) developing, standardising and testing monitoring concepts and strategies, (2) investigating the presently poorly-known short and intermediate-term environmental impacts of nodule collection, that in turn feed into the proposition of potential mitigation measures and the development of spatial management plans, and (3) developing sound methodologies to assess risks and uncertainties that can be implemented in future regulations and guidelines. These goals, together with the sheer small size of the activity involved, show that the framework of the environmental impact assessment presented here is conceptually different to that of a full-scale, long-term industrial mining activity (in the framework of exploitation). It is important to note that the results of the proposed activity presented here are likely to be the primary inputs to Environmental Impact Statements and Assessments for system integration tests and eventually commercial-scale mining at a later stage.

From a technological point of view, the testing of DEME-GSRs 4-m wide vehicle (one-quarter the size of a foreseen future prototype) equipped with hydraulic collector head components focusses on testing its manoeuvrability, reliability and nodule pick-up efficiency as part of an overall mining system, as well as analysing the anticipated environmental impacts in order to inform and improve system design. From a scientific point of view, the JPI-O MiningImpact 2 consortium will set up and evaluate a comprehensive monitoring programme that, amongst others, focusses on three major research topics associated with the test and future nodule mining: (1) the scale of environmental impact caused by a suspended sediment plume, (2) the regional connectivity of species and the biodiversity of biological assemblages and their resilience to impacts, and (3) the integrated effects of disturbance on ecosystem functions, such as the benthic food web and biogeochemical processes.

Due to the small spatial and temporal scale of the testing activity, no serious harm will be caused to the marine environment at any depth within the water column. Moderate, small-scale impacts on faunal communities are expected to occur due to (1) habitat/nodule removal, (2) sediment disturbance and plume formation/deposition, (3) biogeochemical alteration of the sediment (i.e. change of habitat integrity), and (4) noise and light pollution. Toxicity of sediments that are released into the lower water column during nodule collection is very unlikely but will be evaluated. Using an integrated 3D hydrodynamic and sediment transport model developed by the University of Bremen, the distance that the suspended plume in the water column is likely to have spread after 4 days of testing is predicted to vary between 2.5 and 8 km (cut-off value 10 mg/L), depending near-bottom current conditions. Direct sediment fallout from the plume reaches to maximally 2 km from the source (deposition ≥ 0.1 mm). Boundaries of zero deposition

are set at 3.5 km and 8 km from the source, depending on the bottom current dynamics at the time of testing (mean flow versus enhanced flow during eddy passage, respectively). For the determination of geographical scale / sampling scale of the monitoring survey and the definition of impact zones in the Environment Monitoring Plan, these modelled results have been used as orientation, but may be adapted and/or refined prior to testing if necessary (e.g. due to refinement of models or collection of new baseline data shortly before the test takes place). Dedicated monitoring surveys will take place in the area of direct impact (nodule removal), the area of plume deposition surrounding the impact area (transects up to zero impact), and in a close-by, ecologically similar, non-impact reference site.

The project is committed to organising, facilitating and effectively managing the archival of generated data and samples in databases with established structures and capabilities, such as PANGAEA and European museum collections, based on established protocols and best practices for research expeditions, the specific code of conduct for marine sciences, and ISA's and the EU's principles of data and knowledge sharing. Due to the independent nature of the scientific consortium analysing and monitoring the impacts created by the collector vehicle, the project offers a transparent, collaborative, adaptive and effective approach to the development and testing of mining technology. This should promote a greater understanding and comprehensive assessment of the environmental effects of future mining activities, the design of fit-for-purpose monitoring programmes, and environmentally and commercially responsible standard development.



# 1. Introduction

## 1.1 Background and rationale

There has been a steady increase of interest in mining of deep-sea minerals during the last decade, as documented, for example, by the growing number of exploration contracts issued by the International Seabed Authority (ISA) and the “Blue Growth” strategy of the EU’s Horizon2020 program funding marine mining technology projects, i.e. Blue Mining, Blue Atlantis, and Blue Nodules. In this context, the ISA is presently tasked with the drafting of *Regulations on Exploitation of Mineral Resources in the Area* (the most recent version being ISBA/23/LTC/CRP.3\*), which are anticipated to be ratified by the Council and the Assembly by 2020. The current draft contains basic environmental regulations as an integral part of the exploitation regulations, but for most procedural steps more detailed requirements still need to be developed, e.g. specific environmental assessment criteria including quantitative thresholds (e.g. for harmful effects) that will ultimately ensure a level playing field for all contractors involved. Examples where thresholds are needed are impacted seabed habitat and sediment plumes (operational plume at the seafloor; discharge plume at mid-water depths or deeper). Furthermore, the draft exploitation regulations lack a concept of the ISA to foster the development of Best Available Technology for mining activities, specific requirements regarding environmental data to be provided and common standards for environmental surveys and monitoring plans (e.g. guidelines as in ISBA/19/LTC/8 for exploration activities). Acknowledging that, according to the Convention, all natural resources of the seabed and ocean floor and the subsoil of the Area belong to the common heritage of humankind, and considering (1) the extremely slow geological formation of the mineral resources, (2) the slow recovery of biological communities impacted by mining, and (3) the uniqueness of the deep-sea environment and its biodiversity, including the rareness of many species, the ISA is burdened with a high responsibility to meet the provisions of Article 145 of the United Nations Convention of the Law of the Sea (UNCLOS). Hence, it is necessary and timely to scientifically investigate the expected environmental impacts of deep-sea mining.

Impacts from mining activities on the marine environment will differ between resource types, but two consequences appear to be common for all currently discussed mining technologies: the removal of the surface of the seafloor, including its epifauna, and the creation of a plume consisting of mineral debris and/or sediment that will spread and blanket untouched seafloor beyond the boundaries of the mined area. A first phase of the three-year European JPI-Oceans-funded project MiningImpact ([www.JPI-Ominingimpact.geomar.de](http://www.JPI-Ominingimpact.geomar.de)), coordinated by Dr. Matthias Haeckel (GEOMAR, Kiel) between 2015 and 2017 and involving 25 partner institutions from 11 countries, focused on impacts related to the harvesting of polymetallic nodules in the Pacific Ocean, particularly the longer-term (decadal) consequences. A second project phase of the MiningImpact project has now been positively evaluated by the JPI-O board, and is expected to run from 1<sup>st</sup> August 2018 until 28<sup>th</sup> February 2022. The consortium with 30 partner institutions from 9 countries and the ISA will extend its previous work towards three major research interests concerning deep-sea polymetallic nodule mining: (1) the large-scale environmental impact caused by a suspended sediment plume, (2) the regional connectivity of species and the biodiversity of biological assemblages and their resilience to impacts, and (3) the integrated effects on ecosystem functions, such as the benthic food web and biogeochemical processes. In this context, key objectives of the project are:

- to develop and test monitoring concepts and strategies for deep-sea mining operations;

- to develop standardisation procedures for monitoring and definitions for indicators of a good environmental status;
- to investigate potential mitigation measures, such as spatial management plans of mining operations and means to facilitate ecosystem recovery;
- to develop sound methodologies to assess the environmental risks and estimate benefits, costs and risks;
- to explore how uncertainties in the knowledge of impacts can be implemented into appropriate regulatory frameworks.

Whereas the first project phase could only target, sample and investigate previous small-scale, discontinuously created disturbance/impact sites of the deep sea that were several decades to several weeks old, such as the DISCOL (Thiel and Schriever, 1990; Thiel et al., 2001) and IOM BIE experimental impact sites (Kotlinski and Stoyanova 1998; Radziejewska 2002), the second phase will focus strongly on setting up and evaluating a comprehensive monitoring program that will accompany an *in situ* test of a pre-prototype nodule collector vehicle (Patania-II) equipped with launch and recovery system that is currently being developed by the Belgian contractor DEME-GSR. During the test, polymetallic nodules will be harvested in two approx. 100 x 900 m (~0.1 km<sup>2</sup>) small, continuous test areas of the seabed in the Belgian and the German exploration contract areas of the Clarion Clipperton Zone (CCZ) in the NE Pacific Ocean. The pre-prototype mining collector vehicle consists of a 4-m wide collector head (one-quarter the size of a planned future collector) that harvests nodules hydraulically at a speed of 0.2-0.5 m/s. DEME-GSR estimates that it will require 4 consecutive days to remove the nodules in each planned test area, assuming a track width of less than 4 m (i.e., allowing for some overlap). The nodules will be stored in a recipient box inside the collector, which will need to be emptied at the seafloor regularly (anticipated to happen at the end of each 40 to 100-m-long track, depending on the nodule abundance). There is no riser pipe attached to the collector vehicle during the trial, and no nodules will be transported to the sea surface. Besides the directly created footprint on the seafloor (nodule removal, compaction), the propulsion system of the vehicle and the hydraulic collector head mechanism will create an operational sediment plume that will spread outside of the mined area. The associated disturbance will be created in a controlled manner as foreseen for the future industrial exploitation phase. Hence, from a scientific point of view, the DEME-GSR pre-prototype collector trial offers unique opportunities to realistically and independently assess the environmental impact arising from a nodule mining operation at the seafloor for the first time. This is a critical step forward, as upscaling of the “small-scaled” experiments as they have been undertaken in the past, such as the Benthic Impact Experiment II (BIE II: Brockett and Richards, 1994; Tsurusaki, 1997), the Japan Deep-Sea Impact Experiment (JET: Barnett and Suzuki, 1997) and the IOM BIE, is a very difficult if not impossible task.

The extreme environmental conditions within the salt water environment of the deep sea, with pressures of ca. 500 bar and temperatures of ca. 2°C, necessitate the development of an extremely resistant technology for the future mining of manganese nodules. The general aim is to develop a system that is both economically viable and that exerts an as low as possible impact on the environment (Best Available Technology). From a technological point of view, the testing of DEME-GSRs collector vehicle equipped with hydraulic collector head components in the forefront of any larger test-mining activity focusses on testing its manoeuvrability, reliability and nodule pick-up efficiency as part of an overall mining system, as well as analysing the anticipated environmental impacts in order to inform and improve engineering design. Due to the independent nature of the scientific consortium analysing and monitoring the impacts created by the collector vehicle, the project offers a transparent, collaborative, adaptive and effective approach to the development and testing of mining technology. This should promote a greater

understanding and comprehensive assessment of the environmental effects of future mining activities, the design of fit-for-purpose monitoring programmes, and industry-led standard development.

## 1.2 Project proponent and history: German license area

The ISA and the Federal Institute for Geosciences and Natural Resources (BGR) in Hannover, Germany signed an agreement regarding the exploration of polymetallic nodules in the CCZ on 19<sup>th</sup> July 2006, for a contract period of 15 years. The German exploration license area encompasses a total area of 75,000 km<sup>2</sup>, divided into two regions with an area of 15,000 km<sup>2</sup> in the central part and an area of 60,000 km<sup>2</sup> in the eastern part of the manganese nodule belt within the CCZ (FIGURE 1.1). This deep-sea area located between Hawaii and Mexico is characterised by water depths between 4000 and 6000 meters and is densely covered with polymetallic nodules, also called manganese nodules. They on average contain 30% manganese and about 3% of copper, nickel and cobalt. Especially these last three metals form an important future source of raw material. Further trace metals occurring in economically significant concentrations in the nodules are titanium, molybdenum, lithium and neodymium. The manganese nodule resource in the German license area comprises ca. 900 million tons wet weight, which translates to ca. 600 million tons dry weight.

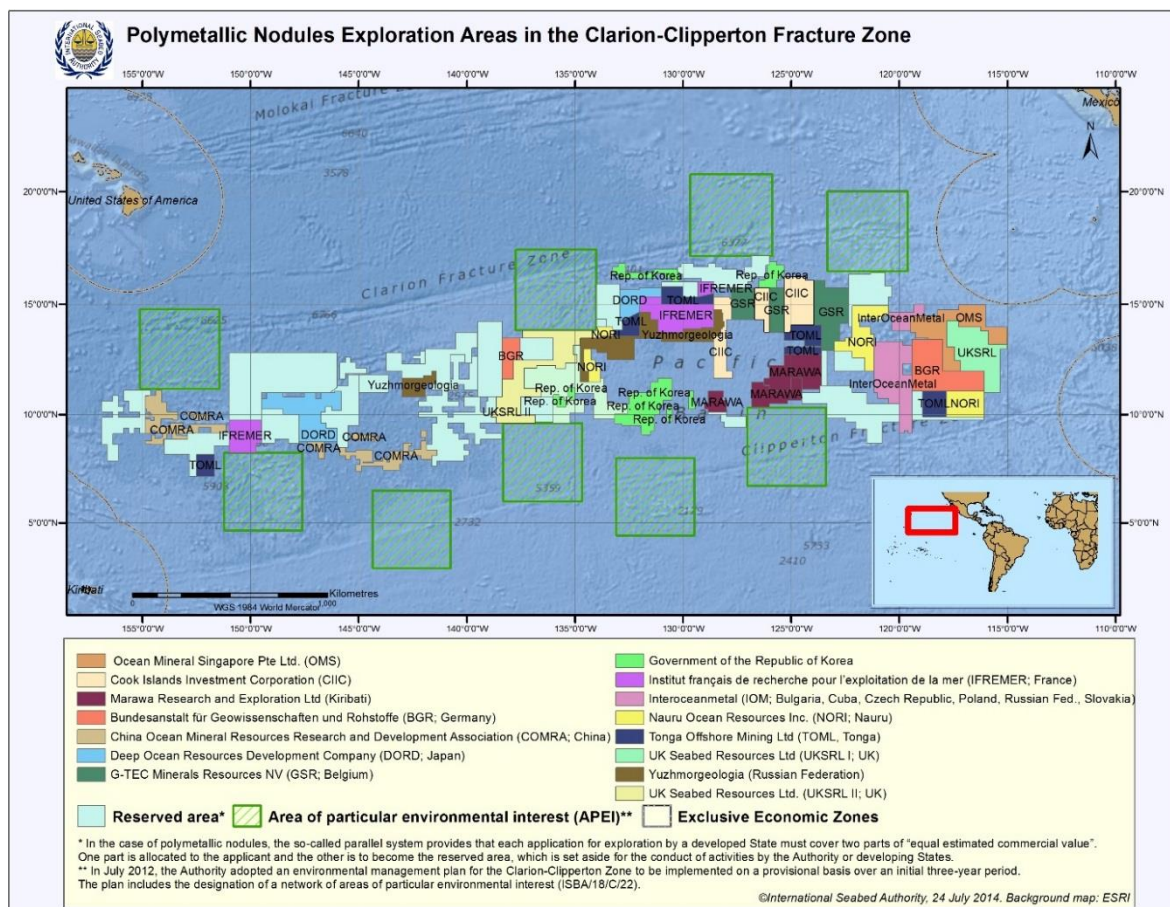


**Figure 1.1:** Manganese nodule exploration contract areas in the CCZ, NE Pacific Ocean (status July 2014). Location of the German (BGR) license area (two sub-regions) is indicated in orange. Source: International Seabed Authority (ISA).

The regulations on prospecting and exploration of manganese nodules adopted by the ISA require each contractor to gather environmental baseline data during the 15 years exploration phase (see CHAPTER 2.1).

Based on such data, the likely effects of possible future mining can be estimated and assessed before intervention within the deep-sea realm actually takes place. Studies of benthic species composition, population densities and connectivity form the most important component of these environmental analyses. In addition to the collection of biological data, detailed analyses of the oceanographic and sedimentological characteristics of the license area must be carried out (e.g. current strengths and directions; particle concentrations and fluxes in the water column; shear strengths, composition and grain size of the sediment; seafloor topography). The BGR has carried out a total of eight exploration cruises to the German license area between 2008 and 2016. Five of these cruises focussed primarily on detailed analyses of the manganese nodule resource potential and its economic value as well as environmental baseline conditions and biodiversity (Wiedicke-Hombach et al., 2009, 2010; Rühlemann et al., 2014, 2015, 2017). A joint French-German cruise (BIONOD) was dedicated to the detailed analysis of benthic communities (Rühlemann et al., 2012), and two cruises (SO-205, SO-240) financed by the German Federal Ministry of Education and Research (BMBF) focussed on processes involved in manganese nodule formation (Rühlemann et al., 2010; Kuhn et al., 2015). The CCZ cruise of the first JPI-O MiningImpact project phase also visited the eastern German license area (Martínez Arbizu and Haeckel, 2015). Biologists from the German Centre for Marine Biodiversity Research (DZMB Senckenberg) in Wilhelmshaven, Germany have accompanied all BGR cruises since 2010 and have, in addition to standard morphological analyses, collected a total of ca. 50,000 individual specimens of benthic fauna for the analysis of deep-sea biodiversity in the German license area based on molecular-genetic techniques. The samples which have been analysed so far generally reflect a high faunal abundance and diversity. In general terms, the German license area can be considered to be one of the best studied areas of the CCZ, particularly when considering the quality and availability of baseline environmental data at and close to the seafloor (as outlined in CHAPTER 4 and CHAPTER 5). It is thus seen to be an extremely suitable site for the testing and environmental monitoring of mining components as outlined in CHAPTER 1.1 above. Furthermore, a ninth exploration cruise to the eastern German license area with the German research vessel SONNE in April/May 2018 will dedicate much of its ship time to the high-resolution analysis of baseline sedimentological, geochemical, oceanographic and biological conditions in the area envisaged for collector vehicle testing in the forefront of the start of the MiningImpact 2 project in August 2018, including the deployment of moorings to measure background current, turbidity and sediment flux conditions in the time period from April 2018 to shortly before the test occurs in April 2019.

### 1.3 Objectives and structure of the proposed project

The main goal of the JPI-O MiningImpact 2 project is to reduce existing knowledge gaps and uncertainties concerning the potential environmental impacts of deep-sea polymetallic nodule mining as set out in CHAPTER 6 and CHAPTER 7. The overall aims of the project are reflected in the project structure (see FIGURE 1.2): three work packages (WPs) address the biodiversity, connectivity and resilience of biological assemblages (WP1), the impact and behaviour of the sediment plume (WP2), and benthic ecosystem functions and processes (WP3), while WP4 facilitates data exchange and archival storage in the project. Furthermore, three cross-cutting themes (CCTs) ensure integration of the different aspects into a coherent work flow at sea to accomplish an effective monitoring of the collector trial (CCT1), to synthesize scientific results into a comprehensive assessment of environmental impacts (CCT2), and to develop joint policy recommendations on risks and best practices of deep-sea mining operations (CCT3). WP5 will coordinate the project activities and communicate and disseminate project results.

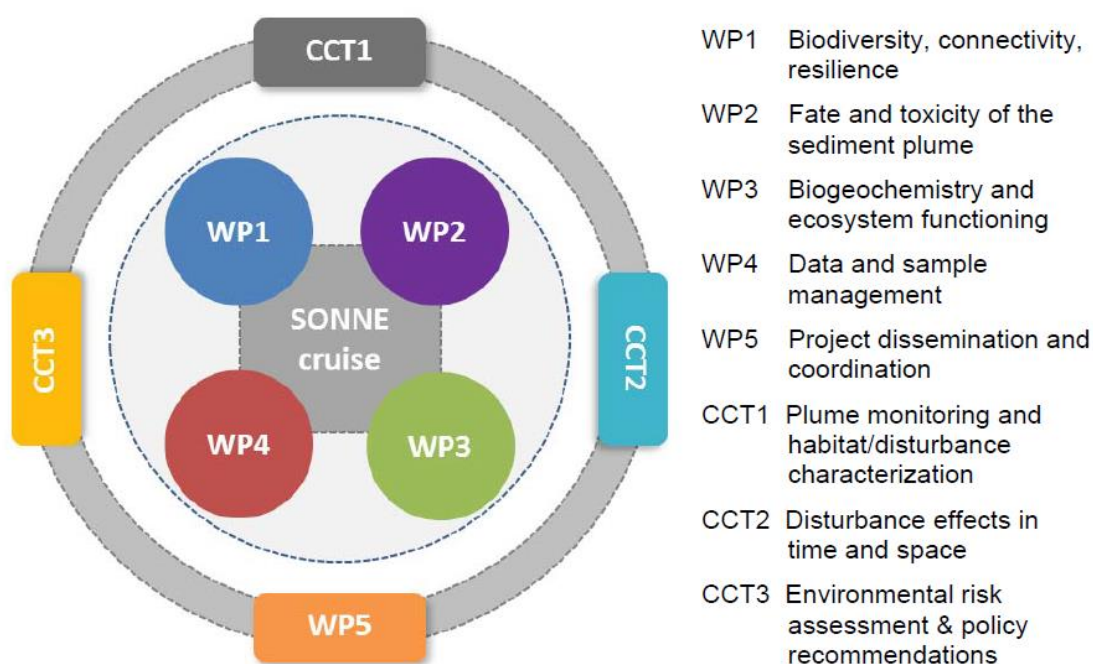


**Figure 1.2:** Structure of the JPI-O MiningImpact 2 project.

### 1.3.1 BIODIVERSITY, CONNECTIVITY, RESILIENCE (WP1)

The primary goal of WP1 is to understand the regional distribution patterns and biodiversity of biological assemblages, i.e. microbes, meiofauna, macrofauna and megafauna, and their resilience to disturbances arising from mining operations.

Specific objectives to be addressed are:

- to assess standing stocks, biodiversity as well as taxonomical and trophic composition of the biota in relation to environmental spatial variability;
- to increase knowledge on taxonomical and functional biodiversity, biogeography and connectivity by applying integrated molecular and morphological approaches;
- to determine biodiversity indicators of “Good Environmental Status” and to assess the short-term impact of nodule collector trial on benthic assemblages as a function of disturbance intensity and habitat variability;
- to assess the resilience of biological assemblages and individual species at various spatial and temporal scales;
- to develop and test molecular methods and protocols for biodiversity assessment and environmental monitoring.

### 1.3.2 FATE AND TOXICITY OF THE SEDIMENT PLUME (WP2)

The primary goal of WP2 is to understand the dispersion, fate and toxicity of the operational sediment plume arising from mining operations.

Specific objectives to be addressed are:

- to monitor sediment plume dispersal, plume sediment redeposition, and numerical modelling of near-field and far-field plume dynamics including particle aggregation processes;

- to characterise the physical and chemical properties of the plume in space and time using both field data and *ex situ* experiments (particle aggregation processes and fate, trace metal dynamics);
- to quantify the spatial and temporal ecological effects of the sediment plume on benthic and planktonic fauna: tolerance to increased suspended particle concentration, physiological and eco-toxicological effects (e.g. bioaccumulation, biomarkers, toxicity bioassays), epigenetic alterations, shifts in coral and deep-water microbial assemblages, reproductive aspects and larvae viability.

### 1.3.3 BIOGEOCHEMISTRY AND ECOSYSTEM FUNCTIONING (WP3)

The primary goal of WP3 is to understand the changes in local spatial variability of sediment physical characteristics and biogeochemical processes in the study area induced by mining operations.

Specific objectives to be addressed are:

- to investigate the local spatial variability of sediment physical characteristics and biogeochemical processes in the study area;
- to quantify the changes induced by the collector trial with respect to the spatial extent of direct (e.g., surface sediment and nodule removal, sediment compaction, pore water release) and indirect mining impacts (sediment blanketing) on physical sediment properties (e.g., shear strength, water content), redox zonation, diagenetic fluxes (e.g., oxygen, nutrients, Mn, Fe, trace metals) and biogeochemical processes including particulate and dissolved organic matter degradation and trace metal reactions;
- to investigate the effects of mining activities on microbial ecology and functions with a focus on organic matter remineralization, productivity, and mortality (microbiological and molecular tools, tracer incubations);
- to investigate the effects of suspended and resettled sediment plumes and differences in nodule coverage on organic matter remineralisation by benthic communities, including microorganisms, meio-, macro- and megafauna (*in situ* experiments and food web models).

### 1.3.4 DATA AND SAMPLE MANAGEMENT (WP4)

The primary objectives of WP4 are:

- to organise long-term storage of the generated data and collected samples;
- to facilitate sharing of data and knowledge between project partners as well as distribution of sample material to partners not able to join the cruises;
- to develop and implement new video annotation and geospatial browsing capabilities for the BIIGLE 2.0 software;
- to develop and implement a central global BIIGLE server to improve collaboration support and knowledge exchange.

### 1.3.5 PROJECT DISSEMINATION AND COORDINATION (WP5)

Building on the experiences and the established contact network of the first project phase, WP 5 will:

- organise workshops with policymakers, NGOs, ISA contractors and interested industry as well as countries planning offshore mining operations in their EEZ to communicate project results and discuss implications;
- communicate the project results to inform the public about the topic of deep-sea mining;
- organise sessions on deep-sea mining at international scientific conferences such as EGU, Goldschmidt, AGU, UMC.

### 1.3.6 PLUME MONITORING AND HABITAT/DISTURBANCE CHARACTERISATION (CCT1)

The project will investigate the dispersal of a mining plume in great detail, complemented by *in situ* and *ex situ* sediment exposure studies. All onsite data will be fed into a near-field plume model which will be used both for ground-truthing of the model and to carry out prognostic plume dispersal simulations under varying hydrodynamic conditions. In this context, CCT1 focuses its efforts on the planning and execution of the monitoring of the sediment plume created by the nodule collector trial. This requires a combination of *in situ* real-time measurements with on-board experiments and shore-based numerical sediment plume simulations (WP2) as well as site selection for baseline and impact sampling (WP1 and WP3). Thus, CCT1 has the following objectives:

- planning of the monitoring cruise, also with regards to an Environmental Impact Monitoring Plan layout: planning of habitat mapping, preparation of the plume monitoring program advised by numerical oceanographic and sediment plume dispersal modelling prior and during the cruise;
- coordination of calibration of sensors and agreement on joint data processing techniques and best practices;
- pre-impact assessment of the habitat distribution by high resolution mapping (hydroacoustic and optical mapping using AUV and ROV) during the cruise;
- coordination of the overall *in situ* monitoring plan of the plume induced by the nodule collector as well as the post-impact assessment;
- coordination and verification of *in situ* and *ex situ* experiments prior to and during the cruise with regards to particle behaviour;
- evaluation of the usefulness and efficiency of employed monitoring technologies and sensors and provide respective recommendations for best practices.

### 1.3.7 DISTURBANCE EFFECTS IN TIME AND SPACE (CCT2)

Given the interactions of multiple stressors and pressures, an integrated assessment of cumulative and interactive impacts is required, reflecting different biological, biogeochemical and physical data, and identifying the sensitivity of different ecosystem components. Furthermore, potential mitigation mechanisms will be investigated by initiating restoration experiments. Specific objectives to be addressed by CCT2 are:



- identification of the scale and magnitude of integrated changes in biological communities and ecosystem function in relation to different disturbance effects;
- development of tools for integrated (cumulative) environmental impact assessment;
- testing of tools and concepts for recovery facilitation.

### **1.3.8 ENVIRONMENTAL RISK ASSESSMENT AND POLICY RECOMMENDATIONS (CCT3)**

One overarching goal of the project is to investigate how the knowledge on environmental impacts and risks as well as concepts for monitoring and spatial management of deep-sea mining operations can be implemented into appropriate legal frameworks of the ISA, the EU and individual countries.

Specific topics to be addressed are:

- identification of pathways towards developing a sound methodology of risk assessment for the utilisation of marine resources that takes into consideration the current state of knowledge on marine ecosystems;
- proposition of methodologies for the risk assessment of the environmental hazard of plumes, such as Weight of Evidence (WOE) and Environmental Hazard and Impact Identification (ENVID);
- development of concepts for minimising harmful impacts on the environment arising from mining, such as: spatial management planning of mining operations; defining criteria for Preservation Reference Zones, conservation areas, marine protected areas; applying the concept of 'good environmental status' from environmental management;
- establishment of non-compliance procedures and a legal framework for a liability regime for environmental damage;
- information exchange with the ISA and their contractors, EU, countries with marine mineral resources, mining-interested industry, NGOs;
- establishment of a systematic approach for estimating the overall benefits, costs and risks stemming from seabed operations, implying undertaking cost-benefit and risk-benefit analysis.

## **1.4 This report**

The most important element of the environmental impact assessment (EIA) presented here is the description of the collector vehicle test in the framework of a scientific project (JPI-O MiningImpact 2) that in itself aims at delivering new and relevant scientific information and knowledge on deep-sea polymetallic nodule mining by (1) developing, standardising and testing monitoring concepts and strategies, (2) investigating the presently poorly-known short and intermediate-term environmental impacts of nodule collection that in turn feed into the proposition of potential mitigation measures and the development of spatial management plans, and (3) developing sound methodologies to assess risks, benefits and uncertainties that can be implemented in future regulations and guidelines. These goals, together with the sheer small size of the activity involved, which is comparable in spatial extent and severity to those of the benthic impact experiments (BIEs) that were carried out in the CCZ in the eighties and nineties (JET BIE, IOM BIE, NOAA BIE), show that the framework of the EIA presented here is conceptually different to that of a full-scale, long-term industrial mining activity (in the framework of exploitation). It is important



to note that the results of the proposed activity presented here are likely to be the primary inputs to Environmental Impact Statements and Assessments for system integration tests and commercial-scale mining at a later stage.

There are no distinct ISA regulations and guidelines for environmental impact assessment during the exploration phase. According to the *Recommendations for the guidance of contractors for the assessment of the possible environmental impacts arising from exploration for marine minerals in the Area* (ISBA/19/LTC/8), each contractor is obliged to submit an impact assessment to the ISA when activities such as those listed in Section IV B of the above-mentioned document are undertaken. Such activities include (1) the use of systems to create artificial disturbances on the seafloor (paragraph 19(b)), and (2) if any one sampling activity by epibenthic sled, dredge or trawl, or a similar technique, exceeds 10,000 m<sup>2</sup> (paragraph 31). The planned activities of testing a collector vehicle on 90,000 m<sup>2</sup> of seafloor (900 x 100 m) in the German license area as outlined in CHAPTER 1.1 above meet both of these requirements for the submission of an impact assessment to the Secretary-General of the ISA. A similar obligation for environmental impact assessment of the collector trial in the Belgian license area exists and will be formulated and submitted to the ISA by the Belgian contractor. There is no obligation for public consultation at this stage of the process (communication with the Secretary-General of the ISA), neither are there any guidelines or templates available that go beyond Section IV C of ISBA/19/LTC/8 (information to be provided by the contractor) to guide contractors in developing impact assessments during the exploration phase. This means that specific requirements regarding the environmental data to be provided and common standards for impact-related environmental surveys and monitoring plans are not available at this point in time.

On the whole, the structure and content of this EIA report has sought guidance from the draft template for an Environmental Impact Statement as laid out in Annex V of the Draft *Regulations on Exploitation of Mineral Resources in the Area* of August 2017 (ISBA/23/LTC/CRP.3\*) and indeed from many of the ISA-related preceding EIA documents (ISA 2012, 2017; Clark et al., 2017), but has some essential differences. Due to the fact that environmental impacts of the collector vehicle test will be greatly limited to the direct vicinity of a small area of seafloor (0.1 km<sup>2</sup>) for a very short period of time (4 days per test area), socio-economic considerations are not included here. The scale of the environmental impact caused by the collector test is in fact well within limits of that which could be considered to be scientifically acceptable for the conduct of marine scientific research in the Area (Article 256 UNCLOS). Also, as nodules will not be transported to the sea surface for commercial purpose there is no developmental context to this EIA (e.g., no transport / materials handling, on-site processing, commissioning and decommissioning, product stewardship, closure plan). Furthermore, as collector vehicle testing ceases in the planned area after 4 days of activity, an ongoing Environmental Management System that follows a clear environmental policy is obsolete and a relatively simple Environmental Impact Monitoring Plan is presented that, for example, does not include long-term conservation goals. In this project, the benefit for the contractor and sponsoring State (Germany) as well as the wider stakeholder community is purely in the form of advancement in applied science and policy related to potential future polymetallic nodule mining in the CCZ.

## 2. Policy, legal and administrative context

### 2.1 Applicable mining and environmental legislation, agreements and policies

The activity that is the subject of the present environmental impact assessment (EIA) is being conducted in "the Area" as defined by the 1982 United Nations Convention of the Law of the Sea (LOS), i.e., on the seabed and ocean floor and subsoil thereof beyond the limits of national jurisdiction (LOS Article 1 (1) (1)). It is the responsibility of the International Seabed Authority (ISA) to organise and control activities in the Area, particularly with a view to administering the resources of the Area (LOS Article 157), in accordance with the legal regime established in Part XI of the Convention (Implementing Agreement) and Part XII of the Convention, respectively.

The activity will take place in the German contract area for the exploration of polymetallic nodules. An agreement on exploration for polymetallic nodules was signed between the ISA and the German Federal Institute for Geosciences and Resources (BGR) on 19 July 2006 for a time period of 15 years. Rules, regulations and procedures for exploration are set out in the ISA Mining Code for polymetallic nodules (ISBA/19/C/17). The testing of collector components planned to take place in the Eastern German license area in April 2019 is part of exploration activities under the current exploration contract.

The activity is governed by the LOS, its 1994 Implementing Agreement (IA) and the rules, regulations and procedures issued by the ISA. Relevant appropriate national requirements by the sponsoring State (in this case Germany) must also be observed (see CHAPTER 2.3). The EIA for the activity planned here has been carried out in accordance with the requirements set out in the legally binding instruments listed above. Note that the International Court of Justice (ICJ) has held that general international law does not "specify the scope and content of an environmental impact assessment" (paragraph 205 of the Judgment of 20 April 2010 in *Pulp Mills on the River Uruguay*, Case No. 135).

Given the absence of specific legally binding ISA regulations, standards, practices and/or guidelines for the development of an EIA during the exploration phase, the present EIA has also sought guidance from the following as appropriate:

- the Recommendations for the guidance of contractors for the assessment of the possible environmental impacts arising from exploration for marine minerals in the Area (ISBA/19/LTC/8);
- the 1 February 2011 Advisory Opinion by the Seabed Disputes Chamber of the International Tribunal for the Law of the Sea: RESPONSIBILITIES AND OBLIGATIONS OF STATES SPONSORING PERSONS AND ENTITIES WITH RESPECT TO ACTIVITIES IN THE AREA (Case No. 17) (which includes guidance relevant here on - in alphabetical order for ease of reference here -: best available technology, best environmental practices, due diligence, environmental impact assessment, and the precautionary approach;
- ISA Technical Studies No. 10 (ISA, 2012) and No. 16 (ISA, 2017);
- the current version of the ISA Draft *Regulations on Exploitation of Mineral Resources in the Area* (ISBA/23/LTC/CRP.3\*).

According to the procedure set out in the above-mentioned Recommendations (ISBA/19/LTC/8), a contractor "is to [submit] an environmental impact assessment to the Secretary-General at least one year before the activity

takes place and at least three months in advance of the annual session of the Authority". The planned date of submission for this EIA is 31 March 2018. The data output of the collector components test planned here will inform equipment design and contribute to the development of an Environmental Impact Statement for eventual future exploitation.

## 2.2 Relevant international and regional agreements

International conventions to which Germany is a party that are potentially relevant to the activities planned in this EIA have been taken into account. These include:

**(1) The Conventions administered or hosted by the International Maritime Organization (IMO):** The activities proposed here require use of vessels at sea. International shipping, safety, and ship-based marine pollution prevention obligations apply to this activity. The proponents must and will ensure that all vessels involved in the activity proposed here comply with these international obligations.

**(2) The 1992 Convention on Biological Diversity (CBD):** The CBD's objectives include in relevant part: "the conservation of biological diversity [and] the sustainable use of its components." (Article 1). The CBD is sometimes invoked as potentially applicable in the context of activities in the Area. Unfortunately, the CBD's relationship to the Law of the Sea Convention with regard to activities in the Area is unclear and has not been judicially interpreted. Furthermore, the extensive qualification of the CBD's obligations with the language "in accordance with [the Contracting Party's] particular conditions and capabilities" and "as far as possible and as appropriate", whose effect has also not been judicially interpreted, render the actual extent of its obligations on Parties unclear with regard to activities in the Area (and in general). In consequence, the applicability of the CBD in this context is both unclear and highly questionable.

## 2.3 National agreements

Activities related to the prospecting and exploration of marine mineral resources in the Area are regulated in Germany by the Gesetz zur Regelung des Meeresbodenbergbaus (Meeresbodenbergbaugesetz – MbergG) that came into effect on 6 June 1995. The main purpose of the MbergG is to assure compliance of sponsored entities with all obligations arising from Part XI and Annex III of the Convention, the Implementing Agreement and all Regulations issued by the Authority. Prospection and exploration activities in the Area are solely supervised by the State Authority for Mining, Energy and Geology (LBEG) in Clausthal-Zellerfeld (Lower Saxony). All German applications for prospecting and exploration activities in the Area require previous approval by both the Secretary-General of the ISA and the LBEG. For the approval process, expert opinion on matters relating to maritime traffic and environmental protection is obtained from the Federal Maritime and Hydrographic Agency (BSH) in Hamburg. The BSH should, in turn, seek for a mutual agreement in opinion on environmental matters with the German Environment Agency (UBA) in Dessau.

The testing of collector components in the Eastern German license area and the associated monitoring of its environmental impacts in the framework of the European JPI-O MiningImpact 2 project is an essential step towards preparing for a pilot mining test and is covered by the exploration contract with the ISA as per its Standard Terms. However, the BGR as contractor is obliged to consult with the LBEG and BSH whether additional requirements for the activity are necessary according to § 4 Article 9 MbergG.

## **3. Project description**

### **3.1 Purpose of the proposed project**

A proposal for a second phase of the European JPI-O MiningImpact project has been positively evaluated and is set to start on the 1<sup>st</sup> August 2018 for a time period of 3.5 years. The consortium of partners from science and industry aims at setting up and evaluating a comprehensive monitoring programme that will accompany tests of a pre-prototype nodule collector vehicle (¼ industrial-scale size) that is currently being developed by the Belgian contractor DEME-GSR. During the tests, polymetallic nodules will be harvested in two approx. 100 x 900 m small, continuous test areas of the seabed in the Belgian and the German exploration contract areas of the CCZ, respectively. This EIA covers the German license test area only; the test in the Belgian license area is subject to a separate EIA that will be submitted by the Belgian contractor. The background and rationale to the proposed project are provided in CHAPTER 1.1, and the objectives of the project are listed in CHAPTER 1.3.

### **3.2 Location**

The collector vehicle test will take place in the Eastern German license area, in an economically prospective nodule field called “Prospective Area #1”, or in short PA1 (see FIGURE 1.1 and FIGURE 4.1 for an indication of the location of the area in a regional context). The target area is in the western part of PA1 (FIGURE 3.1), an area that has been subject to detailed resource analyses as well as environmental analyses during the last few years (see CHAPTER 4 and CHAPTER 5 for details). Starting in 2013, three BGR exploration cruises (Rühlemann et al., 2014, 2015, 2017) and two research cruises with RV SONNE – the JPI-O MiningImpact cruise (Martínez-Arbizu and Haeckel, 2015) and a cruise focussing on the heat flow regime in the crust (Kuhn et al., 2015) – have visited PA1 and carried out detailed investigations and sampling schemes there.

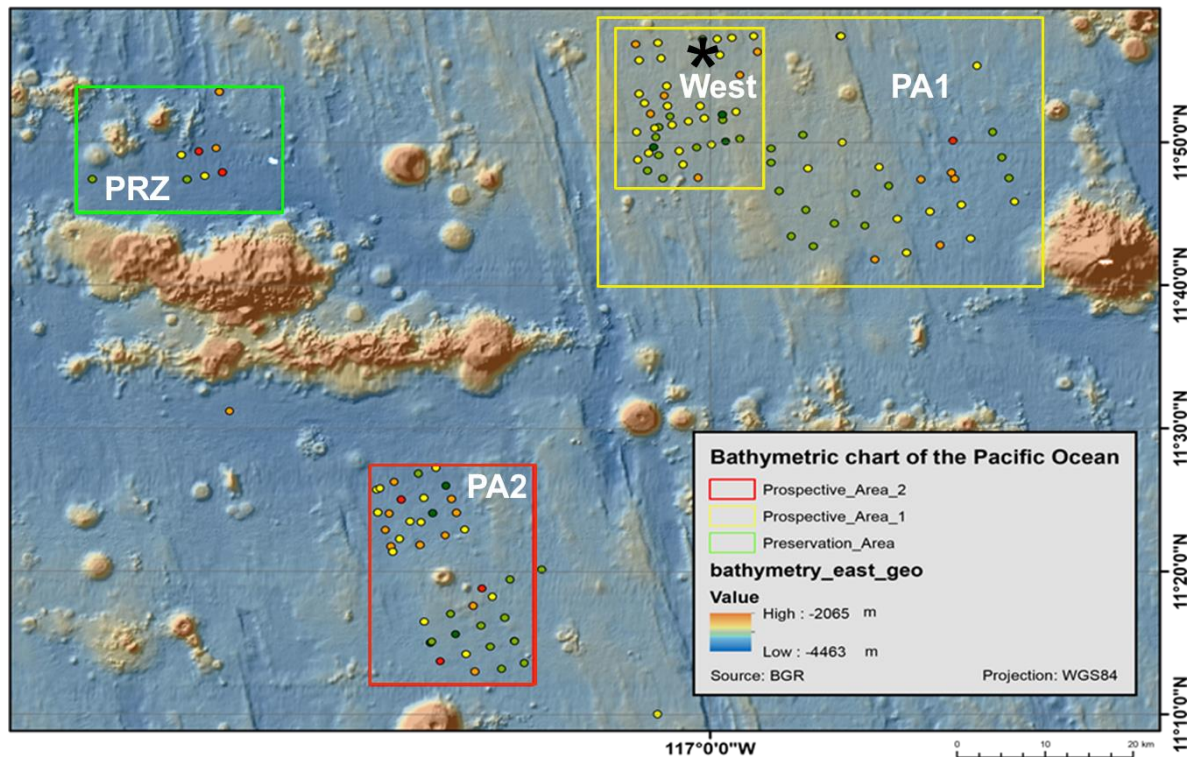


**Figure 3.1:** Bathymetric map of the eastern part of the Eastern German license area showing the locations of two manganese nodule prospective fields PA1 and PA2 as well as the location of a Preservation Reference Zone (PRZ) that was defined in 2013 and has been subject to annual biological investigation. Dots indicate positions of box corer stations (status 2015). The area planned for the collector vehicle test lies in the northern part of the well-investigated area PA1-West, as shown by the black star in the figure.

PA1-West is an area with a relatively flat seafloor, a depth of around 4100 m and a size of ca. 250 km<sup>2</sup> (FIGURE 3.2). It is mostly covered with large nodules (> 4 cm diameter), and represents the best-studied area within the German license area and perhaps even within the whole CCZ (see FIGURE 4.3). The entire German license area has been mapped with 120 m grid size using the Kongsberg 12 kHz multibeam echosounding system EM 120 (e.g. FIGURE 4.1), and parts of PA1-West have additionally been mapped using an EM 122 system and at a high resolution of ca. 1 m with (i) the BGR-owned deep-towed multibeam system HOMESIDE, and (ii) the GEOMAR-owned AUV Abyss. Sediments and nodules of PA1-West have been intensively sampled for nodule geochemical and resource evaluation as well as for biological and environmental analyses. To date, 93 successful box core samples and 32 multicore samples were retrieved from PA1-West (FIGURE 4.3). The average sample distance between box corer samples is 1330 m. Furthermore, six several-km-long video tracks were obtained from the area, as well as photo footage from the GEOMAR ROV Kiel 6000. Biological material for genetic macrofaunal analyses was obtained from 7 epibenthic sled tows. In this regard, the epibenthic sled and the multicorer were deployed in the same area and at the same locations in four consecutive years in a predefined Impact Reference Zone (IRZ – see FIGURE 4.1 for location) in order to obtain information on interannual variability in macrofaunal and meiofaunal assemblages. Water column oceanographic studies have been carried out using 15 CTD casts, and by mooring current meters close to the seafloor (4 positions) over a time period of three consecutive years. Further oceanographic information was retrieved by mooring 2 landers with current meters and a thermistor chain close to the seafloor during a time period of 9 weeks in spring 2015 (MiningImpact cruises). Last but not least, surface waters were sampled by plankton net and rosette to obtain information on plankton assemblages.

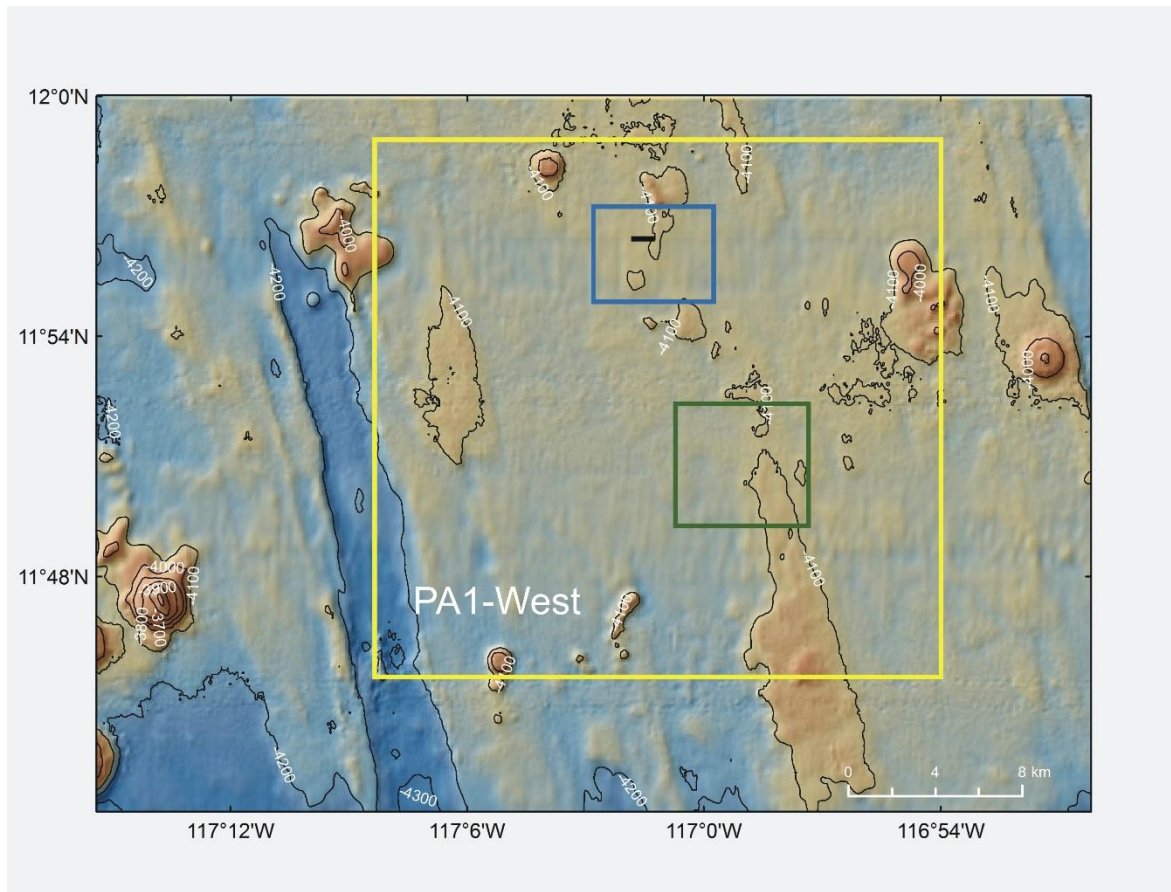


**Figure 3.2:** Bathymetry of PA1-West. The collector vehicle test will take place within the blue rectangular area in the northern part of PA1-West, shown here exemplarily by the black rectangle. The green square represents an area of intensive previous analysis that will be used as a control reference site for the test (see also FIGURE 4.3).

The larger area within which the collector vehicle test will take place lies in the northern part of PA1-West (illustrated by the blue rectangle in FIGURE 3.2) so as to make optimal use of all the baseline data that have been collected in the area so far, but also to be at a reasonable distance away from the area in which yearly samples have been taken and will still be taken in the future for biological time series analyses, and which represents an ideal control reference site for the test (represented by the green square in FIGURE 3.2 and FIGURE 4.3). The exact location of the ca. 100 x 900 m test area (0.1 km<sup>2</sup>) within this larger blue rectangular area with a size of 20 km<sup>2</sup> will to some extent depend on prior habitat mapping efforts using ship- and AUV-based bathymetric and optical information (e.g. on nodule coverage, geology) as well as geological, sedimentological and biological data that will be obtained (i) during a BGR exploration cruise with RV SONNE in April/May 2018, and (ii) shortly before the test (March 2019) during the first cruise leg with RV SONNE as part of the MiningImpact 2 project. One possible location for the collector test based on the best available information at the moment is indicated by the black rectangle in FIGURE 3.2 and FIGURE 4.3, but the exact position will be determined when more information, especially on near-bottom current dynamics and possible direction of plume dispersion, becomes available shortly before the test activity starts (see CHAPTER 8.2 for details on the monitoring approach and programme).



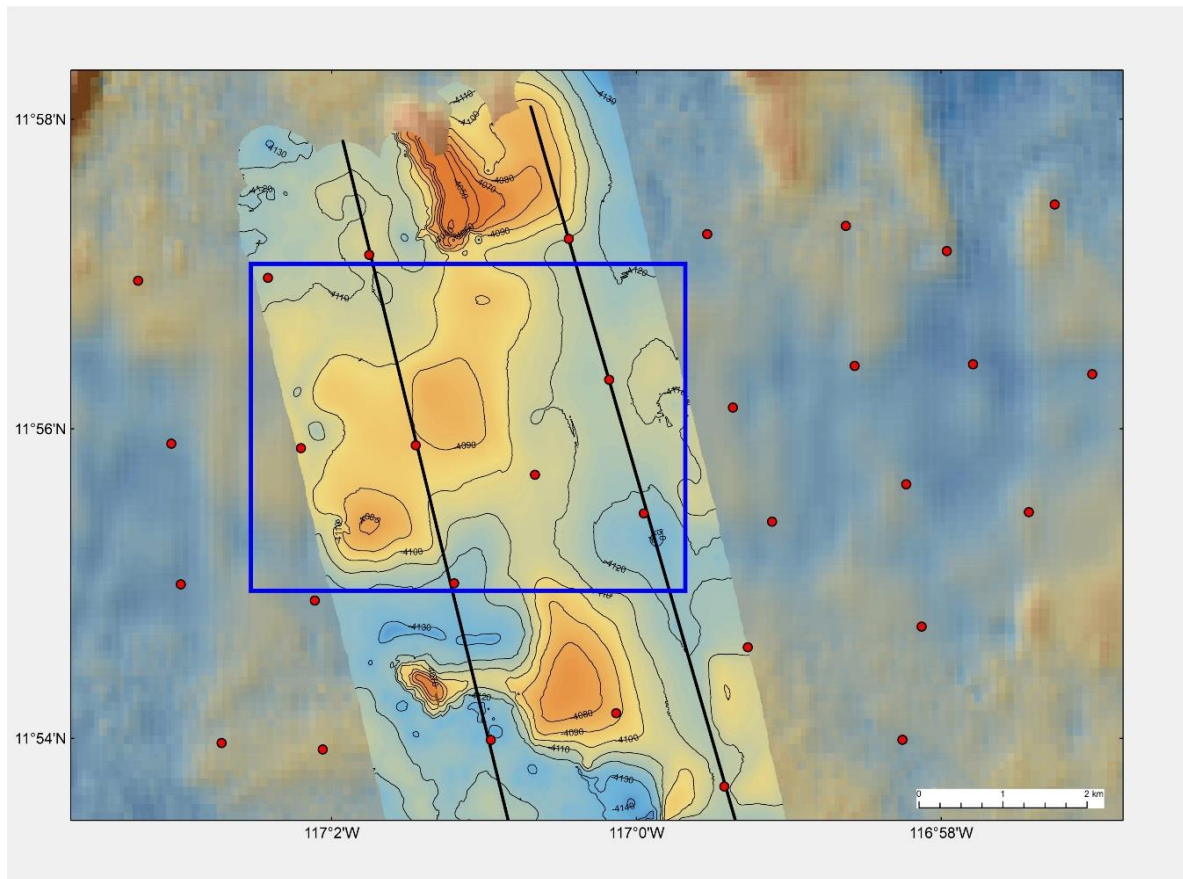


**Figure 3.3:** High-resolution deep-towed bathymetry obtained from HOMESIDE (BGR-owned instrument) with a resolution of about 1 m superimposed on ship-based EM 120 bathymetry (resolution ca. 100 m) of the northern part of PA1-West. The blue rectangle illustrates the larger area that is deemed suitable for the collector vehicle test. Black lines represent video sled tracks from 2016; red dots represent box corer positions.

The 20 km<sup>2</sup>-large area that has been chosen as a suitable site for the collector test comprises a flat abyssal plain that lies in between two small, ca. 60-m-high hills to the north and the south with relatively steep slopes of between 15° and 25° (blue rectangle in FIGURE 3.2 and FIGURE 3.3). These elevated features dip gently to the east, whereas steep flanks occur to the south and west. Depressions or holes were also found at the southern and western flanks of these features, which could be interpreted to be the result of scouring due to currents at the lee side of hills. Slopes are < 3° throughout most of the planned test area (FIGURE 3.4), and the area is free of roundish to oval depressions with depths of up to 6 m, slopes of up to 6° and a size of up to 450 x 120 m that are typical for the well-sampled abyssal plain a couple of kilometres to the south (Martínez-Arbizu and Haeckel, 2015; Rühlemann et al., 2017). Based on acoustic backscatter data of the 12 kHz multibeam echosounding system EM 120, and ground-truthed using box corer nodule size data (see CHAPTER 4.2.1), the area is partly covered with medium to large-sized nodules (> 4 cm) and partly with small nodules (< 4 cm) (FIGURE 3.4). The exact dimensions of the collector test area depends on whether it is carried out in an area with predominantly small nodules or in an area with predominantly large nodules, as these influence the absolute abundances of nodules per square meter that will be picked up by the collector (see CHAPTER 3.3 below), and thus the distance that the collector can drive before tipping its nodules and reversing its direction. For the collector test in the German license area, an area with predominantly small nodules and abundances varying between 18 and 22 kg/m<sup>2</sup> (see FIGURE 4.3, FIGURE 3.4 and FIGURE 3.5 for details) is envisaged. The resultant pattern of nodule collection and the expected dimensions of the collection area (4 days of testing) are described in CHAPTER 3.4.

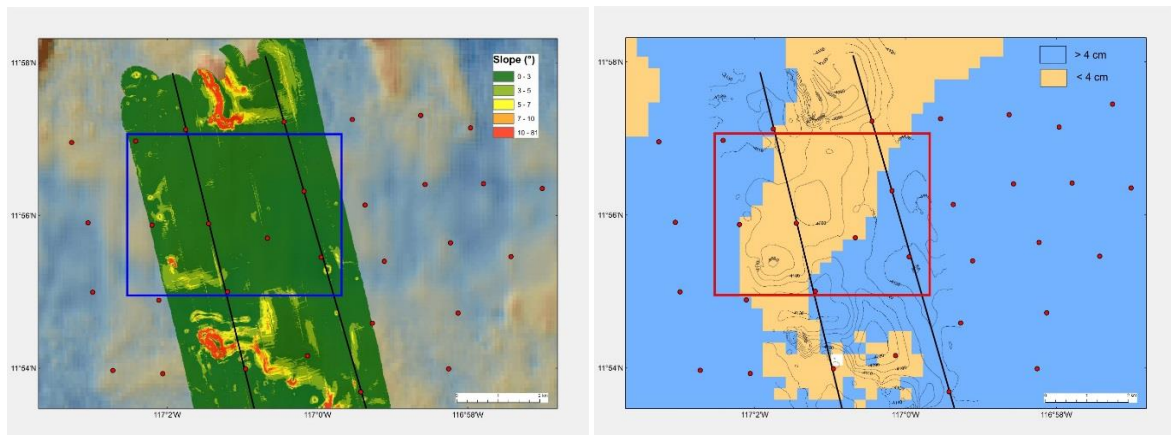


**Figure 3.4:** *Left: Slope angle determined from high-resolution bathymetric data (pixel size 1/1 m) superimposed on ship-based EM 120 bathymetry (resolution ca. 100 m) in the northern part of PA1-West. Right: nodule size distribution as derived from the EM 120 backscatter signal. Blue areas are dominated by medium- to large-sized nodules (> 4 cm) and yellow areas are covered with small-sized nodules (< 4 cm). The blue/red rectangle illustrates the larger area that is deemed suitable for the collector vehicle test. Black lines represent video sledge tracks from 2016; red dots represent box corer positions.*

### 3.3 Mineral resource estimation

The BGR together with Beak Consult GmbH carried out a resource assessment in 2015 based on hydro-acoustic and box corer data for the entire license area as well as for the prospective nodule field PA1-West (Knobloch et al., 2017). A neural network approach was used to analyse the entire license area and typical geostatistics (variography as well as ordinary and universal kriging) were carried out to analyse prospective areas. The average relative prediction error for the neural network approach amounted to ~35%. A classification of the resource assessment of the entire license area according to international standards, such as the JORC code, was not possible mainly because this method can only provide error estimates for sample points, and the number of sample points is small compared to the size of the entire license area. In contrast, the geostatistical analysis of box corer nodule abundance data in prospective areas does provide error estimates even for locations without samples.

For the analysis of the box core data within PA1-West (93 samples, see FIGURE 4.3 for locations), only the geostatistical methods variography and kriging were used. Kriging is a well-known geostatistical method for the interpolation of point data. Its advantage compared to other classical interpolation methods is that it accounts for the spatial variance of a parameter, which is determined and described by a variogram. The variogram model mathematically specifies the spatial variability of the dataset in each geographical direction. Scale, range and nugget effect of the variogram model are required, input parameters for kriging (Akin and Siemens, 1988). The range of the variogram defines the maximum distance between sample points at which samples statistically influence each other. The scale represents the non-random component of the variability of the dataset and the nugget effect represents the random component. For the prediction of a parameter value at any unknown location, the values from the neighbouring known locations are weighted by keeping the estimation error variance low. This error depends on the fitting quality of the variogram function.

For geostatistical analyses, the ArcGIS® extension Geostatistical Analyst® was used. The average sampling distance within PA1-West was calculated to be 1330 m based on the Euclidian distance. For geostatistical calculations, ordinary kriging was applied with a spherical variogram model. Block kriging was applied on the ordinary kriging results in order to estimate the absolute and relative prediction error at a constant block size of 1000 m × 1000 m. No detrending or transformation was applied to the data



prior to analysis. Absolute tonnages of manganese nodules in PA1-West were calculated by adding up the block values. Dry tonnages were obtained by multiplying wet nodule abundances by a factor of 0.69. For the application of geostatistical methods on the dataset of nodule abundances, it is necessary that the input data follow a normal distribution (Gaussian distribution). This assumption was tested and verified using a normal quantile-quantile (QQ) plot.

A spherical variogram model was used. A lag size of 500 m was obtained. The nugget value of 1.5 equals about 14% of the total variance. An anisotropy with a direction of 30° was applied in order to better fit the model to the data, which is likely caused by the local bathymetry in the area. The major range of the variogram is 2500 m and the minor range is 1500 m, i.e. the samples influence each other within a distance of 2500 m in a NE-SW direction (30°) and within 1500 m in a NW-SE (120°) direction around each sample. The regular distribution of sampling points results in a relatively low and homogeneous distribution of the prediction error, i.e. < 20% in many areas without samples.

Results of block kriging with 1000 m square block size are given for the northern part of PA1-West in FIGURE 3.5, which is the area in which the collector test will take place. The average nodule abundance for the whole modelled area PA1-West is  $22.7 \pm 1.8$  kg/m<sup>2</sup>. Assuming that the nodule abundance is normally distributed, one can state that in 95 percent of the cases (95% probability), the true nodule abundance will be inside the interval formed by the predicted value  $\pm 2$  times the prediction standard error. Therefore, with a 95% probability there will be no area in PA1-West with a wet nodule abundance below 14.7 kg/m<sup>2</sup>. The total tonnage of wet manganese nodules based on all data until 2016 sums up to  $5.25 \pm 0.81$  Mio. tons for an area covering 231 km<sup>2</sup>. Average metal contents of the nodules of PA1-West are 31.5% manganese, 1.44% nickel, 1.20% copper, 0.16% cobalt, 0.062% molybdenum, 0.015% lithium and 0.066% REY (rare earth elements and yttrium).

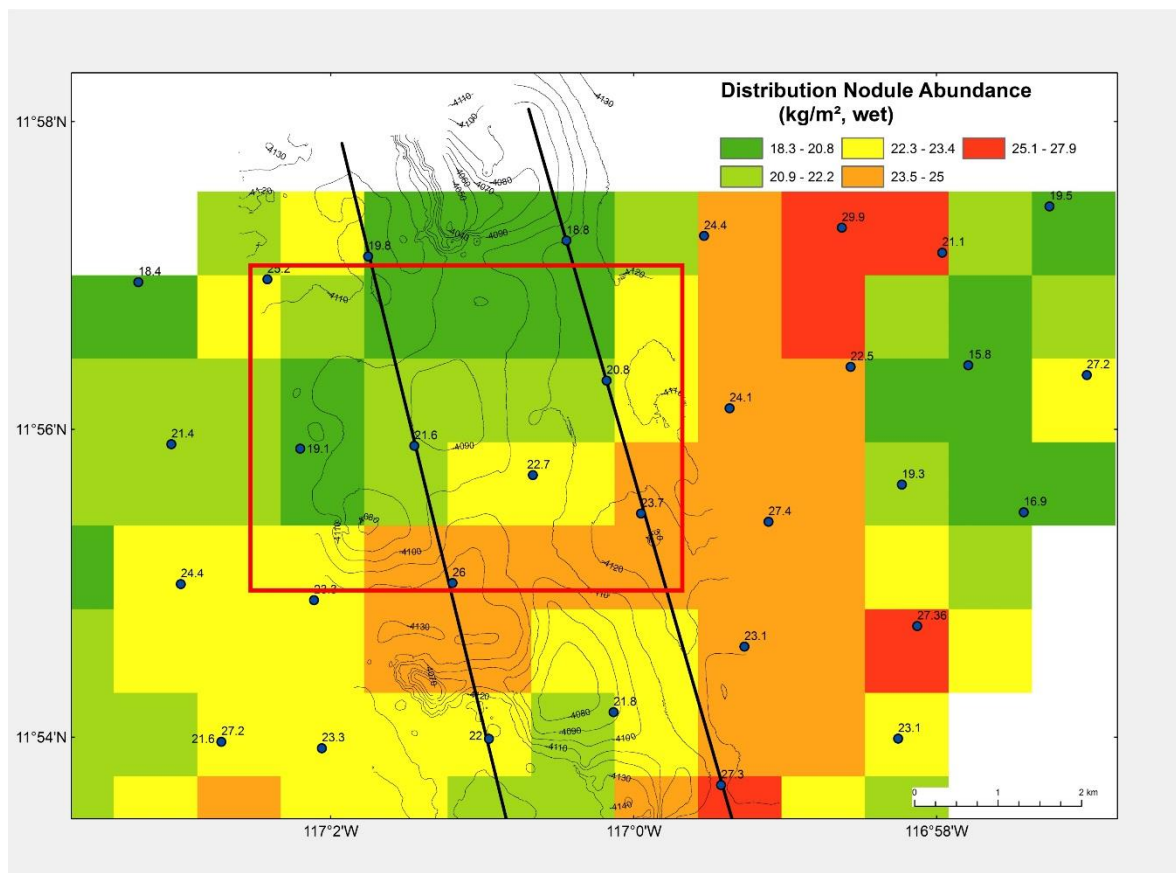


**Figure 3.5:** Prediction of Mn-nodule abundance distribution (wet weight) in the northern part of PA1-West based on ordinary block kriging. The red rectangle illustrates the larger area that is deemed suitable for the collector vehicle test. Black lines represent video sledge tracks from 2016; blue dots represent box corner positions.

The calculated mineral resource of manganese nodules in the analysed area can be classified using geostatistical key values. In a classification guide published by the GDMB society in 1983, a table is provided which links the verbal knowledge classes used in JORC to maximum acceptable average prediction errors for each class. Based on this table, **measured** mineral resources are assumed to have a relative prediction error of less than 10%; **indicated** mineral resources have a relative prediction error between 10% and 20%; and **inferred** mineral resources to have a relative prediction error between 20 % and 30%. Accordingly, with a relative prediction error of 16%, the resource of PA1-West is classified as an “indicated mineral resource”. The range value of the kriging model can also be used to evaluate the continuity of the raw material and its grade (Benndorf, 2015). This can be done by comparing the average sampling distance with the range value of the variogram. Classification can then be as follows: **measured** mineral resources are assumed to have an average sampling distance of less than half of the range value; **indicated** mineral resources are assumed to have an average sampling distance between half of the range value and the range value; and **inferred** mineral resources are assumed to have an average sampling distance of larger than the range value. With a range of the variogram of 2500 m and an average sampling distance of 1330 m within PA1-West, our resource estimation is classified as “indicated mineral resource” in line with the classification based on the relative prediction error.

### 3.4 Description of the pre-prototype collector and testing design

#### 3.4.1 GENERAL REMARKS AND BACKGROUND

CHAPTER 3.4 is structured according to ISA's *Recommendations for the guidance of contractors for the assessment of the possible environmental impacts arising from exploration for marine minerals in the Area* (ISBA/19/LTC/8), Section IV. C. *Environmental Impact Assessment: Information to be provided by the contractor*. It describes the physical characteristics of the pre-prototype test collector Patania II as well as the design of the disturbance experiment. The Belgian company DEME-GSR is currently constructing the Patania II, which will be used for the test in April 2019. The Patania II pre-prototype is the continuation of the "Patania I", which was a Track Soil Testing Device (TSTD) that was tested *in situ* in the CCZ in April/May 2017 in a water depth of 4570 m (FIGURE 3.6 and TABLE 3.1).

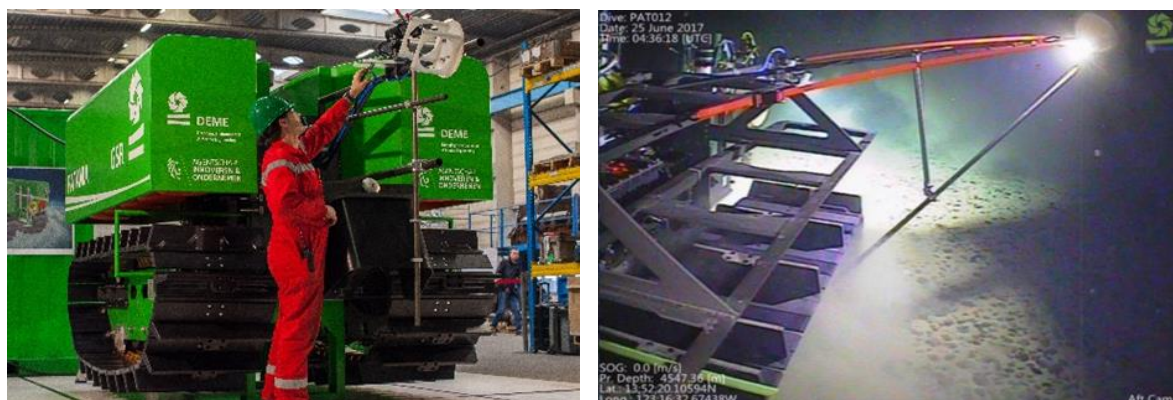


**Figure 3.6:** The Patania I vehicle in the construction hall (left) and on the seabed at 4570 m water depth (right), that was tested *in situ* in the CCZ in April/May 2017.

The tests with the Patania I had seven main objectives:

- (1) Evaluation of the overall performance of a tracked vehicle on the seabed of the CCZ;
- (2) Speed variances and effect on traction and slippage;

- (3) *In situ* pressure-sinkage relationship;
- (4) *Ex situ* shear stress - shear displacement relationships;
- (5) *In situ* thrust – slip relationship;
- (6) Quantitative and qualitative measurements of sediment dispersion generated by the tracks;
- (7) Quantitative and qualitative measurements of sediment dispersion generated by a horizontal water flow parallel over the seabed.

The most important results of the *in situ* tests of Patania I are summarised in TABLE 3.1 below.

**Table. 3.1:** Most important results of the *in situ* tests of the Patania I vehicle in the CCZ in April/May 2017.

Parameter	Measured Value	Unit
Maximum speed driven on seabed	0.65	[m/s]
Total distance travelled on the seabed	14.5	[km]
Total time on the seabed	>30	[hours]
Maximum slope [PAT10]	>15	[%]
Number of <i>in situ</i> plate measurements (sets)	23	[-]
Shear strength – shear displacement measurements ( <i>ex situ</i> samples)	42	[-]

### 3.4.2 DESCRIPTION OF THE PATANIA II COLLECTOR VEHICLE

#### 3.4.2.1 Mineral collection technique

The pre-prototype test collector Patania II is an active system with a hydraulic suction unit constructed and built by the Belgian company DEME-GSR. This vehicle consist of four major subsystems:

- (1) Nodule collection system: consisting of the collector head, the jet water pumps and all sensors to monitor the suction process. The design of the collector head is based on the results obtained from laboratory tests.
- (2) Propulsion system: A two-track system will be used for the propulsion system. The values measured *in situ* with the Patania I have been used for the design of the propulsion system.
- (3) Nodule separation and discharge system: The system is not equipped with a riser for pumping nodules to the surface operation vessel. Hence, a dumping system needs to be incorporated into the design of the Patania II.
- (4) Vehicle systems: comprise all components needed for a proper functioning of the Patania II. This includes Hydraulic Power Units (HPU), telemetry, buoyancy, etc.

These four different sub-components are described in more detail below. The main characteristics and a conceptual design of Patania II are provided in TABLE 3.2 and FIGURE 3.7, respectively.

**Table. 3.2:** Physical and operational properties of the Patania II.

Description	Nominal value	Unit	Comment
Vehicle length o.a.	12	[m]	Including "selfie sticks"
Vehicle width o.a.	4.7	[m]	
Vehicle height o.a.	4.5	[m]	
Vehicle weight in air	35	[mT]	
Vehicle weight submerged	15	[mT]	
Vehicle nominal speed	0.5	[m/s]	
Vehicle maximum speed	1	[m/s]	

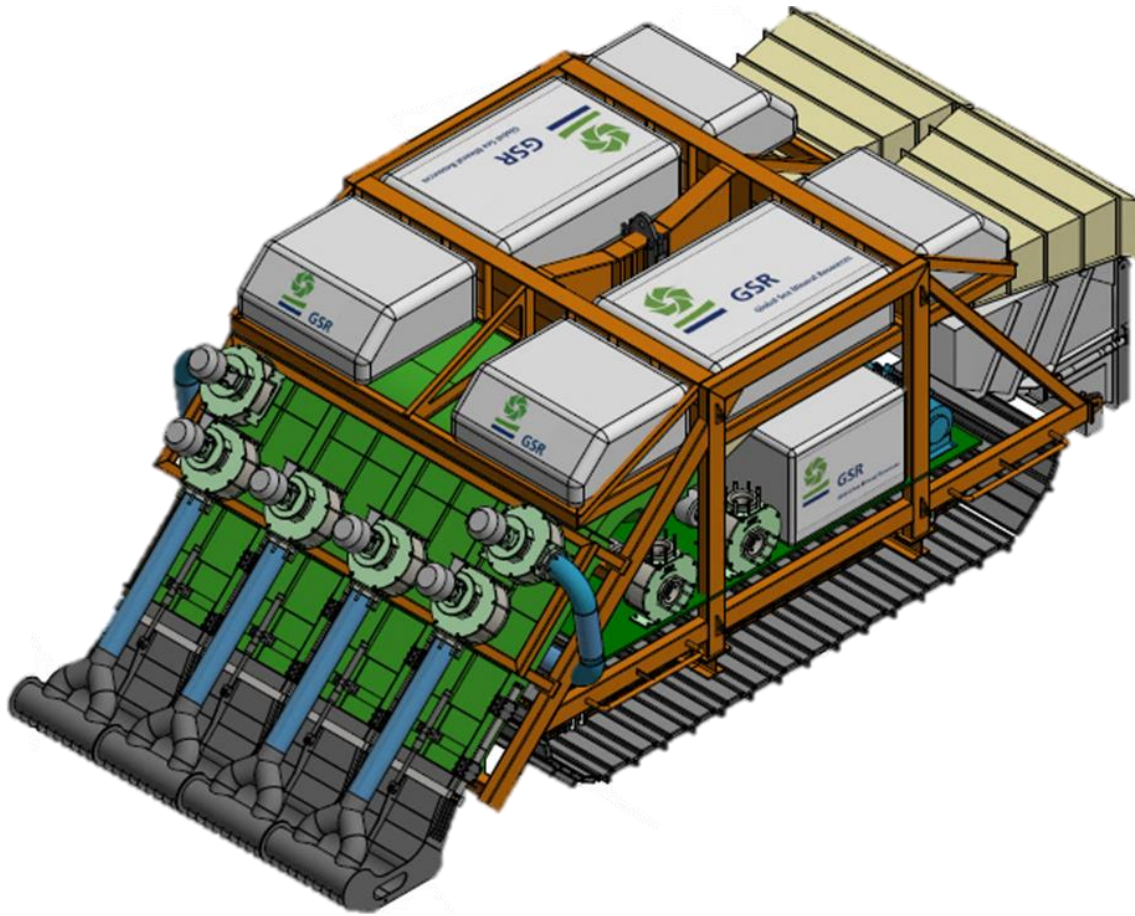


**Figure 3.7:** Conceptual design of the Patania II vehicle that will be tested in the German license area.

### Nodule collection system of Patania II

Four control parameters determine the collection process: (1) the pick-up jet velocity ( $v_{PU}$ ); (2) the transport jet velocity ( $v_{TR}$ ); (3) the height of the collector above the seabed ( $H_{jet}$ ), and (4) the collector forward speed ( $v$ ). The design objective is to be able to verify these parameters during the collection process.

FIGURE 3.8 shows the most important parts of the nodule collector head. A commercial-scale collector system is envisaged to consist of 16 of these modules. The part shown in FIGURE 3.8 is an example of such a module. The Patania II will be equipped with four of these modules. Every module is 1 m wide, and as such determines the total width of Patania II (approx. 4 m). The nodule collection system is based on the results of laboratory tests. One of the main conclusions coming out of the laboratory tests is the importance of the height of the collector above the seabed. Therefore, an important control parameter to be taken into account is  $H_{jet}$ .



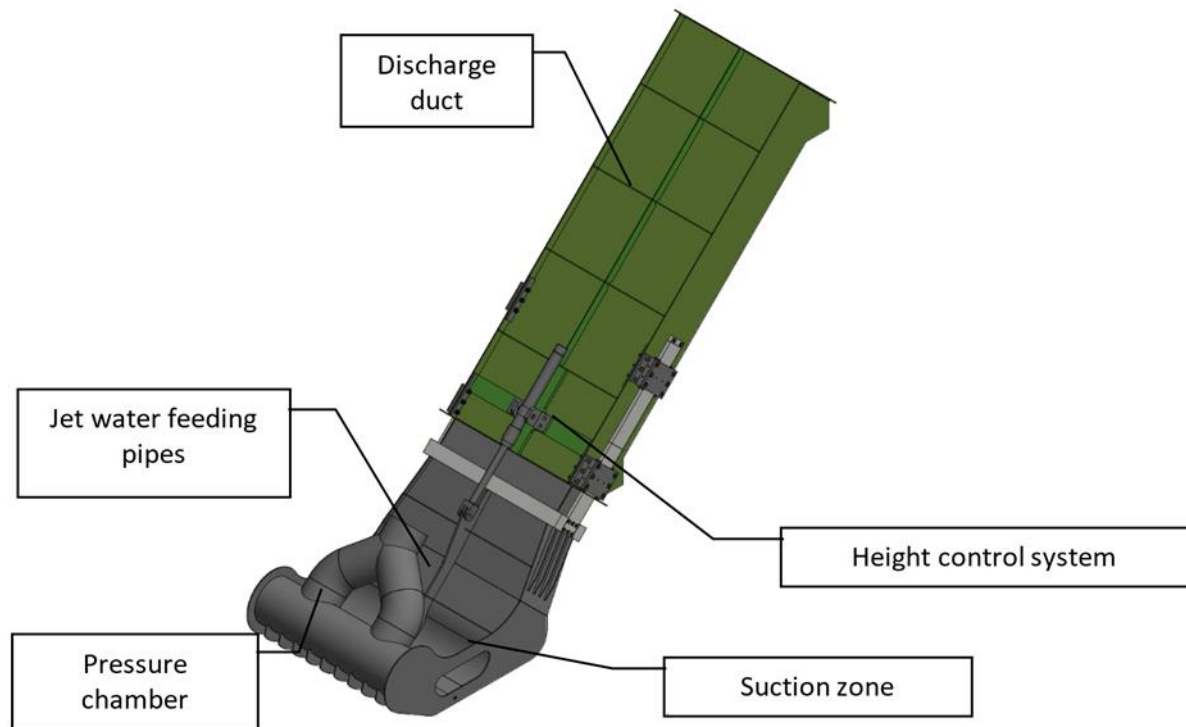


**Figure 3.8:** Nodule collector head.

#### Collector Height control and penetration depth

Two different height reading systems will be installed in front of the collector head (FIGURE 3.9). The primary height measurement will take place using altimeters. However, turbidity might affect the readings, so an additional mechanical back-up system will be installed. Tests with regard to the use of altimeters in a turbid environment will be carried out using altimeters from three different suppliers (Kongsberg, Tritech and Impact Subsea).

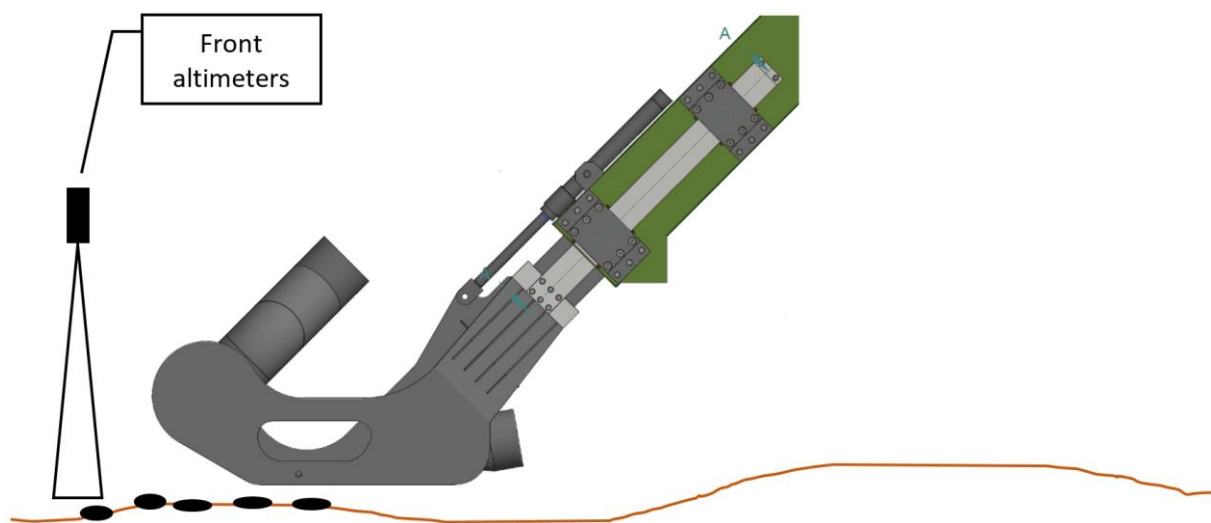


**Figure 3.9:** Collector head height control.

Every head is equipped with its own altimeter, returning the distance to the highest point within its measurement beam. The system processes these measurements and translates them to a certain stroke of the hydraulic piston on top of the discharge duct. Only the forward part is translated up and down. This procedure is automated.

### Flow velocities

Six identical jet water pumps are mounted on the collector: four pumps are used for the pick-up jet and two for the transport jet. A single line diagram of the pump layout is shown in FIGURE 3.10. At current state, a final decision has not been taken as to whether velocity sensors will be mounted in the jet water feeding pipes. Different suppliers have been contacted because of the hyperbaric environment but no appropriate instruments seem to be available. Alternatively, the velocities of the pick-up and transport jets will be controlled by the measurement of rotational speed (rpm) of the jet water pumps. By varying the rpm of the pump, the flow will vary accordingly and as the cross section remains the same, the jet velocity will change. Nominal working point of the pumps is 600 m<sup>3</sup>/h at a head of 10 m.

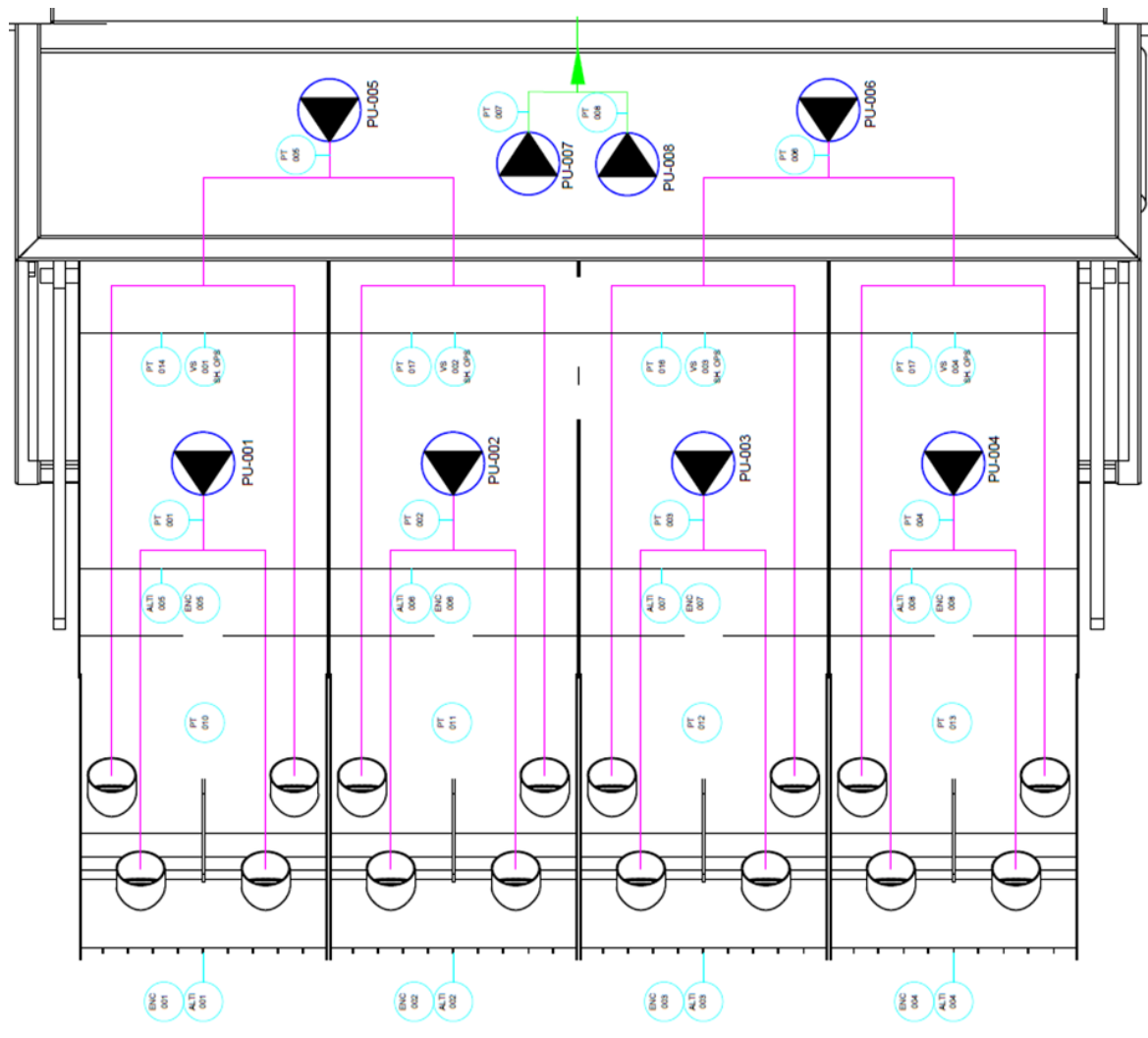


**Figure 3.10:** Layout of one single jet water pump of the Patania II.

### Nodule separation and discharge system

After collection, the nodules move up the collection duct and are deposited in a separation hopper at the end of the collection duct. The larger nodules will fall into this hopper due to gravity. In the hopper, a grating is mounted at the opposite side of the outlet of the collection duct, the inlet of the discharge duct. The majority of the water flow that is used to transport the nodules up the duct passes through the grating towards the diffuser-exhaust. The grating prevents the smaller or fragmented nodules that are entrained by the inlet flow from moving to the diffuser-exhaust. The nodules are subsequently collected at a centralised discharge pipe that pumps the nodules towards the nodule container at the back of Patania II. The nodule payload inside the bucket is shown in purple in FIGURE 3.11. The discharge or dump hatch is the back vertical plate of the nodule container and is controlled hydraulically. A part of the back plate consists of a fine-meshed grating that allows water and remaining sediment to exit the container.

Clogging and blockage remains a significant risk for the hydraulic transport process. Two emergency flushing valves are installed to bring in water into the system. A hopper emergency dump valve is installed in case clogging of the hopper occurs. Although the design is as open as possible, bridge formation of nodules inside the hopper can always take place. In this case, the collector head is lifted from the seabed and a large volume of flushing water is pumped into the system.

“Fresh” water is brought into the process at the central discharge point of the hopper (see FIGURE 3.11). Flow and density measurement systems, together with an emergency discharge valve (gate valve) are installed in the discharge pipe of the hopper towards the nodule container. Approximately 3 metric tons (mT) of nodules (submerged weight, including bunking factor of 60%) can be stored inside the container. The nodule payload inside the bucket is shown in purple in FIGURE 3.11. The discharge or dump hatch is the back vertical plate of the container and is controlled hydraulically. A part of the back plate consists of a fine meshed grating that allows water and remaining sediment to exit the container. If operations require not to collect any nodules (operational mode (1)), the dump hatch remains open and nodules that are being collected are dumped back on the seabed whilst driving.

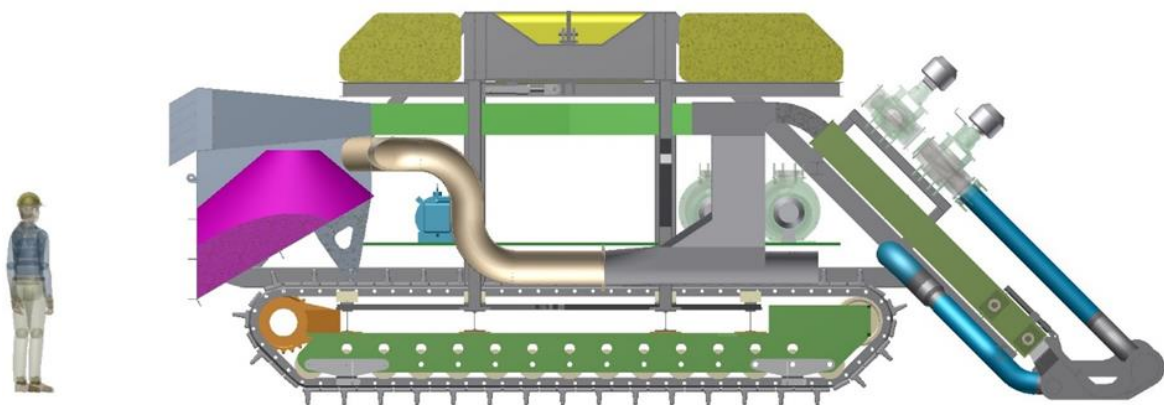


**Figure 3.11:** Nodule separation system. The nodule container at the back of the vehicle is indicated in purple.

### Vehicle systems

#### Power and electronics

An umbilical will be used for supplying electricity to the Patania II. Two types of power conductors are available: 4.2 kV conductors for the electrical motors driving the Hydraulic Power Units (HPUs) and 1 kV conductors (transformed to lower voltages) for the telemetry. Data (video, controls, etc.) will be transmitted via fiber optic cables, also incorporated into the umbilical.

Several ePODs need to be installed on the Patania II to accommodate the electronics that cannot withstand the ambient pressure of 450 bar. The ePODs will be decentralised according to their functionality: (1) nodule collector system, (2) telemetry system and (3) all auxiliary systems.

#### Hydraulic system and track drive

Two (or possibly three) hydraulic power units will be installed on the Patania II to operate all hydraulic systems. These HPU's will be installed underneath the discharge diffuser-exhaust. One of the major consumers of the hydraulic system are the track drives. Two hydraulic motors each drive a track chain. The track pads are mounted on these track chains. Additionally, hydraulic cylinders need to be actuated for different functional objectives. In total 16 hydraulic cylinders are installed on the Patania II:

- 4 units for height control of the collector head (1 cylinder per module)
- 2 units for rotating the separation grating inside the hopper
- 2 unit for emergency discharge off the hopper
- 1 unit for emergency gate valve in discharge line towards nodule container
- 2 units for the dump hatch of the nodule container
- 4 units for a height measurement mechanical back-up system
- 1 unit for an active air relief system on top of the discharge diffuser-exhaust duct.

#### Telemetry

The Patania II will be equipped with a significant amount of sensors. At the current stage, however, the exact types of sensors are still under consideration and we thus cannot provide details here. Whatever the case, the sensors needed for the operation of the Patania II and its environmental monitoring fall into five basic categories:

- (1) Positioning: As on the Patania I, a combination of an Inertial Navigation System/Doppler Velocity Log (INS/DVL) system will be mounted at the front of the Patania II. The DVL will measure the Speed Over Ground (SOG) whilst the INS system will return the absolute position, trim and list.
- (2) Vehicle systems: Sensors measuring hydraulic pressures, hydraulic volumes, pump rpms (such as track drive motors) etc. will be required to follow the status of the Patania II in operation.
- (3) Dredging and nodule collection: Flow and density of the mixture will be measured in the hopper discharge pipe towards the nodule container. The nodule container is mounted on three load cells which provide an indication of the fill level of the container. Additionally, the container will be equipped with proximity switches to provide a back-up measurement of the fill level.
- (4) Environmental sensors: a Conductivity, Temperature and Depth (CTD) measuring probe with a turbidity sensor will be mounted to provide data on the sediment plume.
- (5) Others: in order to measure the load at the end of the umbilical, a load cell will be mounted on the suspension point to the umbilical.

### **3.4.2.2 Depth of penetration into the seabed**

The *in situ* "penetration depth" into the seabed and the "depth of influence" are difficult to predict as the laboratory tests with the hydraulic collector were not specifically designed to provide appropriate values. According to previous *in situ* tests of the Patania I in the CCZ, DEMA-GSR expects that the Patania II caterpillars will penetrate up to 5 cm into the sediment. The depth of influence of the water jets at the



collector head will be investigated *in situ* for the first time during the test runs in 2019. Based on laboratory experiments, DEME-GSR assumes that the depth of influence will be between 5 and 15 cm, depending on the thickness of the fluffy top layer of the seabed. For calculations of rates of sediment mobilisation during the test, e.g. for plume dispersal and deposition modelling (CHAPTER 6.4.3), a depth of sediment removal of 12 cm has been assumed.

### 3.4.2.3 Running gear which contacts the seabed

The Patania II moves on two caterpillars made of a type of Nylon (Ertalon Tracks, commonly used for trenching) that have a width of 1.5 m and an approx. thickness of 12 cm and are equipped with alternating grousers. The total length of each caterpillar is 6 m.

### 3.4.2.4 Methods for separation of the mineral resource and the sediment

The method of separation of nodules from sediment and small particles due to nodule abrasion is explained in CHAPTER 3.4.2.1. Only sediments and very fine abraded nodule fragments mixed with water will pass through the diffuser-exhaust. The discharge outlet behind the collector is at ca. 3 m above seafloor. Depending on the speed of the collector vehicle, which will vary between 0.2 and 0.5 m/s, the amount of wet sediment that will be mobilised by the collector vehicle will vary between 400 and 1000 m<sup>3</sup>/h, = 135 to 337 t/h dry sediment. These values have been used to model particle size dispersion and settlement with distance from the source, as elaborated on in CHAPTER 6.4.3.

### 3.4.2.5 Mineral crushing and processing methods at the seabed

The nodules will not be actively crushed or processed at the seabed.

### 3.4.2.6 Transport of material to the surface

The system does not include a riser for a continuous transport of nodules to the surface. The only way to get the nodules collected in the bucket to the surface is during retrieval of the collector.

### 3.4.2.7 Mineral resource separation and processing on the surface vessel

Does not apply.

## 3.4.3 COLLECTOR TEST DESIGN

### 3.4.3.1 Probable duration of the test

The collector vehicle test (disturbance experiment) in the eastern German contract area will be carried out over a time period of maximally 4 days.

### 3.4.3.2 Test plan

The seagoing campaign to the CCZ for the testing of Patania II will consist of two legs. During the first leg (Deep Sea Functionality Testing), DEME-GSR will test the general functionality of Patania II in the Belgian license area at water depths of about 4600 m. During the second leg (GSRNOD19 impact experiment and component validation), testing in coherent test fields as part of the impact experiments will be carried out first in the Belgian license area, and then in the German license area (April 2019) (TABLE 3.3). These tests will be accompanied by simultaneous environmental impact monitoring from the RV SONNE as part

of the MiningImpact 2 monitoring programme (CHAPTER 8.2.2). The functionality testing is foreseen to mitigate any technical issues before the actual operations within the framework of the MiningImpact 2 programme start. In spite of an entire technical testing program prior to vehicle deployment (FAT testing, land and wet trials, hyperbaric testing), it is not guaranteed that all systems will perform in the deep sea as expected. The conditions are extremely harsh and not always reproducible on land. Additionally, certain components cannot be tested prior to the deployments in the deep sea. For example, a verification of the functioning of the umbilical winch (spooling and fleeting system) or an integrated hyperbaric test of the entire vehicle can only be carried out when the umbilical and the Patania II are fully deployed. Moreover, several consecutive deployments are necessary as the system oil needs time to creep up the umbilical because of the increase in pressure while the vehicle is being gradually deployed.

During the trials with Patania I in 2017, nine different dives spread out over 14 days were required before the Patania I finally touched the seabed. Therefore, the functionality period is foreseen to guarantee operational continuity during the second leg of the campaign. Additionally, a buffer period of 21 days is foreseen to rectify any technical issues that have been identified during the functionality period.

The subsequent GSRNOD19 campaign will have two major operational modes:

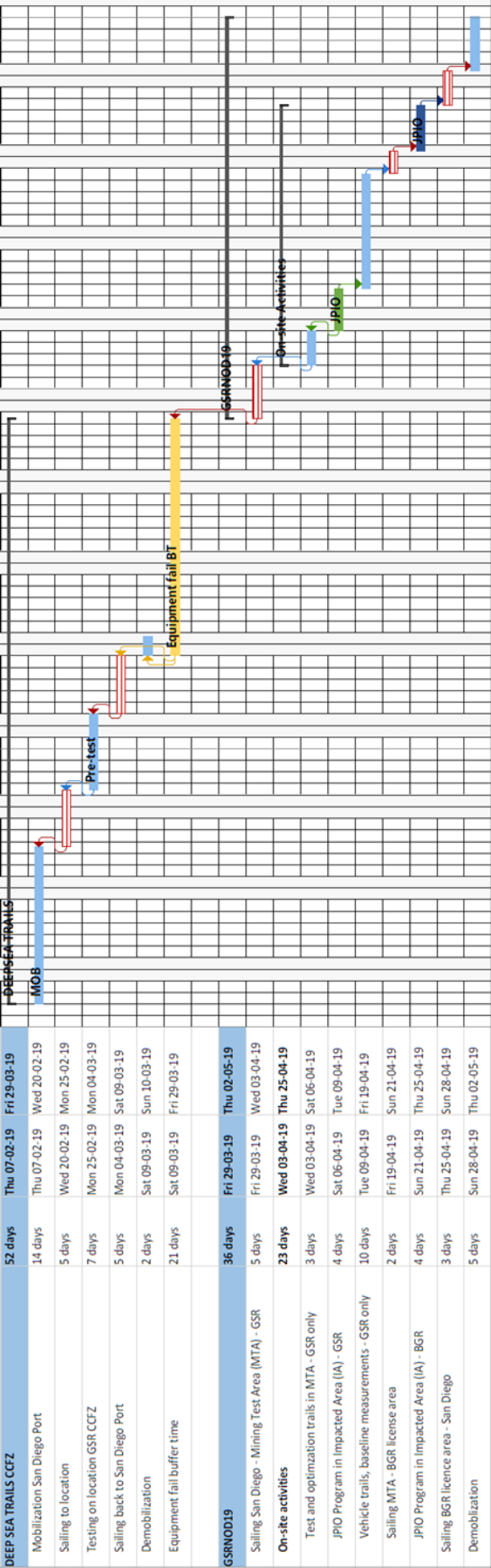
(1) *In situ* validation and optimisation of the nodule collection system as originally tested in the laboratory of the DEME-GSR technical department. The focus is on the optimisation of the collection process. For the validation of the collector principle *in situ* and for further optimisation it is not necessary to store any of the collected nodules. As such, operations can be performed while the dumping valve remains open and collected nodules are reintroduced to the seabed directly after pick up “on-the-go” (same principle as side-casted). The main research topic during this operational mode is operational efficiency of the nodule collector head. Findings of the test runs in the hydraulic laboratory need to be validated *in situ*. These mainly consist of (a) height of the collector head above the seabed and the impact on the collection process, and (b) speed variability and the impact on the collection process. Furthermore, the sediment/nodule concentration during the collection process is an important parameter to further design the operational steering system of the collector and the vertical transport system.

(2) Environmental impact assessment in the context of the JPI-O MiningImpact 2 programme. The objectives of the experiment and the monitoring approach and programme are described in detail in CHAPTER 1.1, CHAPTER 1.3 and CHAPTER 8.

### 3.4.3.3 Spatial scale and test design

For the disturbance experiment in the context of the JPI-O MiningImpact 2 programme, a largely coherent area needs to be cleared from nodules. As the Patania II will not be equipped with a riser system for the test, nodules need to be dumped outside the test area. Several possibilities for dumping have been investigated and a nodule container at the back of the vehicle is the preferred option. The container (cross section shown on FIGURE 3.11) has a dumping valve at the back. When closed, approx. 3 metric tons of submerged nodules can be stored inside the container. Depending on the nodule abundance on the seabed, the Patania II can drive and collect nodules from the seabed over a total distance of 50 m to 150 m before the container needs to be emptied. Consequently, piles of nodules will be deposited on the longitudinal sides of the test area. FIGURE 3.12 gives an example of a possible path of the Patania II on the seabed for an area with a very high nodule abundance.

Table. 3.3: High-level time plan for DEME-GSR’s cruise GSRNOD19.



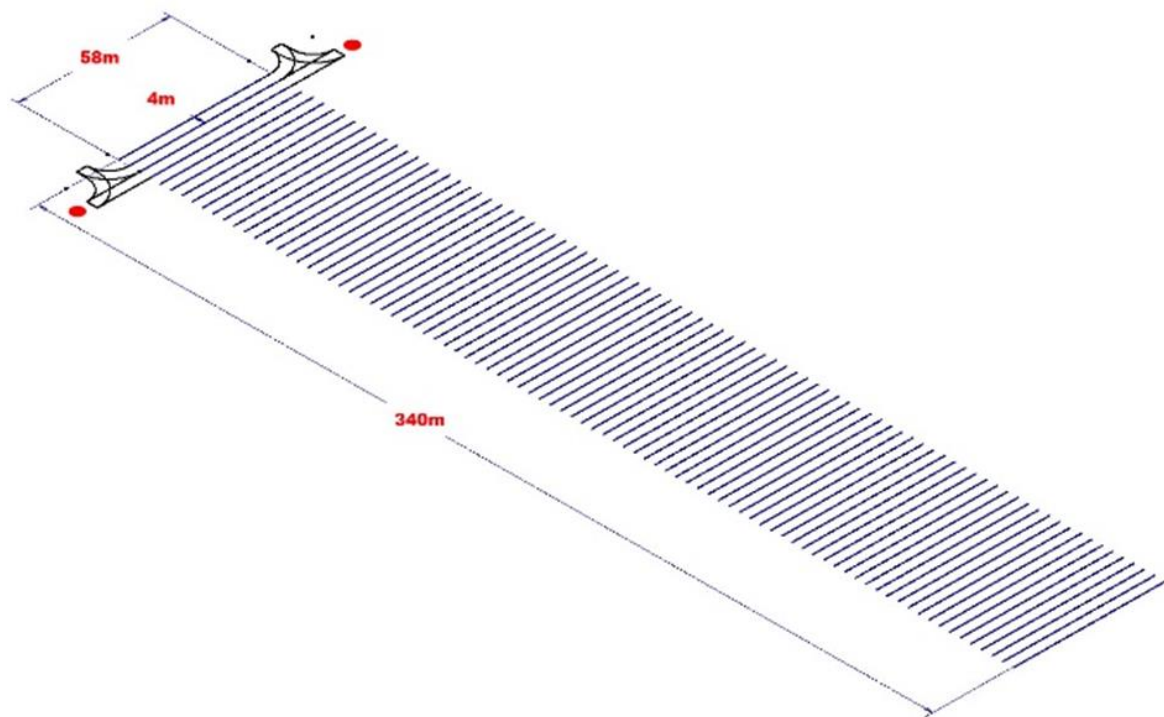


**Figure 3.12:** Example of the pattern of the JPI-O MiningImpact 2 collector vehicle test area for an area with a very high abundance of nodules on the seafloor (25–30 kg/m<sup>2</sup>). Red dots represent the piles of nodules collected.

In the example shown in FIGURE 3.12, the longitudinal distance is set to 340 m but can be changed depending on the progress of the test and the available time. The red dots at the respective ends of the transects indicate the dumping locations. The width of a single lane is equal to the total width of the Patania II, which is assumed to be 4 m. The longitudinal distance will therefore be a multiple of 4 m, depending on the amount of lanes. The example in FIGURE 3.12 shows 85 lanes resulting in a total longitudinal length of 340 m. In the German license area the test will most likely occur in an area with small nodules and an abundance of ca. 20 kg/m<sup>2</sup> (CHAPTER 3.2), yielding a total distance of ~85 m before turning. The longitudinal distance would then amount to maximally 1100 m.

At the end of each lane, a 180° turning procedure as shown in FIGURE 3.13 will be performed. Several phases can be distinguished:

The length of the lanes is determined by the specific nodule abundance that ranges between 15 and 30 kg/m<sup>2</sup> and the volume of nodules in the nodule container of the Patania II. At the end of each lane, the nodule container is fully loaded and the collection process is stopped. To prevent clogging of the system it is not possible to abruptly stop the flow of the water pumps. Water is required to flush the system. As such, at the end of every lane, the nodule collection heads are retracted and only water is pumped through the system.

Subsequently, a 90° turn to portside is executed and all pumps are stopped.

In order to finalise the 180° turn, the Patania II performs a 90° turn back to starboard side with a lateral offset equal to the width of the collector. As such, the front of the nodule collector is facing the target area again. In this position, the nodule container is unloaded by opening the hatch. By starting the water pumps, the nodule container can be flushed and cleaned from any remaining nodules or chunks of sediment. The nodule collector heads are subsequently lowered while the Patania II slowly picks up speed in forward direction. The collection process can then be re-started. **FEHLER! VERWEISQUELLE KONNTE NICHT GEFUNDEN WERDEN..**4 provides an indication of the expected times required for the turning process.

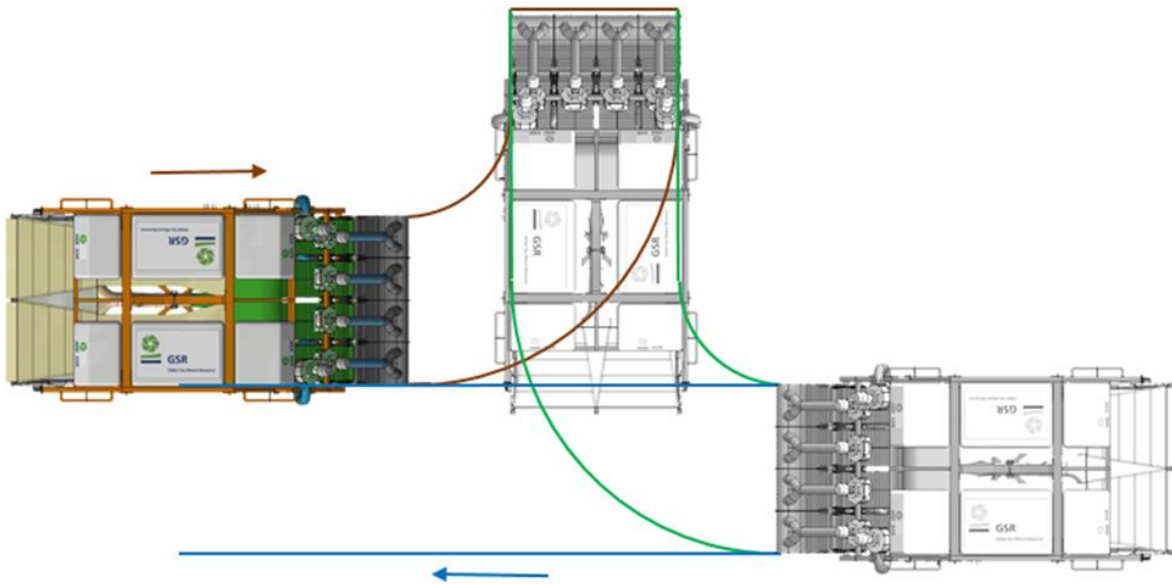


**Figure 3.13:** Turning procedure of Patania II.

**Table. 3.4:** Time required by Patania II to complete a turning process.

Action	Minimum [min]	Maximum [min]
Flushing after lane	2	5
Settling time and retraction of collector heads	0	3
90° turning to port	1	3
90° back turning to starboard side with offset	2	5
Dumping of nodules	1	2
Start-up pump system and flushing of nodule container	2	5
Total time required for turning	8	23
Average time required for turning	15 min	

In order to estimate the percentage operational collection time, several building blocks have been defined. They can be distinguished according to the following categories:

**(1) Start-up:** every time the Patania II is deployed on the seabed, several functional checks need to be performed. These mainly cover all hydraulic and electrical systems. Subsequently, the water pumps need to be started.

**(2) Mowing one lane:** This part gives an estimate of the time required for covering one lane. Again, this depends mainly on the nodule abundance and the net available volume inside the nodule container. **FEHLER! VERWEISQUELLE KONNTE NICHT GEFUNDEN WERDEN.** TABLE 3.5 summarises the breakdown of turning and all associated activities that are required at the end of every lane.

**(3) Technical downtime (assumed simple error):** Part 3 and Part 4 in TABLE 3.5 cover technical downtime. Part 3 assumes a technical issue that can be resolved, but for which the Patania II needs to be recovered. As an example in the overview below, a total of 3 hours is allowed on deck for fault finding and rectification.

**(4) Technical downtime:** Part 4 (TABLE 3.5) assumes a technical issue that can be resolved *in situ*. Full recovery of the Patania II is not required.

Combining the building blocks above and some other operational restrictions, several possible realistic scenarios can be predicted. As an example, two cases are presented in an overview (TABLE 3.5) which yield a total area of nodule removal of 22,000 m<sup>2</sup> and 100,000 m<sup>2</sup>.

**Table 3.5:** Planning breakdown for two different case scenarios.

JPIO Test Program - Detailed planning breakdown	Case 1	Case 2	
<b>Geometrical design assumptions</b>			
Nominal forward speed	0,30	0,50	[m/s]
Max. design forward speed	1,2	1,2	[m/s]
Envisaged collector width	4	4	[m]
<b>Physical properties</b>			
Seawater density	1.048	1.048	[kg/m <sup>3</sup> ]
Nominal nodule abundance	26	15	[kg/m <sup>2</sup> ]
Nodule wet density	2.000	2.000	[kg/m <sup>3</sup> ]
Nodule bulking factor	60%	60%	[%]
<b>Nodule basket - Nodule payload</b>			
Geometric volume of basket	3	3	[m <sup>3</sup> ]
Gross volume of nodules in basket	2,5	2,5	[m <sup>3</sup> ]
Mass of wet nodules in basket (incl. bulking factor)	3	3	[ton]
Mass of submerged nodules in basket	1,43	1,43	[ton]
Corresponding collecting distance	29	50	[m]
<b>JPIO Test Program - building blocks</b>			
Time required for turning	5	5	[min]
Time required for pile dumping (incl. manoeuvring and flushing of basket)	15	5	[min]
<b>Part 1: Start up</b>			
Vehicle system check after touch down	45	45	[min]
Start-up	10	10	[min]
<b>Total time - Part 1: Start-up</b>	<b>55</b>	<b>55</b>	<b>[min]</b>
<b>Part 2: Mowing one lane</b>			
Time required for one lane until nodule basket is full (nom. speed & nodule abundance)	1,60	1,67	[min]
Time required for pile dumping (incl. manoeuvring and flushing of basket)	15	5	[min]
Time required for turning	5	5	[min]
Start-up	5	5	[min]
<b>Total time - Part 2: Mowing one lane</b>	<b>26,60</b>	<b>16,67</b>	<b>[min]</b>
<b>Part 3: Technical downtime (assumed simple error)</b>			
Vehicle recovery	240	240	[min]
Vehicle - Fault finding	60	60	[min]
Vehicle - Fault technical solution (simple)	180	180	[min]
Vehicle re-deployment	240	240	[min]
<b>Total time - Part 3: Technical downtime (assumed simple error)</b>	<b>720</b>	<b>720</b>	<b>[min]</b>
<b>Part 4: In-situ technical downtime</b>			
Fault finding	30	30	[min]
Fault rectification	60	60	[min]
<b>Total time - Part 4: In-situ technical downtime</b>	<b>90</b>	<b>90</b>	<b>[min]</b>
<b>JPIO Test Program - Example</b>			
Part 1: Start up	3	1	[units]
Part 2: Mowing one lane	105	400	[units]
Part 3: Technical downtime (assumed simple error)	2	-	[units]
Part 4: In-situ technical downtime	15	5	[units]
Total time in hours	96	120	[hours]
Total time in days	4,0	5,0	[days]
<b>Distance traveled and area impacted</b>			
Part 2: Mowing one lane	105	400	[units]
Corresponding collecting distance	29	50	[m]
Total travel distance	3.029	20.000	[m]
Area covered per lane	115	200	[m <sup>2</sup> ]
Area covered for total Part 2 units	12.115	80.000	[m <sup>2</sup> ]
Patch x-distance (= Corresponding collecting distance)	29	50	[m]
Patch y- distance	420	1.600	[m]
<b>Synthesis</b>			
Total operational time	4,0	5,0	[days]
Patch x-distance (= Corresponding collecting distance)	29	50	[m]
Patch y- distance	420	1.600	[m]
Total area impacted	12.115	80.000	[m <sup>2</sup> ]

### **3.5 Events that could cause suspension or modification of the planned activities**

Due to the small spatial and temporal scale of the testing activity planned here, no serious harm will be caused to the marine environment at any depth within the water column (see CHAPTER 6 and CHAPTER 7). Thus, no suspension or modification of the planned activities is expected to occur due to serious environmental harm. The only aspects that could potentially cause suspension, delay or modification of the project are delays in technical development (DEME-GSR), problems with ship charter or availability (e.g. when the RV SONNE or the ship of opportunity planned to be used by DEME-GSR for collector vehicle deployment are unexpectedly no longer available ("force majeure")), or when weather conditions in the test area are so poor, e.g. due to the passage of hurricanes, that testing cannot occur, which is very unlikely in the time period planned for the project and would, at most, cause a delay of a few days only (see CHAPTER 6.7). Last but not least, although the JPI-O MiningImpact 2 project has been positively evaluated by the office in Brussels, national funding has not been completely approved for all partners and could lead to adaptations of the monitoring and research contents of the programme (e.g. German partners have handed in their proposals to BMBF but a final approval, especially of the financial capacity available, is still pending).

## **4. Description of the existing physico-chemical environment**

### **4.1 Regional overview**

The Clarion-Clipperton Zone (CCZ) – with a size of approximately  $4.5 \times 10^6 \text{ km}^2$  – is located in the northern part of the Central Pacific in between the Clarion Fracture Zone in the north, the Clipperton Fracture Zone in the south ( $\sim 5^\circ\text{N}$  -  $15^\circ\text{N}$ ), the Mathematician Ridge in the east and the Line Islands Ridge in the west ( $\sim 116^\circ\text{W}$  -  $155^\circ\text{W}$ , see FIGURE 1.1). The geomorphologic and tectonic structure of the CCZ is typical for mid-ocean ridges and adjacent depressions and directly related to seafloor spreading from the East Pacific Rise (Craig, 1979; ISA, 2010). Water depth varies between 3,800 and 4,200 m in the eastern region to 5,400 and 5,600 m in the western region. A system of ridges and valleys with crest-to-crest distances of 1-10 km and elevation extremes between tens to hundreds of metres is aligned approximately perpendicular to these fracture zones. Volcanic structures (single volcanoes and seamount chains) – primarily concentrated in the western and eastern sector – range in height from hundreds of metres to a few kilometres (ISA, 2010).

Lithologically, sediments of the CCZ contain two end members: carbonates (e.g. carbonate silts, clays, and oozes) and siliceous sediments (e.g. red clays, siliceous silts, clays and oozes). Carbonate sediments are predominantly found in the southeast, whereas siliceous red clay is predominantly found in the west-northwest. This trend is caused by two controlling factors: (1) an decreasing primary productivity to the west, and (2) a tectonically-controlled increase in water depth to the west. High sedimentation rates can overcome dissolution rates which favour higher concentrations of carbonates in the south-eastern area. Higher water depths favour the occurrence of siliceous sediments in the central and western part due to a higher solubility of carbonate minerals with increasing hydrostatic pressure (ISA, 2010). The gradients in water depth and productivity not only influence the sedimentation in the CCZ, but also have a major controlling function on abundance and diversity of species.

The eastern German license area with a size of  $61,700 \text{ km}^2$  is located at the easternmost limit of the CCZ (FIGURE 1.1) and is characterised by rough seafloor topography related to tectonic processes (FIGURE 4.1). Water depths range between 1,458 and 4,682 m. The seafloor consists of large deep-sea plains and NNE-SSW oriented horst and graben structures that are several kilometers wide, tens of kilometers long and approximately 100 to 300 meters high. Surface sediments are dominated by siliceous ooze containing small amounts of detrital and volcanic material. The uppermost sediment usually contains a semiliquid layer of 3 to 10 cm thickness. An important characteristic of these sediments is a high organic carbon content (0.4-0.6%) due to the relatively high surface water primary productivity in this easternmost part of the CCZ.

The Eastern German license area is influenced by the North Equatorial Current, flowing westward under the influence of the NE trade winds (FIGURE 4.2). The area lies within the westward extension of the eastern Pacific warm pool.



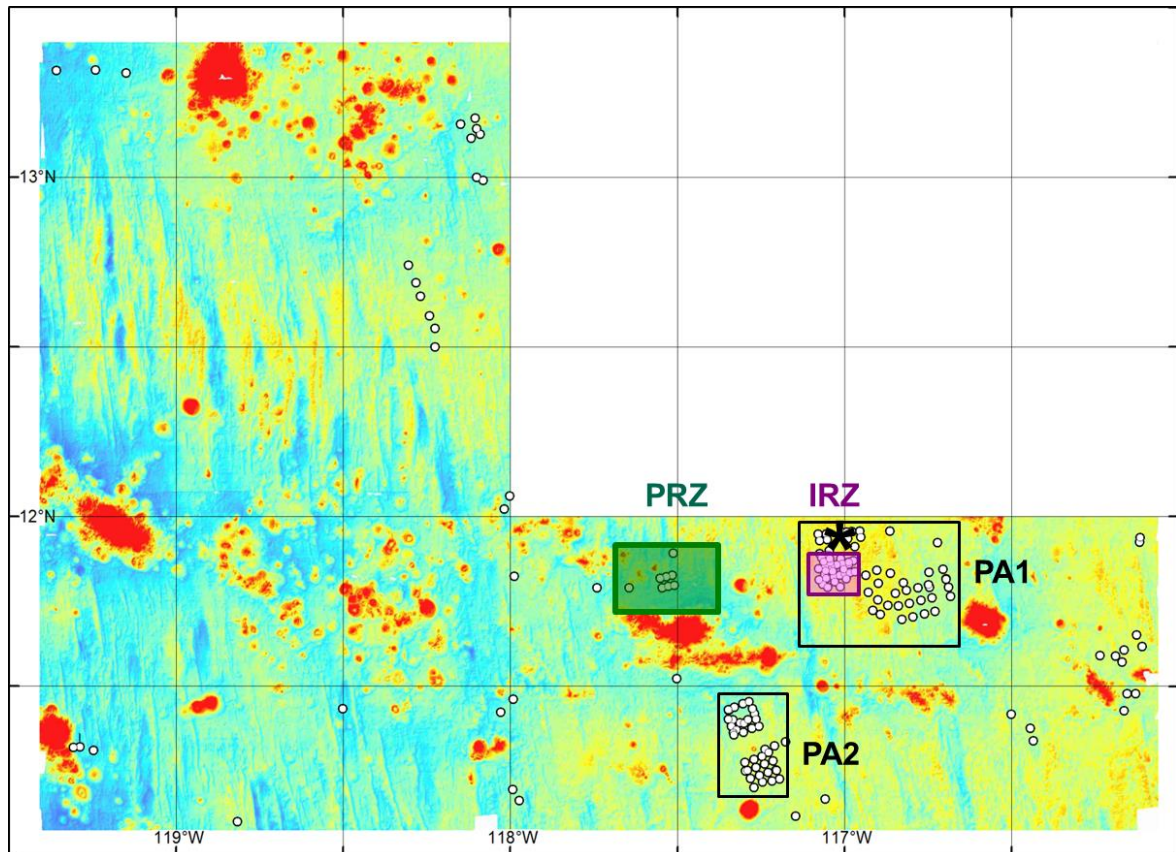


**Figure 4.1:** Topography of the Eastern German license area, showing the presence of numerous seamounts (in red) and NW-SE trending ridges especially in the western part of the area. Two prospective manganese nodule areas are indicated (PA1 and PA2). The locations of a Preservation Reference Zone (PRZ) and an Impact Reference Zone (IRZ) that were defined in 2013 and have been subject to annual biological investigations are indicated in green and purple, respectively. Dots indicate positions of box corer stations (status 2014). The area planned for the collector vehicle test lies in the north-western part of the well-investigated area PA1, as shown by the black star in the figure.

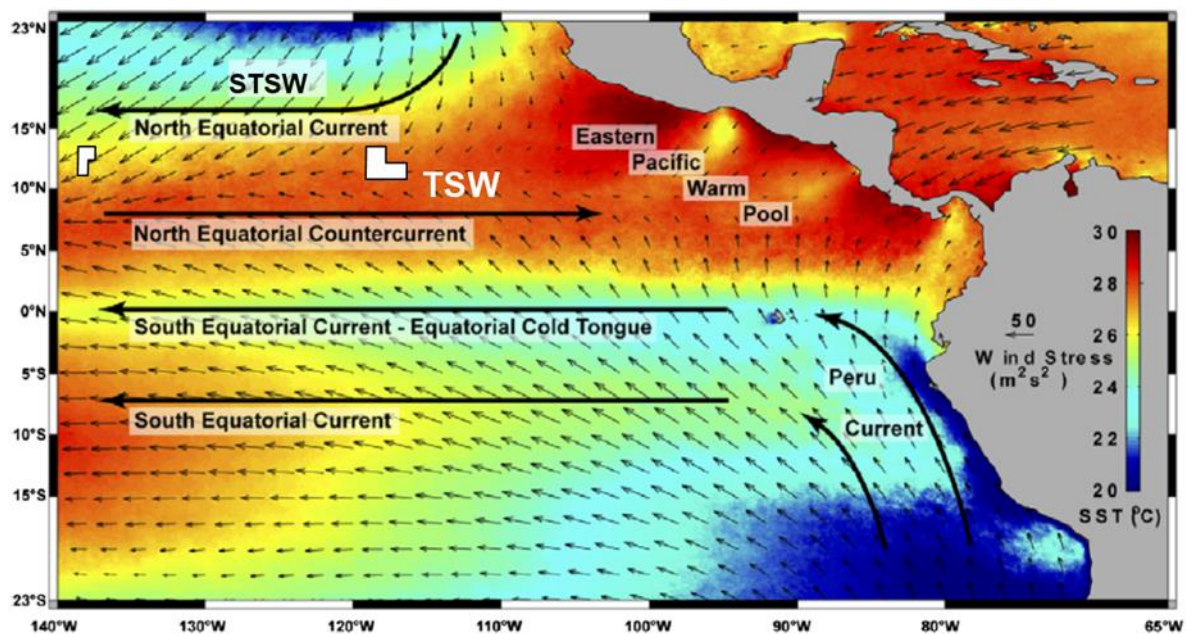


**Figure 4.2:** Average sea surface temperature, wind stress and overview of major surface currents in the eastern tropical Pacific (from Pennington et al., 2006). STSW: Subtropical Surface Water; TSW: Tropical Surface Water. Heavy black lines denote major currents, thin black lines represent FSU/COAPS wind stress climatology (1999-2003), and colours reflect six-year Aqua-MODIS sea surface temperature climatology (1997-2003). The white rectangles denote the positions of the western and eastern parts of the German license area.

In such a large exploration area and with such great water depths, requiring at least 3 h to obtain just one seafloor sample, it is inherent that sample numbers and sizes will remain too small to obtain statistically significant spatial and temporal environmental information throughout large parts of the area. BGR's exploration strategy has thus been to focus strongly on the analysis of two prospective nodule areas PA1 and PA2 in the south-eastern part of the license area, together with a size of ~1500 km<sup>2</sup>, in order to obtain statistically robust data for those areas (FIGURE 4.1). A Preservation Reference Zone (PRZ) and an Impact Reference Zone (IRZ) were defined in this region in 2013 and have been subject to annual biological investigations since then (indicated in green and purple, respectively, in FIGURE 4.1). The area selected for the DEME-GSR collector vehicle test is indicated by the star in FIGURE 4.1.

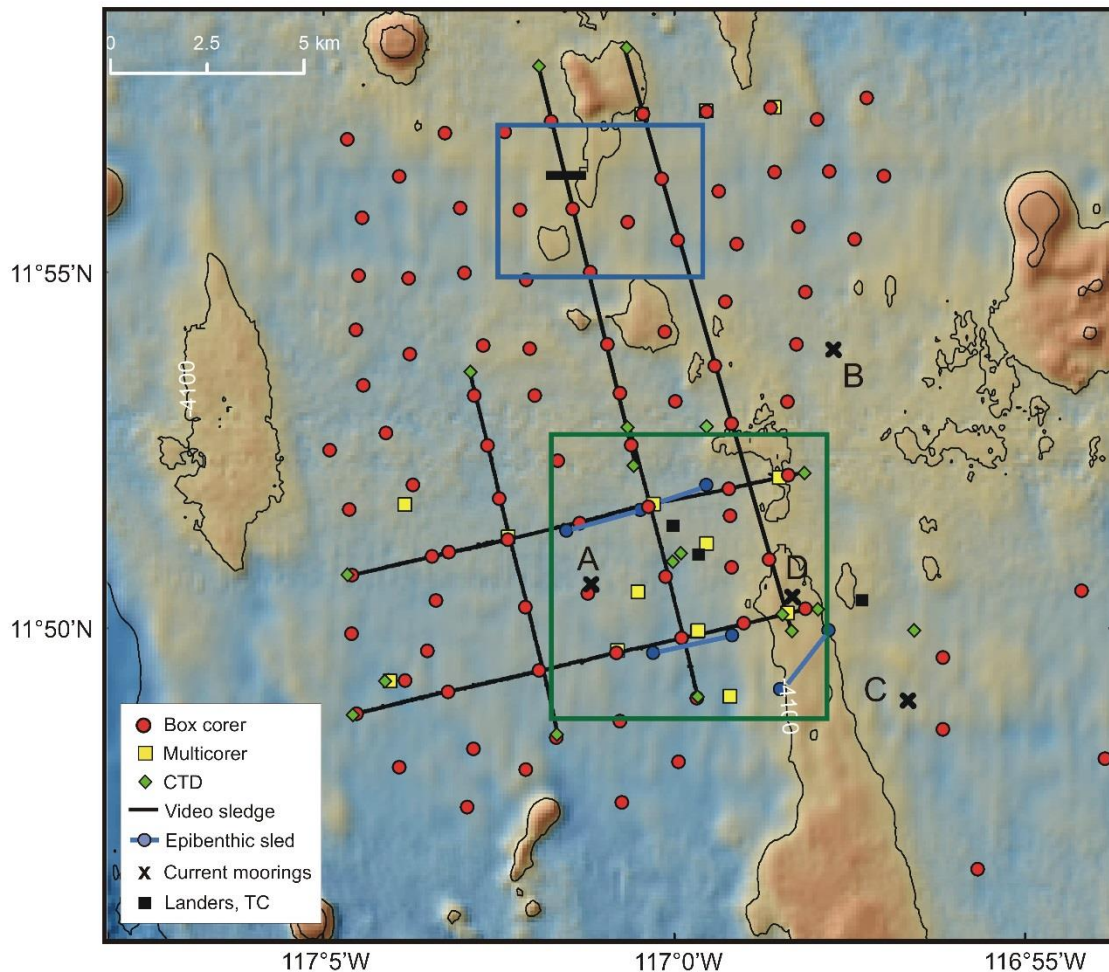


**Figure 4.3:** Locations of deployments of sampling and observation devices in the prospective field PA1-West in relation to bathymetry. The two parallel blue lines represent epibenthic sled tracks that have been sampled in 4 consecutive years for time series analyses, shown here within a green rectangular area that will be used as a control reference site for the collector test. A, B, C, D refer to the positions of 4 long-term ocean bottom current moorings. The test will take place within the blue rectangular area in the northern part of PA1-West, shown here exemplarily by the black rectangle.

The western part of PA1, called PA1-West, is an area with a relatively flat seafloor, a depth of around 4100 m and a size of ca. 250 km<sup>2</sup> (see FIGURE 3.1 and FIGURE 3.2). It is mostly covered with large nodules (> 4 cm diameter), and represents the best-studied area within the German license area and perhaps even within the whole CCZ. The sampling effort in this area is described in CHAPTER 3.2 and summarised in FIGURE 4.3. For the sake of the spatially small-scale collector test planned in the framework of this EIA, we strongly focus our efforts on describing the existing physico-chemical environment on the environmental conditions in the Eastern German license area and, more specifically, in area PA1-West.



## 4.2 Physico-chemical environment in and around the Eastern German license area

### 4.2.1 GEOLOGICAL SETTING

The Eastern German license area is located in the equatorial northeast Pacific Ocean ~900 nautical miles (1700 km) southwest of Manzanillo, Mexico. Magnetic data indicate a crustal age of 18–22 Ma (Barckhausen et al., 2013). Water depths vary between 1458 and 4682 m, with an average of 4240 m (Rühlemann et al., 2011). The entire area has been mapped with 120 m grid size using the Kongsberg 12 kHz multibeam echosounding systems EM 120 and EM 122. The seafloor is characterised by deep-sea plains interspersed with NNW-SSE oriented horst and graben structures that are several kilometers wide, tens of kilometres long and 100 to 300 m high (Rühlemann et al., 2011; FIGURE 4.4). An analysis of the topography shows that for ~80% of the license area the slope of the seafloor does not exceed 3°. Many extinct volcanoes (seamounts) rise a few hundred to almost 3000 m over the surrounding abyssal plains. They are 3–30 km in diameter and seem to appear in clusters with an east-west trending orientation (Rühlemann et al., 2011; FIGURE 4.4). The abyssal plains are punctuated by roughly 300 seamounts with diameters ranging between 3 and 30 km.

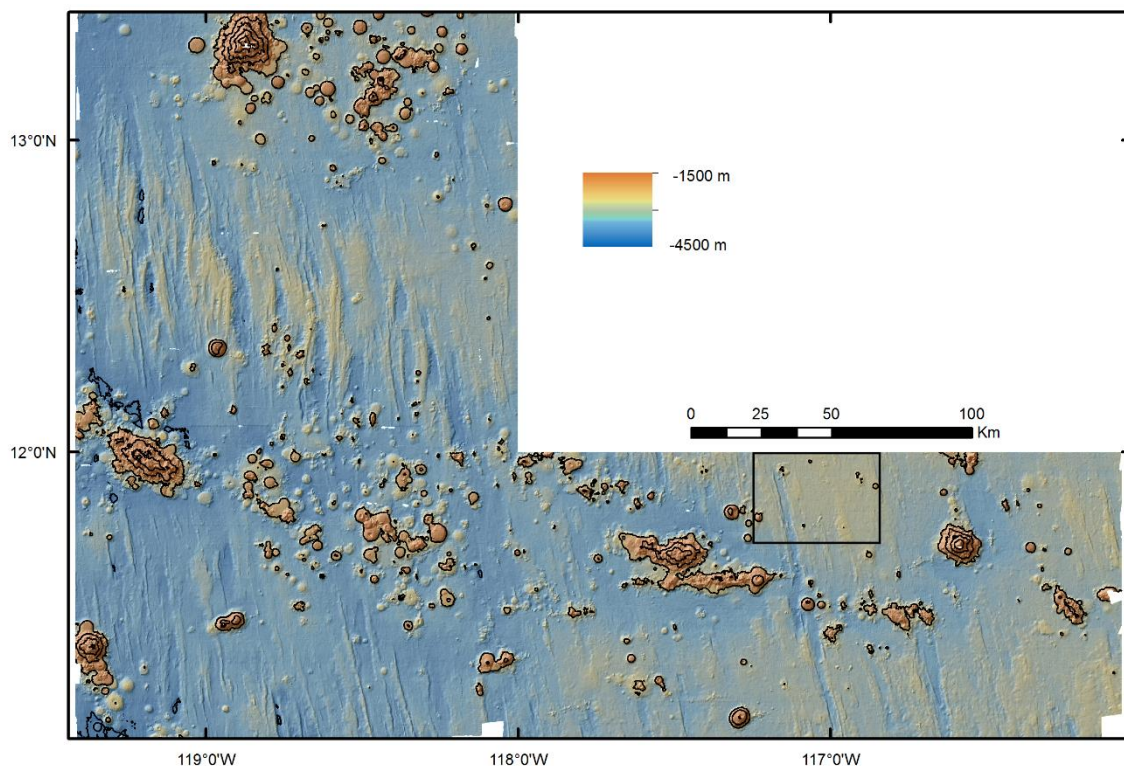


**Figure 4.4:** Bathymetry of the eastern German license area. The inset provides the outline for the maps in FIGURE 4.6.

Manganese nodules cover large areas of the abyssal plains in the license area. Two different types of nodule fields can generally be differentiated: (i) areas dominated by small-sized nodules with a maximum diameter of 4 cm, smooth surfaces, and high numbers of nodules per unit area, and (ii) areas dominated by medium to large-sized nodules with variable diameters above 4 cm (mainly in the range of 5–8 cm), botryoidal surfaces and small numbers of nodules per unit area (FIGURE 4.5). Based on acoustic backscatter data, in combination with the use of seafloor nodule samples and photo analyses for ground-

truthing, the BGR developed an area-wide method to distinguish between areas that are predominantly covered by large or small nodules. According to those analyses, areas dominated by small-sized nodules cover about 64% of the seafloor of the eastern license area, whereas areas with medium to large-sized nodules make up only about 9% of the seafloor. Seamounts and north-south oriented ridges cover about 25% of the license area and flat, sediment-covered areas without nodules comprise only 2% of the entire area.



**Figure 4.5:** Box corer samples from an area dominated by small-sized nodules (left panel) and from an area dominated by large-sized nodules (right panel). These samples derive from a seafloor area covering 50x50 cm each. The differences in size, texture and number are clearly visible.

The area selected for the collector vehicle test is located in the southeast of the Eastern German license area (see CHAPTER 3.2 and FIGURE 4.6). This area is bordered to the east and west by NNW-SSE striking graben structures, to the south by an E-W oriented seamount chain and to the north by the license border. It forms an elevated plateau with an average water depth of 4100 m and a few small seamounts rising about 200 m above it (FIGURE 4.6). The seafloor slope of the plateau based on bathymetry with about 120 m resolution is generally below 3°. Seamounts and graben structures form much steeper morphological features with slopes up to about 50°.

In contrast to the major part of the eastern German license area, the seafloor of the selected region is dominated by medium to large-sized nodules, which is especially true for most parts of the plateau (FIGURE 4.6). Nodule abundances varying between 24 and 33 kg/m<sup>2</sup> are highest in this area, indicating that a few large nodules per unit area cause more nodule mass than a large number of small ones. The reason for this significant distribution of large nodules is unclear. It is speculated that the slightly elevated plateau provides conditions for slightly increased but stable sedimentation rates, which might have caused the formation of larger nodules. In terms of geochemistry, medium to large-sized nodules have slightly higher Mn/Fe ratios (4.3 to 3.4) and also slightly increased Cu+Ni contents (2.6% vs. 2.4%) compared to small-sized nodules (Rühlemann et al., 2011). In contrast, small-sized nodules have slightly increased Co (0.18% vs. 0.16%) and REE contents (750 ppm vs. 650 ppm), indicating a higher hydrogenetic fraction in these nodules.



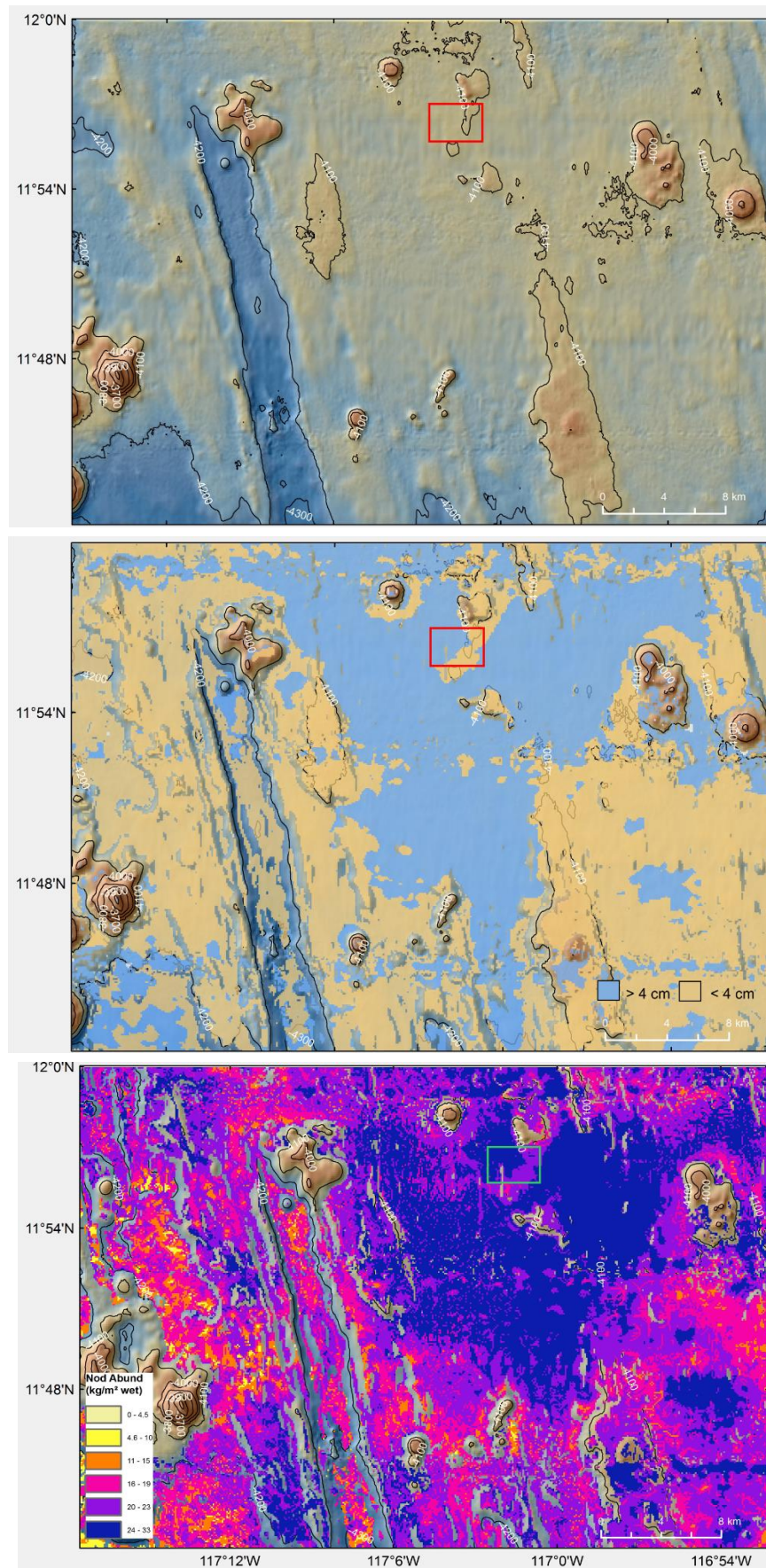


**Figure 4.6:** Bathymetry (upper panel), nodule size distribution (middle panel), and nodule abundance (lower panel) of a selected region from the south-eastern German license area (for location see FIGURE 4.4). The nodule size and abundance maps are clipped with the seafloor slope. Slopes below 3° have been excluded. The rectangle marks the area in which the collector test will take place.

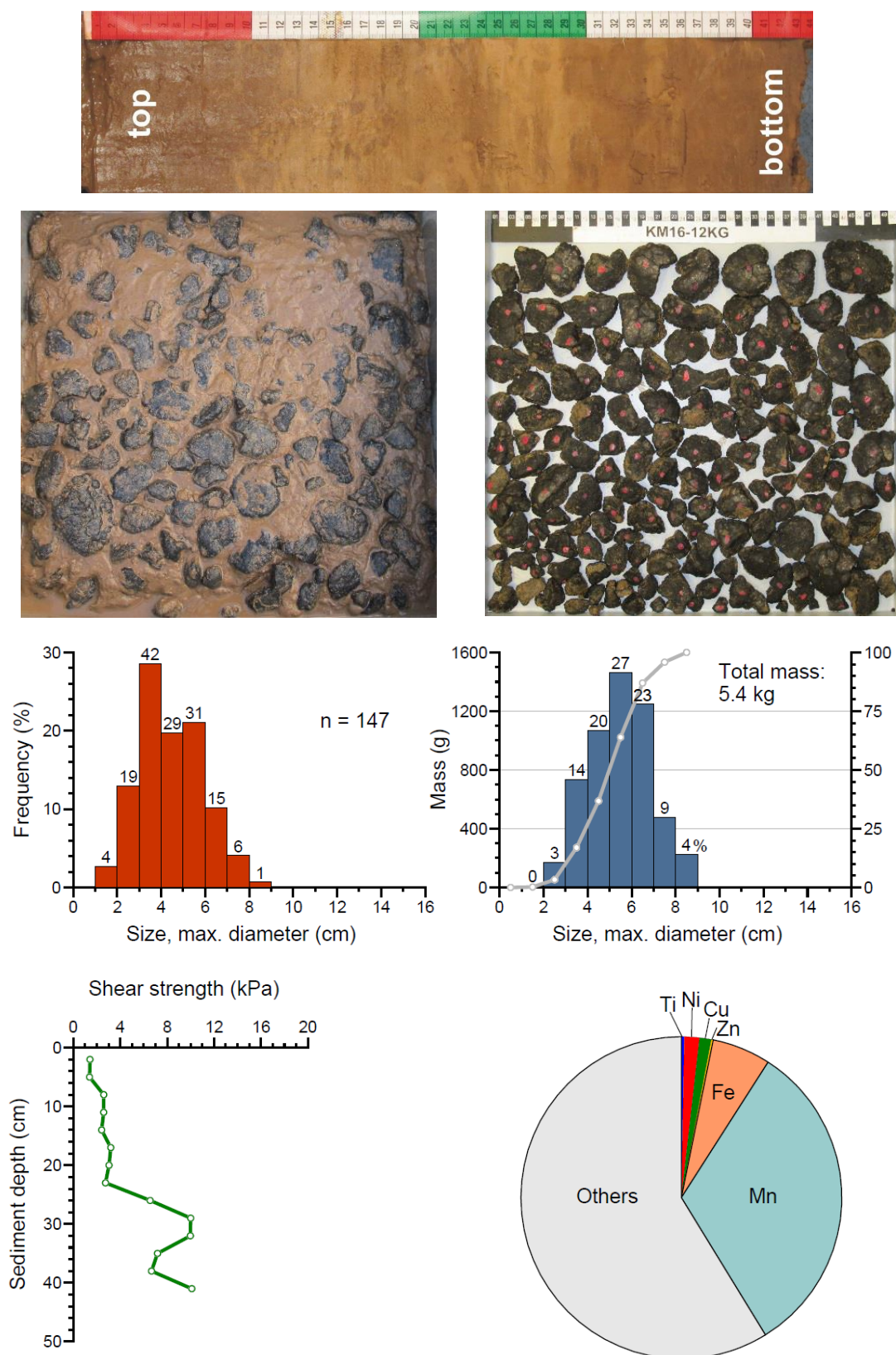


**Figure 4.7:** Compilation of images and data from box core station KM16-12KG taken from the collector vehicle test area. Top image: sediment core of box core station KM16-12KG. Lower images: Photographs of the sediment surface (0.25 m<sup>2</sup>) with nodules (left) and after collecting all surface Mn nodules and displaying them in a white box (right). The lower four diagrams display different statistics: nodule size and mass distributions, shear strength depth profile measured along the sediment core, and average chemical composition of selected nodules (XRF data).

The surface sediments in the area shown in FIGURE 4.6 consist of a mixture of siliceous ooze (radiolarian and diatom tests) and clay minerals with a porosity of about 80%, a water content of about 70% and a wet bulk density of about 1.2 g/cm<sup>3</sup>. The grain size is dominated by the fractions < 2 µm (35% on average) and 2–6.3 µm (30% on average). The grain size fractions between 112 and 355 µm contribute about 20% to the total sediment, which may partly be caused by the presence of Manganese micro-nodules in these size fractions. A typical example of a box core station deriving from the planned collector vehicle test area at a water depth of 4087 m is given in FIGURE 4.7.

#### 4.2.2 METEOROLOGY

This description of atmospheric conditions in the region of the Eastern German license area is based on atmospheric re-analyses, satellite observations and hurricane post-storm analyses. The analyses have been carried out on behalf of the BGR by Maunalani Consulting LLC (Honolulu). The European Interim Reanalysis 'ERA-Interim' (Dee et al., 2011) was used for sea surface temperature, sea level pressure, winds and waves. Daily values of rates of precipitation were obtained from the Advanced Microwave Scanning Radiometer (AMSR-E and AMSR-2) flown on NASA's Aqua spacecraft via the internet site <http://www.remss.com/missions/amsl/>. For hurricane tracks and intensity, the best track data HURDAT2 of the National Hurricane Center of NOAA were downloaded from <http://www.nhc.noaa.gov/>.

The Eastern German license area is located south of the subtropical sea level pressure ridge of the North Pacific High and just north of the sea level pressure trough associated with the Intertropical Convergence Zone (ITCZ). Seasonal variations of sea level pressure, surface winds, cloudiness and precipitation reflect the seasonal march of the ITCZ and changes of the Subtropical High. When the ITCZ is weakest and closest to the equator in March, the eastern part of the German license area is dominated by high sea level pressure, low precipitation (FIGURE 4.8) and cloud liquid water, a measure for clouds, and NE trades (FIGURE 4.9). In August and September, the ITCZ is at 10°N furthest north so that in the license area, sea level pressure is low, precipitation and cloud cover high (FIGURE 4.8), albeit highly intermittent, and winds are highly variable and bimodal between NE trades and south westerlies. Intra-seasonal variability of sea level pressure and winds is elevated, and in part associated with Madden-Julian Oscillation. Sea surface temperatures are lowest in February and highest in August, and are dominated by seasonal and interannual changes.

Of the interannual and decadal climate modes, the El Niño/Southern Oscillation (ENSO) dominates interannual variability, leading to an equatorward shift of the ITCZ and warming in the El Niño phase, with commensurate changes of sea level pressure, precipitation and winds. Anomalies associated with the Interdecadal Pacific Oscillation and the Pacific Decadal Oscillation reflect their shared variance with ENSO. The North Pacific Gyre Oscillation is primary linked with the central equatorial Pacific expression of El Niño variability.

Surface waves in the eastern license area reflect local trades and swells from mid-latitude winter storms. The area is dominated by northerly swells from November to March with largest amplitudes in February, and a preponderance of southerly swells from May to September (FIGURE 4.9). Starting in May and June, smaller easterly and south-easterly swells occur, and peak in September when swells cover a broad fan of easterly directions.



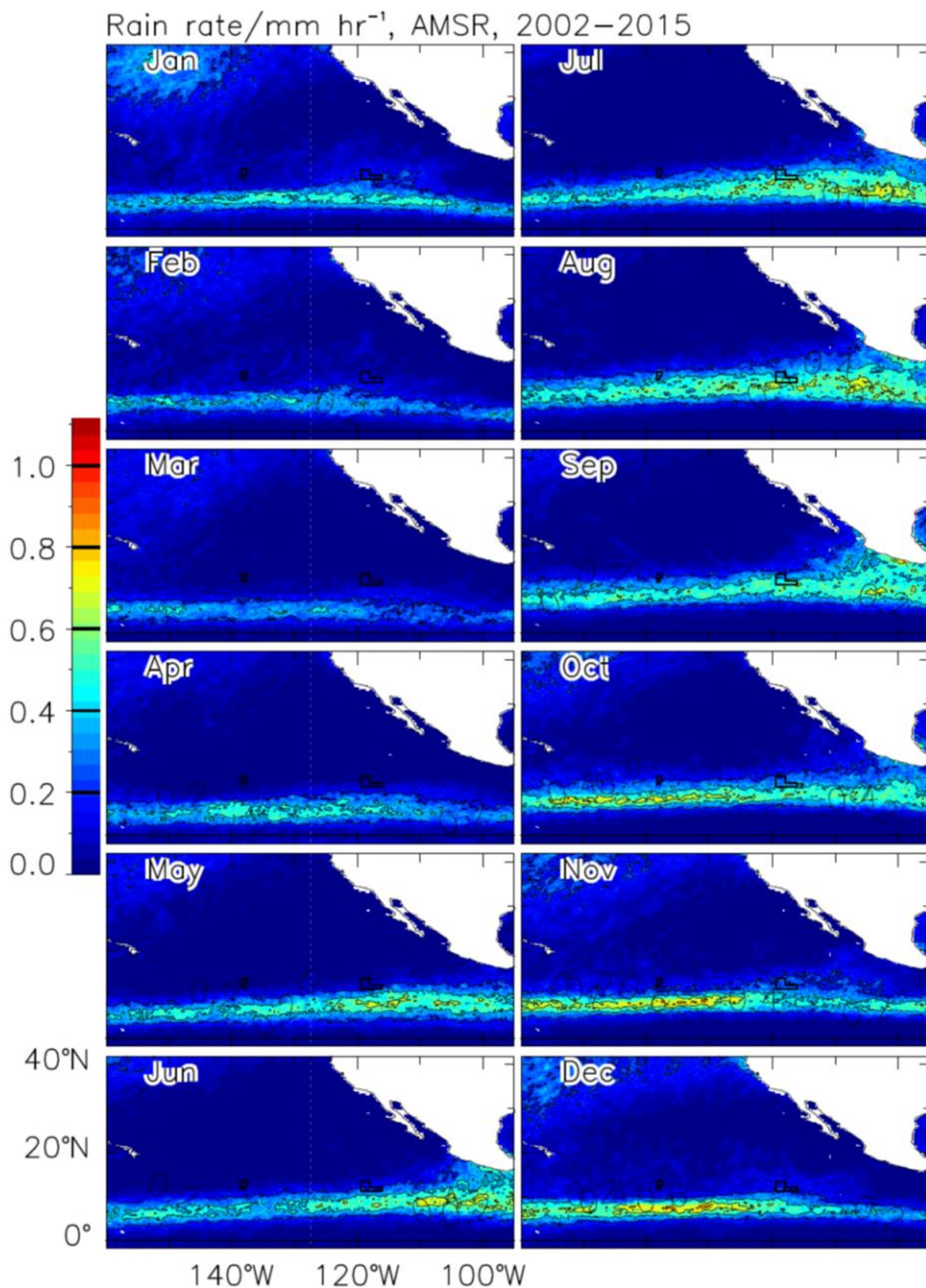


**Figure 4.8:** Mean monthly climatology of precipitation in mm hr<sup>-1</sup> observed with the AMSRE and AMSR2 satellites. Months are indicated in top left of each panel. The colour scale on left applies to all panels. The Eastern German license area is indicated by the small polygon centred on 118°W and 12°N.

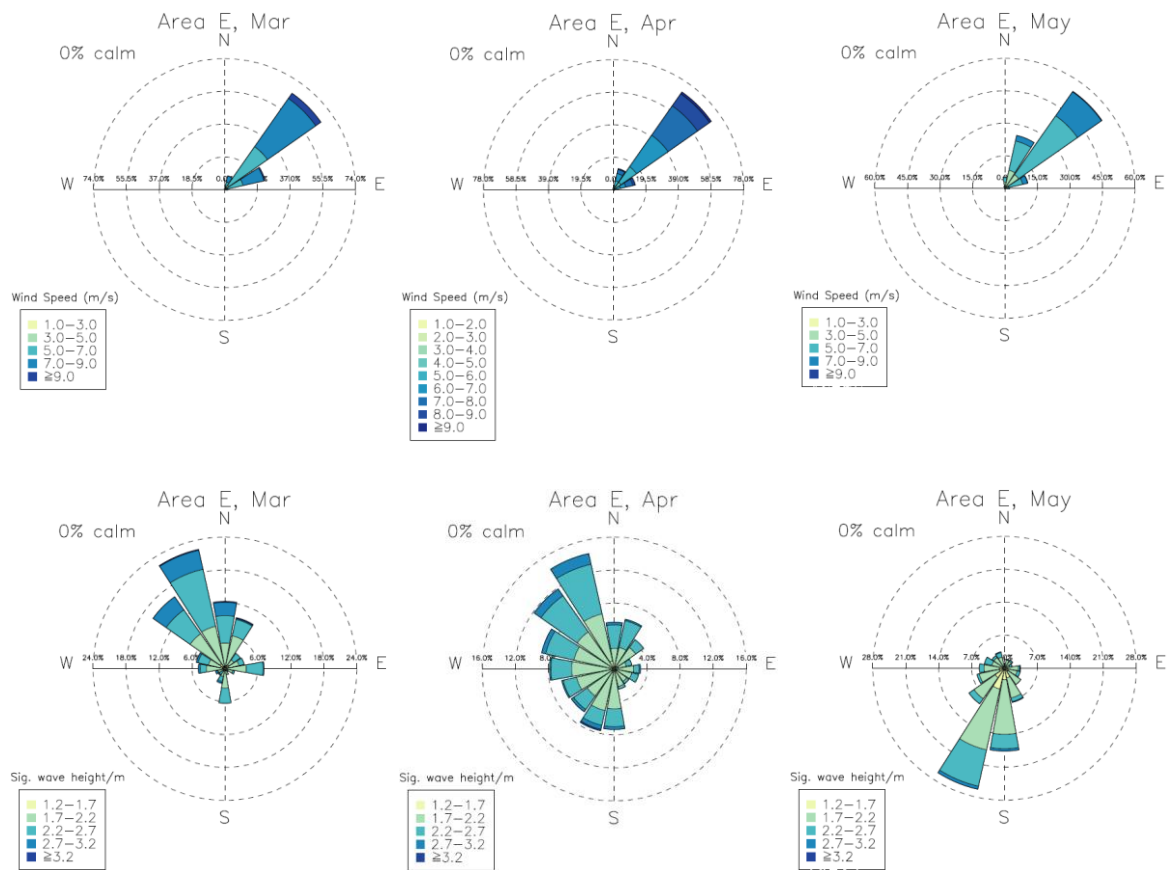


**Figure 4.9:** Wind and wave heights. Upper panels: wind roses for daily averaged surface winds in the Eastern license area for March, April and May, the months for which the collector vehicle test is scheduled in 2019. Lower panels: distribution of daily averaged significant wave height in meters for the same months. Wind direction is defined according to meteorological convention: Easterly winds occupy the bin toward the E, northerlies the directional bin towards north (N) and similarly for westerlies (W) and southerlies (S). Wave direction indicates the direction of wave propagation, towards north (N), west (W), south (S), and east (E). Wave heights or winds with speed less the lowest bin are marked as calm, with frequency of occurrence given in upper left. Shown are the frequency distributions in 15° directional bins, with percentage of occurrence in the radial direction, and values as indicated by the colour key in the lower left of each panel.

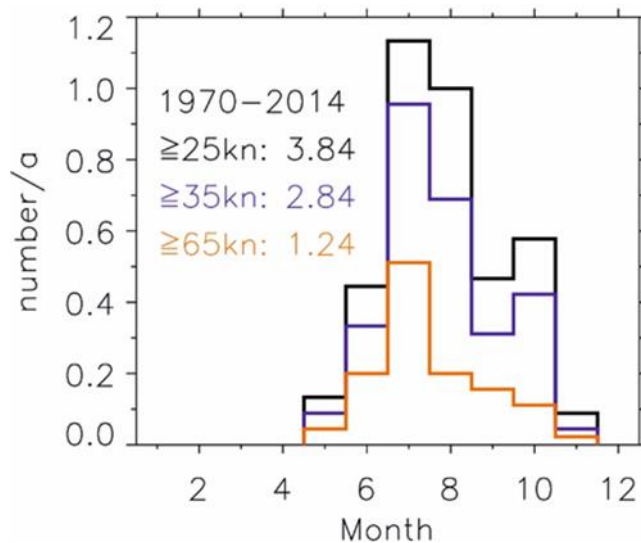


**Figure 4.10:** Average number of tropical depressions, tropical storms and hurricanes per year as a function of month for the Eastern German license area. A storm is counted when its position lies within 10°N to 15°N and between 120°W and 115°W. The averaging period is 1970–2014.

The hurricane seasons starts in May, quickly ramps up to reach maximum intensity in June with over 1.1 wind events per month of tropical depression strength or stronger, of which 1.0 are at or exceed tropical storm magnitude, and, on average hurricane strength is achieved every other year (FIGURE 4.10). Storm counts slowly abate in September and October, but events have occurred as late as November.

On average, the number of cyclonic eddies amounts to 0.5 per month, or 6 cyclones per year. On average, eddy radii are 100 to 200 km, with the largest eddies reaching 300 km, and radial speeds are typically 15-20 cm/s. Eddy lifetime is, on average, 100 days, and propagation is westward with speeds of 10-20 cm/s (see also CHAPTER 4.2.3.5).

## 4.2.3 PHYSICO-CHEMICAL OCEANOGRAPHIC SETTING

### 4.2.3.1 Water column characteristics

This chapter summarises the oceanographic conditions in the Eastern German license area using ocean re-analyses of historical data as compiled in the World Ocean Atlas 2013. The Maunalani Consulting LLC (Honolulu) carried out this synopsis on behalf of the BGR. Furthermore, BGR's own measurements on temperature, salinity, oxygen concentration, chlorophyll  $\alpha$ , turbidity and upper ocean current data from ship-borne ADCPs are presented, which were mainly collected in the months of April and May between 2010 and 2016.

The license area is located at the equatorward edge of the westward flowing, shallow, surface-trapped North Equatorial Current (FIGURE 4.2). The profiles of temperature, salinity and oxygen reflect the vertical distribution of water masses. FIGURE 4.11 provides an example for the variation of water mass characteristics from the sea surface down to 4200 m at the seafloor. Water temperature reaches values as high as 28.8°C and salinity as low as 32.4 psu in the mixed layer. The seasonal cycle results from changes of winds and air-sea fluxes associated with the meridional migration of the ITCZ. Seasonal signals are pronounced in the surface mixed layer (FIGURE 4.12).

Most of the density stratification is due to a vertical temperature gradient, but is reinforced by a halocline. Beneath the warm, low-salinity Tropical Surface Water (TSW;  $T > 25^{\circ}\text{C}$ ,  $S < 34$  psu) a pronounced thermocline /halocline separates surface and sub-pycnocline waters, but does not contain a distinct water mass of any substantial volume (Fiedler and Talley, 2006). This cooler, more saline thermocline water is upwelled at the equator and contributes to the formation of Equatorial Surface Water. The eastern tropical Pacific sub-pycnocline waters are very low in oxygen. This extreme oxygen deficiency is mainly attributable to three factors: (1) high phytoplankton production at the surface; (2) a sharp permanent pycnocline that prevents local ventilation of subsurface waters; and (3) a sluggish and convoluted deep circulation and therefore old age of sub-pycnocline waters (Fiedler and Talley, 2006). The strong increase in chlorophyll  $\alpha$  concentrations to a maximum around 75 m coincides with the depth where oxygen concentrations sharply drop to values of 0.1-0.2 ml/l, indicating that primary production and subsequent remineralization of particulate organic matter under oxygen consumption is an important factor for the formation of the  $\text{O}_2$  minimum zone.

Northern and southern source low-salinity intermediate (sub-pycnocline) water masses (between 500 and 1000 m) meet approximately at the latitude of the license area. Antarctic Intermediate Water (AAIW) forms from the deep, winter mixed layer north of the Subantarctic Front in the southeast Pacific (Hanawa and Talley, 2001) and spreads equatorward and westward in the Pacific. North Pacific Intermediate Water (NPIW) originates from subsidence in the Sea of Okhotsk and at the Oyashio Front in the western North Pacific, with some contribution from the Gulf of Alaska (You, 2003).

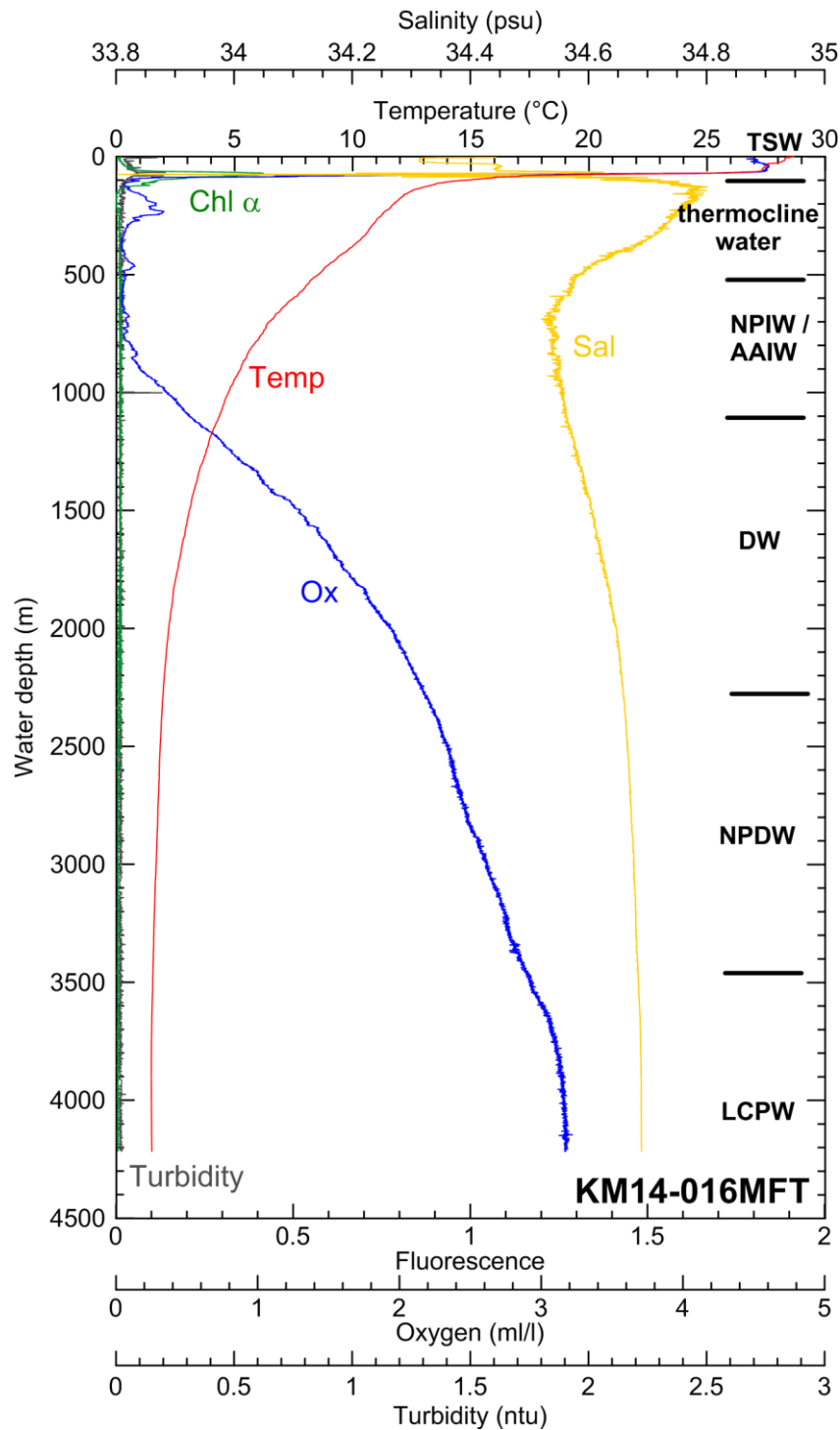


**Figure 4.11:** Water mass characteristics of the Eastern German license area exemplified by the downcast profile of video sledge deployment KM14-016MFT in May 2014. The vertical distribution of water masses is indicated on the right: Tropical Surface Water (TSW), Subtropical Surface Water (STSW), North Pacific Intermediate Water (NPIW), Antarctic Intermediate Water (AAIW), Pacific deep water (DW), North Pacific Deep Water (NPDW), Lower Circumpolar Water (LCPW).

The properties of deep and bottom waters in the Pacific are set by their distant sources in the Antarctic and North Atlantic. The deep water (DW) between 1000 and 2500 m is relatively featureless, with a steady decrease in temperature and increase in salinity. North Pacific Deep Water (NPDW) is the 1.2-2°C cold water mass occurring at a depth > 2500 m. The bottom water (> 4000 m) in the Pacific is Lower Circumpolar Water (LCPW), a mixture of Antarctic Bottom Water formed in the Weddell Sea and North Atlantic Deep Water formed in the northern North Atlantic. LCPW in the eastern tropical Pacific north of

the equator is characterised by relatively high oxygen concentrations. This water mass flows from the Northeast Pacific Basin along the western flank of the East Pacific Rise into the eastern tropical Pacific.

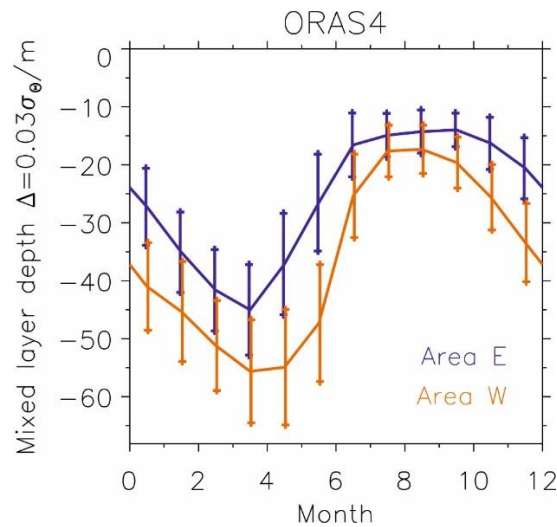


**Figure 4.12:** Seasonal cycle of mixed layer depth in m, with vertical bars denoting the standard deviation, for the western part (W, red) and eastern part (E, blue) of the German license areas. Data are based on monthly estimates, and have been obtained from the ECMWF ocean reanalysis system ORAS4. Mixed layer depths are based on a potential density  $\sigma_\theta$  difference to the surface of  $0.03 \text{ kg/m}^3$ .

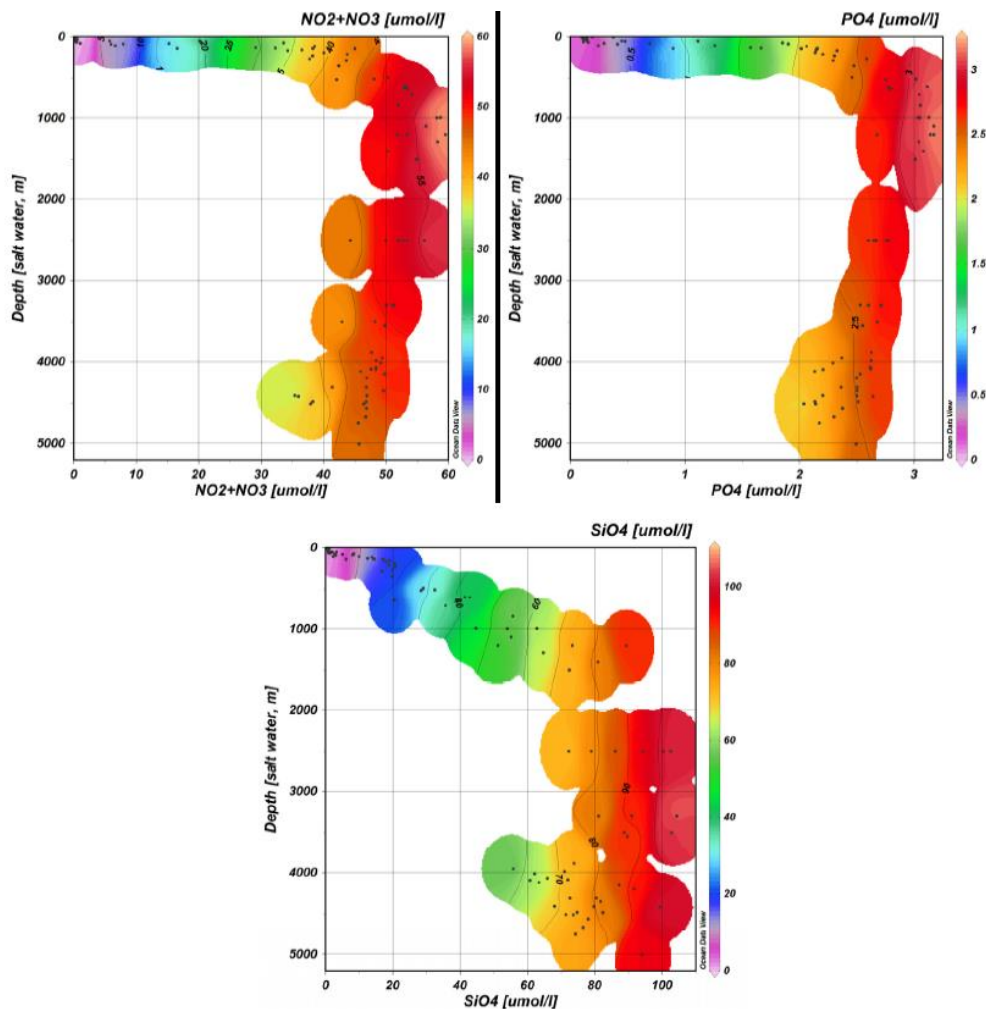


**Figure 4.13:** Nutrient distribution throughout the water column in area PA1-West (from SO-239 cruise report, Martínez-Arbizu and Haeckel, 2015).



Concentrations of the nutrients phosphate, nitrate and silicate were measured in the water column of area PA1-West during cruise SO-239 (2015) (FIGURE 4.13). Further information is available from the data compiled in the World Ocean Atlas 2013, which is based on the World Ocean database (Garcia et al., 2013). These data are very similar to those reported from cruise SO-239. Nutrients showed relatively low concentrations in the upper mixed layer, ranging within 0.1–0.37  $\mu\text{M}$  for  $\text{PO}_4$ , 0.23–1.38  $\mu\text{M}$  for  $\text{SiO}_4$ , and 0.09–0.60  $\mu\text{M}$  for  $\text{NO}_x$  ( $\text{NO}_3 + \text{NO}_2$ ). Concentrations increase with depth towards the upper limit of the thermocline (which coincides with the deep chlorophyll maximum) due to the remineralization of sinking organic matter, followed by a sharper nutricline in the Oxygen Minimum Zone (OMZ). Phosphate and nitrate reached maxima (2.78–3.17  $\mu\text{M}$  and 53.3–59.49  $\mu\text{M}$ , respectively) generally at the lower limit of the OMZ (~1000–1200 m); while silicate showed a maximum (81.07–104.25  $\mu\text{M}$ ) deeper than the OMZ, between 2500 and 3300 m. This is consistent with differences of remineralization processes governing silicate on the one hand and nitrate or phosphate on the other. Beneath the nutricline, the nutrient concentrations show a slight decrease down to near-bottom waters, where they reach values between 2.04 and 2.64  $\mu\text{M}$  for  $\text{PO}_4$ , 35.37 and 49.72  $\mu\text{M}$  for  $\text{NO}_x$ , and 60.66 and 99.29  $\mu\text{M}$  for  $\text{SiO}_4$ .

#### 4.2.3.2 Chemical composition of bottom water

There is only limited information available for the chemical composition of bottom water in the German license area. Few data were obtained from water samples collected from the overlying water in MUC cores (10 cm). The nutrient and dissolved oxygen concentrations determined in cruise SO-205 samples are 35–37  $\mu\text{M}$  nitrate, ~2  $\mu\text{M}$  phosphate and 148–164  $\mu\text{M}$  oxygen, which is in good agreement with CTD near bottom values (TABLE 4.1).

Due to the very low concentrations and high contamination risks during sampling and analyses, trace metal concentrations in open ocean waters are difficult to obtain and rarely available. In the Eastern license area the deepest water mass is the lower circumpolar water (LCPW). Dissolved (< 0.2  $\mu\text{m}$ ) trace element concentrations (filtered through a 0.2  $\mu\text{m}$  filter) in deep water masses in the Pacific determined during GEOTRACES transects GP16 and GP13 are provided from the Geotraces Intermediate Data Product 2017. The concentrations in Pacific Deep Water (PDW) and in Lower Circumpolar Water (LCPW) are as follows: Mn (0.1–0.25 nM), Fe (0.25–0.7 nM), Co (~0.025 nM), Ni (6–9 nM), and Cd (0.7–1 nM). During cruise SO-240, dissolved (< 0.2  $\mu\text{m}$ ) trace element concentrations were determined in MUC bottom water samples from the sediment-water interface, the ranges for Al, V, Cr, Fe, Mn, Co, Ni, Cd, and As are summarised in TABLE 4.2. Especially the concentrations of Fe, Mn, Co, and Ni are 2–4 orders of magnitude higher than in the LCPW. This strong enrichment can either be related to (1) resuspension of sediment during sampling, with an enrichment of colloids/nanoparticles in the dissolved fraction passing a 0.4  $\mu\text{m}$  or 0.2  $\mu\text{m}$  filter, (2) a strong benthic flux, or (3) contamination during sampling.

Trace element concentrations in deep ocean water are determined by physical transport (i.e., water mass mixing) and biogeochemical controls (remineralization, dissolution, sorption) either *in situ* or along the flow path of the water mass. In recent years, increasing evidence for the importance of processes at the sediment-water boundary for many trace element cycles has been published (Middag et al., 2015; Van de Fliert et al., 2016; Zheng et al., 2016; Homocky et al., 2016; Haley et al., 2017). Scavenging of trace elements in the Bottom Boundary Layer (BBL) or dissolution promoted by sediment resuspension have shown to be highly effective in modulating benthic metal fluxes (Middag et al., 2015; Homocky et al., 2016). Filtered seawater generally includes colloids and nanoparticulates as well as aqueous species, and significant proportions of “dissolved” trace metals passing through a 0.4  $\mu\text{m}$  or 0.2  $\mu\text{m}$  filter are in fact present as colloidal/nanoparticulate aggregates (e.g., Fe (oxyhydr)oxides or Fe-organic matter colloids; see references in Raiswell and Canfield, 2012). In Atlantic intermediate and deep waters, dissolved Fe < 0.2  $\mu\text{m}$  was found to be evenly partitioned ~50:50% into truly dissolved Fe and colloidal Fe phases, which





#### 4.2.3.3 Upper ocean currents

The Eastern German license area is located in the North Equatorial Current and the zonal component of currents is westward (negative) at the surface with a rapid decay in the upper thermocline (FIGURE 4.14). Surface maximum zonal velocities are 8 cm/s toward the west. Meridional currents are northward at the surface, consistent with the wind forcing by the trades and Ekman dynamics, and reach values of 5 cm/s. Below the surface mixed layer, the currents remain northward. The speed of the meridional currents at a depth of 100 m is a few centimetres per second only.

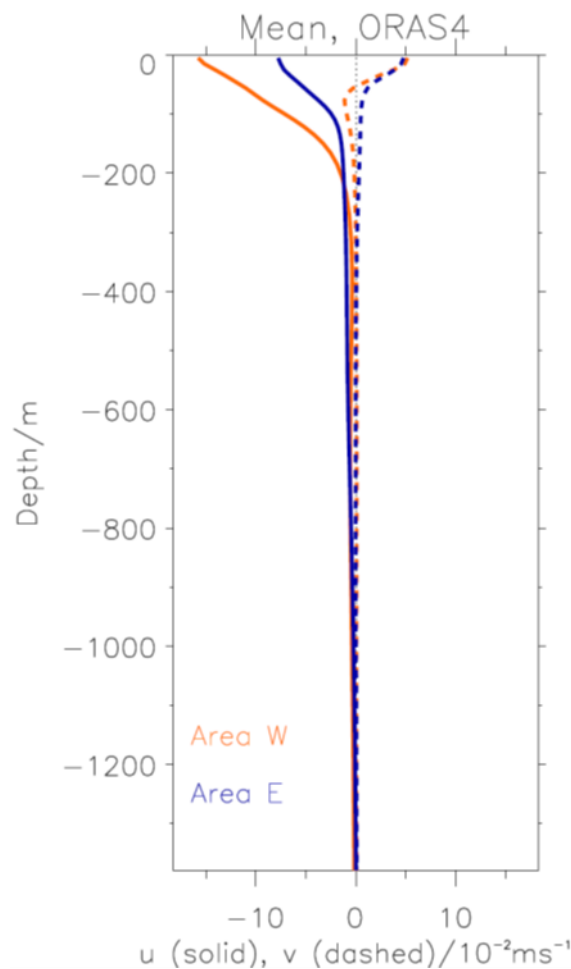


**Figure 4.14:** Long-term average of (solid) zonal and (dashed) meridional current in  $10^{-2} \text{ m s}^{-1}$ , as a function of depth in m for the western part (W, red) and eastern part of the German license area (E, blue), respectively. Data from the ocean reanalysis ORAS4.

Zonal surface currents show a strong seasonal cycle consistent with the meridional migration of the ITCZ. In boreal winter, the convergence zone and its zonal wind minimum are at their southernmost position and trades in the license areas are strongest. The license area is under the influence of the North Equatorial Current, with westward speeds of up to 12 m/s and in excess of 20 m/s (FIGURE 4.15). In boreal summer, surface currents weaken when the ITCZ and associated weak winds are at their most northward position. In the Eastern German license area, currents are close to zero in September. Below the thermocline, a noticeable seasonal cycle persists. Currents at a depth of 300 m remain westward and have hints of a semi-annual component, with speed minima in May and October. Below a depth of 700 m, zonal currents are reverse to eastward from February to June and are westward for the remainder of the year.

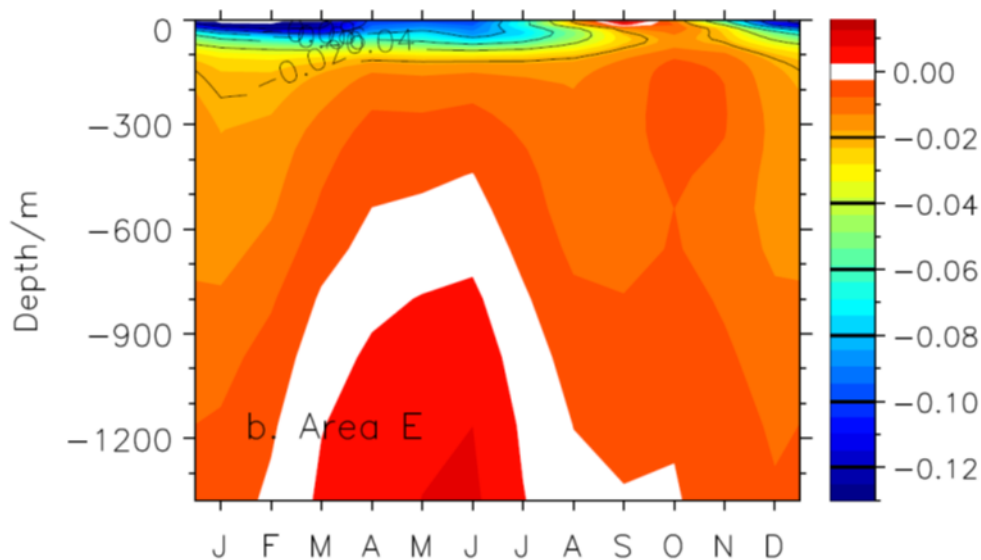


**Figure 4.15:** Zonal velocity in  $\text{m s}^{-1}$  at the Eastern German license area as a function of month and depth in m. The average seasonal cycle is calculated using monthly averages from 1992 to 2015, and by averaging four points surrounding the centre position of the license areas. Data is based on ORAS4.

Meridional currents (FIGURE 4.16) again reflect seasonal changes of the trade winds. Currents are strongest northward in boreal winter with speeds slightly above 10 cm/s. Below the thermocline, meridional currents reflect the annual Rossby wave (Kessler 1990), and meridional currents are toward the north in boreal winter, and to the south in boreal summer. Speeds below the thermocline are of the order of a few cm/s.

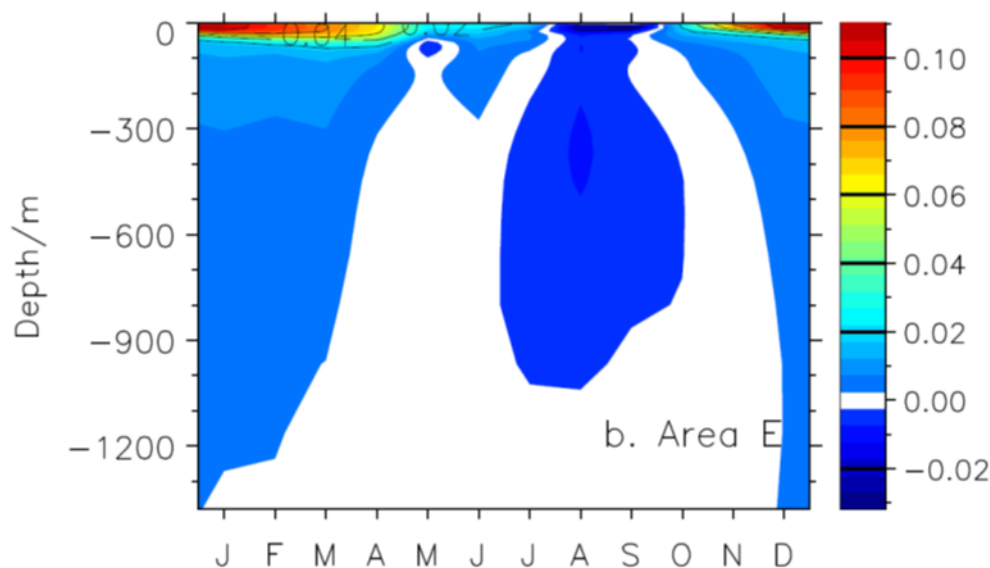


**Figure 4.16:** Meridional velocity in  $\text{m s}^{-1}$  at the eastern German license area as a function of month and depth in m. The average seasonal cycle is calculated using monthly averages from 1992 to 2015, and by averaging four points surrounding the center position of the license areas. Data is based on ORAS4.

Since the ORAS4 data covers the period from 1992 to 2015 with monthly averages, current anomalies, including year-to-year changes, have been characterised for the four seasons January to March, April to June, July to September and October to December. The distribution of current speed and direction are presented as a 'current rose'. Note that in contrast to wind direction that depict from where winds are blowing, current direction denotes the direction in which the water is flowing. Surface currents (FIGURE 4.17) are fairly steady and swift from January to March, with top monthly mean speeds larger than 26 cm/s. During fall and winter seasons, monthly mean currents become much more variable.

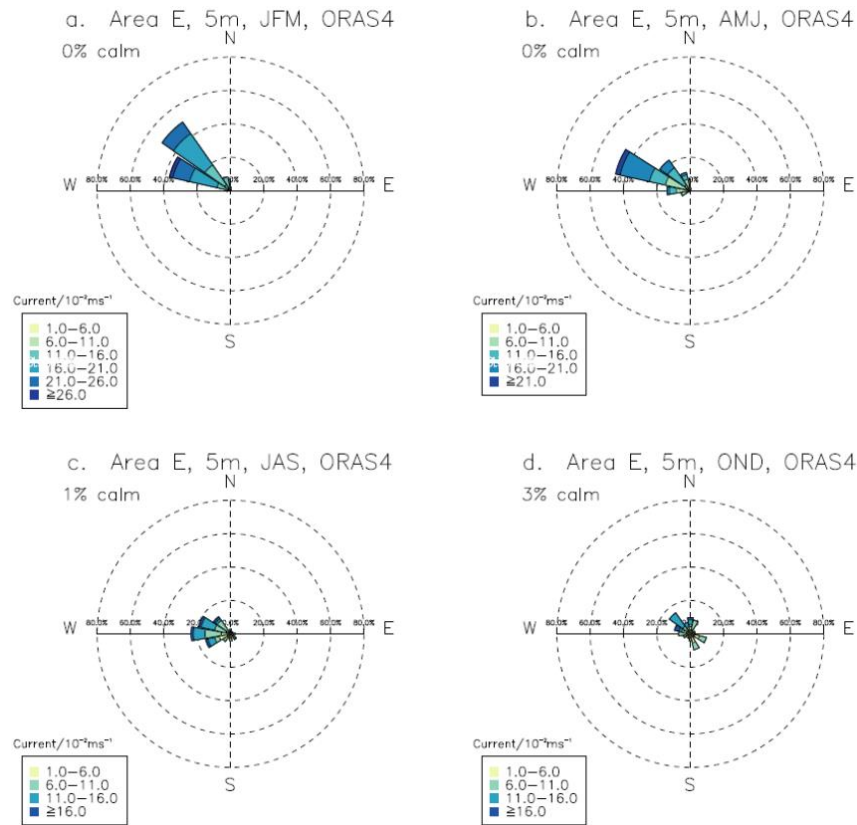


**Figure 4.17:** Current rose in  $10^{-2} \text{ m s}^{-1}$  in the Eastern German license area at 5 m depth for (a) January-March, (b) April-June, (c) July-September and (d) October-December. Data is based on monthly means of ORAS4.

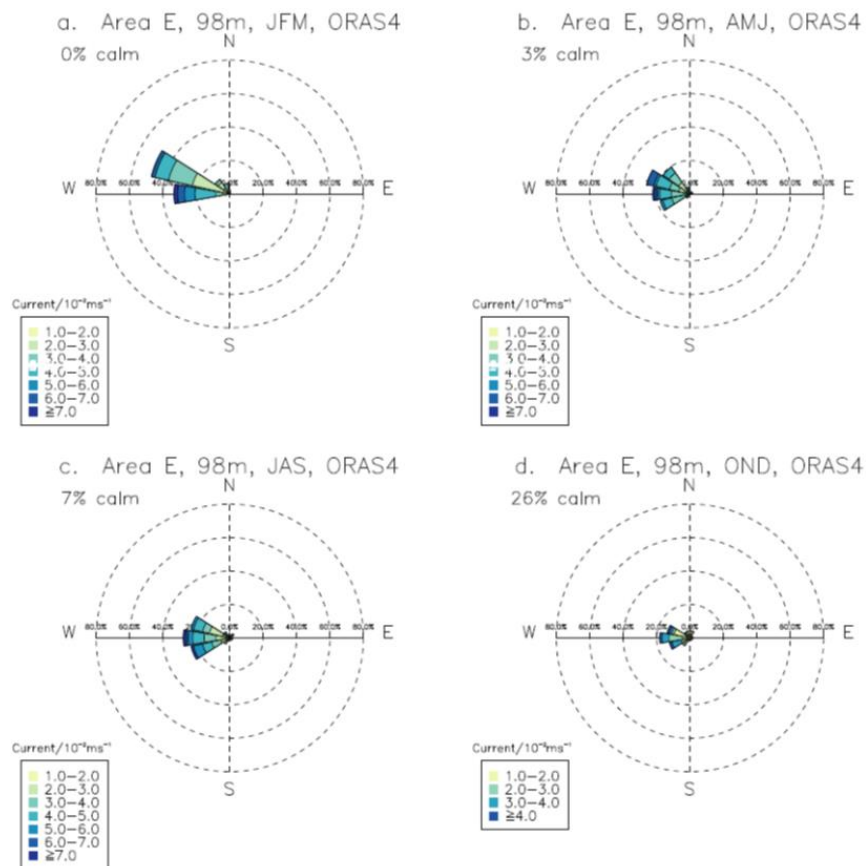


**Figure 4.18:** Current rose in  $10^{-2} \text{ m s}^{-1}$  at 98 m depth for (a) January-March, (b) April-June, (c) July-September and (d) October-December. Data is based on monthly means of ORAS4.

Comparison with currents at a depth of 100 m suggests that winter variations are largely an Ekman response to wind forcing. In the thermocline at a depth 100 m, currents direction is shifted toward the east, consistent with the lack of Ekman currents with west-south-westward currents more frequent from April to June. Seasonal change in speed distributions are modest with top speeds hovering around 10 cm/s. Currents at 100 m depth (FIGURE 4.18) mirror the distributions at the surface, but with a more westward component, and less directional variability in the October to December season. This season shows also more frequent occurrences of calm conditions, defined by speeds less than 1 cm/s.

At a depth of 500 m the centre of the oxygen minimum, currents are largely westward in January to March, with top speeds of 2.5 cm/s and calm conditions occurring about 10% of the time (FIGURE 4.19). In the April to June season currents are variable, and calm conditions prevail for 60% of the months. For the seasons from July to December, currents again are intermittent and toward the west and south-westward section, with calm condition occurring in 40% of the months.

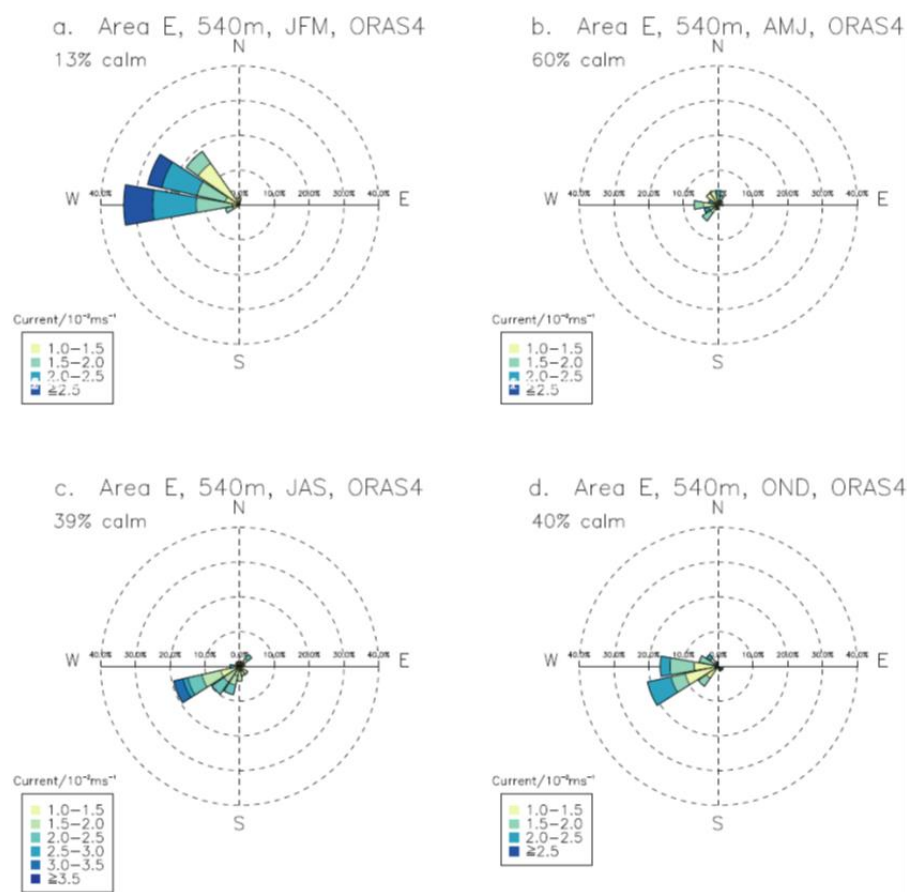


**Figure 4.19:** Current rose in  $10^{-2} \text{ m s}^{-1}$  at 540 m depth for (a) January-March, (b) April-June, (c) July-September and (d) October-December. Data is based on monthly means of ORAS4.

As the depth increases to 1000 m, occurrence of calm increases (FIGURE 4.20), with no-zero currents similar to those at 500 m, with westward flow in January to March, north eastward flow in July through September with speed of less than 1 cm/s for most of the time.

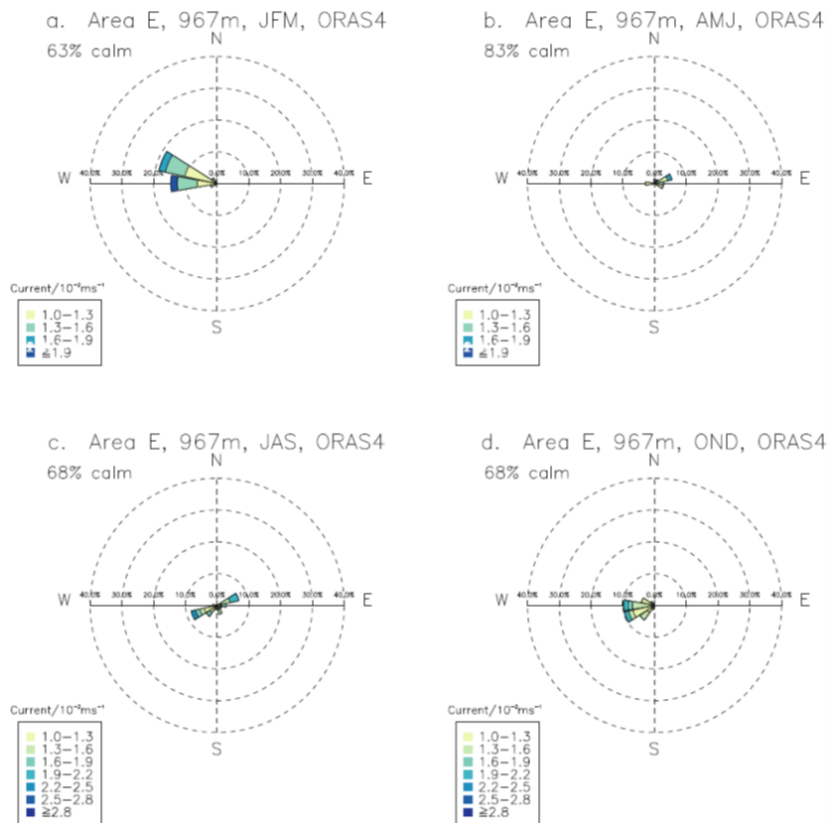


**Figure 4.20:** Current rose in  $10^{-2} \text{ m s}^{-1}$  at 967 m depth for (a) January–March, (b) April–June, (c) July–September and (d) October–December. Data is based on monthly means of ORAS4.

#### 4.2.3.4 The current regime close to the seafloor

Long-term data on current speed and direction as well as background turbidity have been collected in the area PA1-West at the depths that will be influenced by the operational plume arising from the testing of collector systems and equipment, i.e. near the seafloor. For these purposes, three moored systems (long-term Ocean Bottom Moorings, OBM), equipped with oceanographic instrumentation to obtain high resolution data from close to the seafloor, were deployed between April 2013 and May 2016. Furthermore, one additional OBM was deployed in the same area between May 2014 and May 2016 (see FIGURE 4.3 for exact locations). These measured high-resolution current and turbidity data have contributed to (1) the assessment of hydrographic conditions that are characteristic of the area (e.g. background mean flow velocities, tidal wave activities, inter-seasonal and near-inertial fluctuations, degree of local stratification/mixing, etc.), and (2) the configuration, implementation and calibration of existing and specifically adapted deep-sea 3D ocean circulation-sediment transport models that provide information on the probable fate of mining-induced discharged sediments under varying discharge scenarios at both the local (near-field) and the regional (far-field) scale in and beyond the (test-)mining area. Both aims have been tackled within the frameworks of the European-funded MIDAS and JPI-O MiningImpact 1 projects.

#### Current profilers

The OBM were constructed to be as short as possible so that the current profilers would hang just a few meters above the seafloor (configurations are summarised in Rühlemann et al., 2017). In this way, the current profilers could be programmed to collect data on current variability in the lower ~100 m of the water column. They measured at 45 minute intervals throughout a time period of approximately 1 year, were then retrieved and redeployed, from April 2013 to May 2016, respectively. Three of the four OBM



were equipped with two different current profilers: an upward-oriented Teledyne RDI ADCP (Acoustic Doppler Current Profiler) Workhorse Sentinel with a frequency of 600 kHz, and a sideward-oriented Aanderaa Seaguard Recording Current Meter (RCM) with a frequency of 2 MHz (both rated to 6000 m water depth). These OBM were deployed approximately 8 km apart in a triangular fashion in PA1 for the first time on the 11th April 2013 during the MANGAN 2013 cruise (Rühlemann et al., 2014), and then redeployed at exactly the same positions on the 12th May 2014 during the MANGAN 2014 cruise (Rühlemann et al., 2015) and the 6th June 2015 during the SO-240 cruise (Kuhn et al., 2015) (shown by the crosses in FIGURE 4.3). The fourth OBM was equipped with an upward-oriented Teledyne RDI ADCP Workhorse Quartermaster with a frequency of 150 kHz. This OBM was deployed for the first time on the 13th May 2014 in a centralised position between the 600 kHz OBMs, and redeployed at the same position on the 6th June 2015 (FIGURE 4.3, central cross).

### ADCP Data

ADCPs principally require a sufficient concentration of particles in the water column for the backscatter of their acoustic signals. Knowing that particle concentrations close to the seafloor are very low (e.g. from turbidity measurements on the video sledge), the functionality of ADCPs in this deep-sea environment was questionable before deployment. Fortunately, all ADCPs did deliver reliable current data from the seafloor, although the range of especially the 600 kHz ADCPs was low with the number of usable bins being restricted to bins 4 to 8 only (translating to a height of ca. 12 to 16 m above the seafloor).

Only the results of the three 600 kHz ADCPs are presented here. FIGURE 4.21 shows the variations in current speeds measured at all three sites throughout the three year measuring period, showing comparable patterns in current magnitudes, albeit with local-scale small differences. Frequency analyses of the current speed data indicate a clear semi-diurnal tidal cycle (M2) with an amplitude of  $> 2$  cm/s, as well as a clear diurnal tidal cycle (S1) and cyclicity in the near-inertial (fi) range ( $\sim 50$  h) related to ocean geostrophic currents and/or internal inertial waves (FIGURE 4.22).

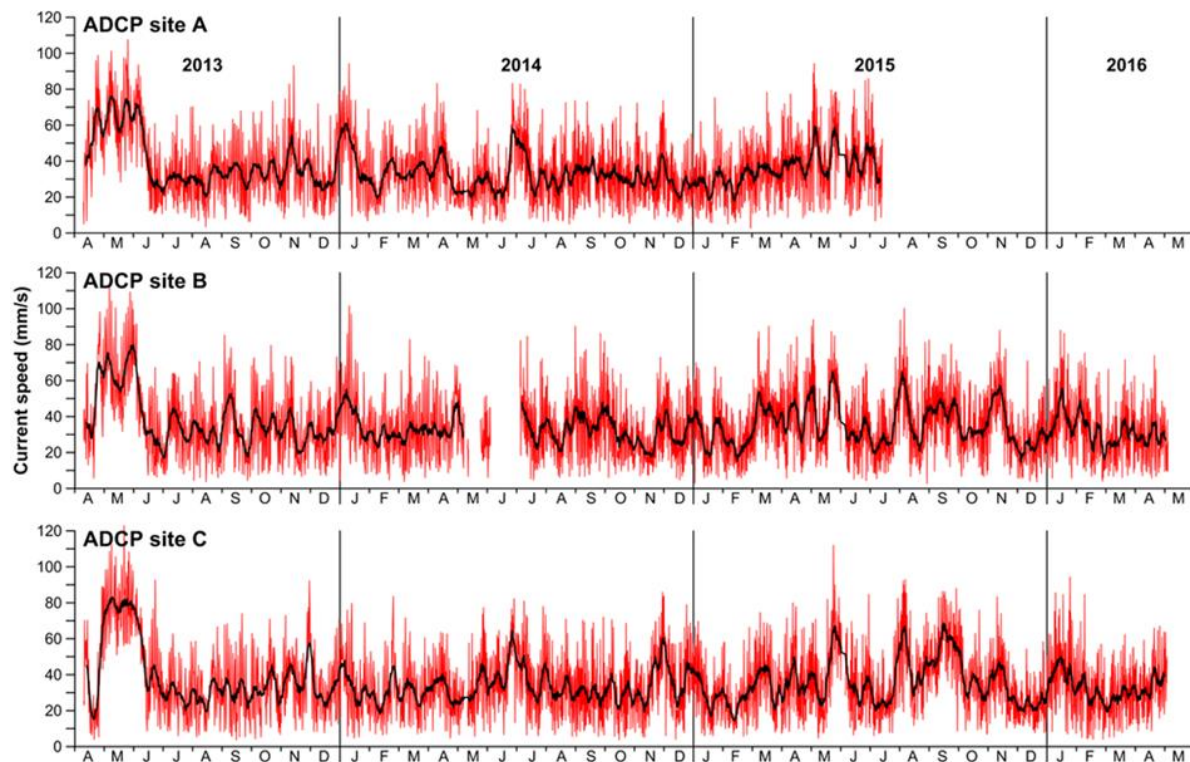


**Figure 4.21:** Comparison of averaged current speeds (black lines) measured by 600 kHz ADCPs in the water layer 12–16 m above the seafloor at the three OBM sites A, B and C in PA1-West (for positions see FIGURE 4.3) over the whole 3-year deployment period from April 2013 to May 2016.

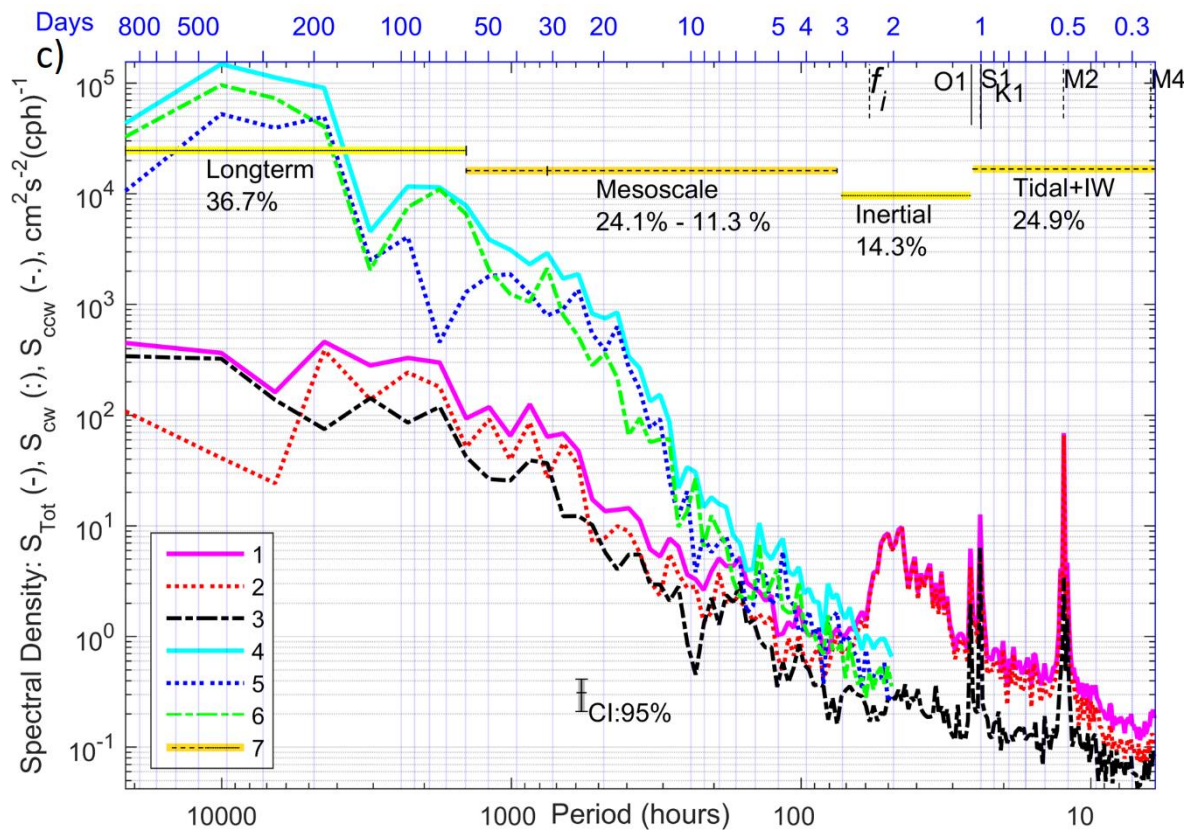
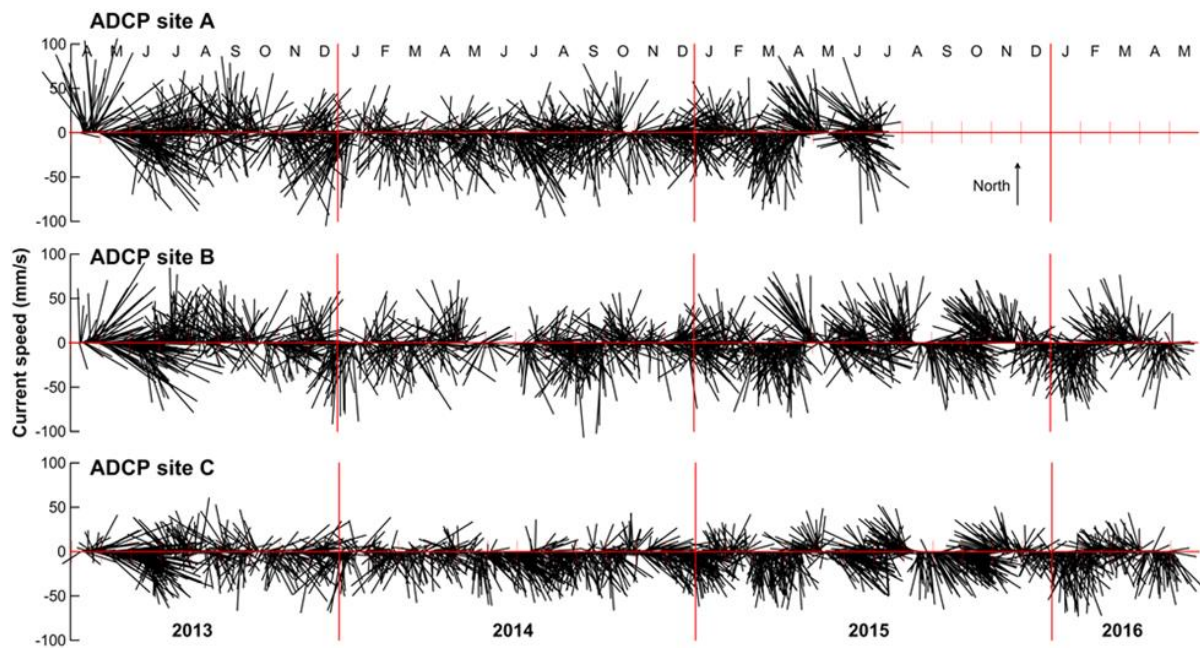


**Figure 4.22:** Rotary spectral density estimates of seabed currents at mooring site B over the period 11.04.2013–02.06.2015 are shown with lines 1,2,3 for total, clockwise (cw) and counter-clockwise (ccw) components and similar lines 4,5,6 for the surface currents at that site. Confidence Intervals (CI=95%) are included. Integration intervals over long-term, mesoscale, inertial and tidal + internal wave's bands and their contribution (%) in total spectra are shown by the yellow lines. Figure from Aleynik et al. (2017).

Average speeds are very similar when comparing sites (A, B and C) and deployment years, varying between 3.27 and 3.85 cm/s. The maximum attained current speed in the water layer 12-16 m above the seafloor was 14.2 cm/s (at site C). A distinct event of greater current speed and predominantly eastward current flow characterises May 2013 in all three sites, the event being most conspicuous at site C (FIGURE 4.21). This event has been related to the passage of a large westward-propagating eddy that transmitted its energy from the surface right down to the seafloor with a lag of 8-12 days (see CHAPTER 4.2.3.5 below; Aleynik et al., 2017). In fact, several El Niño-related eddies have passed over the license area in 2014 and specifically in 2015, whose signals can be traced by enhanced current speed on the ocean floor (CHAPTER 4.2.3.5; Aleynik et al., 2017).

Current directions can be erratic during some phases but have a clear unidirectional component during other phases (e.g. during the period of eddy passage in May 2013). In general, low frequency cycles with an approximate 60-90 day period are observable in the current direction data (FIGURE 4.23), with clockwise anticyclonic variation dominating the observed pattern.

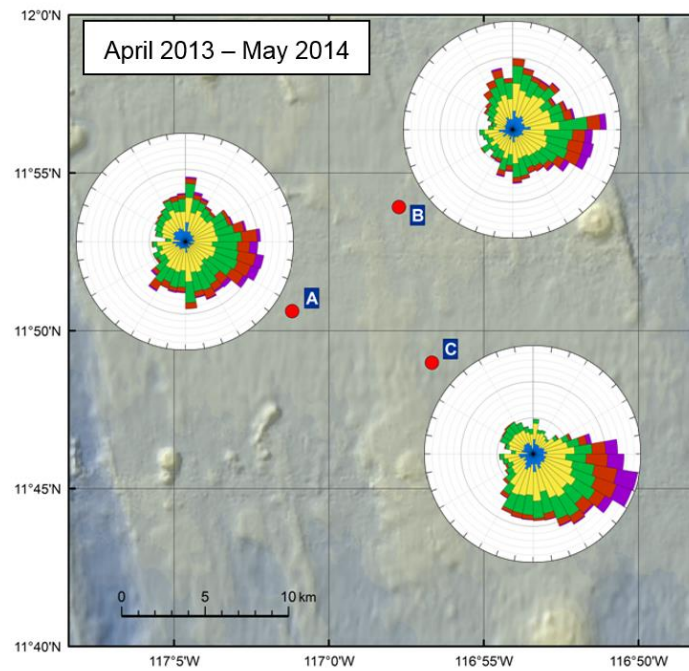




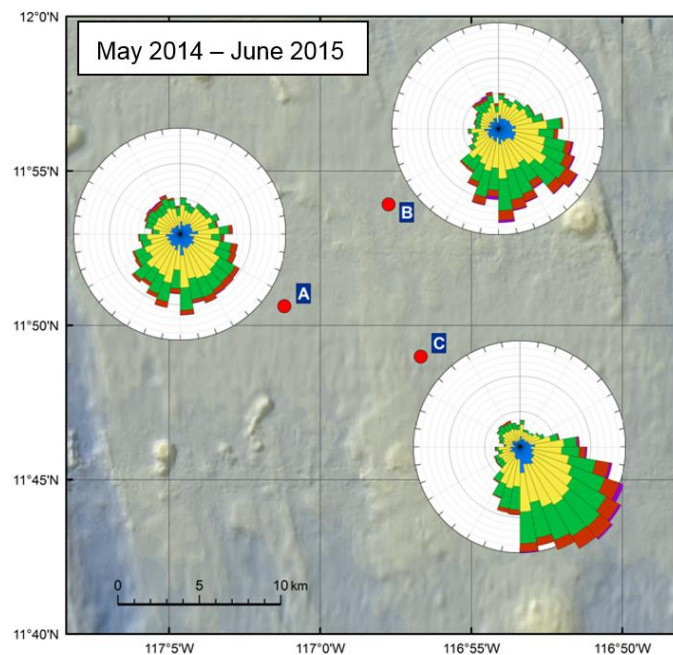
**Figure 4.23:** Stick-plots of ocean bottom current speeds and directions as measured by 600 kHz ADCPs in the water layer 12–16 m above the seafloor at the three OBM sites A, B and C in PA1-West (for positions see FIGURE 4.3) over the whole 3-year deployment period from April 2013 to May 2016.

FIGURE 4.24, FIGURE 4.25 and FIGURE 4.26 show radial plots of the ADCP data (current speeds and directions plotted as a function of their frequency of occurrence) at sites A to C in relation to topography during the three different deployment years. An average over all three deployment years is provided in FIGURE 4.27. In comparison, the following tendencies become apparent:

- a predominant SE current direction predominates during the first two deployment years, but an additional strong NW component arises during the last deployment year, showing that current directions are not easy to predict and susceptible to change in strong dependence of hydrographic conditions at the sea surface (eddy action, wind action);
- strongest currents ( $> 8$  cm/s) are always associated with E-SE flow direction (FIGURE 4.27);
- the E-SE component of flow and its current speeds are most distinctive at site C, perhaps due to the occurrence of a slight topographic high to its west (elevated by ca. 50 m). The northward and westward component of flow is strongly reduced at this site;
- during flow periods with a strong SE current component (speeds  $> 6$  cm/s), a sediment plume could potentially drift 10–12 km away from its source position in 4 days' time;
- no clear relationship between current speed and the occurrence of large nodules (sites A and B) or small nodules (site C) could be found.



**Figure 4.24:** Radial plots of current speeds and directions in the water layer 12–16 m above the seafloor as measured by 600 kHz ADCPs at the three OBM sites A, B and C from April 2013 to May 2014 plotted as a function of their frequency of occurrence: the radius represents a relative frequency of 6%. Colours reflect increasing current speeds from < 20 mm/s (blue) to > 80 mm/s (purple). OBM positions have been plotted on a map of the topography of the area.



**Figure 4.25:** Radial plots of current speeds and directions in the water layer 12–16 m above the seafloor as measured by 600 kHz ADCPs at the three OBM sites A, B and C from May 2014 to June 2015 plotted as a function of their frequency of occurrence: the radius represents a relative frequency of 6%. Colours reflect increasing current speeds from < 20 mm/s (blue) to > 80 mm/s (purple). OBM positions have been plotted on a map of the topography of the area.

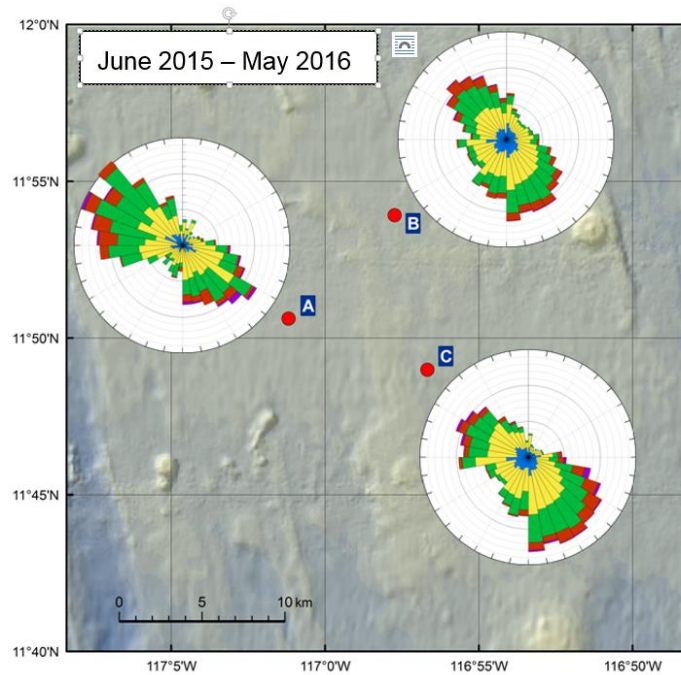


**Figure 4.26:** Radial plots of current speeds and directions in the water layer 12–16 m above the seafloor as measured by 600 kHz ADCPs at the three OBM sites A, B and C from June 2015 to May 2016 plotted as a function of their frequency of occurrence: the radius represents a relative frequency of 6%. Colours reflect increasing current speeds from < 20 mm/s (blue) to > 80 mm/s (purple). OBM positions have been plotted on a map of the topography of the area. Due to early surfacing of the OBM at site A, the diagram for site A covers the period from May to July 2015 only.

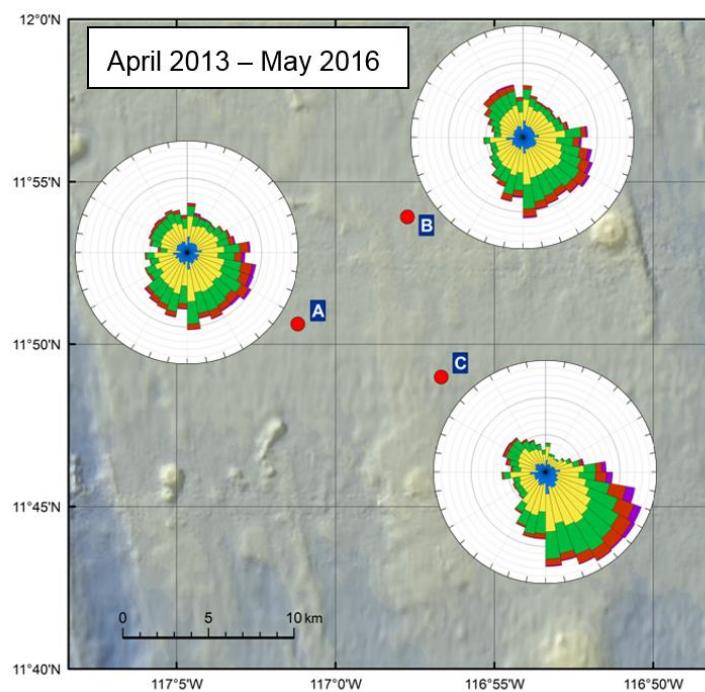


**Figure 4.27:** Radial plots of current speeds and directions in the water layer 12–16 m above the seafloor as measured by 600 kHz ADCPs at the three OBM sites A, B and C over the whole 3-year deployment period from April 2013 to May 2016 plotted as a function of their frequency of occurrence: the radius represents a relative frequency of 6%. Colours reflect increasing current speeds from < 20 mm/s (blue) to > 80 mm/s (purple). OBM positions have been plotted on a map of the topography of the area.

### Turbidity measurements at site B

The turbidity sensor on the RCM of site B measured average background turbidity values of 0.08 FTU during the time period between 11.04.2013 (first deployment) and 22.07.2013, without showing any changes during the eddy event of increased current strength in May 2013, suggesting that no natural resuspension occurred close to the seafloor during the period of increased current strength (FIGURE 4.28). A phase of greatly increased turbidity with maximum values of 4.18 FTU (i.e. an approximate 40-fold increase compared to background values) followed in September and October 2013, dropping to average values of 0.27 FTU from 08.11.2013 onwards. This impressive increase in turbidity which is not correlated to changes in current strength may be explained by an increase in surface water chlorophyll concentrations in the upper water column as registered by satellite imagery, and the consequent increase in particle fluxes to the seafloor (Rühlemann et al., 2015). In the second deployment year, a turbidity spike of similar dimensions was not observed. An average turbidity value of 0.21 FTU was registered, with peaks of max. 3.5 FTU occurring sporadically in the first quarter of 2015. Again, these are not associated with the passage of surface eddies (FIGURE 4.30; Aleynik et al., 2017). Unfortunately, the turbidity sensor did not measure properly during the third deployment year.

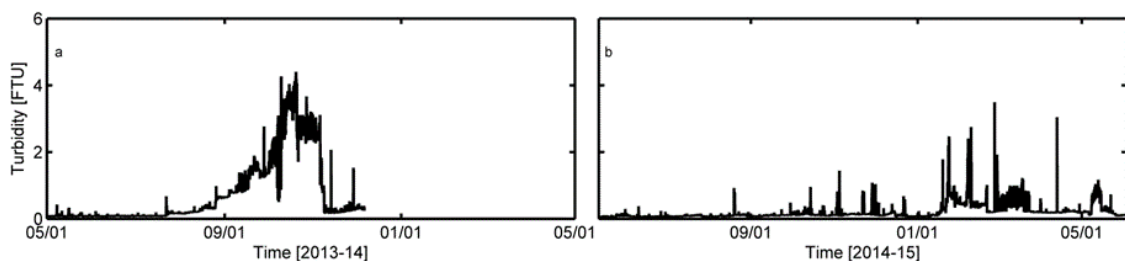


**Figure 4.28:** Turbidity data obtained from OBM site B at a height of 2–2.5 m above the seafloor during the first two years of deployment (April 2013 to June 2015).

#### 4.2.3.5 Controlling factors on abyssal currents and the significant influence of eddies on the abyssal current regime

Harvesting of polymetallic nodules in the CCZ will generate plumes of suspended sediment which are anticipated to be ecologically harmful. While the deep sea is low in energy, it also can be highly turbulent, since the vertical density gradient which suppresses turbulence is weak. Our observations from mooring data (see the last CHAPTER 4.2.3.4) show that the low-energy environment more than four kilometres below the surface unexpectedly becomes an order of magnitude more energetic for periods of weeks in response to the passage of mesoscale eddies (FIGURE 4.21).

Despite the well-known fact that surface-generated, full-depth eddies are important contributors for the material transport to the interior ocean from continental margins (Zhang et al., 2014; Zhang et al., 2016) and hydrothermal vent systems of mid-ocean ridges such as East Pacific Rise (Adams et al., 2011), little is known on their near-seabed effects over abyssal plains. In the Central Tropical Pacific, the influence of surface eddies on the currents at abyssal depths has, however, already been registered in two occasions (Demidova et al., 1993; Kontar and Sokov, 1994).

As part of the MIDAS programme, the Scottish Association of Marine Sciences (SAMS) quantified the links between remotely wind-induced surface current patterns, tidal action, bottom topography and deep ocean flow enhancement based on the deep-ocean oceanographic data presented in CHAPTER 4.2.3.4, in order to predict the resulting impact on sediment plume dynamics in the eastern German nodule licence area. This work was recently published in Aleynik et al. (2017) and is presented here.



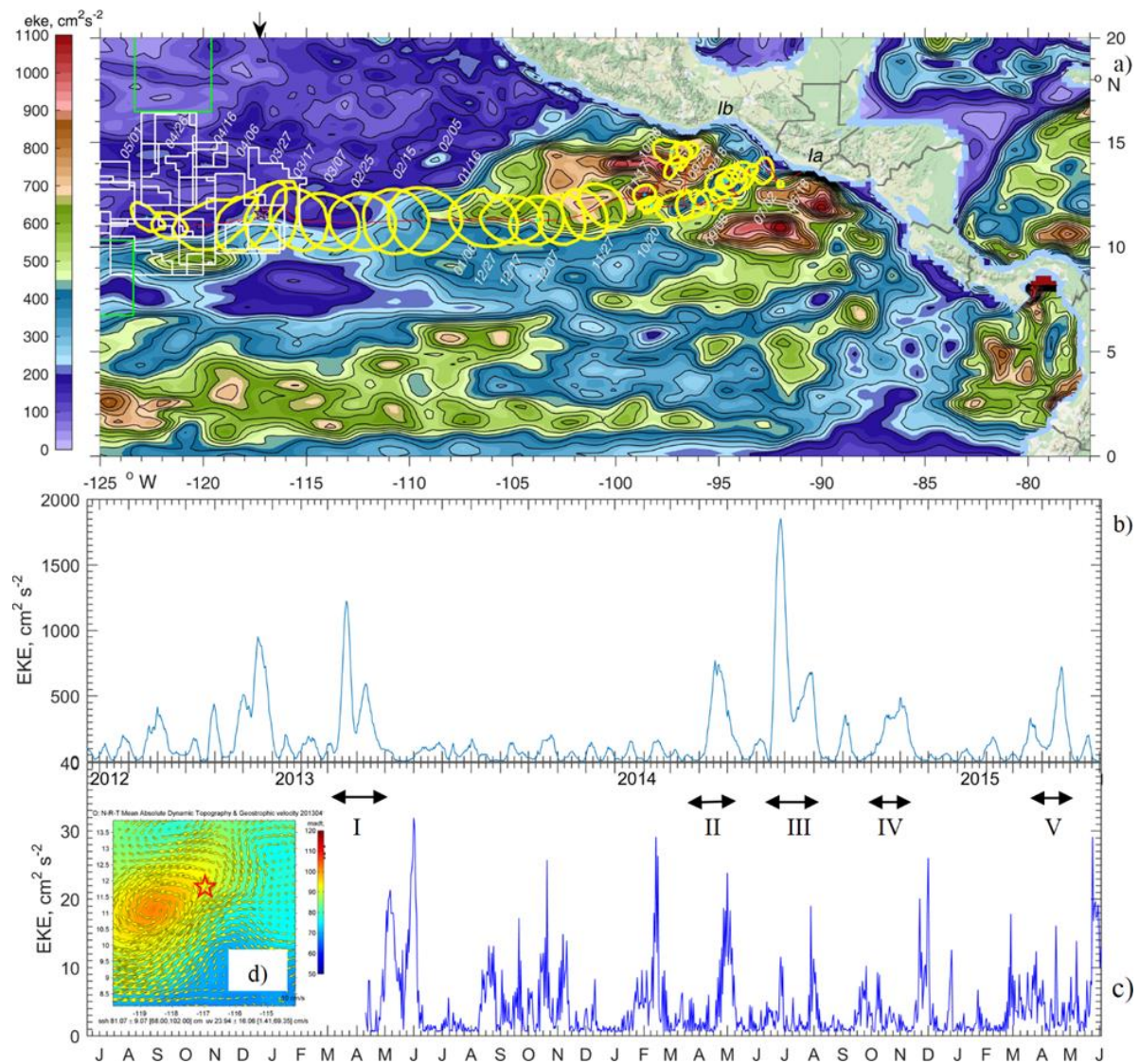


**Figure 4.29:** **a)** The track of a mesoscale eddy (I) over 318 days from the coast towards the CCZ (licence areas shown with white and APEIs with green lines) and the BGR moorings site (star). Yellow lines encircle a local maximum (>80 cm) sea surface height (SSH) anomaly (AVISO) at 10-day intervals. Colours reflect mean surface Eddy Kinetic Energy (EKE) over the period 18.06.2012 to 01.05.2013. **b)** Time series of EKE at the surface and **c)** in a layer 15-20 m above the seabed at mooring site B; eddies I-V are indicated with black arrows. Inset **(d)** shows SSH anomaly (colours) and geostrophic currents (arrows) on the date of moorings deployment (11.04.2013). Figure from Aleynik et al. (2017).

In-situ, deep-ocean current measurements were compared to sea-surface dynamic topography and surface geostrophic currents derived from satellite altimetry (AVISO: <http://www.aviso.altimetry.fr/duacs/>). In spring 2013, an unusually consistent increase and doubling of flow speed up to 8 cm/s was detected at all three mooring sites over a timespan of several weeks, with peak values (17-24 cm/s) exceeding the normal background average of 3.8 cm/s by 4-6 times at 12-16 meters above the bottom (mab) (FIGURE 4.30). The tidal contribution to total current variability over the whole deployment period is estimated by subtracting the variance of a synthetic time series, constructed using harmonic tidal analysis, from the total variance of the observed series. The 67 tidal constituents detected contribute only  $34.3 \pm 0.5\%$  to the total variance (FIGURE 4.22). Half of this variance is provided by the 8 largest constituents. To identify the other greater driver(s) capable of providing two-thirds of the energy required to sustain variability of abyssal flow, rotary spectral, wavelet transform and coherence analyses were performed. This allowed a differentiation between the relative contributions of the tides, the inertial oscillations related to wind-induced internal waves and the full-depth mesoscale eddies.

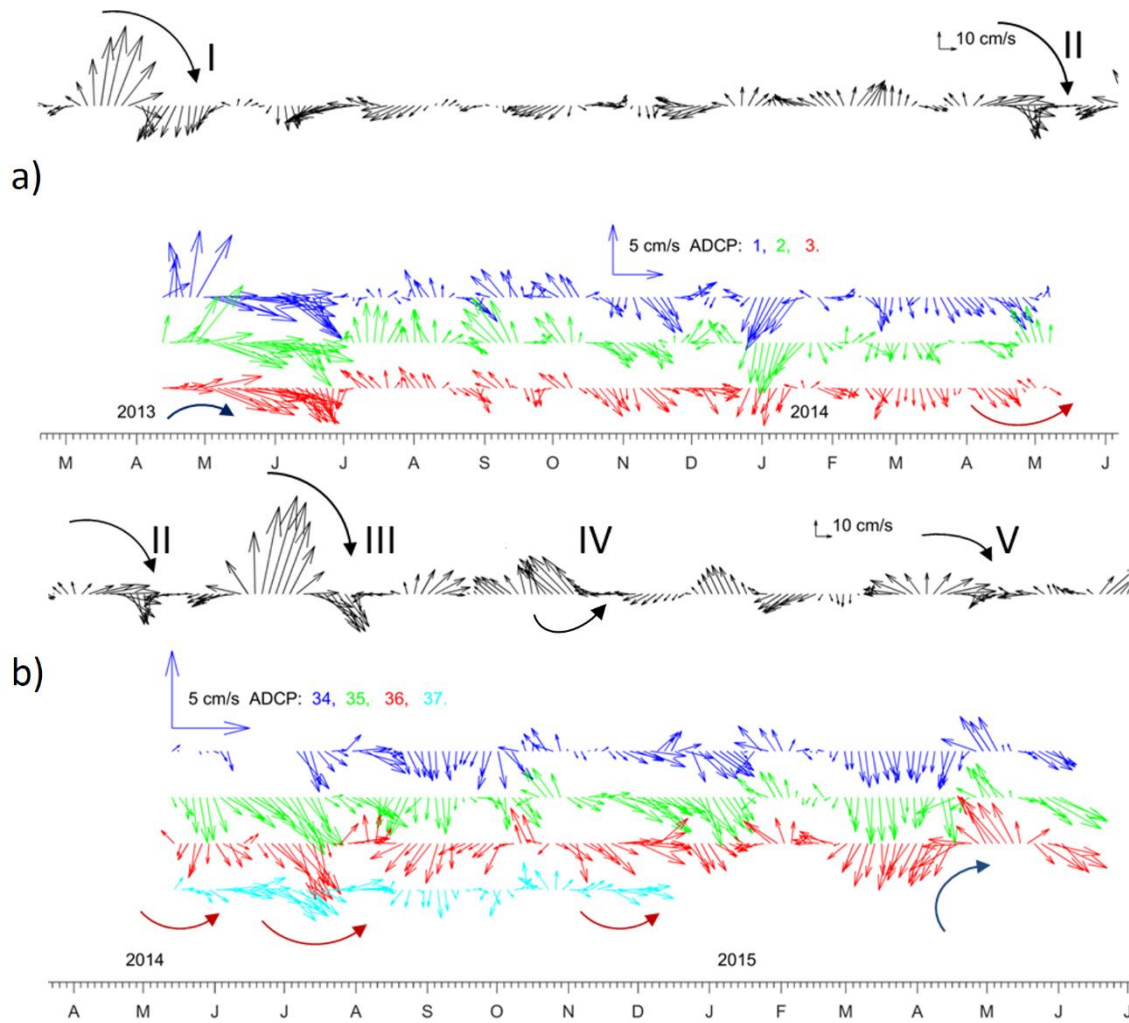


**Figure 4.30:** Surface geostrophic velocity (AVISO) (black) and residual currents at mooring sites A, B and C (1,2,3) (a) and A, B, C and D (34,35,36,37) (b) shown in colours (3-daily averaged, layer 15-20 mab) during two consecutive deployment years. The curved arrows indicate current veering during passage of eddies I-V (FIGURE 4.29). Figure from Aleynik et al. (2017).

Combined total and rotary spectra of the daily mean velocities (FIGURE 4.22) reveal that energy at the sea surface was higher than energy at the seabed below the inertial frequency  $f_i$  (with periods longer than 2.5 days). Clockwise (negative) rotary power density  $S_{cw}$  was also higher than counter-clockwise  $S_{ccw}$  in both time series at the same frequencies.  $S_{cw}$  of the seabed oscillations at near-inertial frequencies was as high as the major diurnal ( $S_1$ ,  $O_1$ ,  $K_1$ ) and only slightly lower than semidiurnal ( $M_2$ ) tides. Large-scale variations also have peak periods of 10, 30, 90 days at the sea surface, and 8, 12, 36, 90 days in the deep ocean layer.

The westward propagation of large surface eddies over the mooring sites is revealed by veering velocity vectors at depth. With a delay after passage of the eddy centre over the site, currents veered anticyclonically in all three current meter records (FIGURE 4.30A). Direct lag correlation between surface and seabed daily averaged currents was found to be insignificant. Only small peaks ( $|r|=0.2\div0.4$ ) with a delay of 10-20 days for velocity magnitude, north-south and east-west components were registered. To quantify the link between the surface and near-bed currents, complex coherence over rotary-decomposed vectors were calculated from pairs of spatially-separated time series (Gonella, 1972). Non-negligible coherence between *co*- and *counter*-rotating currents above the 95% significance level was detected at all three mooring sites with an approximate one week delay.

If a westward-propagating, warm, anti-cyclonic, clockwise-rotating (in the Northern Hemisphere) eddy centre passes to the south of the mooring sites, then bottom vectors turn in a clockwise manner. If an eddy centre passes to the north of the sites, an opposite, anti-clockwise rotation is recorded. In two of the five mesoscale eddy cases (I,V), the direction of bottom vector rotation matches the surface (FIGURE 4.30), which indicates that these eddy centres propagated south of the moorings and the northern edge of the eddy passed over it. The detected lag was 7-8 days. Thus, approximately one week is required for the eddy-induced, low-frequency signal to arrive at 4100 m depth with an estimated downward transfer rate of 300 m/day. The daily average horizontal drift speed of the first eddy centre varied from 5 to 20 cm/s. At the time the eddy signal was detected at the seafloor, its surface manifestation had propagated ~50 km westward. Therefore, the eddy's axis was effectively tilted from the vertical by  $4.5^\circ$  to the west, which is similar to the estimated tilt of baroclinic eddies formed near the shallow shelf in the South China Sea (Zhang et al., 2016) and the Salish Sea (Canals et al., 2009). This small axis tilt explains the delay in receiving the eddy signature at the bottom.

### Eddy origin and energy source

Satellite-derived sea-surface dynamic topography (AVISO) shows that the number of eddies passing over the moorings significantly increased in the second year of observations (eddies II-V on FIGURE 4.29B, FIGURE 4.30B). Such eddies draw their energy mainly from the narrow Central American mountain Gap Winds, driven by pressure gradient variations between the Pacific and the Gulf of Mexico, and are associated either with North American cold-air outbreaks (Chelton et al., 2000) or with intrinsic variability of the Trade Winds. Annually,  $3.5 \pm 1.2$  Gulf of Tehuantepec (T) and  $2.2 \pm 0.9$  Papagayo (P) giant anticyclonic eddies separate from their origin sites (Palacios and Bograd, 2005; Willett et al., 2006) to propagate westward for a year or two before their initial energy is mostly exhausted by sub-mesoscale motion, by merging with another eddy, or by collapsing and disintegrating as a result of collision with comparable horizontal-scale features in seabed topography, such as the East Pacific Rise. All five anticyclonic eddies could be tracked back to their origin. The travel duration from the starting point (P, Ia) and (T, Ib-V) to the moorings in the eastern German licence area was  $246 \pm 64$  days, with an average propagation speed of 12 km/day. A week before each P and T eddy was formed, a strong wind event (cyclonic tropical storm or hurricane) with wind speed exceeding 15-20 m/s was recorded (TABLE 4.3).

Possible generation of anticyclonic eddies during the low wind summer seasons and their observed enhanced frequencies shortly before and during El-Niño periods has been explained in literature by the link with equatorially-generated, freely-propagating, intra-seasonal and intra-annual Kelvin waves. These waves are seamlessly transformed into coastally-trapped waves (CTWs) on their arrival at the Central American coast, and become amplified with poleward propagation along the coastal waveguide. CTWs induce eddy shedding from the narrow coastal current. The vertical axis tilt inside such an eddy core is a signature of baroclinic instability due to vortex compression and stretching over varying bathymetry. The stronger northerlies (offshore Gap Winds) become statistically significant only in May and September of El-Niño years. Baroclinic Kelvin waves with a 30-90 day period are produced in the western and central Pacific under equatorial winds and have an enhanced signal during the Southern Oscillation (SO) warm phase. Surface EKE (defined as half of the horizontal velocity deviation from mean squared) was averaged over the most recent seven low and eight high episodes when the SO Index (6-month running-averaged) was outside a 0.5 standard deviation threshold of the 1993-2016 mean (FIGURE 4.31C).



**Table 4.3:** Parameters of mesoscale eddies tracking from Papagayo (Ia) and Tehuantepec (Ib-V) in a period from June 2012 until May 2015: dates at origin and destination locations, drift duration, mean, maximum speed and its standard deviation, hurricanes names, dates and maximum wind speed. Table from Aleynik et al. (2017).

ID	At origin			At destination			N	Mean  V	STD $\sigma_v$	Pick V	Hurricane name	Date	Wind speed
	Date yyymmdd	Lon °W	Lat °N	Lon °W	Lat °N	Date yyymmdd						yyymmdd-dd	
Ia	120618	90.875	13.625	116.9952	11.2487	130329	284	0.14	0.06	0.30	Carlotta	120612-16	175
Ib	120916	95.50	15.50	99.00	12.50	121030	44	0.16	0.05	0.30	Kristy	120912-17	95
II	131020	96.75	14.75	117.5763	11.2128	140420	182	0.16	0.06	0.33	Raymond	131018-30	205
III	131102	95.70	14.95	116.6564	11.0477	140706	246	0.13	0.05	0.30	Sonia	131101-04	75
IV	131225	96.25	14.95	117.0297	11.8435	141120	330	0.11	0.08	0.89			
V	141008	95.50	15.50	116.1081	10.8378	150412	186	0.15	0.04	0.26	Simon	141001-07	215
mean				nearest to	moorings	BGR-site	246	0.14	0.06	0.40			

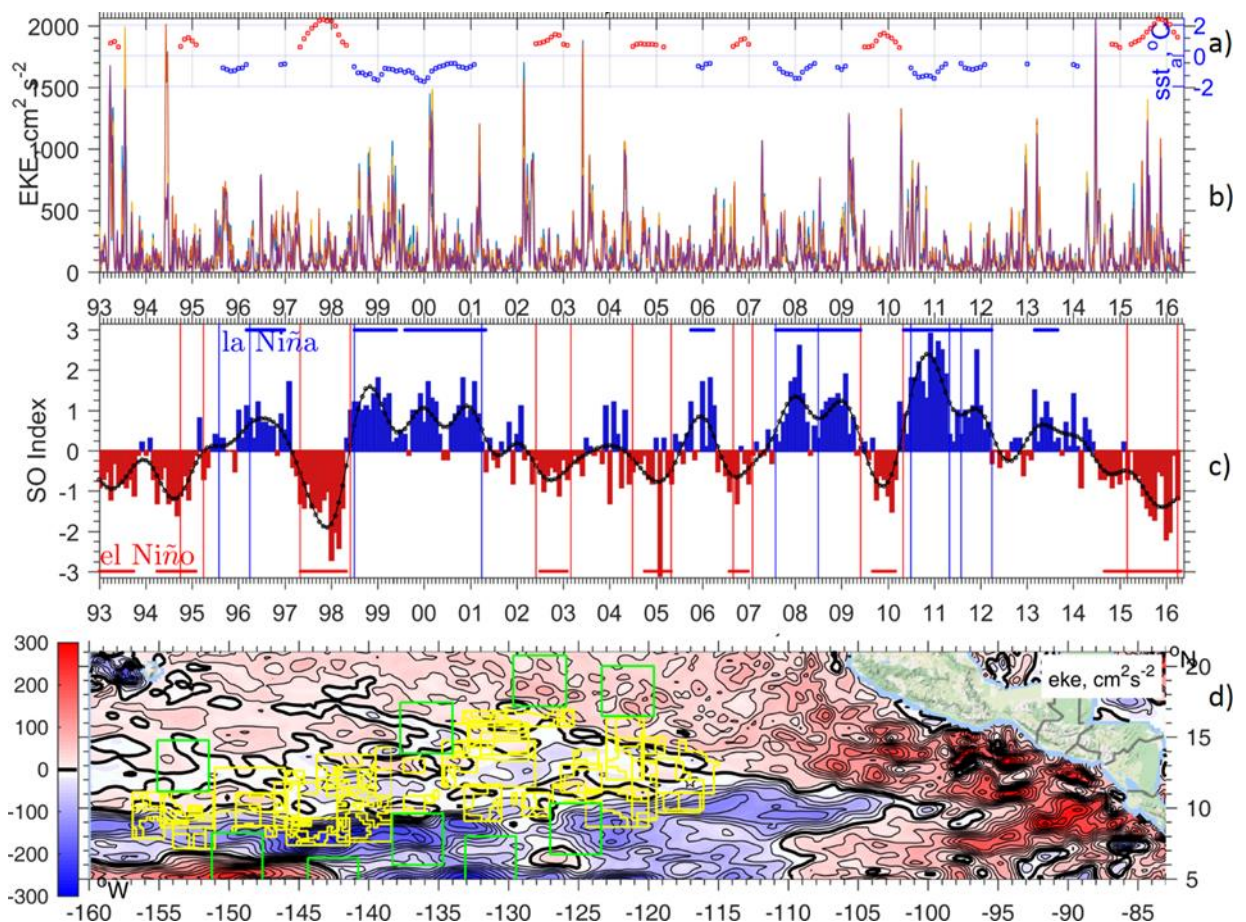


**Figure 4.31:** a) Sea Surface Temperature (SST) anomalies in the Central Pacific. b) Surface Eddy Kinetic Energy (EKE) over the BGR mooring sites. c) The Southern Oscillation Index (SOI), which represents the pressure difference between Tahiti and Darwin and is referred to as a precursor/indicator of El-Niño (red) and La-Niña (blue) strength; 6-month running averaged SOI is shown by the black line. d) The difference between the mean EKE (isoline increment is  $25 \text{ cm}^2/\text{s}^2$ ) of the altimetry-derived (AVISO) ocean surface currents between El-Niño and La-Niña periods calculated over the time period 1993-2016. CCZ licence areas are shown with yellow and APEIs with green lines. Figure from Aleynik et al. (2017).

Over the past 23 years across a wide band (600-1000 miles) along the Central American western coast, the surface EKE was higher (up to  $300 \text{ cm}^2/\text{s}^2$ ) during El-Niño phases in comparison with La-Niña (FIGURE 4.31D). Therefore, and in consensus with Palacios and Bograd (2005), the role of Southern Oscillation in

the modulation of the intensity and increasing the number of eddies at their origin is evident. The spikes in surface EKE above the mooring sites (FIGURE 4.29B, FIGURE 4.31B) reflect the increase in the number of mesoscale eddies emerging and passing over the site during the latest El-Niño period (mid 2014 - early 2016).

The effects that mesoscale eddies have on the current regime at abyssal depths inherently shows that future mining operators in the CCZ should be concerned about possible effects of large-scale surface climatic phenomena on abyssal conditions. In the above we have shown that near-bed velocities in excess of 10 cm/s are related to long-lived coastal-origin eddies, which have the potential to strongly affect the direction and speed of spreading of mining plumes. Whether eddy-induced bed velocities may cause significant resuspension at 4 km depths remains to be seen, but there is no doubt that these eddies influence the fate of any pre-existing plume. They should thus definitely be taken into account in the design of any kind of deep-sea mining operation and have thus been accounted for in probable plume spreading scenarios for the collector test proposed here (see CHAPTER 6.4.3). Furthermore, the data above show that the possibility of detecting and tracing eddies in advance could help anticipate and assess the behaviour of both natural and man-made plumes in a representative range of conditions over potential mining sites and could well serve as an important management tool.

## 4.2.4 SEABED SUBSTRATE CHARACTERISTICS

### 4.2.4.1 Dry bulk densities; shear strengths; grain-size analyses

Physical properties of sediments such as water content, dry bulk densities (DBD) and shear strengths have been routinely obtained from box core sediments (0-40 cm depth) during and after BGR exploration cruises (195 box cores in total from the eastern and western license areas). TABLE 4.4 gives a quick indication of the typical ranges of values and average values of these sediment properties as measured in the box core sediments of the eastern and western license areas.

**Table 4.4:** Total current number of measurements, typical ranges of values and average values of sediment properties as measured in box core sediments (0-40 cm depth) from the eastern and western license areas (2008 – 2015).

	Nr. of measurements	Typical range of values	Average value
Dry bulk density (g/cm <sup>3</sup> )	~ 2150	0.2 – 0.6	0.34
Shear strength (kPa)	~ 2450	0.5 - 20	4.42
TOC (%)	~ 1830	0.1 – 0.65	0.34
CaCO <sub>3</sub> (%)	~ 1600	0 – 3.5 (max. 8)	0.51
Grain size surface sediment SO-205 (x-ray granulometry; sedigraph)	20	16 – 47% clay (< 2 µm) 27 – 56% silt (2 – 63 µm) 13 – 45% sand (> 63 µm)	34.1% clay 38.4% silt 27.5% sand
Grain size surface sediment (sieving with 125 and 63 µm sieves and 4.2 l water; x-ray granulometry; sedigraph)	19	20 – 37% clay (< 2 µm) 53 – 70% silt (2 – 63 µm) 5 – 13% sand (> 63 µm)	29.1% clay 62.5% silt 8.4% sand
Grain size surface sediment (sieving with 63 µm sieve and 1.4 l water; x-ray granulometry; sedigraph)	121	15 – 37 % clay (< 2 µm) 20 – 60 % silt (2 – 63 µm) 12 – 60 % sand (> 63 µm)	23.6% clay 33.1% silt 43.2% sand

### Dry bulk density

Water content, dry bulk density (DBD) and porosity are important properties of marine sediments and are usually interrelated. The dry bulk density is also related to the softness of the sediment, its vulnerability to erosion, resuspension and other mechanical properties such as shear strength. Dry bulk density is the

mass (weight) of the dry solids divided by the total volume of the wet sediment sample (Eq. 1); that is, dry bulk density is the ratio of the mass of the mineral grains to the total volume:

$$\rho_d = M_s/V \quad (1)$$

in which  $\rho_d$  is the dry bulk density ( $\text{g/cm}^3$ ),  $M_s$  is the mass of the salt-free dry sample (weight of the solid portion of the sample), and  $V$  is the total volume (volume of the wet sample).  $M_s$  needs to be corrected for the salt remaining as solids after drying the sediment sample. The corrected dry weight is determined by equation (2):

$$M_s = M - M_f = (M_d - s M)/(1 - s) \quad (2)$$

where  $M$  is the total wet mass,  $M_f$  is the mass of the salt water,  $M_d$  is the uncorrected dry mass, and  $s$  is the salinity (expressed as a decimal; i.e., 35 ppt = 0.035). To determine the dry bulk density of box cores (up to 40 cm long), the samples were frozen at  $-20^\circ\text{C}$  and then freeze-dried. Samples were taken with 10 ml syringes and wet volume and wet weight (mass) were determined prior to the drying process. After freeze-drying the dry weight was measured.

The DBDs in the upper 40 cm of the sediment in the eastern and western license areas range from 0.2 to  $0.6 \text{ g/cm}^3$ , with an average value of  $0.34 \text{ g/cm}^3$  based on analyses of ca. 2150 samples (TABLE 4.4). Highest values for DBD and shear strengths cluster on a plateau in the north-eastern part of the Eastern license area. In contrast, most of the lower shear strength and DBD values occur in the deeper parts of the abyssal plain. This apparent relationship between shear strength and topographic location might be caused by differences in bottom current velocities. In PA1, the average DBD in the uppermost 10 cm of the sediment is  $0.31 \pm 0.03 \text{ g/cm}^3$  (FIGURE 4.32). In PA2, the Gaussian distribution of DBD is somewhat broader, but most values lie between 0.25 and  $0.35 \text{ g/cm}^3$  and the average DBD of  $0.30 \pm 0.03 \text{ g/cm}^3$  is very comparable to that of PA1. The low standard deviation shows that DBD does not vary much laterally throughout and between both areas ( $\sim 2000 \text{ km}^2$  in PA1;  $\sim 1200 \text{ km}^2$  in PA2).

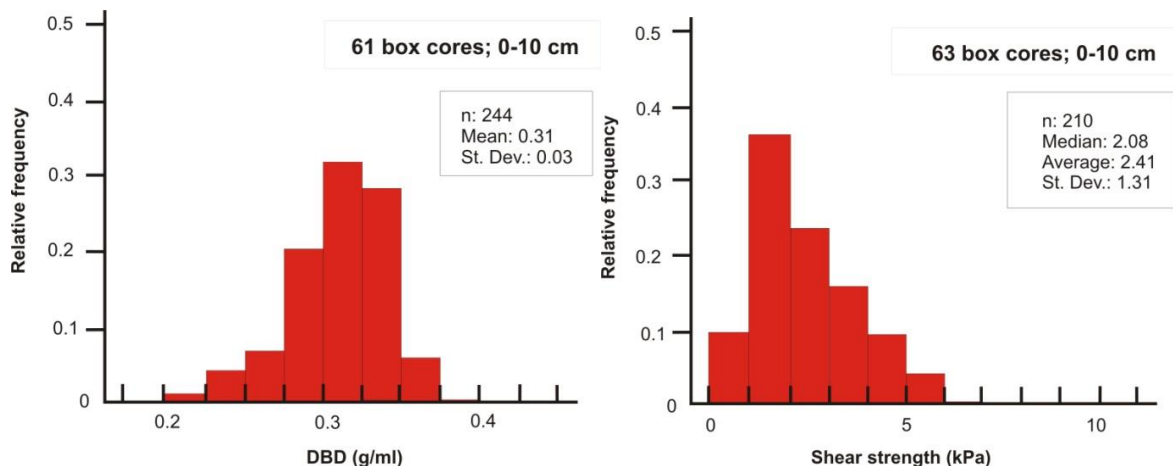


**Figure 4.32:** Dry bulk density (left) and ex situ shear strength (right) values of the upper 10 cm of box core sediments originating from Prospective Area #1 (PA1).

### Shear strength

Short sediment cores obtained from the box corer were split into two equal halves, and the undrained shear strength of the predominantly cohesive clayey sediments in one half of the core was measured at ca. 3 cm sampling intervals using a "Strassentest Baustoff-Prüfungssysteme" fallcone penetrometer type 318-D with a digital display. The cone and vertical sliding rod of the penetrometer have a total weight "GK" of 79.9 g (= 0.78 N), and the apex angle of the cone is  $30^\circ$ . The tip of the cone was positioned to just

touch the surface of the sediment to be measured. The cone was then released so that it could penetrate into the surface of the sediment, and was fixed after 5 sec. The undrained shear strength “ $\tau_u$ ” of the sediments (in N/m<sup>2</sup> or Pa) was determined from the penetration depth “ $s$ ” (in m) according to the following equation (Hansbo, 1957):

$$\tau_u = \frac{k \cdot G_k}{s^2} \quad (3)$$

The dimensionless factor “ $k$ ” depends on the cone angle and, to a lesser extent, on the sensitivity to adhesion. Its value is 0.85 for undisturbed, cohesive marine clayey samples and a cone apex angle of 30° (Houlsby, 1982).

*Ex situ* shear strengths in the upper 40 cm of the sediment in the eastern and western license areas range from 0.5 to 20 kPa, with an average value of 4.42 kPa (TABLE 4.4). *Ex situ* shear strength values in the uppermost 10 cm of sediment in PA1 range from 0.4 to 6 kPa, with an average value of  $2.41 \pm 1.31$  kPa (FIGURE 4.32). The high standard deviation shows that shear strengths in the upper 10 cm of sediment fluctuate much more strongly than DBD throughout PA1. In PA2, shear strength values of the sediments range between 0.4 and 3.8 kPa in the topmost 10 cm of the sediments. The average value is  $1.73 \pm 0.88$  kPa. Thus, the sediments of PA2 appear to be softer and have a lower variability in shear strength than the sediments of PA1. The difference could be related to the nodule size, as PA2 has a predominant coverage of small nodules whereas PA1 has a coverage of both large (PA1-West) and small (PA1-East) nodules.

### Grain-size analyses

There are many different methods for determining the grain-size distribution of deep-sea sediments, such as using the classical pipette method, x-ray granulometry (XRG, e.g. sedigraph), or laser diffraction (e.g. Malvern Mastersizer 2000). 161 samples from two long sediment cores from the eastern German license area (SO205-15KL and SO205-54KL) were investigated for differences in density, water content and particle size in the framework of a Master thesis at the University of Tübingen, Germany (Belz, 2015). Particle size distributions were investigated by laser diffraction and SEM image analysis and compared to previous results from Mewes et al. (2014) based on x-ray granulometric techniques (XRG; Sedigraph). Results on average grain size, size distribution as well as down-core trends were significantly different depending on the method used (FIGURE 4.33). These differences are attributed to differences in method-dependent sample preparation and the general difficulty in accurately measuring heterogeneous deep-sea siliceous oozes with considerable amounts of platy (e.g. clay) and elongate (e.g. diatoms, spicules) components. There is currently no routine method for the particle size measurement of such sediments. Belz (2015) concludes that laser diffraction may be the tool of choice for particle size measurements that best reflect the natural *in situ* composition and size range, which is important for understanding and modelling environmental effects of sediment disturbances during future mining operations. XRG may better determine the geological grain size which is of special interest for geochemical investigations. SEM analyses are fundamental for detailed studies of the sediment as even smallest components can be resolved, however, a comprehensive estimation and quantification of particle size and range as carried out in this study turned out to be difficult.

Furthermore, the grain-size distributions determined by XRG are strongly dependent on whether ultrasonic and/or dispersing agents are used (e.g. Dreiseitl et al., 2013). In the following we show by comparison of three almost identical but slightly different grain-size methods using a sedigraph that the use of dispersing agents, the amount of sieving steps and the quantity of water used during sieving greatly

alters the stability of larger aggregates and thus the resulting distribution of grain size in deep-sea sediments of the CCZ.

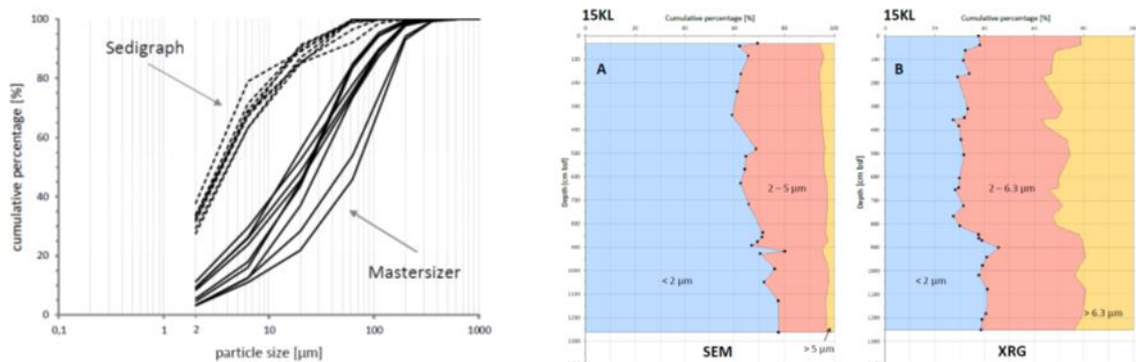


**Figure 4.33:** **Left:** Cumulative plot of particle sizes in core SO205-15KL measured by Mastersizer 2000 (continuous line) and Sedigraph (broken line). The Mastersizer 2000 generally measured distinctly coarser particle sizes than the Sedigraph method. Especially the fine fraction  $< 2 \mu\text{m}$  is underrepresented by laser diffraction compared to the Sedigraph method. **Right:** Comparison of particle size distributions in three size-classes (clay, fine silt,  $>$  fine silt) between SEM analysis (A) and XRG (B) for sediments of core SO205-15KL. Overall, average particle sizes derived by SEM are finer ( $3.26 \mu\text{m}$ ) compared to XRG measurements ( $\sim 5 \mu\text{m}$ ). Figures from Belz (2015).

#### Method 1

Grain sizes were determined for 20 surface sediment samples obtained during the SO-205 cruise to the eastern license area in 2010 based on standard x-ray granulometric techniques (sedigraph) used at the BGR. During this method, 10 g (precision  $\pm 0.001$  g) of the sediment sample were suspended using approximately  $150 \pm 50$  mL 0.01 M ammonia solution in 250 mL PE bottles. These suspensions were allowed to stand over-night, after which they were sieved over a  $63 \mu\text{m}$  sieve. Both fractions were oven-dried at  $60^\circ\text{C}$ . The fraction  $> 63 \mu\text{m}$  was dry-sieved using a  $125 \mu\text{m}$ ,  $200 \mu\text{m}$ ,  $630 \mu\text{m}$ , and a  $2000 \mu\text{m}$  sieve. In total, 3 g of the fine fraction  $< 63 \mu\text{m}$  was re-suspended in PTFE bottles using 80 mL Na-pyrophosphate and placed in the autosampler of the XRG machine (Sedigraph, Micromeritics). The intermediate drying step is necessary as XRG requires a relatively large solid concentration which should be within a narrow range. After mounting of the autosampler, an automatic procedure started where suspensions were stirred and treated with ultrasound. This was followed by the XRG measurement which was operated using a focused horizontal x-ray beam. Grain sizes were calculated as equivalent sphere diameters based on Stokes' law.

According to this method, sediments of the eastern license area contain 16-47% clay ( $< 2 \mu\text{m}$ ), 27-56% silt ( $2-63 \mu\text{m}$ ) and 13-45% sand ( $> 63 \mu\text{m}$ ). Average values of 34.1% clay, 38.4% silt and 27.5% sand were obtained (TABLE 4.4).

#### Method 2

In the framework of a student project, a detailed survey of the grain-size analysis method described above (method 1) was carried out with the aim of optimising the method for our deep-sea sediments as much as possible. An analysis of the fraction  $> 63 \mu\text{m}$  showed that this fraction contained many large aggregations of nodule fragments, phyllosilicates and skeletal remains of radiolarians that, without cohesion, would have passed through the sieve. Experimentation with ultrasonic treatment (35 kHz) showed that a short period of ultrasonic treatment (15 s) managed to break up many of the aggregates without tearing the larger micronodules / nodule fragments and radiolarians apart. However, the use of 2



min of ultrasonication was enough to break up the entire fraction  $> 63 \mu\text{m}$ , so that nothing remained on the sieve and a much larger clay fraction was registered (cf. Dreiseitl et al., 2013).

Grain sizes were determined for 19 surface sediment samples distributed randomly throughout the eastern and western German license area based on a slight adaptation of the standard x-ray granulometric techniques (sedigraph) used at the BGR described above (method 1). During this method, sediments were completely desalted by centrifugation and freeze-dried. 10 g (precision  $\pm 0.001$  g) of the sediment sample was suspended in 150 ml water, treated by ultrasonication for 15 s (35 kHz) and then sieved over a  $125 \mu\text{m}$  and a  $63 \mu\text{m}$  sieve using 4.2 l of water. The fraction  $< 63 \mu\text{m}$  was placed in the autosampler of the XRG machine (Sedigraph, Micromeritics).

The resulting average grain-size distributions are shown in TABLE 4.4. According to this method, sediments of the CCZ contain 20-38% clay ( $< 2 \mu\text{m}$ ), 48-79% silt ( $2-63 \mu\text{m}$ ) and 5-13% sand ( $> 63 \mu\text{m}$ ). Average values of 29.1% clay, 62.5% silt and 8.4% sand were obtained.

### Method 3

Consequently, 121 surface sediment samples from both the eastern and the western license areas were analysed using a slightly modified method to the one described above (method 2). In order to save time, the sieving process after ultrasonication treatment was reduced to the use of one sieve only ( $63 \mu\text{m}$  sieve) using 1.4 l of water. All other analytical procedures remained the same.

The resulting average grain-size distributions are shown in TABLE 4.4. According to this method, sediments of the CCZ contain 15-38% clay ( $< 2 \mu\text{m}$ ), 12-79% silt ( $2-63 \mu\text{m}$ ) and 5-71% sand ( $> 63 \mu\text{m}$ ). Average values of 23.6% clay, 33.1% silt and 43.2% sand were obtained.

### Comparison of methods 1, 2 and 3

In comparison, the use of dispersing agents (method 1) or ultrasonication and considerable amounts of water during the  $63 \mu\text{m}$  sieving process (method 2) tends to break up aggregates and leads to a relative increase of the clay and silt fractions compared to the sand fraction. This is especially true for method 2, where the large volume of water used during sieving additionally broke up aggregates and pushed its components through the  $63 \mu\text{m}$  sieve. In method 3, many more aggregates remained in the sand fraction compared to the two-sieve, thorough rinsing process of method 2 (43.2% vs. 8.4% sand fraction; TABLE 4.4).

For the purpose of determining grain-size distributions for input into sediment-transport models as part of sediment plume modelling procedures, the grain-size distributions obtained by XRG involving complete desalinisation, the use of dispersing agents and a short period of ultrasonication treatment will give us very conservative values ("geological" grain sizes), as (i) larger aggregates occurring in the natural environment are broken down to smaller components, and (ii) the high quantities of clay minerals in our deep-sea sediments are in fact extremely cohesive and flocculation in a natural salt water environment (in contrast to the desalinated water used during grain-size analyses) would greatly increase particle size and particle settling velocities. Unfortunately, experiments to determine the "natural" grain sizes in salty water using the pipette method failed due to the rapid rate of flocculation, the presence of salt crystals as part of the residue and the impracticability of using the Stokes' Law. Instruments such as sedigraph, sediment or laser mastersizer are not resistant to corrosion. In order to obtain good parameter values for sediment settling velocities and the cohesive properties (flocculation) of deep-sea sediments as input for reliable sediment-transport models, analyses at the Jacobs University in Bremen focus on studying the natural behaviour of sediments from PA1 using LISST suspended particle size analysers, roller tanks,

Gust erosion chambers and a nodule-filled flow channel (racetrack flume) (see CHAPTER 4.2.4.2 below). In contrast to the methods described above, the LISST has the advantage that it can measure particle sizes and sinking velocities under *in situ* salinity and temperature conditions. These analyses have delivered first parameters for input into hydrodynamic plume models (see CHAPTER 6.4.2) and will continue during the MiningImpact 2 project.

#### 4.2.4.2 Particle sinking velocities and aggregation

As it appears to be extremely difficult to analyse “natural” grain size distributions in the deep-sea sediments of the CCZ (see CHAPTER 4.2.4.1 above) – the results being very sensitive to the method used – OceanLab of the Jacobs University of Bremen was contracted by the BGR to carry out a preliminary analysis to characterise the sediments of the eastern German license area through the analysis of their natural, dynamic behaviour under *in situ* conditions based on laboratory studies (particle size distributions, settling velocities, concentration and turbulence-dependent flocculation potential (aggregation), erosion and resuspension potential). Values of these parameters are important inputs to the plume modelling exercises that are described in CHAPTER 6.4.2. The topmost 10 cm of 9 multicores collected during cruise SO-240 (Kuhn et al., 2015) and deriving from different working areas in the eastern German license area were analysed. *In situ* conditions of 34.5 p.s.u. and 1.5°C were used in all experiments.

##### Particle size analysis

A combine approach using a LISST-100X (Laser In-Situ Scattering and Transmissometry; Sequoia Scientific) coupled with an industrial camera (DFK 23UX174, The Imaging Source) mounted with a telecentric lens (TEC-M55MPW) was used to determine sediment particle sizes (Mikkelsen et al., 2005; Hill et al., 2013). This set-up allowed to detect a broad range of particle sizes ranging from 2.5 µm up to several mm. The median “natural” particle size of the analysed CCZ sediments was found to vary between 15 and 52 µm [ $\pm 2$  µm]), with a majority of sediment samples showing a median particle size around 22 µm.

##### Aggregation processes

Aggregation and disaggregation processes of particulate matter occur continuously in the ocean. Such processes depend on collisions between particles due to Brownian motion, fluid shear and differential settling. In this study, the aim was to simulate a dispersal of sediment plumes of four different particle concentrations (35, 105, 175 and 500 mg/l dry sediment) into the ocean interior below the permanent thermocline, where currents are strongly reduced and aggregation due to differential settling is the dominant aggregation process. The first three concentrations are recommended for the disposal of drill cuttings and were used for comparison with this offshore waste disposal (Pabortsava et al., 2011). An additional concentration of 500 mg/l was used to take into account the much higher disposal concentration behind deep-sea mining collectors such as the one proposed in this EIA. Core sample 68MUC, which represents the median size distribution of the 9 analysed sediment cores, was selected as a representative sample. Fixed amounts of surface sediments were diluted in filtered sea water (34.5 psu) and transferred into a 1.15 l roller tank. For the determination of aggregation due to differential settling (no shear), the rotation speed was fixed at 3 rpm to avoid effects of shear caused by centrifugal forces. For the determination of aggregation due to turbulent shear ( $G = 2.4, 5.7$  and  $10.4 \text{ s}^{-1}$ ), a horizontal Couette device which consists of an inner fixed cylinder and a rotating outer cylinder was used at a temperature of 1.5°C. Shear rates in the oceanic environments are typically only around  $10^{-2} \text{ s}^{-1}$ . The duration of the experiment was discussed with modellers and fixed to approximately three hours. The aggregation dynamics over time were followed using the LISST-100X and camera set-up described above.

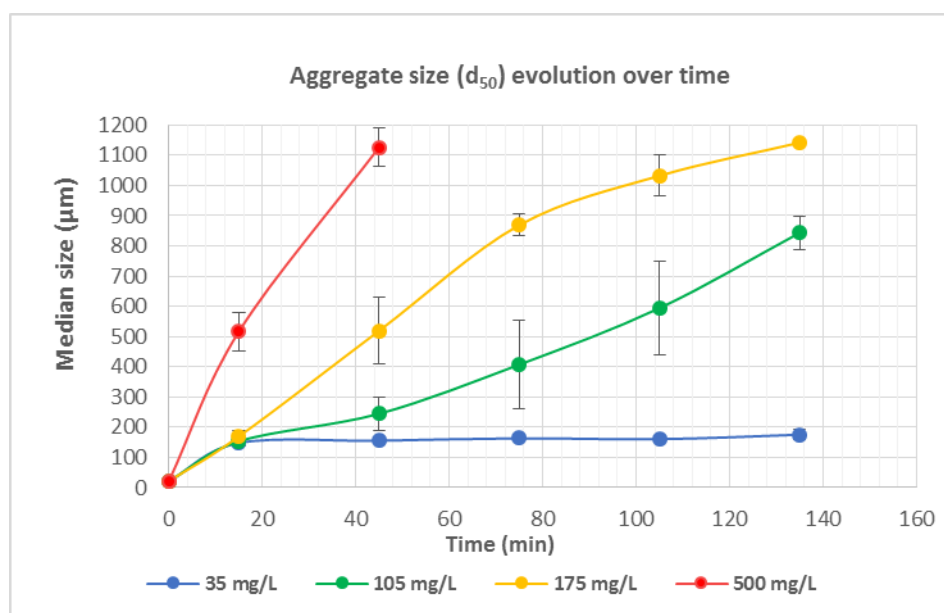


**Figure 4.34:** Median size ( $d_{50}$ ) of produced aggregates over time (under differential settling = zero shear).

The results of these and other experiments on particle behaviour are being prepared for publication (B. Gillard et al., in prep.). Both the discharge of 105 and 175 mg/l of surface sediment with  $d_{50}$  of ca. 20  $\mu\text{m}$  under zero shear resulted in the formation of large aggregates ( $\approx 900 \mu\text{m}$  in diameter) after 2 hours of settling (FIGURE 4.34). Between 30 and 70% of the clay particles were scavenged by aggregation within this time. Under a plume concentration of 500 mg/l, which is the expected concentration behind a nodule collector, this aggregation process already ended after 45 minutes. It could be shown that  $> 90\%$  of the clay fraction and  $> 80\%$  of the larger particles up to a size of 63  $\mu\text{m}$  were scavenged via aggregation within this time.

Experiments to analyse the effects of turbulent shear were carried out with plume concentrations of 175 and 500 mg/l. The discharge of surface sediments with  $d_{50}$  of  $\approx 20 \mu\text{m}$  resulted in the formation of large aggregates of 300- 900  $\mu\text{m}$  diameter within 10 to 30 minutes of turbulent condition for both concentrations, which is  $\approx 4$  times faster than under differential settling. A plume concentration of 500 mg/l under a shear rates ( $G$ ) of 2.4 (comparing to a water speed of ca. 20 cm/s) produced aggregates within 10 minutes. Under high turbulence of  $>10 G$  the aggregation process produced generally smaller aggregates which indicates disaggregation.

### Determination of settling velocity

The aggregate size vs. settling velocity relationship was investigated using a settling cylinder (square cross-section) (Thomsen and Gust, 2000). The particles were 360° down-illuminated and settling rates and particle sizes were determined by camera analysis. Differential settling of particles as a function of their size was determined. The results indicate that, at zero shear, aggregates formed under low plume concentrations depict generally higher settling velocities than particles of similar size formed under higher plume concentrations. This may be due to a process of “hindered settling”, when particles start to interfere and hinder each other, thereby reducing their settling velocity. As shown above, particle concentrations of 500 mg/l (dry sediment) resulted in the formation of large aggregates ( $\approx 1000 \mu\text{m}$  in diameter) after 45 minutes of settling. The settling velocity of these large aggregates ( $d_{50}$ ) was found to be only 0.2 cm/s (165 m/day). As such, these mineral plume aggregates settle considerably slower than sediments of similar size, but almost one order of magnitude faster than typical organo-mineral aggregates from the

benthic boundary layer of the deep sea (Thomsen et al., 2002). A clear deviation from the model-based calculations for sediments based on Stokes Law and from the recalculated settling velocities of Ferguson and Church (2004) for plume aggregates larger than 100  $\mu\text{m}$  is apparent, showing that the use of sinking velocities based on Stokes Law for e.g. plume modelling purposes, as has been done in the past (Nakata et al., 1997; Aleynik et al., 2017), does not reflect realistic particle behaviour in the plume.

Under turbulent shear  $G$  of  $2.4 \text{ s}^{-1}$ , the settling velocities of large aggregates in a plume of 500 mg/l are slightly higher than in the no shear situation. The aggregates formed are slightly smaller (800  $\mu\text{m}$ ), but settling velocities ( $d_{50}$ ) are slightly higher at 0.24 cm/s (210 m/day). However, the fine sediment fraction ( $d_{25}$ ) does not appear to be scavenged by the large aggregates at all and stays in suspension (9  $\mu\text{m}$  size; settling velocity of only 1 m/day).

These values have been used as primary input parameters for the plume modelling exercises in CHAPTER 6.4.3, in which an output plume concentration behind the collector has been set to 500 mg/l and the two scenarios  $G = 0$  and  $G = 2.4$  represent hydrodynamic conditions close to the seafloor during mean current flow and during the time of eddy passage (see CHAPTER 4.2.3.5), respectively.

#### 4.2.4.3 Pore water and sediment geochemistry

##### Pore water oxygen profiles

Most of the oxygen profiles deriving from the upper few centimetres of sediments retrieved with the multicorer or box corer show a strong decrease in concentration within the upper 1-2 centimetres and then decline only slightly with depth or stay on a more or less constant level over the remaining sediment interval of about 30–40 cm. Differences occur in the concentrations of oxygen at the sediment surface, which appear to be significantly higher at sites without nodules or with small nodules ( $\sim 200 \mu\text{mol/l}$ , FIGURE 4.35 c,d) than at sites with large nodules on the sediment surface (100-150  $\mu\text{mol/l}$ , FIGURE 4.35 a,b). Oxygen profiles measured with a respirometer also clearly reveal higher oxygen consumption in sediments without nodule coverage, suggesting that biological activity in the sediment decreases as nodule size increases. The strongest oxygen consumption takes place in the upper 5 cm of the sediment, where the  $\text{O}_2$  concentrations decrease sharply from 100-200  $\mu\text{mol/l}$  at the sediment surface to 30-40  $\mu\text{mol/l}$  at 5 cm sediment depth. In deeper sediments, concentrations tend to decrease more gradually.

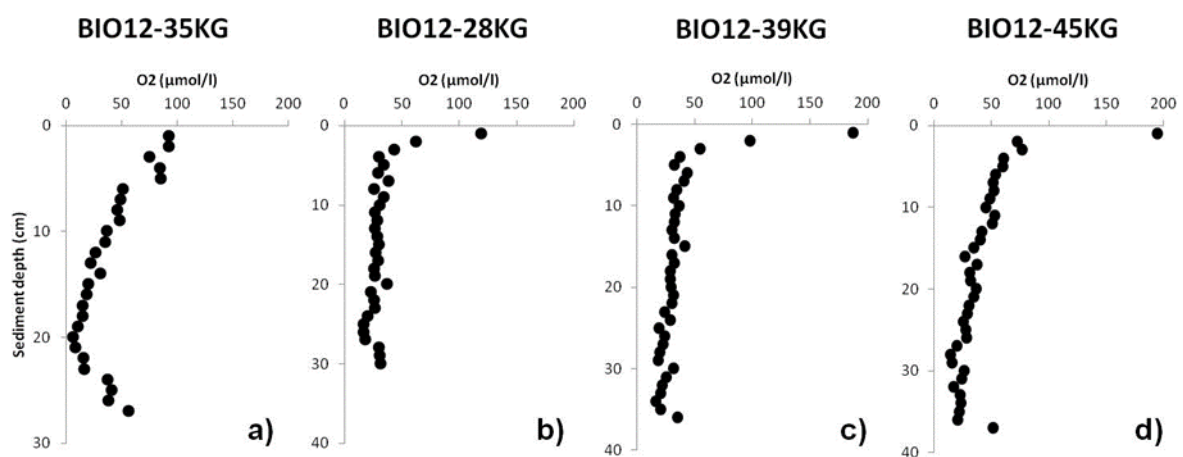


**Figure 4.35:** Oxygen profiles in box cores from PA1 with large nodules on the sediment surface (a, b), and in box cores from the PRZ with small nodules on the sediment surface (c, d).

Down-core pore water oxygen profiles of long sediment cores deriving from the Eastern German license area generally show decreasing oxygen concentration values that reach suboxic conditions (zero  $O_2$  concentration) between 1.5 and 3 m sediment depth (Mewes et al., 2014; Mogollon et al., 2016). These values increase to 4 m and more in the French and Belgian license areas, and oxygen is not completely consumed in APEI 3 (SO-239 cruise). However, re-increasing oxygen concentrations with depth have been found in the vicinity of seamounts (e.g. Teddy Bare seamount; Mewes et al., 2016), and the SO-240 cruise revealed that all sites located close to and at the foot of seamounts showed oxygen concentrations that first decreased with sediment depth and then re-increased again towards the basaltic basement (FIGURE 4.36). Sites located at a greater distance to seamounts did not show this type of oxygen-depth profile, but rather the typical oxygen penetration depth of 1 to 3 m described above. Oxygen apparently diffuses up into the basal sediments from the underlying crust as a result of low-temperature fluid/seawater circulation processes in the permeable basaltic crust (FLUM project; Kuhn et al., 2015), thus demonstrating the influence of seamounts on the redox environment of the overlying sediments. These results imply that the amount of organic matter reaching the seafloor is not the only factor determining the redox-zonation and oxygen penetration depth of these sediments, but rather that local transport and circulation patterns of fluids/seawater within seamount structures also play an important role. All in all, significant spatial variations in pore water profiles and biogeochemical fluxes are observed on km-scale. Unfortunately, *in situ* measurements of microbial POC degradation and respiration rates are currently missing and need to be performed during the proposed cruises in MiningImpact 2.

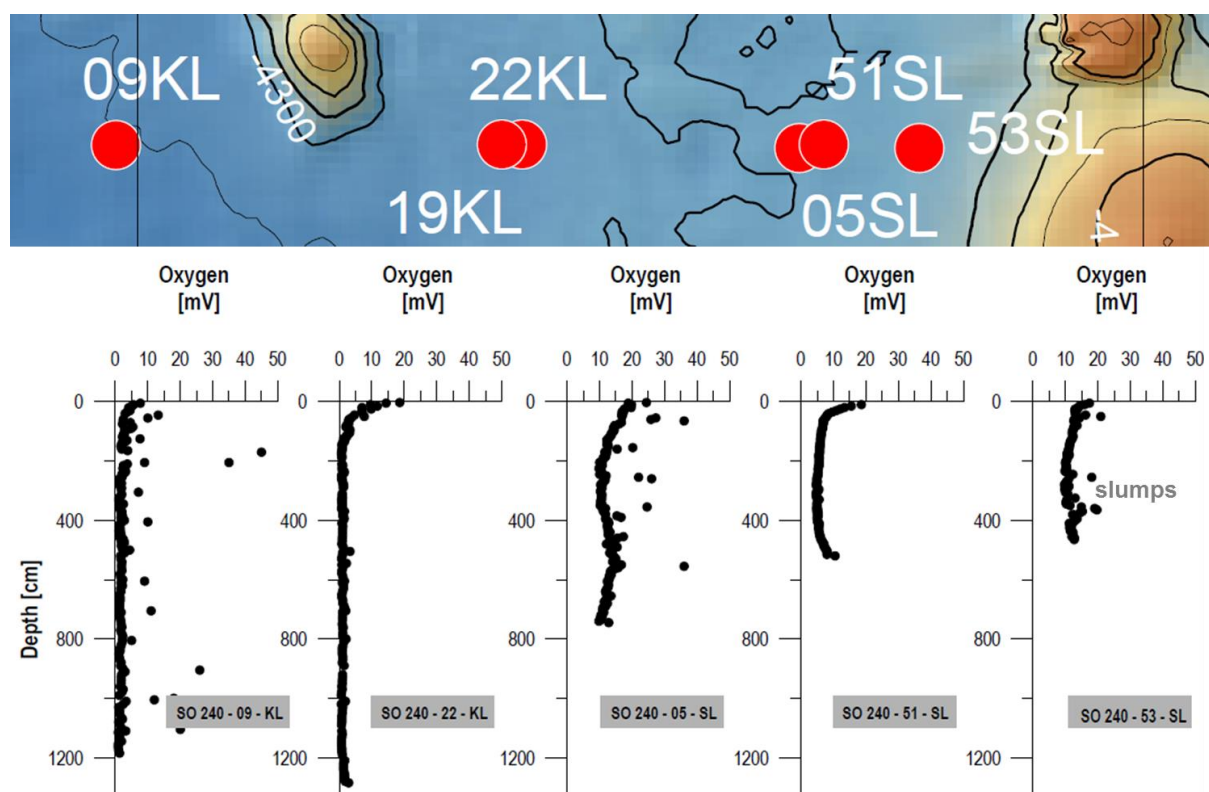


**Figure 4.36:** Oxygen concentration-depth profiles in long sediment cores deriving from sites located along a transect west of the Teddy Bare seamount in the northern part of the Eastern German license area. Figure from SO-240 cruise report (Kuhn et al., 2015).



In the northern part of the Eastern German license area, pore water concentration profiles for silica, phosphate and alkalinity as typical examples for nutrient content in the sediment are comparable between sites. Whereas silica often shows a typical increase with depth within the uppermost sediments, phosphate concentrations are low and fluctuate within a narrow concentration range of ca. 1 to 3  $\mu\text{mol/l}$ . At almost all sites sampled during cruise SO-240, phosphate concentrations show a decrease with increasing sediment depth. Alkalinity values are similarly low and show very similar and uniform values over depth of about 2.5 mmol (eq)/l at all stations (Kuhn et al., 2015).

### SO 240 - 22 - KL

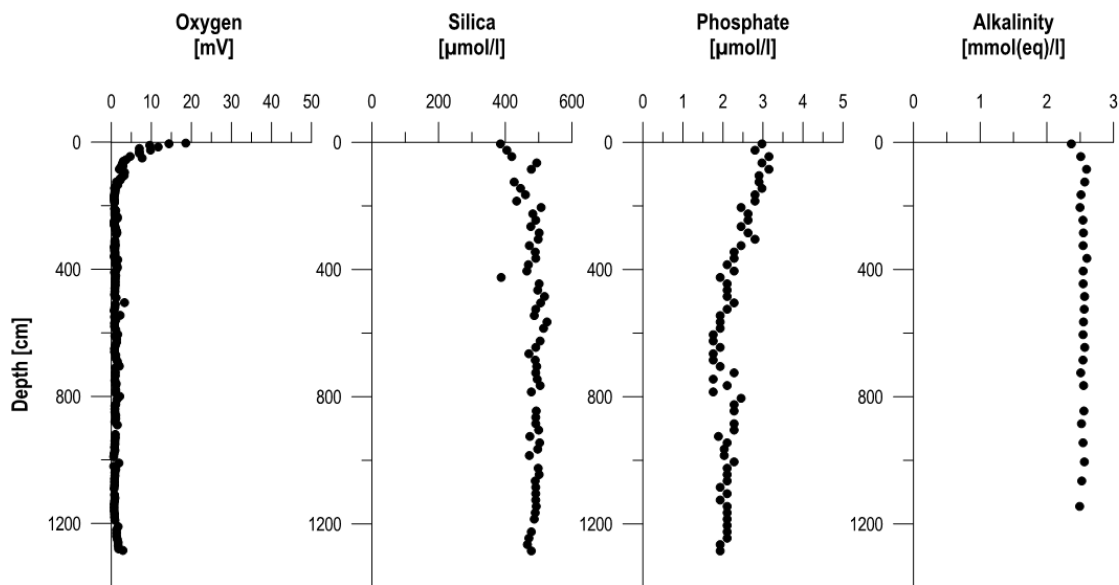


**Figure 4.37:** Typical pore water nutrient profiles in a piston core derived from an abyssal plain site close to the Teddy Bare seamount in the northern part of the Eastern German license area (see FIGURE 4.36 for location). Figure from SO-240 cruise report (Kuhn et al., 2015).

### Sediment geochemistry

Sediment samples from 37 box core stations scattered across the eastern license area were investigated for their total element concentrations using X-ray fluorescence. Rare Earth Elements and Yttrium (REY) were measured using a Laser Ablation ICP-MS. TABLE 4.5 shows total element concentrations in the box core sediments. The variability of Co, Cu, Mo, Ni and Zn is similar to that of Mn (see CoV in TABLE 4.5), which indicates that these metals are either bound to the Mn-oxide phase or display a similar geochemical behaviour. The sum of rare earth elements in surface sediments (at 1 cm and 4 cm depth) ranges from 194 to 236  $\mu\text{g/g}$  in the eastern area. Sediments display a significant negative Ce anomaly, a slightly positive anomaly of medium REE (Sm – Dy), and heavy REE (Ho – Lu) are more enriched than light REE (La – Nd).

**Table 4.5:** Statistics of total element concentrations in box core sediments (0-40 cm) from the eastern license area.

	Min.	Max.	Mean	Median	St.dev.	CoV
<b>SiO<sub>2</sub></b>	35.8	52.7	48.7	50.2	4.4	9
<b>TiO<sub>2</sub></b>	0.38	0.61	0.51	0.52	0.06	12
<b>Al<sub>2</sub>O<sub>3</sub></b>	8.84	13.9	11.8	11.8	1.34	11
<b>Fe<sub>2</sub>O<sub>3</sub></b>	4.54	6.81	5.93	6.02	0.58	9.8
<b>MnO</b>	0.06	1.17	0.33	0.3	0.25	<b>76</b>
<b>MgO</b>	2.11	3.27	2.78	2.83	0.27	9.6
<b>CaO</b>	1.07	16.7	3.4	1.21	4.5	<b>132</b>
<b>Na<sub>2</sub>O</b>	2.72	5.32	4.44	4.52	0.66	15
<b>K<sub>2</sub>O</b>	1.45	3.06	2.63	2.78	0.43	16
<b>P<sub>2</sub>O<sub>5</sub></b>	0.21	0.34	0.28	0.28	0.03	12
<b>LOI</b>	14.5	23.5	17	16.4	2.48	15
<b>Ba</b>	0.75	1.24	0.94	0.92	0.15	16
<b>Co</b>	20	76	42	39	15	<b>36</b>
<b>Cu</b>	54	308	157	151	61	<b>39</b>
<b>Mo</b>	3	7	4	4	1.24	<b>28</b>
<b>Ni</b>	57	259	101	83	<b>48</b>	<b>47</b>
<b>Pb</b>	4	11	7	6	1.62	24
<b>V</b>	72	110	92	95	9.8	11
<b>Zn</b>	10	41	25	25	10	<b>41</b>
<b>Zr</b>	106	173	141	141	19	14

Oxides, LOI (loss on ignition), Ba in wt-%; Elements in µg/g; St.dev.: Standard Deviation; CoV: Coefficient of Variation in % (=St.dev./Mean\*100); N=37

The H<sub>2</sub>O<sub>2</sub> leachable fraction of the sediments was also analysed. The most significant feature is the Mn content of the surface sediments, which ranges between 3000 and about 7000 µg/g and decreases strongly in the layer 10 to 30 cm below the sediment surface. This Mn decrease could be observed in more than 37 box cores and is a common feature of the license area. It is related to diagenetic Mn mobilisation in sediments and the enrichment of Mn in surface nodules (Kuhn et al., 2017a). Metals related to Mn such as Co, Cu, and Ni display the same distribution patterns in the upper 30–40 cm of sediment. One other important observation is that in most cores, the Ni content is higher than the Cu content in the surface sediments, but this relation is inverted in sediments below the seafloor in some box cores.

### Total Organic Carbon (TOC) and carbonate concentrations

The total carbon content (TC) and the content of organic carbon (TOC) were determined using a LECO CS 230. TC was measured on untreated samples at 1800°-2200°C. TOC was measured after sample treatment using 2N HCl at 80°C to remove carbonate. The latter was calculated from the difference between TC and TOC.

The TOC content at the sediment surface in the eastern license area typically ranges between 0.4 and 0.65 wt.%, values that are typical for mesotrophic ocean areas (FIGURE 4.38). Highest TOC contents occur in the easternmost area. In contrast, TOC values in the western license area are much lower at ca. 0.25 wt.%. The significant difference between these areas can be attributed to the higher bio-productivity in surface waters of the eastern area. The surface water chlorophyll content as an indicator of bio-productivity is 0.1-0.2 mg/m<sup>3</sup> in the east and 0.07-0.08 mg/m<sup>3</sup> in the west (ISA, 2010). TOC concentrations

in sediment cores deriving from the eastern license area decrease with depth to ca. 0.2 wt.% below 30 cm bsf, which is a prominent feature in all box cores (FIGURE 4.38).

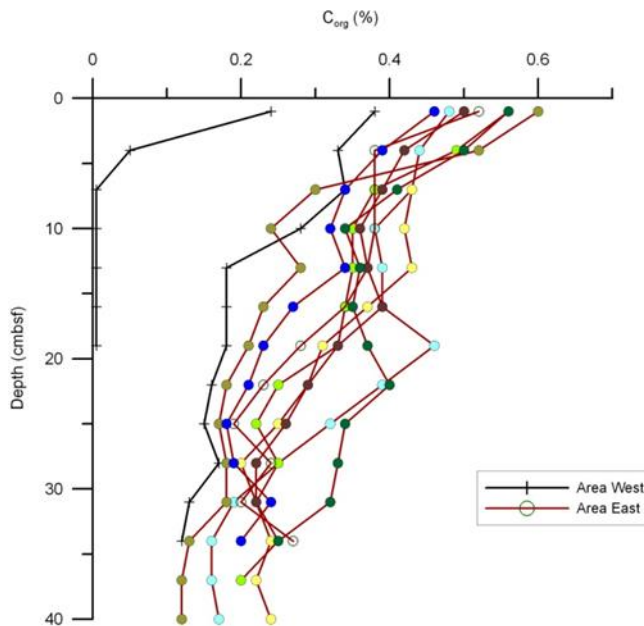


**Figure 4.38:** Total organic carbon (TOC) content of box core sediments from the eastern and western license areas. Note that TOC values are distinctly higher in the eastern area.

The carbonate concentrations ( $C_{carb}$ ) are generally low, not exceeding 1 wt.% in most of the (sub)surface samples (~0.08-0.9 wt.%). However, there are some box cores with  $CaCO_3$  contents between 1 and 10 wt.%, and in the eastern part of the license area some box cores show prominent  $C_{carb}$  peaks between 13 and 31 cm sediment depth with significantly higher  $CaCO_3$  concentrations (10-66 wt.%; FIGURE 4.39).

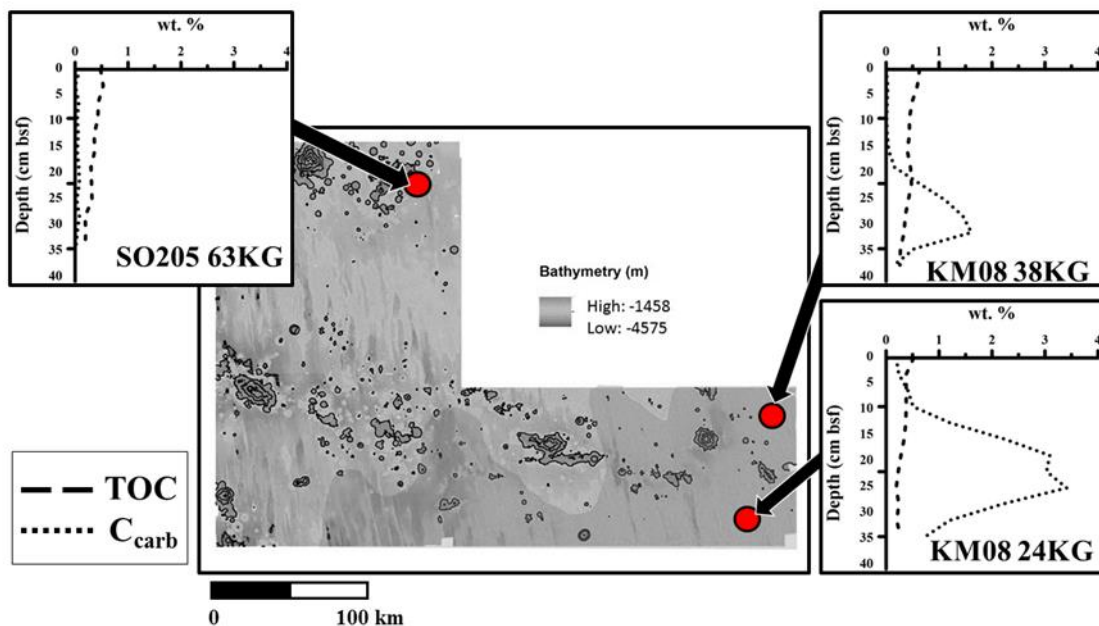


**Figure 4.39:** Total organic carbon (TOC) and carbonate ( $C_{carb}$ ) concentration profiles at selected box core sites in the eastern license area. Sediments in the south-east are characterised by a prominent  $C_{carb}$  peak at depth (dark grey area in the map) which does not occur in the north-west. Figure from Widmann (2014).

#### 4.2.4.4 Sedimentation rates

AMS radiocarbon age dating was carried out on samples from 4 box core sites, in which a carbonate-rich horizon between 25 and 31 cm bsf consisting of significantly increased amounts of planktonic foraminifera was sampled (Hoppe, 2015). Samples were converted to graphite prior to AMS carbon dating. The measurements were carried out at the commercial laboratory Beta Analytic Inc. following their standard procedure. The inferred radiocarbon ages range between ~ 28 and > 43.5 ka BP (TABLE 4.6). The average sedimentation rate of the upper 25-31 cm of sediment based on these AMS ages amounts to 0.6-0.9 cm/kyr.

**Table 4.6:** AMS radiocarbon ages of foraminifera-rich layers in four box cores.

Sample	Depth (cm)	Measured Age (BP)	Conventional Age (BP)	2 Sigma Calibration	Sedimentation Rate (cm/kyr)
SO205-45KG	28	34900 +/- 270	35310 +/- 270	38790 - 40035	0.79
SO205-18KG	25	NA	> 43500		0.57
KM08-38KG	31	41500 +/- 550	41950 +/- 550	44050 - 45840	0.74
KM08-21KG	25	27980 +/- 130	28380 +/- 130	31420 - 31955	0.88

Sediment thickness is highly variable in the license area reaching from 0 to about 100 m with an average of 40 m (Kuhn et al., 2017b). Dating of four long sediment cores from the Eastern license area covering the last ca. 10 million years has been attempted using (a) the decay of the authigenic  $^{10}\text{Be}/^9\text{Be}$  ratio, whose exponential decrease with core depth reflects average sedimentation rates over millions of years, and (b) diatom stratigraphy. Sedimentation rates of surface sediments (last 100.000 years) range between 0.4 and 0.9 cm/kyr (BGR data and Mewes et al., 2014). Older sediments (up to 10 Ma) were deposited with rates varying between 0.02 and 0.35 cm/kyr. There are significant variations in the sedimentation rates from different locations which are caused by (1) the primary production in the surface waters, (2) different rates of consumption of organic material during its pathway through the water column, and (3) speeds of near-bottom currents, which are affected by seafloor topography (seamounts, ridges, pits, etc.) (see also CHAPTER 6.4.2.1).

#### 4.2.5 NATURAL HAZARDS

Natural hazards in the Eastern German license area may include volcanism, seismic activity and the occurrence of cyclones and/or hurricanes.

The numerous seamounts in the eastern German license area are all of submarine volcanic origin. Their formation is related to the seafloor spreading of the East Pacific Rise 18–22 Ma (Barckhausen et al., 2013). Ash particles found in different depths of sediment cores derive from the American continent, indicating that there has been no submarine volcanic activity in the license area for at least the last 10 Million years (BGR data).

Seismic measurements carried out during cruise SO-240 in 2015 (Kuhn et al., 2015) have shown that numerous faults have fragmented the basaltic crust beneath the sediments. Most of the faults are limited to the basaltic crust but there are some faults protruding the sediments and reaching the seafloor. The formation of the faults is again related to the seafloor spreading process during which the oceanic lithosphere was formed on the East Pacific Rise about 18–22 Ma ago. There is no information on recent seismic activity in the area.

The average number of tropical storms and hurricanes that pass through the Eastern German license area is described in CHAPTER 4.2.2 and FIGURE 4.10.

#### 4.2.6 NOISE

Sound is carried in water much faster than in air. It is used by sea mammals, fish and some invertebrates as communication. Artificial sound can disturb animals and inhibit their communication. However, for most animals (and especially for deep-sea animals), the direct effect of sound is unknown (Ortega, 2014).

The principal sources of ambient ocean sound are (1) ocean turbulence and microseisms at the lowest frequencies (0.1 to 10 Hz) (Webb, 1992); (2) wind-related surface noise (between 1 and 30 kHz) (Naumann, 2008); and (3) thermal noise of water molecules (100 kHz and more) (Dahl et al., 2007). Biogenic background noise is created by whales, dolphins, fishes and invertebrates for communication, navigation, echolocation and feeding purposes. The range of frequencies used by living organisms extends from less than 10 Hz to more than 200 Hz.

The frequency range from shipping activities is broad (50-150 Hz up to 10 kHz), since it is largely related to distance from the source (i.e. the vessel) or the type of noise emission (Dahl et al., 2007). Drilling and dredging noise does impact biological activity (Richardson et al., 1990). Commercial shipping produces low frequency noise, such as noise from the propeller, hydrodynamic hull flow, engines and other machinery (McKenna et al., 2012). However, shipping traffic through the CCZ is infrequent as shown by FIGURE 4.40.

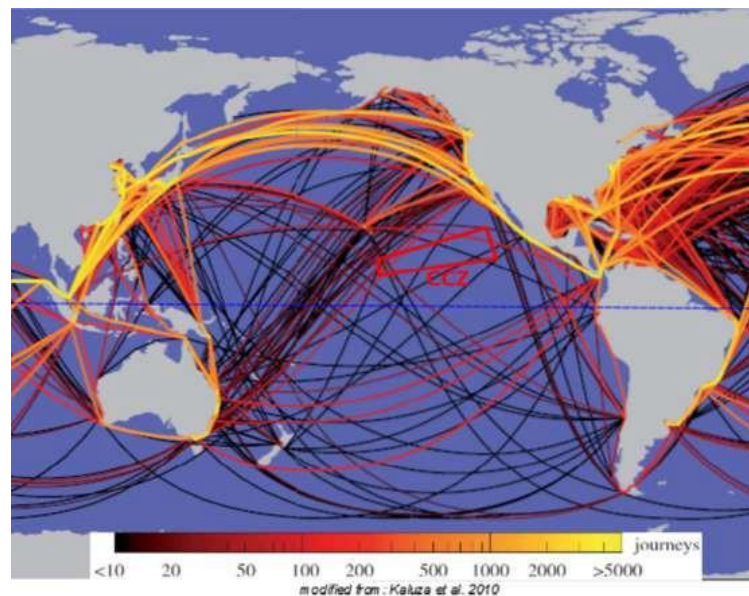


**Figure 4.40:** Shipping routes across the Pacific Ocean.



## 5. Description of the existing biological environment

### 5.1 Regional overview

The CCZ is a spatially very heterogeneous environment, characterised by gradual changes of environmental conditions such as nodule sizes and densities, differences in surface productivity and depths (ISA 2010, Wedding et al., 2013). The CCZ and, more specifically, the Eastern German license area (see CHAPTER 4.1 for a geographical and geological overview), is known to be highly diverse, harbouring a high number of different species and a substantial proportion of species are unknown to science (Glover et al., 2002; Ramirez-Llodra et al., 2010; Janssen et al., 2015). Overall, benthic faunal densities are low and most species are considered to be rare. This is a typical characteristic of deep-sea diversity, which constitutes a major challenge when assessing biogeography and connectivity patterns (Glover et al., 2002; Janssen et al. 2015). However, taxonomic studies during the last decade have drastically increased the number of known species (Dahlgren et al., 2016; Glover et al., 2016b; Wiklund et al., in press), showing that even relatively limited research efforts can significantly increase the baseline ecosystem knowledge of the region. The relevance of molecular approaches for biodiversity and connectivity assessments in the CCZ has been recognised (Janssen et al., 2015) and the first phase of the JPI-O MiningImpact project has provided a quality reference database of vouchered and barcoded specimens from the CCZ as well as relevant knowledge on the distribution and connectivity of several common macrofauna species (Glover et al., 2016a; Taboada et al., in press). However, studies addressing connectivity in abyssal areas are few (Taylor and Roterman, 2017) and better data from REM taxa (i.e. Rare, nodule-Endemic and Megafauna) are required that represent both the majority of the macrofauna and the vulnerable sessile suspension feeders in nodule areas. Issues such as connectivity, regional community analysis and (regional) spatial modelling approaches are not inherently linked to the work carried out by individual contractors within their license areas, but rather form larger-scale scientific topics needing project and contractor collaboration. Taxonomic impediment, lack of standardisation of data collection, and the required spatial and temporal scales for sampling and analysis are further issues that need to be tackled collaboratively, to name but a few.

Analyses of biodiversity and benthic faunal abundances are prone to statistical uncertainties. For example, the number of macrofaunal organisms obtained from one box core deployment, i.e. the macrofaunal sample size, is so small that we still have no clear perception of the actual number of deep-sea species living in the abyssal CCZ. A total macrofaunal density of 37-202 individuals per box core sample (0.25 m<sup>2</sup>) has been registered for the Eastern German license area (n = 139), with high numbers of rare species. For polychaetes this means that there are about 5-30 specimens per core, but in general only one or two species are found in the sample that occur with more than 3 or 4 individuals. Detailed analyses based on individual species' distributions (e.g. those used in genetic connectivity and population genetic analyses) will thus only work for several species of polychaetes or isopods. In all other efforts, low sample sizes give many estimates (e.g. diversity) a descriptive character and lumping species into higher taxonomic groups (key taxa) or functional groups is probably the only way forward to obtain robust information on spatial and temporal variations in macrofaunal densities and biomass. The number of meiofaunal specimens and species obtained from multicorer deployments are statistically more robust as at least 5 cores from one sampling site are used for analysis, with ca. 600-4000 individuals occurring in the top 5 cm of each core (n = 77), facilitating the direct comparison of distant samples. Nevertheless, the

quantity of rare species is extremely high and so the grouping into key taxa and/or functional groups is just as important as for the macrofauna.

Key biological conclusions from the first phase of the MiningImpact project are that (1) deep-sea ecosystems associated with polymetallic nodules support a highly diverse fauna, (2) deep-sea faunal communities show a high variability on both small and large spatial scales, but their connectivity over the relevant scales required for the definition of Preservation Reference Zones and for conservation purposes (e.g. APEIs) remains unknown, (3) temporal variations of faunal abundances remain uncertain due to the paucity of long-term ecological time series, and (4) loss of seafloor integrity by removal of nodules and surface seafloor reduces population densities and ecosystem functions (e.g. nutrient remineralisation, microbial growth, bioturbation activity).

Despite many of the unknowns and restrictions described above, the Eastern German license area and in particular the prospective area PA1-West (IRZ) and its associated PRZ (FIGURE 4.1) probably represent the best-studied area of the whole CCZ in terms of biological sampling and analysis. For environmental baseline studies, it is important to analyse a whole range of organisms of preferably all size categories and life history traits as the organisms presumably might be unequally affected by a potential mining activities. This chapter provides a comprehensive dataset of all size classes of the benthic fauna of the CCZ and contributes significantly to the understanding of biodiversity in the manganese nodule belt. The distribution, abundance, community structure and biodiversity of benthic faunal species within the German license area has been studied by the German Center for Marine Biodiversity Research (DZMB, Senckenberg am Meer, Wilhelmshaven, Germany) since 2010. The sampling effort in PA1-West is described in CHAPTER 3.2 and summarised in FIGURE 4.3.

## **5.2 Biological communities in and around the Eastern German license area**

### **5.2.1 SURFACE**

#### **5.2.1.1 Seabirds and marine mammals**

No detailed surveys and distribution assessments of the distribution of seabirds and marine mammals during ship cruises have occurred in the Eastern German license area so far, despite the fact that they are excellent bio-indicators (as they are relatively easily observed) and constitute the upper trophic levels of the food chain. Their distribution potentially reflects prey abundance (e.g. phytoplankton, zooplankton, nekton and fish) and is thereby a reflection of the ecology and the biological production of the upper water column.

Birds and mammals were recorded on a non-standardised but daily basis from the bridge of the ship only during the MiningImpact SO-239 cruise (Martínez-Arbizu and Haeckel, 2015). A total of 15 bird species, most of them rare, were observed across the CCZ during the cruise, of which 6 species were seen in the German license area. Fairly abundant occurrences of Leach's Storm Petrel and especially the Masked Booby were registered. The latter have had a tradition of resting on the ship during exploration cruises in groups of up to 40 specimens during the last few years and appear to be resident in the area. Only 1 Minke whale was observed in the CCZ during SO-239 (in the Belgian license area). No whales have ever been observed in the German license area during any of the BGR exploration cruises. Several specimens of marine turtles and sharks have been observed, but always in extremely low numbers.

### 5.2.1.2 Phytoplankton

Not much is known on the phytoplankton diversity, standing crop and primary production in the Eastern German license area or its surroundings. Over 1000 taxa of phytoplankton are known from the Pacific (Semina, 1974). Analyses from the 1970ies from the US American DOMES project (Deep Ocean Mining Environmental Study) in the area between 5 and 20°N and 128 and 155°W showed that average phytoplankton concentrations are in the range of 20,000 cells/l, with diatoms, dinoflagellates and coccolithophorids making up half of that number (Fryxell et al., 1979). Coccolithophorids were dominant at some depths, and ~85% of the total chlorophyll a concentration in the upper water column was made up of nanoplankton, *Emiliania huxleyi* being the dominant species (El-Sayed and Taguchi, 1979). Many of the oceanic species are widely distributed. Half of the diatom species found in the DOMES analyses were, for example, also found in the Mozambique Channel, as were 57% of the dinoflagellate species (Fryxell et al., 1979). Nevertheless, small-scale horizontal patterns in phytoplankton distribution occur, and diversity indices reveal the complexity of phytoplankton communities in the CCZ (Fryxell et al., 1979).

In the Eastern German license area, water samples from the photic zone (uppermost 200 m of the water column) have been taken from area PA1-West using a CTD-rosette and plankton nets (1) for baseline investigations of the diversity of phytoplanktonic dinophysoid dinoflagellates, a major lineage of the group of dinoflagellates with special morphological characters, in the CCZ, and (2) for the isolation and cultivation of representative phytoplanktonic species from the study site, which amongst others will be used in aggregation experiments to simulate the effect of a phytoplankton plume on particle behaviour in a sediment plume as described in CHAPTER 4.2.4.2.

Phytoplanktonic dinophysoid dinoflagellates are mainly heterotrophic organisms that occur in very low abundances at unknown depths between the water surface and about 200 m water depth. Many of the species are only known from very few light-microscopic observations alone. 132 dinophysoid species were recorded from the Eastern tropical Pacific by Kofoid and Skogsberg as early as 1928. However, samples for the analysis of dinoflagellates from the German license area in the CCZ were taken during the MANGAN 2013 and 2016 cruises for the first time (Rühlemann et al., 2014). 65 dinophysoid dinoflagellate species were observed during these investigations, including 4 potentially new species (Zinßmeister et al., 2016). Some of the species found were represented by a single cell only.

### 5.2.1.3 Zooplankton

Zooplankton communities have never been studied in the German license area. Merely one plankton sample obtained from PA1-West (0-250 m depth) has been analysed for the diversity and distribution of zooplankton species, in order to set up a molecular library of zooplankton for the genes 18s (hypervariable regions V1- V2) and the COI gene (barcoding gene). Once the library is functional, it will be used to assign the reads of Next Generation Sequencing (NGS) metabarcoding to barcoded species. Metabarcoding is a method that deals with large numbers of undescribed species by regarding the community as a whole instead of individual species. Such an approach can also be archived via molecular identification in metabarcoding (Bik et al., 2012). Analyses of zooplankton samples obtained during the next baseline exploration cruise to the collector test area in April/May 2018 will be fed into the library and first metabarcoding sequencing tests will be performed to test the efficiency of the method.

82 species of zooplankton were found in the sample by morphological examination; the dominant group was the Ostracoda (*Vargula* sp. 1). The subclass Copepoda had the highest species richness (57 spp.), and rare species such as *Clytemnestra gracilis*, *Clytemnestra* sp.2, *Miracia gracilis* and *Macrosetella* sp. 1 were also found. The molecular method, in which amplicons were sequenced in 2 runs on an Illumina MiSeq Sequencer, identified 70 different species in the Bayesian tree of mtDNA COI sequences. This first

test shows that the method of Miseq metabarcoding is very promising for a rapid future identification of zooplankton.

### 5.2.2 MIDWATER

Midwater zooplankton, mesopelagic and bathypelagic fish, and deep-diving mammals present in midwaters have never been studied in the German license area, and we are not aware of studies from neighbouring contractors or from overarching scientific projects that have dedicated monitoring or research capacities to these midwater pelagics. We refrain from carrying out more detailed literature analyses of these organisms in the framework of this EIA as no environmental impacts are expected within this water mass (see CHAPTER 7.3).

### 5.2.3 SEAFLOOR

In the soft sediment of the seafloor of the CCZ, the dominant metazoan meiofaunal groups are nematodes, followed by harpacticoid copepods, while polychaetes and isopod crustaceans dominate the macrofaunal taxa, and typical megafauna is comprised of ophiuroids, holothurians, fish and large komokiaceans and xenophyophore protists (Gollner et al., 2017). Diversity is very high on a local scale as well as throughout the entire CCZ. Changes in benthic faunal composition, abundance and diversity have been related to variations in surface primary productivity and the corresponding flux of organic carbon to the abyssal seafloor. Abundance and biomass of all faunal size classes (meio, macro- and megafauna) typically decrease along the productivity gradient from eutrophic (eastern CCZ) to oligotrophic (western CCZ) environments (Martínez-Arbizu and Haeckel, 2015). Evidence of a wide geographic distribution exists for some genotypic clusters (e.g., polychaetes and isopods), that appear to be related not only to life history but also to distance (Janssen et al., 2015). However, assessing population and ecological connectivity across the CCZ is currently limited by low sample numbers, a patchy sampling scheme restricted to certain license areas within the CCZ, and the high proportion of undescribed species (Gollner et al., 2017).

Spatial heterogeneity is known to influence the structure and composition of benthic communities, as well as the rate of deposition of sinking particulate organic matter in abyssal plains (Morris et al., 2016). In the CCZ, there is increasing evidence that at the local scale, nodules influence the structure and composition of both infaunal (Miljutina et al., 2010) and epifaunal communities (Vanreusel et al., 2016).

The distribution, abundance, community structure and biodiversity of benthic faunal species within the Eastern German license area have focused and are still focusing strongly on the study of macrofaunal polychaetes and isopods, as (1) these taxa dominate abyssal macrofauna communities in terms of abundance and species richness (e.g. Paterson et al., 1998; Glover et al., 2001), and (2) these taxa are representatives of different life strategies, with polychaetes being the most common infaunal organisms (living in the sediment) whilst isopods are the most common epifaunal organisms (living on the sediment). Furthermore, success rates in molecular (DNA) extraction, amplification and sequencing processes are relatively high in these organisms and allow detailed determinations. Nevertheless, substantial effort has also gone into the determination of megafaunal, epifaunal and meiofaunal diversity and distribution patterns.

Molecular (DNA) analytical methods suggest that morphological techniques typically underestimate the number of species and overestimate species ranges in marine habitats (Knowlton, 2000; Van Soosten et al., 1998; Creasey and Rogers, 1999). However, morphological studies of organisms are pivotal to understanding and calibrating genetic results. DZMB has successfully overcome this problem by applying

a reverse taxonomic approach as developed by Janssen et al. (2015): i.e. mega-, macro- and meiofaunal organisms have been analysed with molecular methods in order to determine the distribution range of species and the faunistic similarity between the different areas, after which the identity of shared MOTUs (molecular operational taxonomic units, i.e. putative species) is tested using traditional morphological methods. Up to now, this approach appears to provide the most robust estimates of biodiversity and species ranges and is being adopted by other contractors in the CCZ.

A further aim of DZMB has been to carry out a population genetic study throughout the eastern license area on the basis of the five most abundant polychaete and isopod species, in order to infer the degree of genetic exchange among their populations, to determine some of the important factors influencing extinction and immigration rates and to address fundamental questions regarding connectivity of the deep benthos among pristine and potential impacted areas prior to mineral exploitation: (a) Is there a significant genetic structure between populations across the license area in terms of spatial or temporal scales? (b) Do the life history strategies of species reflect the observed patterns of genetic connectivity? (c) Which conclusions can be drawn in terms of the efficacy of PRZs and IRZs to preserve benthic fauna in part and enable successful recolonisation?

### 5.2.3.1 Megafaunal diversity

#### Morphological analyses of megafauna

Megafaunal composition and richness has been examined during all BGR exploration cruises through the preliminary analysis of in situ still and video images of the seafloor taken by the HD camera installed on the video sledge. A high variety of different megafaunal organisms was observed on the seafloor. Megafauna catalogues were produced during each cruise, which were subsequently submitted to the ISA. 89 morphospecies from 9 different phyla, of which 26 morphospecies were considered to be widespread throughout the eastern license area, were described during the BIONOD 2012 cruise; 162 morphospecies from 16 different phyla were identified in PA1 during the cruise MANGAN 2013, and 121 morphospecies from at least 7 different phyla and 11 different classes were identified during the cruise MANGAN 2014. During the MANGAN 2014 cruise, a comparison between the eastern (PA1, PA2) and the western German license areas showed that only 31% of all morphospecies occurred in both areas, whereas 39% were only observed in the eastern and 30% only in the western area.

Video observations made during the SO-239 and SO-240 cruises reveal a different fauna on seamounts compared to that of the abyssal plains. Echinoderms and poriferans are most abundant in the deep-sea plains, whereas anthozoans are most abundant at the seamounts and on their slopes (Martínez-Arbizu and Haeckel, 2015). Every analysed seamount was found to be different. Especially the Ophiuroids on seamounts were found to be completely different to those in the abyssal plains.

A total of 49 megafaunal specimens mainly belonging to the groups Porifera, Anthozoa and Ophiuroidea were collected for detailed morphological and biomolecular analysis during 5 ROV dives (SO-239) in the eastern German license area (PA1 nodule field, two seamounts fringing the PRZ and the IRZ, one 3-year-old EBS track in PA1 and one EBS track directly after deployment). Two amphipod baited traps/landers deployed in PA1 were also successful in sampling several amphipods and fish. In total, specimens of 18 different taxa of amphipods and fish were collected from across the CCZ (Martínez-Arbizu and Haeckel, 2015). Two standardised video transects were carried out with the ROV along the 3-year-old EBS track in PA1 and along a freshly produced EBS track in the PRZ. Surveys conducted along experimental tracks revealed an extremely impoverished epifauna compared to undisturbed areas in the vicinity (see CHAPTER 5.2.3.7).



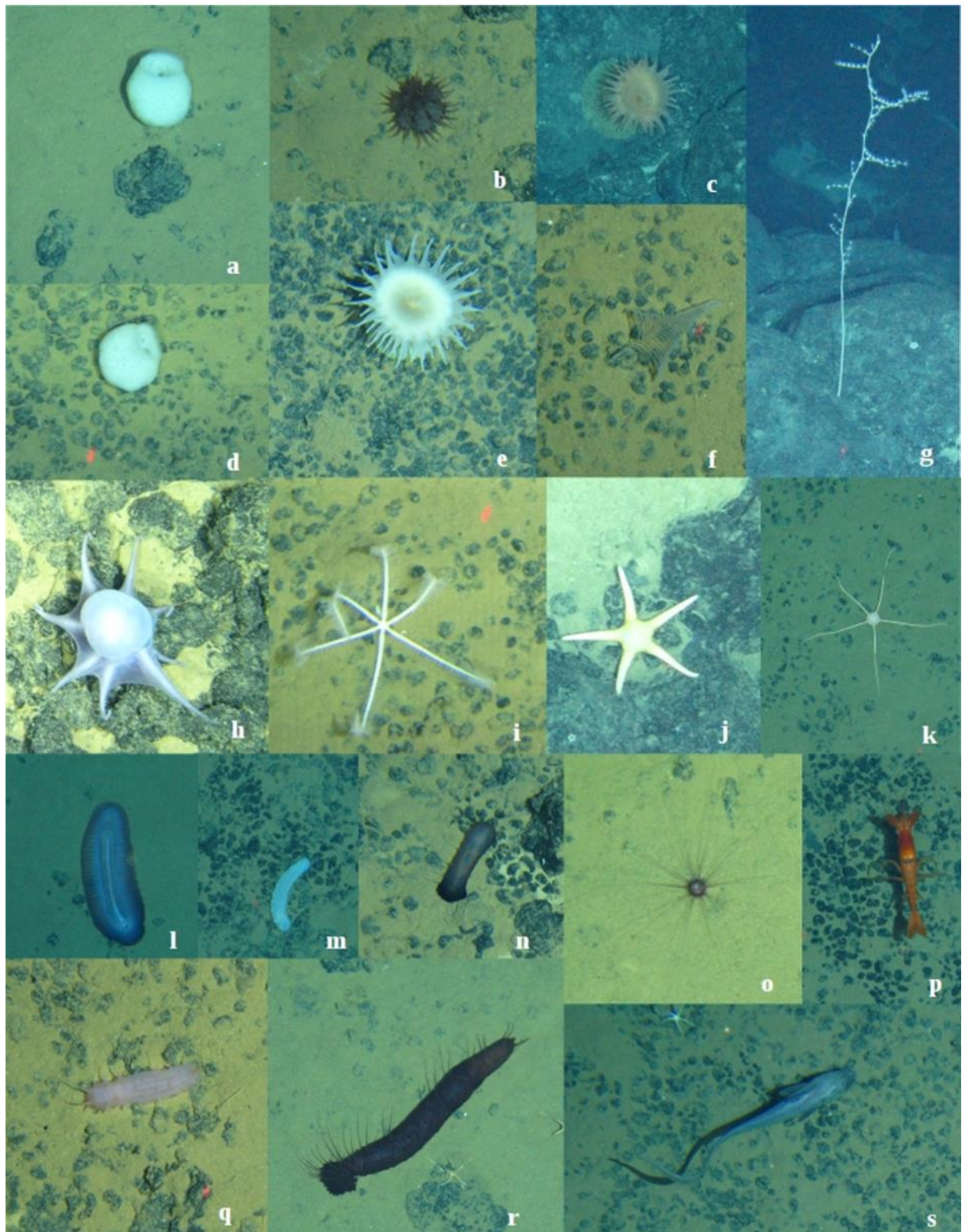


**Figure 5.1:** Typical megafaunal organisms observed by video sledge during cruise SO-240 from the Eastern German license area. a,d: Porifera; b-c, e-f: Cnidara, Hexacorallia; g: Cnidara, Octocorallia; h: Mollusca, Cephalopoda; i,j: Echinodermata, Asteroidea; k: Echinodermata, Ophiuroidea; l-n, q-r: Echinodermata, Holothuridea; o: Echinodermata, Echinoidea; p: Crustacea, Mysida; s: Pisces, Actinopterygii.

### Molecular analyses of Ophiuroidea

Specimens of the Echinodermata have been investigated genetically based on sequencing of part of the mitochondrial COI gene (barcoding approach). Echinodermata comprise an essential part of the megafaunal fauna of the deep sea (Hughes et al., 2011). Most Echinodermata, such as Ophiuroidea and Asteroidea, are mobile and therefore they do not rely on the nodules as hard substrate. During a long-term study in the north-eastern Pacific, the Echinodermata represented more than 99% of the mobile megabenthic fauna (Ruhl, 2007). However, in another study in the same area, just more than half of the megafaunal taxa (mobile and sessile) were Echinodermata (Foell and Pawson, 1986). Despite their widespread abundance, the influences of activities such as deep-sea mining on these organisms remain uncertain (Bluhm, 2001).

Ophiuroids were sampled from license areas across the CCZ during cruise SO-239 using the ROV. Nine different species could be identified. Six of these species occurred only once, one species occurred with three individuals and two species occurred in higher abundances. In the UK license area that was sampled during the cruise Abyssline 1 with R/V Melville in October 2013, six species were found additionally to the species observed during SO-239. However, the two most abundant species of SO-239 also occurred in the UK license area.

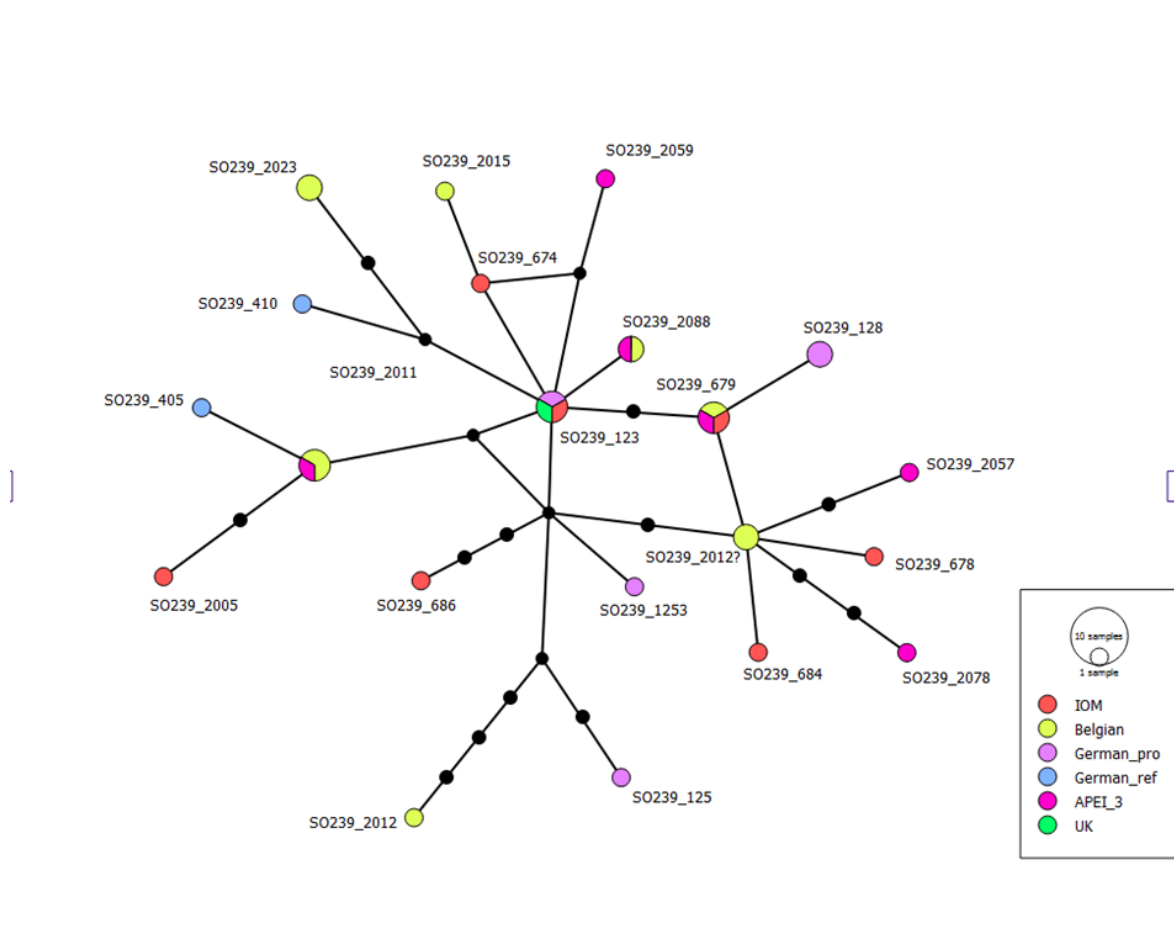


**Figure 5.2:** Haplotype network of *Ophiomusium glabrum* Lütken & Mortensen, 1899. Specimens were obtained from different areas of the CCZ and genetic analyses are based on the mitochondrial COI gene.

The species that occurred most frequently has been determined as *Ophiomusium glabrum* Lütken & Mortensen, 1899. This species has an extremely broad distribution as it does not only occur in the deep sea, but has also been reported from depths varying between 1820 m and 4028 m (Baker, 2016). In the CCZ it has been sampled in all areas except for seamount sites. Although individuals of *O. glabrum*

display a large morphological variation, no barriers seem to prevent gene flow between the populations in different areas (FIGURE 5.2). A reason for this broad range might be the planktonic larval stadium (Ward et al., 2008). Drifting through the water column, juveniles can reach distant areas that are unreachable for adult individuals.

One clade of species has been found exclusively in the Eastern German license area and has been hypothesised to consist of an endemic species-complex of this area. However, individuals fitting into this species-complex have been found also in the DISCOL area (Peru Basin) about 3000 km away. An explanation might be that differences in megafaunal abundance can even be observed between different years at the same deep-sea location (Ruhl, 2007). The species composition observed during cruise SO-239 can only be regarded as a snapshot of the ophiuroidean community.

### 5.2.3.2 IRZ vs. PRZ: Faunal composition and population genetic analyses

#### Macrofaunal composition and densities derived from boxcorer samples

Twenty-five different macrofaunal taxa were found in box cores obtained from the Impact Reference Zone (IRZ) and Preservation Reference Zone (PRZ) during the MANGAN 2013 cruise (for locations of the IRZ and PRZ, see FIGURE 4.1). In terms of mean abundances per square meter, the most abundant taxa were the copepods ( $>300 \mu\text{m}$ ; Harpacticoida  $131 \pm 21 \text{ ind./m}^2$  and Calanoida  $52 \pm 9 \text{ ind./m}^2$ ), followed by the polychaetes ( $91 \pm 9 \text{ ind./m}^2$ ), tanaids ( $67 \pm 7 \text{ ind./m}^2$ ) and isopods ( $27 \pm 4 \text{ ind./m}^2$ ). All other taxa such as Crustaceans (Amphipoda, Cumacea, Ostracoda, Mysidacea, Decapoda), Nematoda, Mollusca (Bivalvia, Gastropoda, Scaphopoda, Solenogastres, Polyplacophora), Sipunculidae, Echinodermata (Asteroidea, Echinoidea, Ophiuroidea), Chaetognatha, Pantopoda, Acari, Cnidaria and Bryozoa were found to be scarce and are not present at each sampling site.

Total macrofaunal abundances (indiv. per  $\text{m}^2$ ) based on data from MANGAN 2013, 2014 and SO-240 were calculated for the IRZ, PRZ and the northern part of the eastern license area (LA-north, cruise SO-240). Total abundances range between 148 and 712 ind./ $\text{m}^2$  in the IRZ, between 452 and 720 ind./ $\text{m}^2$  in the PRZ and between 336 and 808 ind./ $\text{m}^2$  in LA-north (FIGURE 5.3). A Mann-Whitney-U-test reveals significantly higher abundances of macrofaunal organisms in the PRZ compared to the IRZ ( $p < 0.01$ ).

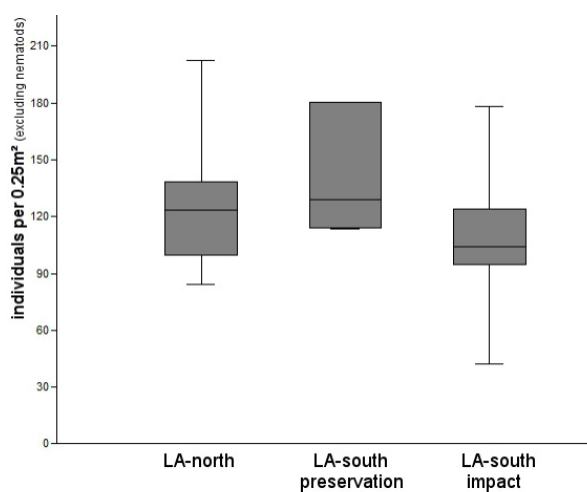


**Figure 5.3:** Total macrofaunal abundances per  $0.25 \text{ m}^2$  in the northern license area (LA-north), the IRZ and the PRZ based on box core samples collected during MANGAN 2013, MANGAN 2014 and SO-240.



Small but significant differences in macrobenthic community composition are found between the northern and southern parts of the eastern German license area. The samples in the north contain higher relative amounts of polychaetes, whereas those in the south contain relatively greater amounts of crustaceans. The relative community composition does not appear to be related to the absence or presence of nodules, nor is there a relation with nodule size or working area. A non-metric, multi-dimensional scaling plot (nMDS plot) shows no differentiation between the IRZ and PRZ in terms of community composition. The analyses of macrofaunal organisms obtained from box cores thus reveal that differences between the macrofaunal assemblages are especially due to different abundances and are not related to community composition at major taxa levels. However, a pairwise one-way analysis of similarities test (ANOSIM) does reveal significant differences between macrobenthic communities living close to and far away from a seamount (SO-240), being caused mainly by a higher abundance of macrofaunal organisms in box cores that are located near to a seamount in comparison to those box cores that are located further away from a seamount.

### Macrofauna collected by epibenthic sled

#### Morphological comparisons

The comparison between the relative abundance data of macrofauna as obtained from EBS deployments during cruises MANGAN 2013 (KM13), MANGAN 2014 (KM14), SO-239 and MANGAN 2016 (KM16) within the IRZ and the PRZ at exactly the same geographic locations reveals only very slight differences from the one year to the other at higher taxonomic levels (FIGURE 5.4). The most common taxa were Polychaeta, Peracarida (Isopoda, Tanaidacea, Cumacea and Amphipoda) and Maxillopoda (Copepoda, Ostracoda and Tantulocarida). Bivalvia and Ophiuroidea were also sampled in lower numbers. The proportion of polychaetes decreased from about 30% to 25-20% in both areas from 2013 to 2014, decreasing further in the IRZ but increasing slightly in the PRZ in 2015. The PRZ is characterised by higher relative abundances of molluscs (Bivalvia) during all three years. The proportions of the remaining taxa do not differ significantly between the three years.

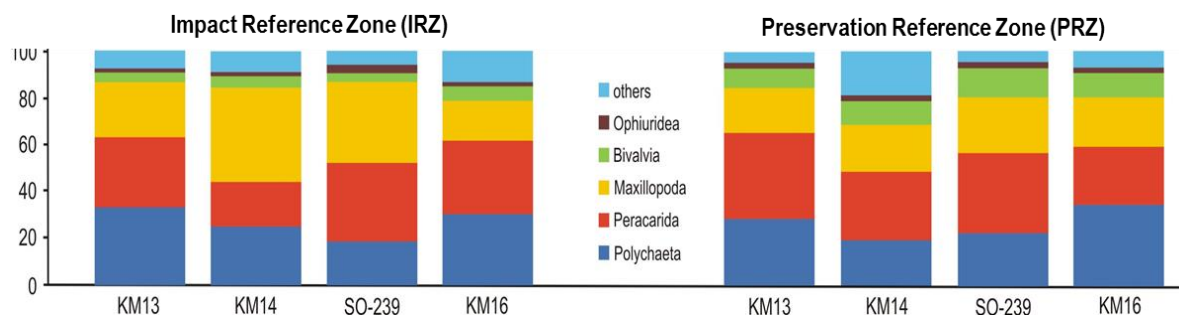


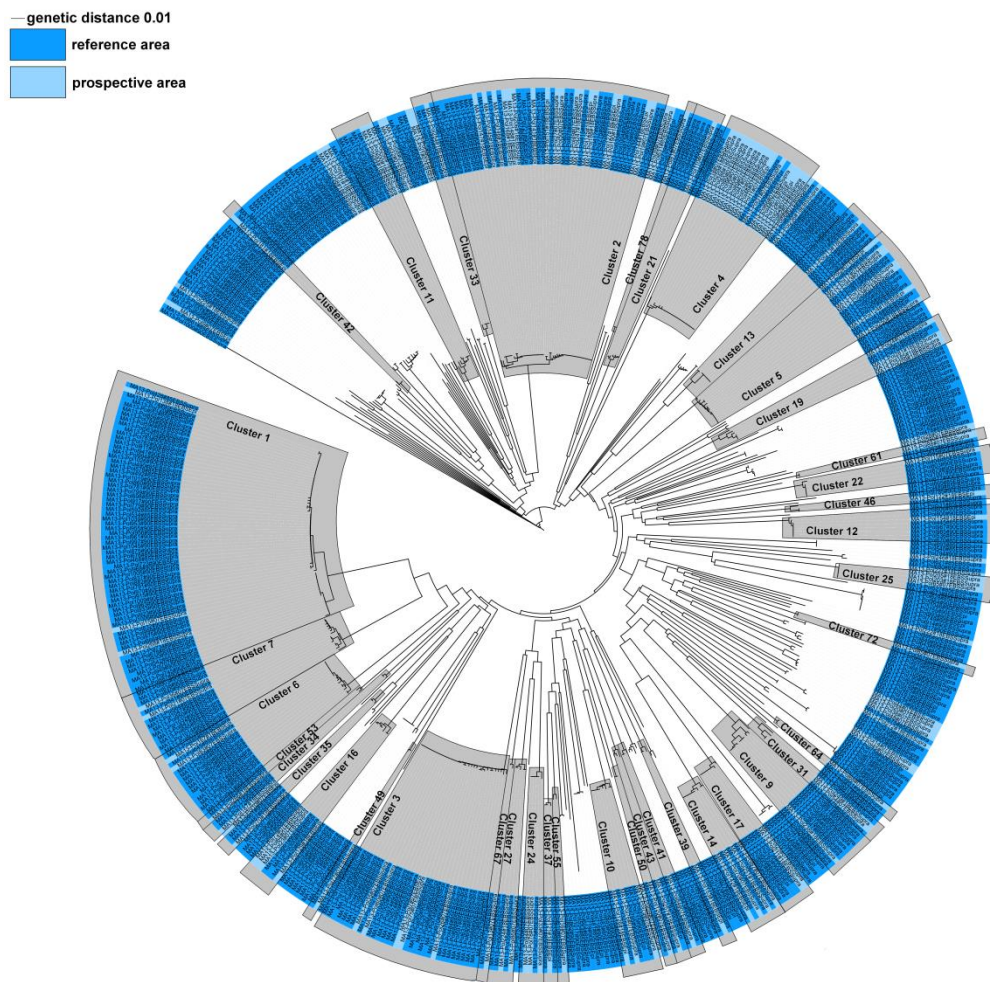
**Figure 5.4:** Comparison between the relative abundances (in %) of taxa present in the impact reference and preservation reference zones in 2013 (MANGAN 2013), 2014 (MANGAN 2014), 2015 (SO-239) and 2016 (MANGAN 2016).

A comparison of family dominance structure in the isopods collected during the MANGAN 2014 cruise showed slight differences between different sampling sites and working areas. However, the relative abundance of each family differed strongly between sampling sites and areas, i.e. also between two samples taken from the same area. In total, 72 morphospecies could be determined, most of which were provisionally new. Some morphospecies (e.g. *Nannoniscus* sp. 2 and *Sugoniscus* cf. *parasitus* Menzies & George, 1972) have been previously recorded from elsewhere in the German license area and thus seem to be wide-spread. Overall, similarity levels in species composition were very low both between and

within working areas. This is because many species were restricted to one or two stations, while only 4% of all species occurred in all three areas (PA1, PA2, PRZ).

#### Genetic analyses on polychaetes and isopods

Genetic analyses using sequences of the mitochondrial cytochrome c oxidase subunit I (COI) were carried out on 1068 polychaetes and 715 isopods collected by EBS from the IRZ and PRZ during the MANGAN 2013 cruise. 550 successful sequences of polychaetes were collected. Clustering with CD-HIT provided 147 MOTUs with a similarity of 97% (FIGURE 5.5). Out of these 147 MOTUs, 67 were singletons, representing 12% of all analysed specimens. 40 MOTUs were shared between the PRZ and IRZ (27% of all MOTUs). 5 MOTUs were found in the IRZ only, whereas the remaining 35 MOTUs were found in the PRZ only. 349 successful sequences were obtained from isopods. Clustering with CD-HIT provided 83 MOTUs with a similarity of 96% (FIGURE 5.6). Out of these 83 MOTUs, 45 were singletons (13% of all analysed specimens), while 38 were represented by more than one sequence/specimen. However, these 38 MOTUs do represent 87% of all specimens. Only 11 MOTUs are found in both the IRZ and the PRZ (~29%), whereas 15 were found in the PRZ (~40%) and 12 in the IRZ (~32%).

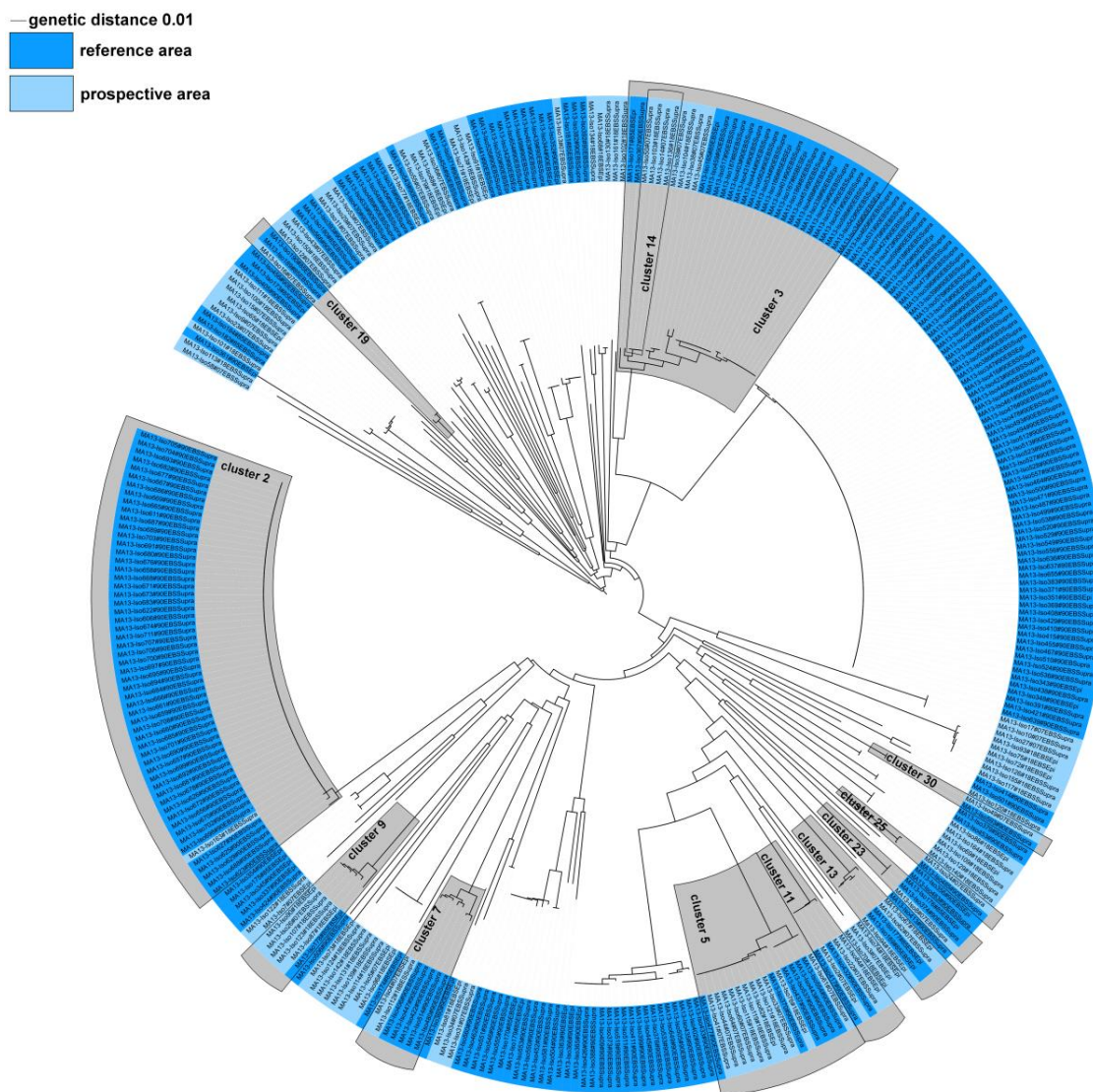


**Figure 5.5:** Phylogenetic tree of 550 polychaetes collected during the MANGAN 2013 cruise, based on their COI sequences. Light blue specimens derive from the IRZ; dark blue specimens derive from the PRZ. Figure from Raschka (2014).

The similarity of MOTUs between sampling sites is low due to the significant occurrence of rare species and perhaps also due to continuous turnover rates (Raschka, 2014). Despite the small geographical distance between both sites, phylogenetic differences within one area are almost as high as the differences



between areas, as shown by nMDS-plots for both isopods and polychaetes (Raschka, 2014). In consideration of potential future mining of the IRZ, the preliminary results above show that roughly one-third of the putative species live in both areas. Many more putative species were found exclusively in the PRZ than in the IRZ. The results suggest that a) these species are endemic to the PRZ or, more likely, that b) the amount of analysed samples is too small to obtain an accurate picture of the entire community. Presently it is still difficult to estimate the number of samples that would be required to reflect the whole community with any sort of statistical significance.

432 successful COI sequences were obtained from 672 polychaetes collected during the MANGAN 2014 cruise. Preliminary analyses conducted by CD-Hit show that the most frequently represented MOTUs from MANGAN 2013 have also been found in MANGAN 2014 as they have been assigned to the same genotypic clusters. 692 isopods were also collected for sequencing and genetic analyses. Further comparative work, also with material collected in 2015 during cruise SO-239 and in 2016 during cruise MANGAN 2016, is still in progress.

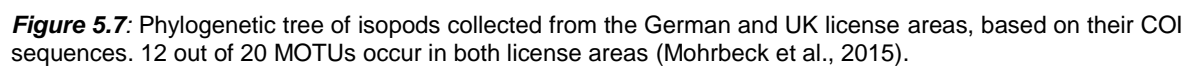


**Figure 5.6:** Phylogenetic tree of 349 isopods collected during the MANGAN 2013 cruise, based on their COI sequences. Light blue specimens derive from the IRZ; dark blue specimens derive from the PRZ. Figure from Raschka (2014).



 UK1 License Area    
  Eastern German License Area

 0.1 genetic distance



Population genetic analyses of diversity, divergence and demography were carried out with a strong focus on the most abundant polychaete and isopod species that were encountered during the last 5 years throughout the eastern German license area (8 sampling sites). One of the main objectives was to estimate the degree of genetic divergence between putative populations found i) in areas that are considered to be potential future mining areas (PA1 [IRZ], PA2), and ii) in areas that are designated as preservation areas (PRZ). Absent or low divergence would indicate high genetic connectivity, i.e., gene flow between sub-populations affects evolutionary processes within these populations. Alternatively,

pronounced or complete divergence would indicate no genetic connectivity, i.e., there is restricted or no gene flow and populations evolve largely or completely independent. Additional analyses on diversity and demography provide insight into aspects of population dynamics.

Five polychaete and three isopod species were identified for which the number of available nucleotide sequences was high enough to perform population genetic analyses and to estimate divergence, diversity and demography parameters from different putative populations as shown in FIGURE 5.8 and listed in TABLE 5.1.

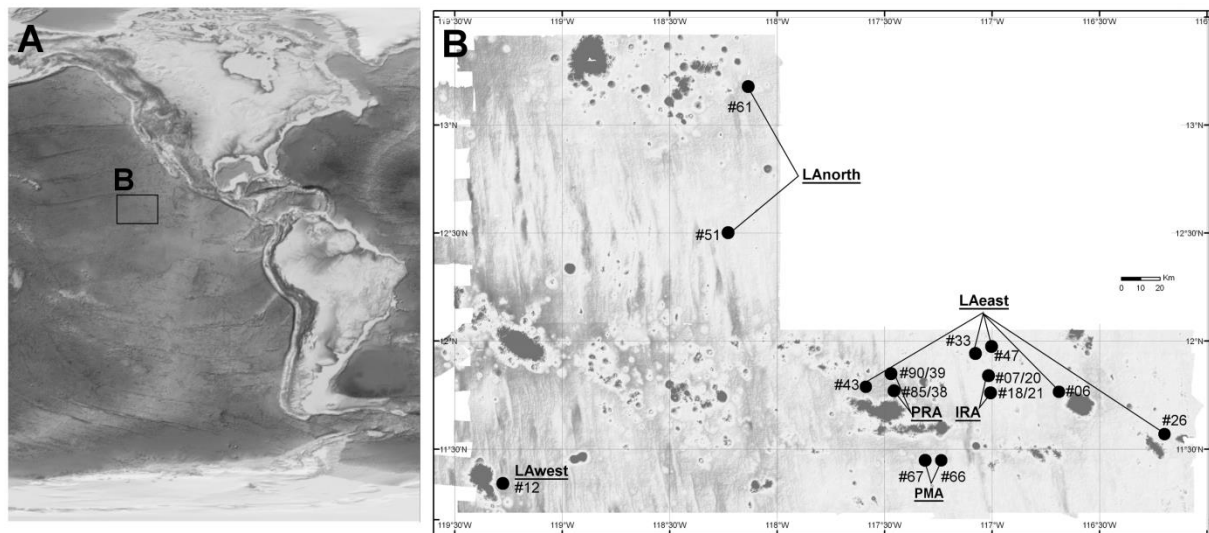


**Figure 5.8:** A: Location of the eastern German license area; B: Locations of EBS samples used for population genetic analyses. PRA = Preservation Reference Zone; IRZ = Impact Reference Zone; PMA = Prospective Area #2 (PA2).

### Divergence analyses

Many specimens were independently sampled at particular sites in successive years (2013, 2014; compare samples in TABLE 5.1) and this raised the question as to whether the COI nucleotide sequences of these samples can be pooled for further analyses. One basic concern is that these independent samples might have been taken from different and independently evolving populations that are distributed over very small spatial scales only and have different haplotype frequencies. The same concern applies to the case that haplotype frequencies within the same population might change within the short term of one year. In order to address this question, divergence between samples from the same area but obtained during successive years was estimated based on an Analysis of Molecular Variance (AMOVA). AMOVA leads to the distribution of the total amount of genetic variation of samples as variance components (1) within each population, and (2) between populations.

The possibility to pool samples from successive years provided the basis for divergence estimates between populations encountered in different areas. A first set of analyses with AMOVA investigated small-scale divergence between two areas within the PRZ (PRZ-north and PRZ-south) for four polychaetes and three isopods. Divergence between polychaete populations of all four taxa in areas PRZ-north and PRZ-south was absent. In contrast, there was evidence for divergence between isopod populations found in PRZ-north and PRZ-south in the case of *Macrostylis* sp.2 and *Eugerdella* sp. 1.

**Table 5.1:** List of samples from different cruises obtained for population genetic analyses. Numbers of specimens are given as size classes: + =  $n < 4$ ; ++ =  $4 < n < 9$ ; +++ =  $n > 9$ ; IRZ = Impact Reference Zone, PRZ = Preservation Reference Zone, PMA = Prospective Area #2 (PA2).

Cruise/ Year/ Sample site	license area	Species/MOTU							
		Polychaeta					Isopoda		
		<i>Paralacydonia weberi</i> Cluster 0	<i>Sigalionidae</i> sp.1 Cluster 1	<i>Bathylgocinde profunda</i> Cluster 2	<i>Polychaeta</i> sp.1 Cluster 3	<i>Polychaeta</i> sp.2 Cluster 4	<i>Macrostylis</i> sp.2 Cluster 1	<i>Eugerdella</i> sp.1 Cluster 3	<i>Eugerdella</i> sp.2 Cluster 4
SO-205	EBS12	German	++	++	+	+	+	-	-
	EBS26	German	-	-	-	++	+	-	-
	EBS47	German	++	-	+	+	+	-	-
	EBS61	German	+	-	-	+	-	-	-
BIONOD 2012	EBS06	German	-	-	-	+	+	+	-
	EBS33	German	+	-	-	+	+	+	-
	EBS43	German	-	-	-	-	+	-	+
	EBS51	German	+	-	+	-	-	-	-
	EBS67	French	+	-	-	-	-	+	+
	EBS73	French	-	+	-	-	-	-	-
	EBS80	French	-	+	-	-	-	-	-
	EBS107	French	+	+	-	+	-	-	-
MANGAN 2013	EBS07	German (IRZ-north)	++	+	++	++	++	-	++
	EBS18	German (IRZ-south)	+++	+	-	+	+	-	++
	EBS85	German (PRZ-south)	+++	+++	+++	+	++	++	-
	EBS90	German (PRZ-north)	+++	+++	+++	++	+++	++	++
MANGAN 2014	EBS20	German (IRZ-north)	++	+	++	++	-	+	+
	EBS21	German (IRZ-south)	+++	-	++	+	+	-	+
	EBS38	German (PRZ-south)	+++	+++	+	++	+++	+++	+
	EBS39	German (PRZ-north)	+++	++	+++	+	+++	++	++
	EBS66	German (PMA)	+++	-	-	++	-	-	+
	EBS67	German (PMA)	-	-	-	-	+	-	+
Total number of specimens		136	94	58	52	71	67	35	33

The second set of analyses explored divergence between (1) the PRZ and IRZ, and (2) between the three different areas (PRZ, PMA [PA2], IRZ), based on a hierarchical AMOVA. This approach allows distributing the total amount of genetic variation observed between three hierarchical levels: (1) between areas (either PRZ vs. IRZ, or PRZ vs. PMA vs. IRZ), (2) between populations found in each of the respective areas, and (3) within all populations (ignoring any hierarchy level). No divergence between

populations deriving from different areas was found, either by comparing the areas PRZ and IRZ (exemplified for three polychaete and one isopod lineage) or by comparing the areas PRZ, IRZ and PMA (exemplified for one polychaete lineage).

The data presented here indicate different levels of population divergence at small spatial scales (below 100 km) for selected polychaete and isopod species. While there was no indication of profound divergence for all four polychaete lineages and for one isopod species (*Eugerdella* sp.2; cluster 4), there is a signal for weak divergence between populations in two isopod lineages (*Macrostylis* sp.2; cluster 1 and *Eugerdella* sp.1; cluster 3). Weak population divergence is indicative for differences in mitochondrial haplotype frequencies at both localities, mainly due to random effects (genetic drift). This pattern is usually seen when populations exchange migrants, but individuals at any one locality preferentially mate with each other. Consequently, although migration between these localities is expected to occur, specimens at each locality form locally-specific, genetic populations. In contrast, the lack of population divergence as seen for the polychaete species and for one isopod species shows that these species do not form locally-specific genetic populations, i.e. individuals occurring at localities that are 100 km apart can still be considered as belonging to one single population and there is a high degree of gene flow between populations. Future investigations have to confirm this pattern based on a sampling scheme that allows the collection of many more specimens per locality to strengthen statistical analyses.

### *Diversity and Demography*

Complementary investigations on genetic diversity and demography were performed using the same populations of polychaete and isopod species as used for analysing divergence as outlined above. Population samples as listed in TABLE 5.1 were analysed to investigate their intra-population diversity, haplotype distribution and haplotype network, and to assess whether populations show a haplotype frequency distribution as expected for expanding populations (i.e. one with genetic exchange). Results of these investigations show that the majority of populations among polychaete and isopod species are genetically diverse (the haplotype diversity is mostly larger than 0.5) and that the haplotype frequency distribution is typical for non-expanding populations, i.e. the high haplotype diversity and the large number of shared haplotypes indicates that the population structure is not changing in successive years (i.e. in the PRZ and IRZ) and that there is no divergence in population structure, i.e. there is sufficient gene flow between the populations of the eastern, western and northern parts of the license area.

This study shows a general pattern of no to scarce genetic structure between the populations of the selected macrobenthic taxa at spatial and temporal scales within the German license area. Therefore, gene flow between the PRZ and the IRZ does occur, and no geographical barriers are present that could impede a successful recolonisation of the most abundant macrofaunal taxa after polymetallic nodule mining. Nonetheless, these conclusions cannot be translated into recommendations for conservation during mining activities or into predictions for recolonisation after mining at the moment, but they can be used to strengthen working hypotheses for future research. Account must also be taken of the fact that temporal variations in population diversity are probably not sufficiently large to be detected over the very short timescale of one year intervals as has been the case in the IRZ/PRZ.

### **Epifauna collected by box corer**

While macrofaunal taxa such as the Isopoda and Polychaeta have frequently been barcoded in the past in order to determine their connectivity over larger spatial scales (e.g. see chapters above and CHAPTER 5.2.3.3), different taxa have different life traits, and therefore they might be selectively influenced by potential future manganese nodule mining activities.

Especially sessile organisms, which largely depend on manganese nodules as their substrate, will probably be greatly impacted by the removal of the nodules. Thus, Bryozoans have been chosen as another taxon to be investigated for their connectivity using a barcoding approach. After a mobile larval stadium, individuals of this taxon settle on the hard substrate and form sessile colonies (Hurlbut, 1991). In the Pacific deep sea, bryozoans are commonly found using nodules as hard substrate (Rühlemann et al., 2015; Kuhn et al., 2015) and have frequently been obtained as epifauna in box core samples during previous exploration cruises.

All Bryozoans obtained from box cores during the last BGR exploration cruises to the areas PA1-West, PA2 and the PRZ ( $n = 824$ ) were sorted out and investigated molecularly and morphologically. Sequencing of part of the COI gene was successful for 369 individuals. Based on an ABGD-analysis (simple distance), the individuals cluster into 42 groups. The largest set of individuals clustered into one group containing 101 individuals that occurred in similar abundances in all three areas. It was not possible to distinguish different populations in the different areas based on a haplotype network, suggesting good connectivity within this taxon. Nevertheless, a high number of mutations between individuals ( $> 40$ ) occurs within this group. Although the ABGD-analysis suggests that this group is only one species, this result appears questionable and perhaps the sequencing of other genes can reveal a better resolution of this group.

The second most abundant group contains 74 individuals, and distinctly less mutations were observed. Nevertheless, no geographical pattern with separated populations could be observed for this group either (FIGURE 5.9). In addition to occurring in the three main sampling areas, this species also occurs in PA1-East. The results show that connectivity at a 100-km-scale is good between macrofaunal/epifaunal Bryozoans, despite the fact that they are sessile.

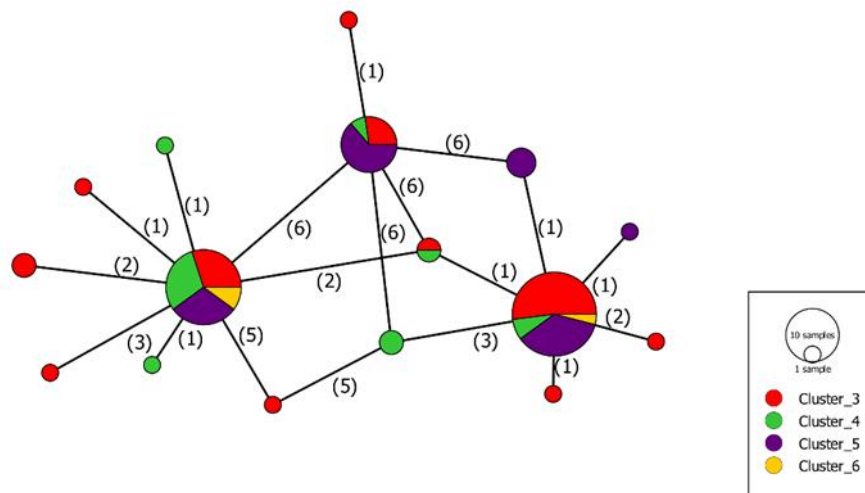


**Figure 5.9:** Haplotype network of the second most abundant Bryozoan taxon in the Eastern German license area from different areas (clusters). Red = PA1-West; green = PA2; purple = PA1-East; yellow = PRZ.  $N = 74$ .

### Meiofaunal composition and densities derived from multicorer samples

Total meiofaunal abundances within the upper 5 cm of sediment obtained by multicorer during the MANGAN 2013 cruise range from 96 ind./10 cm<sup>2</sup> to 452 ind./10 cm<sup>2</sup> in the IRZ, and from 154 ind./10 cm<sup>2</sup> to 602 ind./10 cm<sup>2</sup> in the PRZ (FIGURE 5.10) (Janssen et al., submitted). As with macrofaunal densities, a Mann-Whitney-U-test confirms significantly higher meiofaunal densities in the PRZ ( $p < 0.01$ ).

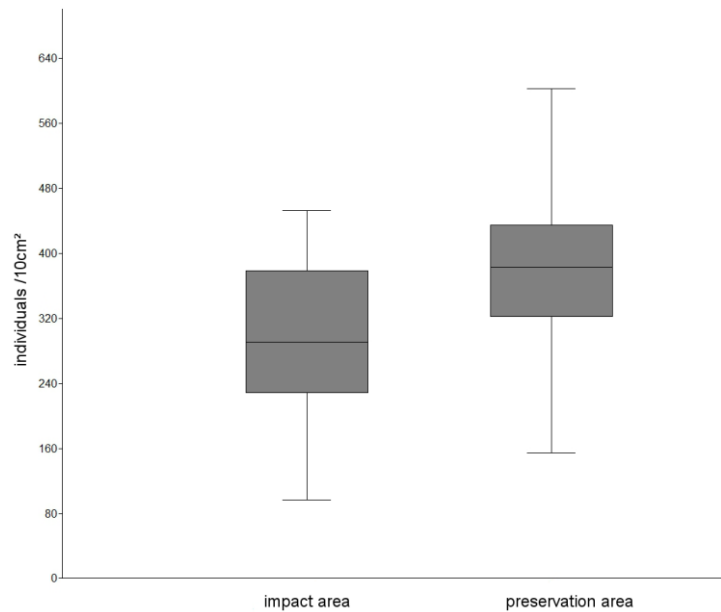


**Figure 5.10:** Total meiofaunal densities (individuals per 10 cm<sup>2</sup>) in the IRZ and PRZ as determined from the upper 5 cm of MUC samples obtained during the MANGAN 2013 cruise.

In general, nematodes form the dominant taxon (82-95% in the entire eastern German license area), followed by copepods (+nauplii) (3-14%) and annelids (1-2%). About 12 major taxa were identified in the eastern German license area (Janssen et al., submitted). Statistical analyses show no differentiation between the IRZ and PRZ in terms of community composition at a higher taxonomic level, regardless of nodule abundance or size. Preliminary analyses of meiofaunal organisms from MUCs have thus revealed that differences between the meiofaunal assemblages are especially due to different densities in the two analysed areas and are not related to community composition at major taxa levels.

Temporal changes in benthic communities in the deep sea remain poorly investigated (Glover and Smith, 2003), and the annual variability in meiofaunal abundance has not been investigated at all. In addition to the time series analyses of macrofaunal assemblages using EBS deployments in the PRZ and IRZ (see chapter above) starting in 2013, the temporal variation of meiofaunal assemblages can be analysed by comparing the results of multicorer analyses that were carried out in the exact same areas as the EBS deployments throughout the same 4 consecutive years. Here, a first comparison of meiofauna on higher taxonomic level is presented for the years 2013 and 2014.

The average overall meiofaunal abundance in both the IRZ and the PRZ is similar in both years. However, the dispersion is distinctly higher in 2013 and both the highest and lowest abundance are beyond the range observed in 2014 (FIGURE 5.11). This heightened dispersion might be caused by the different original sampling sizes.



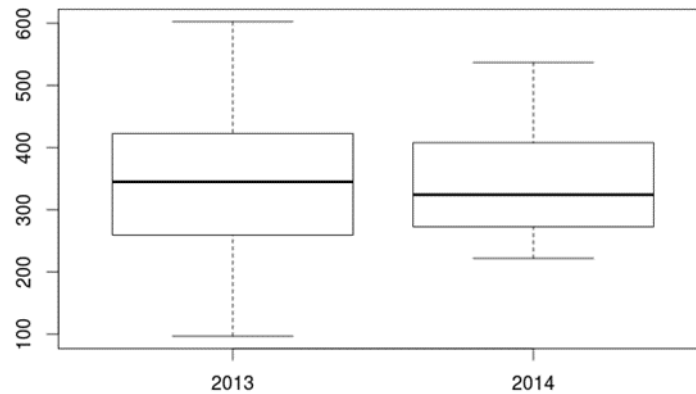


**Figure 5.11:** Overall abundance of meiofaunal organisms per 10 cm<sup>2</sup> of sediment obtained from both the IRZ and PRZ in 2013 and 2014.

Differences between the two reference areas were investigated by comparing the overall meiofaunal abundance at the IRZ and the PRZ separately. In both years, the abundance was slightly lower in the IRZ than in the PRZ (FIGURE 5.12). As a Shapiro-Wilk test indicated that the abundance was normally distributed in both years, a Welch's t-test was computed for both years. Indeed, there are significant differences between the PRZ and the IRZ in 2013 ( $p=0.009$ ) as well as in 2014 ( $p=0.003$ ). A Kruskal-Wallis test showed a similar result ( $p=0.01$  for both years).

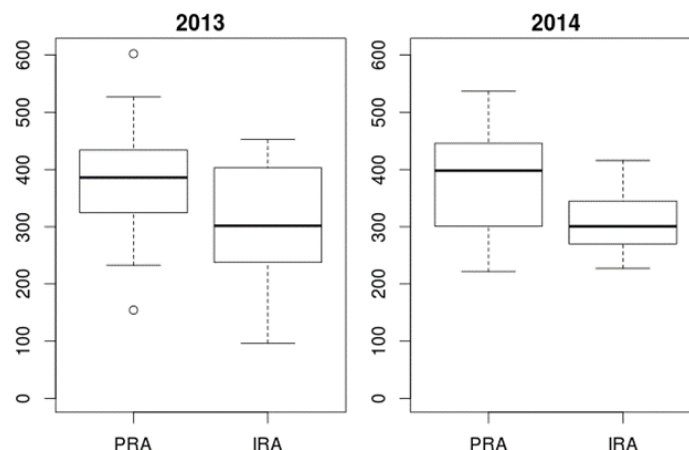


**Figure 5.12:** Overall abundance of meiofaunal organisms per 10 cm<sup>2</sup> of sediment in the Preservation Reference Zone (PRZ) and the Impact Reference Zone (IRZ) in 2013 and 2014.

### The Nematode community

In most marine sediments, Nematoda are the most abundant higher taxon (Giere, 2009) and this is also the case in the CCZ. In the Eastern German license area, Nematoda comprise 93.3% of the meiofauna. While local diversity is high in this taxon, regional diversity has been estimated not to be especially elevated (Lamshead et al., 2003, Lins et al., 2016) and an occurrence of only 400 species has been estimated for the CCZ (Lamshead et al., 2003). Therefore, and due to their high abundance, Nematoda have been suggested to be good bio-monitoring indicators in the CCZ (Lamshead et al., 2003).

Samples obtained from the time series sites (IRZ, PRZ) with the multicorer during cruise SO-239 were analysed for their Nematode content. A total of 1095 individuals were investigated in the PRZ and 798 individuals in the IRZ. To compare the different sub-samples adequately, counts were aggregated as relative abundances. A total of 79 genera could be determined. The most abundant genera are *Acantholaimus* Allgen, 1933 (22.4%) and *Monhystrella* Cobb, 1918 (17.5%), followed by *Daptonema*

Cobb, 1920 (7.0%) and *Halalaimus* de Man, 1888 (6.4%). All other genera comprise less than 5% of the overall abundance (Fig. 5.6.1). Comparing the two areas, *Acantholaimus* (IRZ: 23.8%; PRZ: 19.9%) and *Monhystrella* (IRZ: 16.9%; PRZ: 18.2%) are first and second most abundant in both cases. In the IRZ, they are followed by *Daptonema* (8.7%) and *Halalaimus* (7.9%). However, the third most abundant genus in the PRZ is *Theristus* Bastian, 1865 (6.4%), followed by *Daptonema* (5.3%) and *Halalaimus* (4.8%), although *Halalaimus* comprises less than 5% of all individuals here.

Comparing the diversity of the two different areas, based on the Shannon Index ( $H'$ ), diversity is higher in the PRZ than in the IRZ (FIGURE 5.13) and a similar pattern can also be seen for the genus richness ( $G$ ). One reason for the higher values of Shannon Index and genus richness might be the elevated number of genera exclusively occurring in the PRZ (23 genera) compared to the IRZ (8 genera). However, the differences in the number of additional genera within the PRZ seem to be larger than within communities observed in the IRZ. Pairwise comparing all samples, they usually share 54.5% of all genera observed in both samples. But although differences between samples are this large, the magnitude of differences is similar between all samples, leading to similar beta-diversity across both areas. This finding is consistent with previous observations of high local diversity and limited turnover in the deep sea (Lambshead and Boucher, 2003).

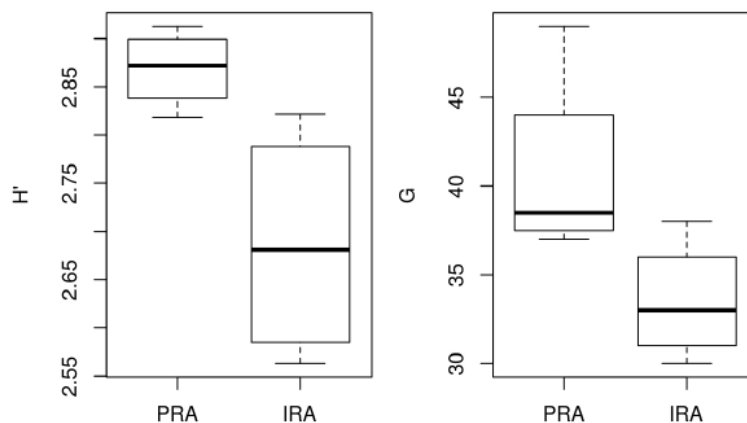


**Figure 5.13:** Diversity ( $H'$ ) and genus richness ( $G$ ) compared for the Nematoda of the PRZ and the IRZ as obtained by MUC sampling during cruise SO-239 (2015).

#### The Copepod community

Although the very short fragment of 18S rDNA (the SSU region) has previously been used for genetically delimitating copepod species, the studies on material from the German license area show that its use is problematic for abyssal copepods, as first morphological analyses show that sequences which meet the threshold of 99%, i.e. are genetically grouped into one MOTU, are morphologically different, making species identification tedious. Furthermore, the success rate for extracting, amplifying and sequencing the SSU gene in 1002 meiobenthic copepods deriving from the IRZ and PRZ was low and constituted roughly 44% (442 sequences). Out of the 442 analysed sequences, 358 (81%) originated from 5 MUC deployments in the PRZ, whereas only 84 (19%) originated from 5 MUC deployments in the IRZ. The success rate for amplifying other genes (i.e. 28S, 12S) was found to be very low (< 10%) in our area and thus was not considered to be applicable for further analyses.

Nevertheless, using the SSU gene as described above, 297 MOTUs were identified in the IRZ and PRZ. Further morphological determinations of MOTU clusters (at a similarity threshold of 99-100%) have to be carried out before significant statements on copepod distribution ranges can be provided

but as a first result, we can state that even at a similarity threshold of 99%, the number of singleton MOTUs is high (> 80%), indicating a very high species diversity (FIGURE 5.14).

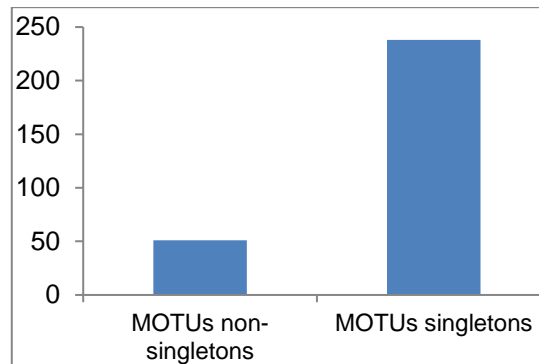


**Figure 5.14:** Total number of singleton and non-singleton copepod MOTUs (18S\_SSU) from the IRZ and PRZ in the eastern license area (MANGAN 2013 cruise) at a similarity threshold of 99%.

### Preliminary conclusions on the IRZ and PRZ

- Significantly higher abundances of macrofaunal and meiofaunal organisms are found in the PRZ compared to the IRZ.
- No differentiation between the IRZ and PRZ in terms of community composition at major taxa levels (macrofauna; meiofauna) or from year to year (macrofauna) over a four-year period (2013–2016) was found.
- The most abundant macrofaunal taxa are polychaetes, tanaids and isopods. Overall, similarity levels of e.g. isopod species are very low both between and within the sampling areas. This is because many species are restricted to one or two sampling sites only, i.e. there is a high degree of faunal patchiness which almost certainly is also a reflection of insufficient spatial coverage and small sample size.
- Genetic analyses of polychaetes and isopods of the IRZ and PRZ show that ca. 12% of all analysed specimens are singletons for both groups of organisms. Roughly one third of all putative species live in both areas, whereas many more putative species were found exclusively in the PRZ than in the IRZ. This could be due to a higher degree of endemism, but may also be related to small sample size. The most frequently represented polychaete MOTUs from MANGAN 2013 have also been found during MANGAN 2014.
- The most abundant meiofaunal taxa are the nematodes, followed by copepods and annelids. Diversity and species richness of nematodes are higher in the PRZ than in the IRZ. Genetic analyses of copepods in our area are problematic in terms of taxon identification, but at least show that the number of singleton MOTUs is high (> 80%), indicating a very high species diversity.
- Preliminary analyses of genetic connectivity of the five most abundant polychaete species and the three most abundant isopod species of the eastern German license area reveal high haplotype diversity for the COI sequence in all cases, indicating that there is no divergence in population structure and that the population structure is not changing in successive years (i.e. in the PRZ and IRZ). Therefore, there appears to be sufficient gene flow between the populations of the PRZ and the IRZ, and no geographical barriers are present that could impede a successful recolonisation of the most abundant macrofaunal taxa after polymetallic nodule mining.

### 5.2.3.3 Connectivity: Macrofaunal and meiofaunal comparisons between the German and French license areas

Based on all biodiversity analyses carried out so far, including those that were carried out in the French license area in the framework of the BIONOD cruise in 2012, a high species diversity (> 800 species) with a high number of singletons (70% of all macrofaunal species and 90% of all meiofaunal species are represented by only one specimen) and varying distribution ranges of organisms at the family and species level are noted. Abundances are significantly higher in the eastern German license area than they are in the French area, which lies ca. 1300 km westwards. This is probably related to the lower surface productivity and associated lower benthic food supply in the French area. A study was conducted to make detailed morphological and molecular comparisons between the benthic species of both areas using a reverse taxonomic approach (Janssen et al., 2015).

The French and the German license areas share several benthic species. This particularly applies to polychaete species: out of the 95 polychaete taxa found more than once, 27 taxa (~28%) were found in both the French and German license areas, 56 taxa were present in the German license area only, and 12 taxa in the French license area only. However, isopod species appear to be restricted to smaller areas: out of the 30 isopod taxa found more than once, only 2 taxa (~7%) were present in both the German and French license areas, 14 taxa were found in the French area only and 14 taxa in the German license area only. Out of the 28 meiobenthic copepod taxa found more than once, only 3 taxa (~9%) were present in both the German and French license areas, 8 taxa were found exclusively in the French license area and 15 taxa exclusively in the German license area.

#### Macrofauna collected by epibenthic sled

##### Morphological comparisons

Morphological results from the EBS samples have revealed that macrofaunal abundance levels are relatively low in the French license area compared to the German area. Overall, malacostracan crustaceans were the most dominant groups examined in both areas. Polychaetes appear to be more abundant in the German area and form a greater component of the macrofauna, comprising ca. 20% of the macrofauna in the German area in comparison to only ca. 11% in the French area.

At the Polychaete family level, the French area shows a much greater dominance by three families (65%), whereas the German area shows much greater evenness. Although Opheliidae (19% with relative abundance (RAD)), Spionidae (17% RAD) and Paralacydonidae (14% RAD) are important groups in both areas, Opheliidae and Polynoidae are much less abundant in the German area, whereas important components of the German polychaete fauna, such as Scalibregmatidae, Sigalionidae and Nereidae, are very rare or absent in the samples from the French area (FIGURE 5.15). Analysed polychaete specimens belonged to 21 supraspecific taxa: Acrocirridae, Opheliidae, Nereididae, Goniadidae, Ampharetidae, Hesionidae, Spionidae, Magelonidae, Paralacydonidae, Pholoidae, Poecilochaetidae, Polynoidae, Paraonidae, Sphaerodoridae, Scalibregmatidae, Cirratulidae, Sigalionidae, Sabellidae, Phyllodocidae, Nephtyidae and Lacydoniidae. Most abundant MOTUs represented in both the French and German license areas were morphologically assigned to *Paralacydonia* cf. *weberi* (Horst, 1923) (with RAD of 14% (excluding singletons)) and *Bathyglycinde profunda* (9% RAD).

The Desmosomatidae are the most dominant Isopod crustacean family in both areas, followed by the Munnopsidae (FIGURE 5.16). While the Macrostylidae are more important in the French area, Nannoniscidae are more abundant in the German area. In Isopoda, analyses indicated seven supraspecific taxa: Desmosomatidae, Macrostylidae, Munnopsidae, Nannoniscidae, Haploniscidae, Haplomunnidae and Dendrotionidae. The most abundant morphospecies was assigned to a new species

of Macrostylidae (*Macrostylis* sp.5; 15% RAD (excluding singletons)). The most abundant taxa for which sequences could be obtained and which were recorded in both the French and German license areas, were Macrostylidae (29% RAD) and Desmosomatidae (26% RAD).

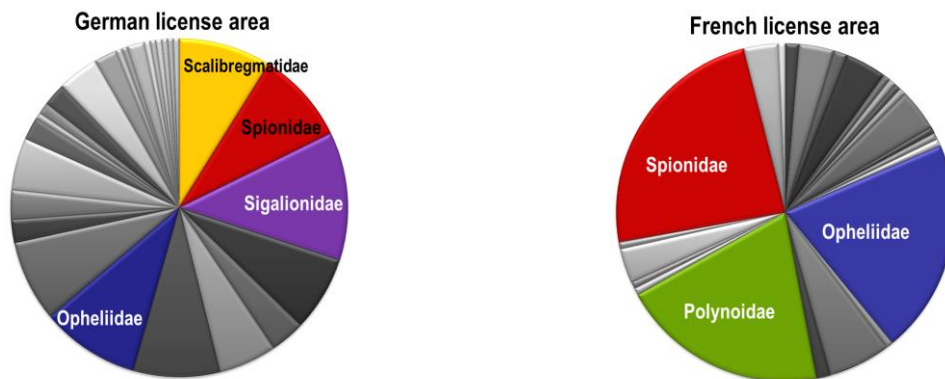


**Figure 5.15:** Relative abundances of polychaete families in the French and German license areas.

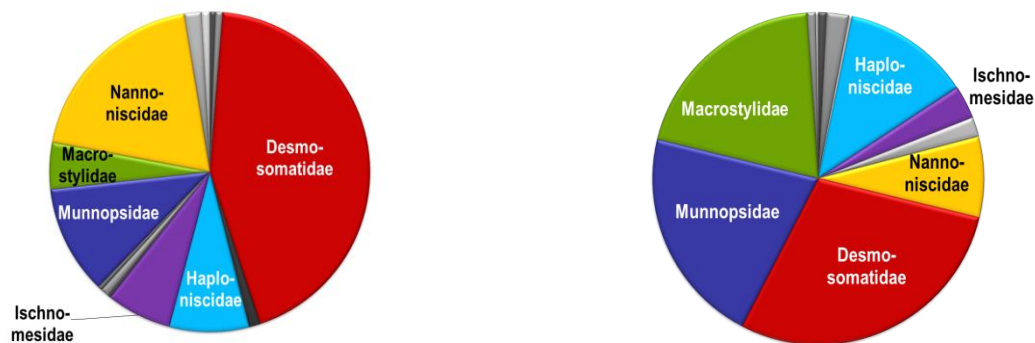


**Figure 5.16:** Relative abundances of isopod families in the French and German license areas.

### Molecular (DNA) comparisons

From the 1900 specimens analysed, COI amplification and sequencing was successful for 556 polychaete and 150 isopod specimens, i.e. 44% and 31% of the total number of polychaetes and isopods selected for genetic analyses, respectively. Of these, 436 polychaete and 76 isopod sequences were obtained from the German license area, whereas 120 polychaete and 74 isopod sequences could be retrieved from the French license area.

### *Polychaetes*

Using CD-HIT, the 556 COI sequences clustered into 233 MOTUs at a similarity level of  $\geq 97\%$  (FIGURE 5.17). Of the 233 MOTUs, a total of 95 MOTUs (40%) were represented by more than one sequence, while 138 sequences were singletons (i.e. 60% of MOTUs, but 25% of total sequences were recorded only once). Out of 95 MOTUs found more than once, 27 MOTUs (~28%) were found in both the French and German license area, 56 MOTUs (~59%) were exclusively found in the German license area, and 12 MOTUs (~13%) occurred only in the French license area. Including singletons, 158 MOTUs were present exclusively in the German license area compared to 48 in the French license area. An nMDS of unweighted UniFrac metric displays no evident grouping of the French and German stations. A pairwise one-way analysis of similarities (ANOSIM) test shows that the genetic distance of polychaete assemblages between the German and the French license areas does not differ significantly from chance (Global  $R = 0.13$ ,  $p = 0.15$ , number of permutations = 999), suggesting that the within-group variability is as high as the between-groups variability.

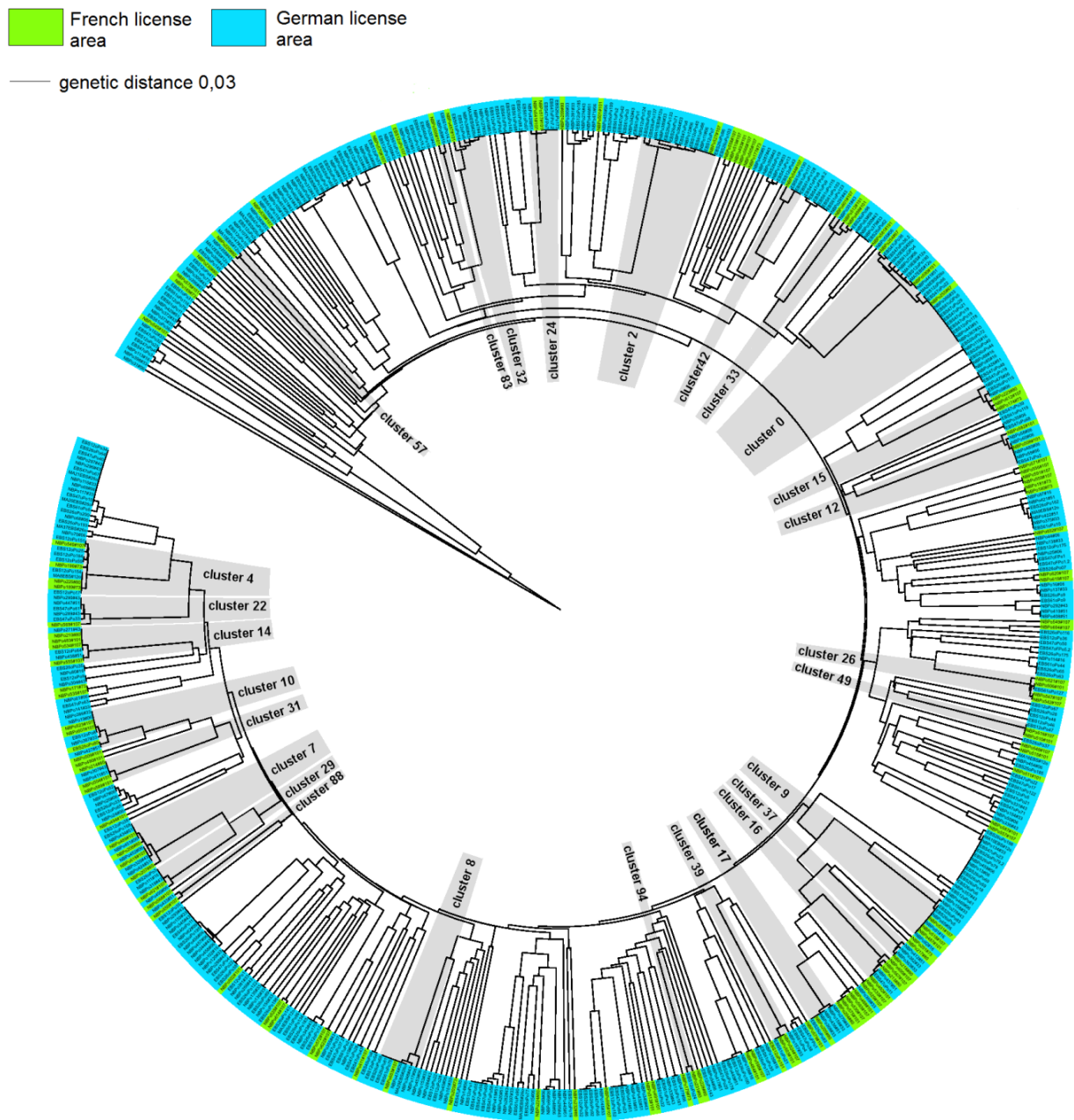


**Figure 5.17:** Phylogenetic tree of 556 polychaete COI sequences deriving from the French (green) and German (blue) license areas. Clusters represent MOTUs which are present in both areas.



*Isopoda*

In total, 95 MOTUs were identified (at  $\geq 97\%$  similarity) (FIGURE 5.18). Of these, 30 MOTUs ( $\sim 30\%$ ) were represented by more than one sequence and 65 MOTUs were singletons ( $\sim 70\%$  of MOTUs,  $\sim 50\%$  of total sequences). Out of the 30 MOTUs that were represented by more than one individual, only two MOTUs (7%) were present in both the German and French license areas (i.e., *Eurycope* aff. *linearis* and *Prochelator* sp. 1). This is in contrast to morphological analyses, which recorded three species occurring in both the French and German claims. Fourteen MOTUs (47.5%) were found exclusively in the French and 14 MOTUs (47.5%) were restricted to the German license area. Including singletons, 45 MOTUs were found exclusively in the German and 48 in the French license area.

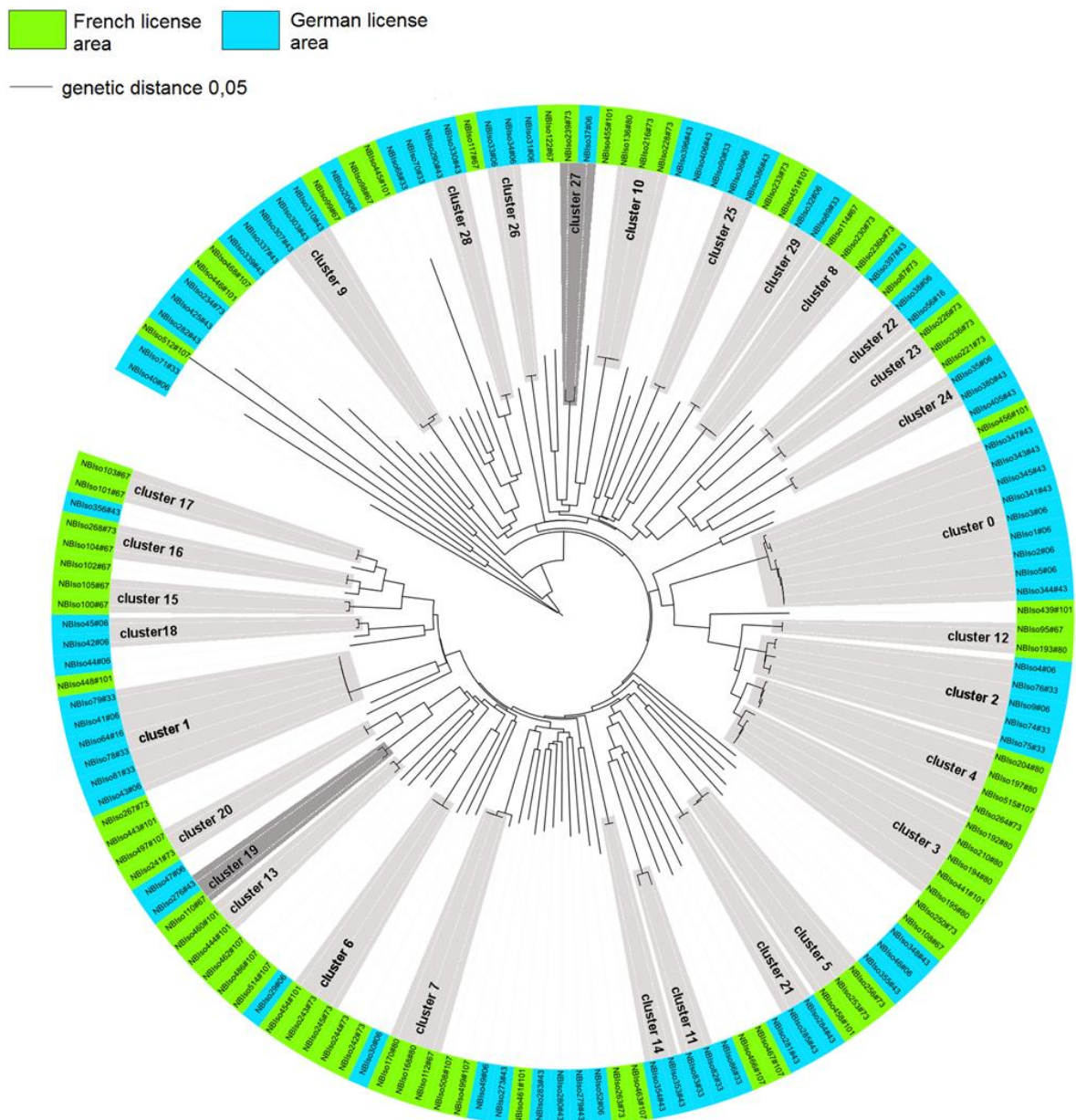


**Figure 5.18:** Phylogenetic tree of 95 isopod COI sequences deriving from the French (green) and German (blue) license areas. Light grey clusters represent MOTUs that are only present within one particular license area; dark grey clusters represent MOTUs that are present in both areas.

An nMDS of unweighted UniFrac metric displays a slight grouping of the French and German isopod assemblages. An ANOSIM test shows that the genetic isopod assemblages of the German and the French areas differ significantly (one-way ANOSIM, Global R = 0.38,  $p = 0.016$ , number of permutations = 999), but the R value is low. A Mantel test reveals a significant positive correlation ( $r = 0.56$ ,  $p < 0.01$ ) of genetic and geographical distances between all stations and thus confirms the previous findings. This positive correlation was found to be stronger for isopods than for the polychaetes. Thus, although most of the isopod genera, i.e. *Macrostylis*, *Haploniscus*, *Eurycope*, *MIRZbillicoxa* and *Eugerdella* display a wide distribution within the CCZ and are represented within both the French and the German license areas, these analyses show that the distribution of isopod species is conspicuously restricted to smaller areas.

## Meiofaunal organisms

### Molecular comparisons of Copepoda

From 1190 copepod specimens analysed, amplification and sequencing of the 12S gene was successful for 302 copepods. A total of 185 copepod sequences were obtained from the German license area and 117 copepod sequences from the French license area. The success rate of sequencing 12S from copepod specimens was, on average, only 25%. Comparison of the reference sequence of every MOTU with BOLD and GenBank databases resulted in very low matching success, as most of the abyssal species in this area are new to science. However, the copepod sequences from the CCZ have been compared with 32 copepod sequences deriving from the Kuril-Kamtschatka Trench (North Pacific; KURAMBIO SO-223 cruise (2012); 40-43°N, 147-157°E; water depth 4900-5800 m). These two regions are about 9000 km apart.

Using CD-HIT, the 302 successful 12S sequences of the CCZ and the 32 sequences of the Kamtschatka Trench clustered into 284 MOTUs with  $\geq 97\%$  similarity (255 MOTUs from the CCZ and 29 MOTUs from the Kamtschatka Trench). From those 284 MOTUs, only 28 MOTUs (~10%) were represented by more than one specimen and 256 MOTUs were singletons (227 MOTUs from the CCZ and 29 MOTUs from the Kamtschatka Trench). Out of the 28 MOTUs found more than once, only 3 MOTUs were present in both the German and French license areas, 8 MOTUs were found exclusively in the French license area and 15 MOTUs exclusively in the German license area (FIGURE 5.19). Only 2 MOTUs could be identified which are found in both the CCZ and the Kamtschatka Trench. Including singletons, 157 MOTUs were found exclusively in the German license area and 93 exclusively in the French license area. Out of 302 analysed copepod individuals in the CCZ, 227 sequences of individuals were found which have a sequence identity of less than 97% to any other analysed sequence, singletons thus comprising 75% of all analysed copepod individuals.

Morphological analyses of the 3 MOTUs containing specimens from both the German and French license areas (Clusters 0, 1 and 8 in FIGURE 5.19) have revealed that these clusters contain similar species, thus confirming CD-Hit clustering. Therefore, the analyses reveal that out of 302 individuals, there are only 3 species (21 individuals) that are found in both the German and the French license areas. Moreover, the results reveal a wide distribution within the Pacific Ocean of 2 species (Clusters 7 and 14) that have been found in the Kamtschatka Trench as well as in the French or German license areas.

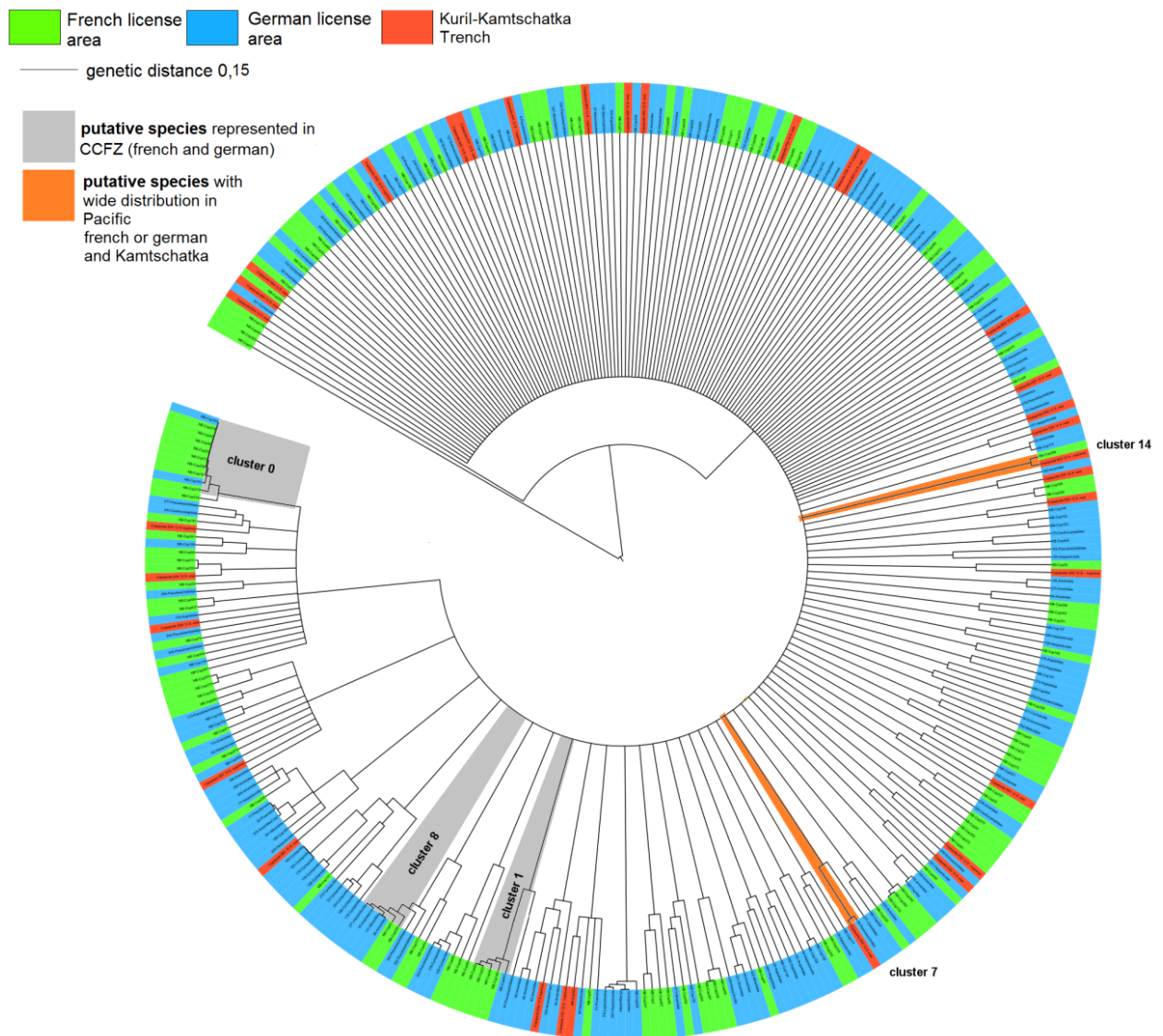


**Figure 5.19:** Phylogenetic tree of 302 copepod 12S sequences deriving from the French (green) and German (blue) license areas, as well as from the Kamtschatka Trench (red). Clusters represent MOTUs which are present in both CCZ areas (grey) or have a wider distribution in the Pacific (orange).

#### 5.2.3.4 Meiofaunal communities and their dependence on abiotic parameters

Meiofauna is known to be influenced by a variety of environmental variables. In the deep sea, the availability of nutrients has been described as a main driver of meiofaunal abundance (Galéron et al., 2000; Danovaro et al., 2002) and community structure (Zeppilli et al., 2014). Other important factors influencing meiofaunal communities of the deep-sea habitat can be water depth (Danovaro, 2000; Rex et al., 2006; Bik et al., 2012), currents (Levin and Thomas, 1989; Guidi-Guilvard et al., 2009) and the grain size of the sediment (Carman et al., 1987). In the CCZ, nodules are another factor strongly characterising the deep-sea plain. The nodules themselves are known to be a habitat with a distinctly different fauna compared to the ambient sediments (Thiel et al., 1993) and Singh et al. (2016) observed differences in nematode communities between nodule-bearing and nodule-free areas.

### Correlation analyses

Janssen et al. (submitted) carried out a local and regional-scale investigation of the relationships between metazoan meiofaunal communities (assemblages, diversity) and their surrounding environment (nodule coverage and facies, grain size, total organic carbon, ocean surface bioproductivity) in the German and French license areas of the CCZ. The main results are:

- A Spearman's rank correlation analysis indicates that there is no significant correlation between total meiobenthic density and the displacement volumes of nodules per core. In detail, the correlation analysis reveals that there is a significant negative correlation for densities of nematodes, but that the densities of the other major taxa do not correlate significantly with the displacement volume of nodules.
- However, a correlation analysis between the displacement volume of nodules and the total number of taxa does show a significant positive correlation (e.g. Singh et al., 2016).
- A Spearman's rank analysis of correlation between the meiofaunal communities, sediment characteristics and TOC reveals a strongly significant positive correlation ( $r_s = 0.9$ ,  $p < 0.05$ ) between the content of silt in the sediments and meiofaunal density, but there is no correlation with clay or sand content. In terms of community composition, silt content correlates significantly with the relative abundance of nematodes ( $r_s = 0.9$ ,  $p < 0.05$ ) and rotifers ( $r_s = -0.9$ ,  $p < 0.05$ ). In contrast, clay content shows a significant correlation with the relative abundance of copepods ( $r_s = 0.9$ ,  $p < 0.05$ ). No significant correlation between the total meiofaunal density and composition of taxa and TOC content was found.
- The „nodule crevice“ nematode community at family and genus level was found not to be significantly different from the nematode community of surrounding „bare“ sediments, although the nodule crevices do favour some nematode species (Singh, 2015).

Thus, one of the main factors determining the total meiobenthic density at the local scale appears to be the presence or absence of nodules at the sampling site, whereas size and abundance of nodules do not show a material effect on this parameter. The presence of nodules, as it is, positively affects the meiobenthic diversity (at least in terms of number of major taxa found), in contrast to its insignificant influence on total meiobenthic density. In the German license area, nodules were found everywhere, and the total density did not differ significantly between several working areas, in spite of differences in nodule size (facies) and their abundance (measured as displacement volume). In the French license area, in contrast, the total density in nodule-free areas was twice as high as that in nodule-bearing sites, whereas the difference between facies was also insignificant. Despite similarities in total density throughout the whole German license area, significant variations in relative abundance of some meiobenthic groups was registered in some working areas. In general, the total density was one and a half times higher in the German license area compared to the French license area. One possible explanation for this is the sufficient decrease in primary production from the east to the west in the CCZ. In summary, while at local scale the difference in structure of meiobenthic communities (at the level of major taxa) between working areas with varying nodule abundance is small, the difference between two distant (1300 km apart) license areas is significant.

As the biota of nodule-bearing and nodule-free sites from within the same nodule area is similar in many respects, the latter sites that are not impacted during commercial mining could well serve as donor areas providing colonisers for areas impacted during mining operations (Singh et al., 2016).

### Spatial modelling exercises

Today, distribution models are a common tool for bio-monitoring of possible anthropogenic threats to a natural environment in terrestrial, limnic and marine habitats (Bailey et al., 1998; Reiss et al., 2015). A main advantage of such distribution models is that they are conceptually simple, descriptive and can be applied based on relatively few data (Reiss et al., 2015). However, due to this simplicity it can be challenging to appropriately interpret the results in the context of ecosystem management. Nevertheless, only using point source data for biological monitoring is extremely expensive and possibly not sufficient in the deep-sea (see section above).

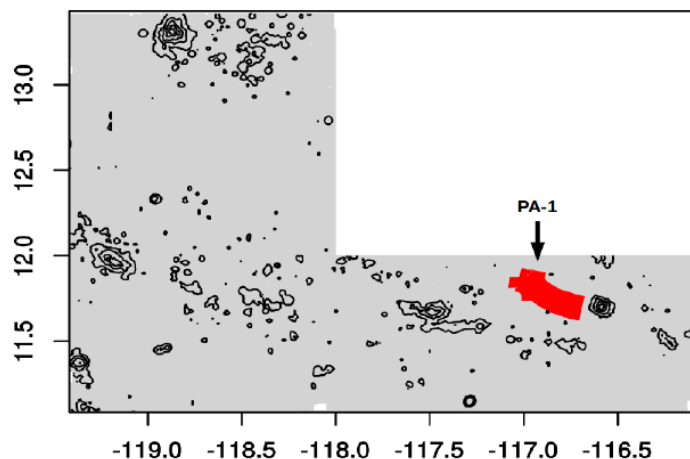


**Figure 5.20:** Map of the modelled area PA1 in the Eastern German license area.

Continuous environmental layers are only scarcely available in the deep sea (Ostmann et al., 2014; Reiss et al., 2015) although they are obligatory for the investigation or prediction of any biological variable across a continuous spatial scale. For the analyses carried out in the Eastern German license area and more specifically in PA1 (FIGURE 5.20), continuous layers are available for water depth (bathymetry), backscatter (function of nodule size), slope, aspect, roughness and topographic ruggedness index (TRI). Another environmental variable that is available as a continuous spatial layer across the whole German license area is the modelled abundance of polymetallic nodules (see CHAPTER 4.2.1).

In the prospective area PA1 many more environmental parameters have been investigated as point source data using box core samples. Such parameters include sediment grain size, wet and dry bulk densities, TOC, TIC, TC, and characteristics of the nodules (wet weight, mean size, size ratio, number, metal content). However, to use these variables as predictors for meiofaunal patterns they were converted to continuous environmental layers with random forest regression as suggested by Ostmann et al. (2014) for environmental variables in the surroundings of Iceland. As predictors for these environmental variables, backscatter and all available bathymetric variables (water depth, slope, aspect, roughness, TRI and distance to the next seamount) were used.

Distribution modelling was carried out using the package “randomForest”. According to the residual sum of squares across trees, model performance is decent for overall abundance ( $0.15 \pm 0.01$ ), richness ( $0.23 \pm 0.01$ ) and diversity ( $0.12 \pm 0.01$ ) but distinctly worse regarding the individual taxa, except for the Nematoda, and similar results were obtained for the residual sum of squares for the final model. The proportion of residuals compared to fitted values is bad only for the rare taxa Gastrotricha, Kinorhyncha, Loricifera, Tardigrada and Tantulocarida. Similarly, the stratified pairwise Pearson's correlation coefficient is worst for these rare taxa and best for Nematoda and meiofaunal diversity. Nevertheless, different distribution patterns can be observed for different taxa and meiofaunal traits. Resulting spatial predictions of the abundant meiofaunal taxa in PA1 are shown in FIGURE 5.21.



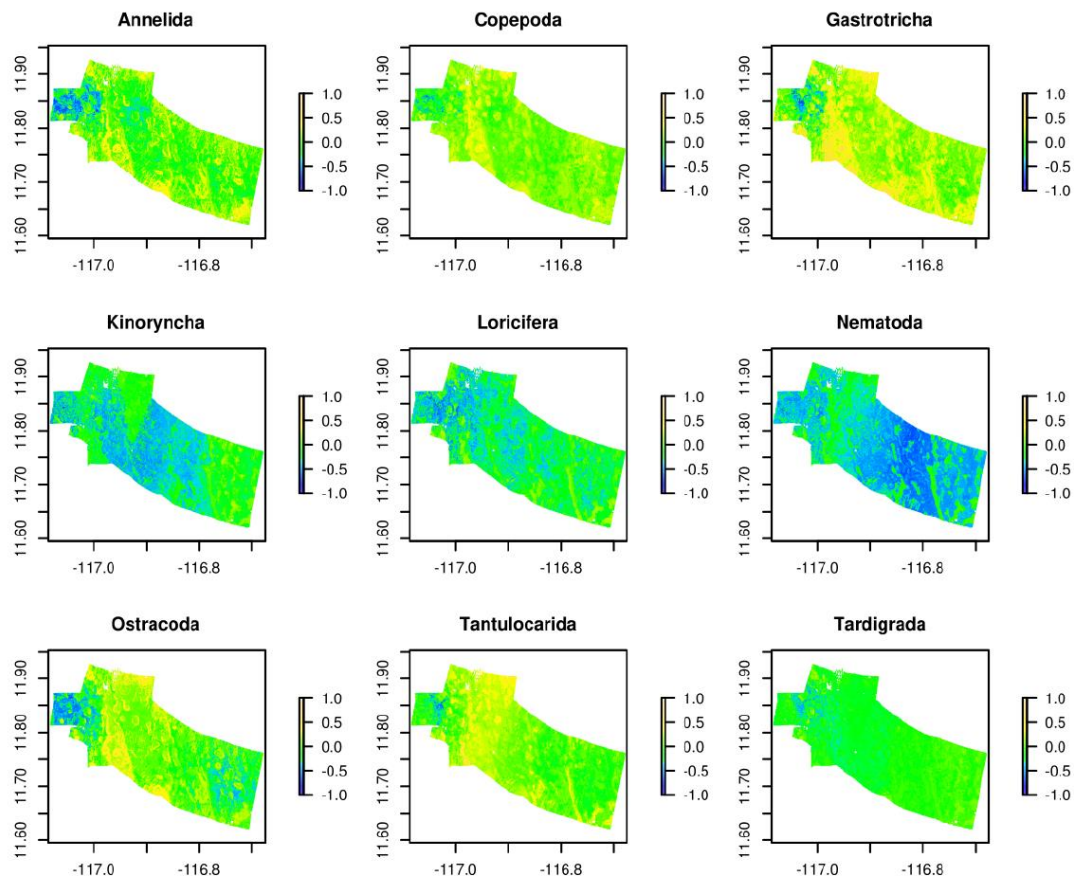


**Figure 5.21:** Spatial predictions of abundant meiofaunal taxa in PA1, converted to values between 1 and -1.

It proved possible to relate and predict meiofaunal distribution patterns based only on bathymetry, backscatter and coverage with polymetallic nodules. Investigating the importance of the predictor variables within the random forest models, especially the distance to the next seamount appears to be an important predictor variable. Furthermore, carbon content is among the six most important environmental factors for all meiofaunal response variables except for the abundance of Tantulocarida. Gradients in particulate organic matter (POM) have often been described as a main driver for biodiversity in the CCZ (Smith et al., 1997; Hannides and Smith, 2003; Lutz et al., 2007). As POM was not available in this study, the carbon content of the sediment might act as another approximation for the nutrient availability. This environmental variable has often proven to be an important influence for meiofauna (e.g. Danovaro et al., 2002; Zeppilli et al., 2014). No relationship was found with grain size or DBD, which probably relates to the very small spatial differences in these parameters across PA1.

All in all, the model results show the potential for area-wide habitat and species abundance and diversity classification – which will be a very important tool for habitat mapping and conservation planning in the future. However, the model does require a better spatial distribution of point meiofaunal data covering varying habitats, such as seamounts and hills, in addition to the abyssal plains.

### 5.2.3.5 Bioturbation

Bioturbation coefficients, delivering a quantitative measure of bioturbation, have been determined by analysing the radioactive disequilibrium between  $^{210}\text{Pb}$  and  $^{214}\text{Pb}$  (as a measure of  $^{226}\text{Ra}$ ) in 4 surface sediment cores from the eastern and western license areas using the methodologies and techniques described for the DISCOL area (Peru Basin) by Suckow et al. (2001). 49 radiometric analyses were carried out. In all 4 cores and in all samples, a significant radioactive disequilibrium between  $^{214}\text{Pb}$  and

$^{210}\text{Pb}$  and the presence of excess  $^{210}\text{Pb}$  activity even at depth (FIGURE 5.22, FIGURE 5.23) would imply that sampling has not been deep enough to obtain the whole bioturbation signal completely.

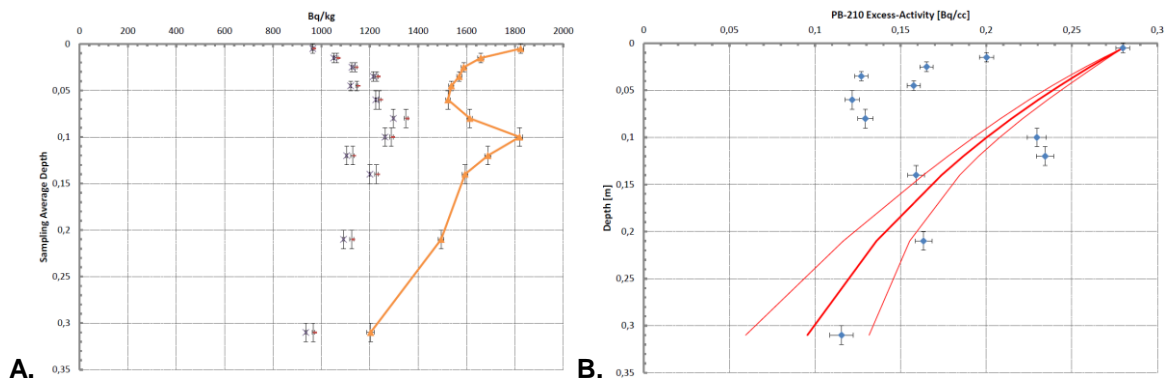


**Figure 5.22:** Radionuclide depth profiles for KM08-47KG in the western license area. **A.** Blue crosses:  $^{214}\text{Pb}$ ; red dashes:  $^{214}\text{Bi}$ ; orange line:  $^{210}\text{Pb}$ . **B.** Fitted depth profile of  $^{210}\text{Pb}_{\text{exc}}$  (blue diamonds) with positive and negative uncertainties.

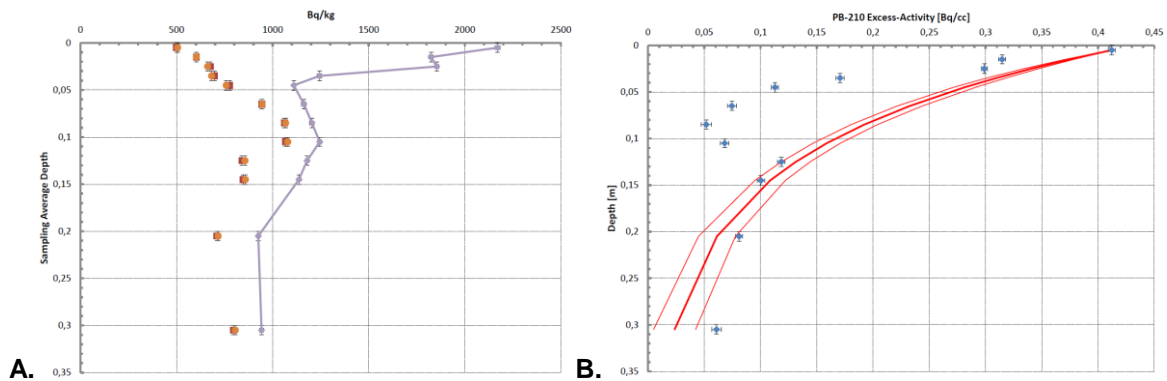


**Figure 5.23:** Radionuclide depth profiles for SO205-46MUC in the eastern license area. **A.** Red squares:  $^{214}\text{Pb}$ ; orange dots:  $^{214}\text{Bi}$ ; blue line:  $^{210}\text{Pb}$ . **B.** Fitted depth profile of  $^{210}\text{Pb}_{\text{exc}}$  (blue diamonds) with positive and negative uncertainties.

These results are not in line with conventional results of bioturbation depths for Pacific deep-sea sediments and also deviate from estimations based on  $^{230}\text{Th}$  measurements from the German license area that are being worked on at AWI in the framework of the MiningImpact project and rather suggest a bioturbation depth of around 8 cm. Surprisingly, though,  $^{210}\text{Pb}$  activity in the DISCOL area (measured by NIOZ) also does not decrease down-core to 'background' level supported by decay of  $^{238}\text{U}$  series radioisotopes within the sediment. This could indicate mixing of fresh sediment to depths of 30 cm or more, which is unexpected because of the scarcity of fauna in the area, so analytical issues cannot be excluded. Further analyses are required and will also be a target during the MiningImpact 2 project phase.

### 5.2.3.6 Microbes

#### Microbial characterisation

In order to characterise the microbial community presumably involved in the process of manganese nodule formation, DNA was extracted from four different parts (hydrogenetic, diagenetic, core, edge) of manganese nodules deriving from the area PA1-West (Blöthe et al., 2015). As a control, DNA was also extracted from the sediment surrounding the nodule. Cell numbers and microbial diversity were analysed with quantitative, real-time PCR and via clone libraries for 16S rRNA genes. Cell numbers of diagenetic

and circular edge nodule parts were determined to be as high as ca.  $1.7 \times 10^8 - 3 \times 10^8$  cells/g and similar values ( $1 \times 10^8$  cells/g) were obtained for the top 2 cm of the sediment surrounding the nodule. Cell numbers inside the nodule and in the hydrogenetic part of the nodule were lower by one order of magnitude (ca.  $10^7$  cells/g). Bacterial cell numbers were always higher than the numbers of Archaea.

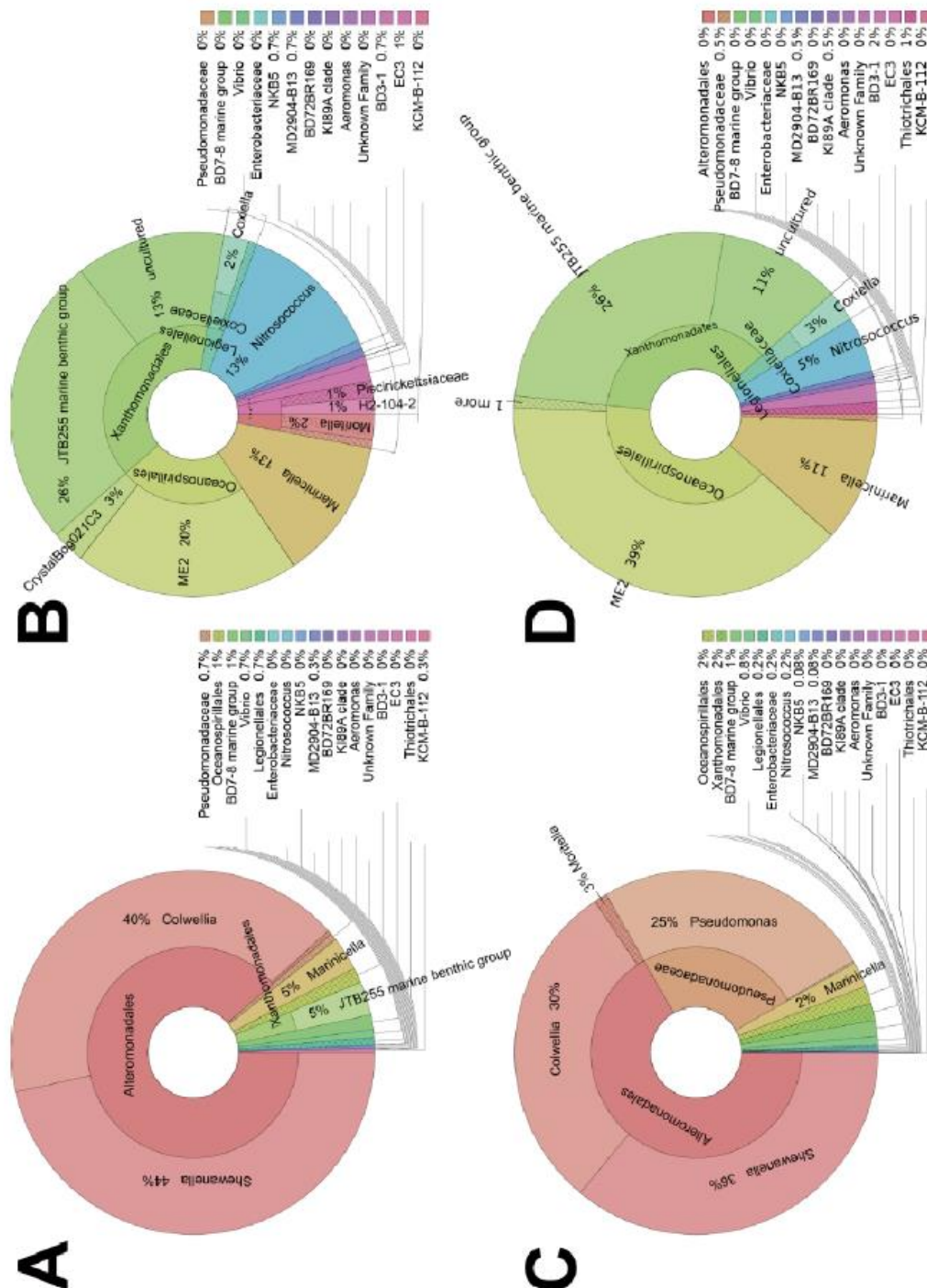


**Figure 5.24:** Detailed classification of the sequences affiliated to the Gammaproteobacteria deriving from the Easeterm German license area. (A) Results from nodule 48MUC and (B) the surrounding sediment. (C) Results from nodule 19MUC and (D) the surrounding sediment.

Bacterial species highly similar to *Shewanella benthica* were found in all clone libraries from the nodule but not in the surrounding sediment. This observation could be verified using two further molecular methods. Using molecular 16S rRNA gene techniques (clone libraries, pyrosequencing, and real-time

PCR), it could be shown that polymetallic nodules provide a suitable habitat for prokaryotes with an abundant and diverse prokaryotic community dominated by nodule-specific Mn(IV)-reducing and Mn(II)-oxidizing bacteria (Blöthe et al., 2015). These bacteria were not detected in the nodule-surrounding sediment. The high abundance and dominance of Mn-cycling bacteria in the manganese nodules argue for a biologically driven closed manganese cycle inside the nodules relevant for their formation and potential degradation. Nearly all obtained archaeal 16S rRNA gene sequences belonged to the Marine Group I Crenarchaeota and clustered in the MG I Alpha-group around the autotrophic ammonium oxidising archaea *Nitrosopumilus maritimus*. In the upper sediment, Proteobacteria (33-45%) and particularly Gammaproteobacteria (9-35%) were found to be dominant (FIGURE 5.24). Further dominating sequences belonged to the groups of Alphaproteobacteria.

### Microbial activity in sediments

In order to study the microbial activity rates in sediments of the eastern German license area, selected sediment samples from multicores as well as piston/gravity cores were incubated and potential respiration rates measured (MPI, Bremen, Germany). Potential respiration rates were estimated from the production of  $^{14}\text{CO}_2$  produced during incubation of sediment with  $^{14}\text{C}$ -acetate using the method described in Picard and Ferdelman (2011). The incubation times varied depending on the sediment.

Incubation experiments indicate that heterotrophic microbial communities are present and active in sediments of the Eastern German license area, which are characterised by low organic matter content. Activity rates were generally highest at the surface and decreased with increasing depth. The strongest decrease in activity occurred within the first 20-30 cm. Activity rates in PA1-West were measured in two cores (FIGURE 5.25). Activity is slightly higher in 46MUC in the sample nearest to the surface. However, it seems that activity decreases more rapidly at this location than at the location of 48MUC. Elevated rates at depth were observed at 170 cm in 46MUC/55KL. Similar increases of activity at depth were observed in the North Atlantic Gyre and were related to changes in lithology, to darker layers and to bioturbation (Picard and Ferdelman, 2011).

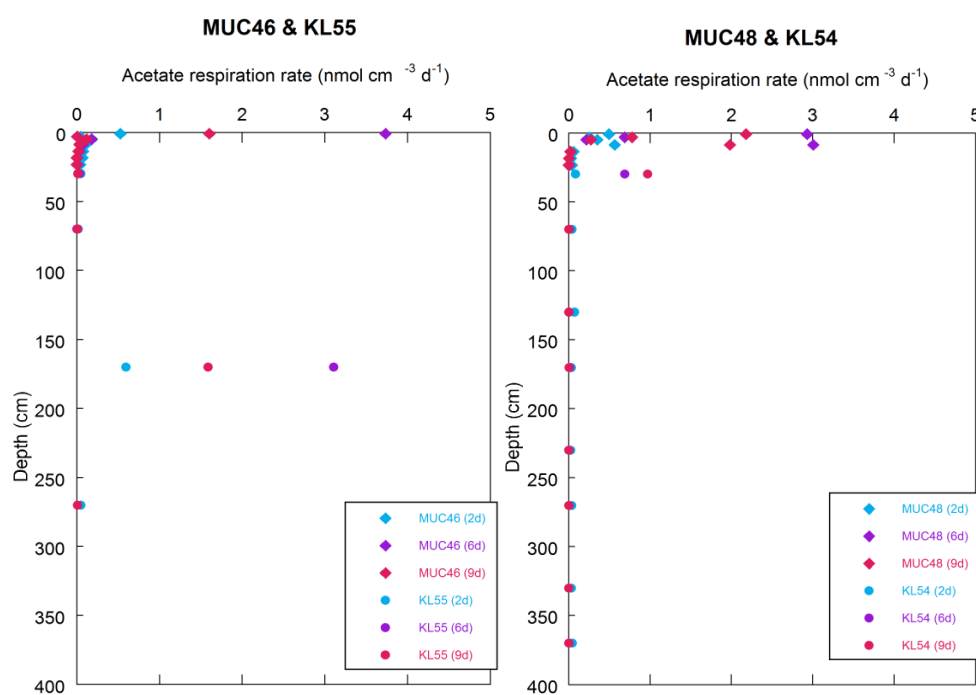


**Figure 5.25:** Microbial activity rates at two stations in PA1-West.



### 5.2.3.7 Epifauna

The nodule surface is often inhabited by sessile metazoan epifauna, such as Hydrozoa, Anthozoa and Porifera, resulting in higher epifaunal densities where nodule coverage is dense (Vanreusel et al., 2016). Also, smaller organisms belonging to the meiofauna size class, such as nematodes, harpacticoid copepods, tardigrades, and foraminiferan protists inhabit the crevices of nodules (Gollner et al., 2017). Several larger epifaunal, but also endofaunal species appear to be widespread across the CCZ (Janssen et al., 2015). Overall densities of sessile taxa in nodule areas are variable (14-30 individuals per 100 m<sup>2</sup>; FIGURE 5.26). Anthozoans are the most abundant sessile group within the epifaunal size class larger than 3 cm (> 63%), followed by sponges (Porifera, 6-36%) (FIGURE 5.26).

Mobile epifauna (> 3 cm) are represented by echinoderms (Holothuroidea, Ophiuroidea, Echinoidea, and Asteroidea) in both nodule-rich and nodule-free areas. Densities vary between 4 and 15 individuals per 100 m<sup>2</sup> in nodule-rich sites, largely due to the contribution of ophiuroids (Vanreusel et al., 2016). Densities are more than two times lower in nodule-free sites (1-3 ind./100 m<sup>2</sup>) compared to nodule fields in the same geographical area, with a particularly large decrease (>50%) in ophiuroids and echinoids (Vanreusel et al., 2016), suggesting that even the mobile epifauna is dependent on nodules or on the sessile organisms that are attached to them (sketch in FIGURE 5.26).

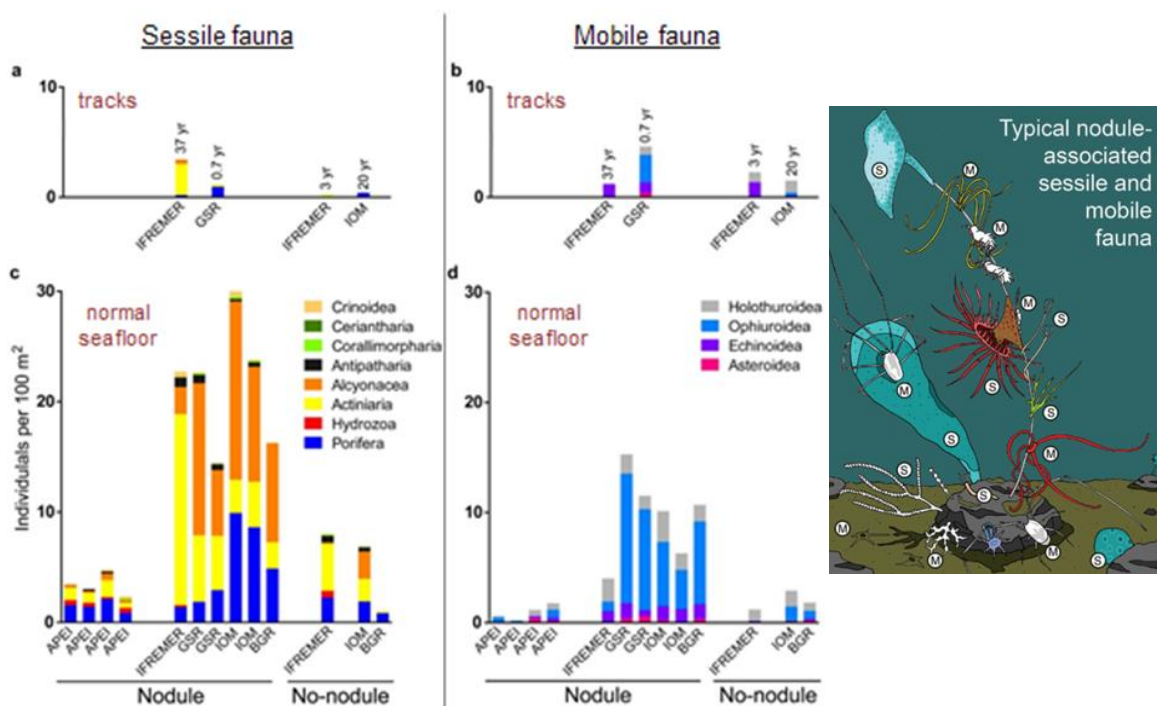


**Figure 5.26: Left:** Epifaunal abundances (sessile and mobile) on the normal seafloor of the CCZ w/o nodules in comparison to abundances in various old disturbance tracks (1979 OMCO track, 1995 IOM-BIE, 2013 IFREMER EBS, 2015 GSR EBS) (Vanreusel et al., 2016). **Right:** Sketch depicting the observed close association between mobile (M) and sessile (S) fauna and the nodules that provide the necessary hard substrate (A. Purser, AWI).

Although megafaunal epifauna is usually observed via video tracks and photographic images (see also CHAPTER 5.2.3.1), smaller organisms are not visible on these images and therefore, they have to be investigated differently. To do so, the macrofaunal epifauna was obtained from the areas PA1, PA2 and the PRZ using the box core during the three last BGR exploration cruises and counted to higher taxonomic levels. A total of 2574 individuals could be observed, 824 of which are Bryozoans (see also CHAPTER 5.2.3.3).



The most frequent taxon is Bryozoa ( $n=824$ ), followed by Komokiaceae ( $n=620$ ) and Polychaeta ( $n=561$ ) (FIGURE 5.27). Foraminifera ( $n=148$ ) and Xenophyophora ( $n=161$ ) are also quite abundant. Other taxa that occur frequently are Cnidara, Echinodermata, Bivalvia, Brachiopoda, Porifera, Crustacea and Gastropoda.

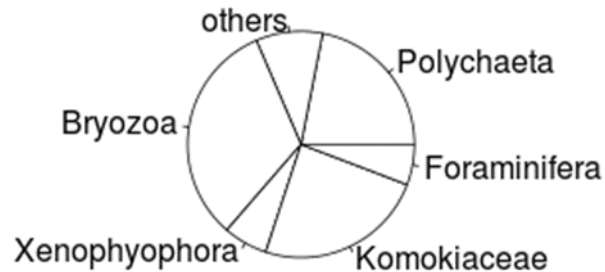


**Figure 5.27:** Relative abundances of the most abundant epifaunal taxa observed during the cruises MANGAN 2013, MANGAN 2014 and MANGAN 2016 in the areas PA1, PA2 and the PRZ.

In terms of the epifaunal densities obtained in the box cores, a largely variable number with a mean of  $19 \pm 13$  individuals could be found in one core, despite the fact that cores without any epifauna had already been neglected. A similar pattern can be observed for the individual taxa. Including sediment-dwelling species, box core samples are usually dominated by Polychaeta, Isopoda and Tanaidaceae (Borowski and Thiel, 1998; Janssen et al., 2015; Wilson, 2016). All of these taxa have also been found as epifauna, although only Polychaeta occur in higher amounts. However, the species collected as epifauna are predominantly sessile individuals. Most Polychaeta are tube-constructing and often use the manganese nodules on the sediment surface as hard substrate. A similar pattern applies for the Foraminifera, including Komokiaceae and Xenophyophora. The encrusting fauna of manganese nodules has been described to be dominated by Foraminifera and other protozoans (Mullineaux, 1987).

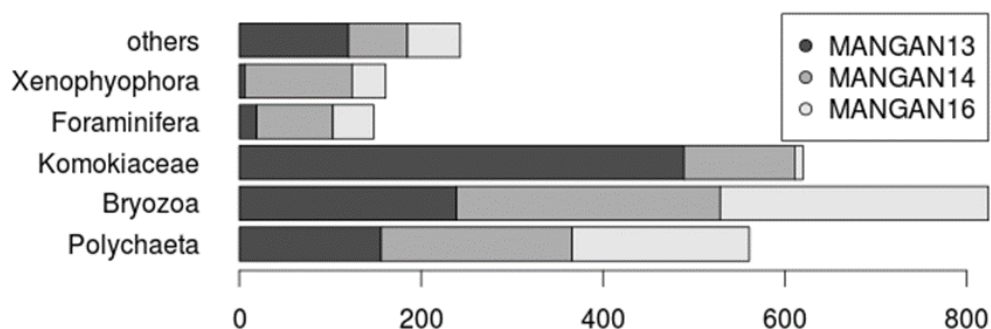


**Figure 5.28:** Number of epifaunal individuals obtained from box cores taken during the cruises MANGAN 2013, MANGAN 2014 and MANGAN 2016.

The number of individuals collected in box cores varies distinctly between cruises (FIGURE 5.28) and a significant General Linear Model (ANOVA:  $p=0.001$ ) can be computed. However, these differences can especially be observed regarding the taxa Komokiaceae (ANOVA:  $p=0.001$ ), Porifera (ANOVA:  $p=0.005$ ), Foraminifera (ANOVA:  $p=0.005$ ) and Xenophyophora (ANOVA:  $p=0.001$ ) and can possibly be traced back to difficulties concerning the determination of these taxa.

The overall weight of the manganese nodules within the box core has also been used as a possible factor influencing abundance. It was possible to compute a significant General Linear Model (ANOVA:  $p=0.004$ ) but in this case, only the Bryozoans appear to be significantly influenced (ANOVA:  $p=0.002$ ). However, it

is important to consider that Bryozoans, as well as Cnidaria, are colony-forming (Hurlbut, 1991) and therefore fragments might be counted as whole individuals, thus distorting the actual abundance.

#### **5.2.3.8 Demersal scavengers and fish**

Demersal scavengers and fish have hardly been analysed in the German license area. Two amphipod baited traps/landers were deployed in PA1-West during the SO-239 cruise and were successful in sampling several amphipods and fish. In total, specimens of 18 different taxa of amphipods and fish were collected from across the CCZ (Martínez-Arbizu and Haeckel, 2015). The lander system Anonyx of the Herriot-Watt University (Edinburgh) equipped with cameras and baited traps will be deployed several times during the next BGR exploration cruise (SO-262) to the Eastern German license area in order to quantify scavenger biodiversity and relative abundance, amongst others also in the planned collector test area.

## **6. Description of impacts on the physico-chemical environment**

This section provides an overview of potential impacts that the collector vehicle test will have on the physico-chemical environment, in a descriptive form that is based on the best scientific information that is available at this time. The aim of the MiningImpact 2 project is to assess the immediate, short-term and intermediate-term (2 year) physical and chemical impacts of the collector vehicle test on the seafloor and its overlying waters, as well as the response of benthic organisms to the impact, which in turn is crucial for the recovery of benthic standing stocks and biodiversity and for the maintenance of associated ecosystem functions. We thus refrain from providing detailed assessments or prognoses on the extent of impacts here (except for a detailed modelled assessment of the potential range of the sediment plume, see CHAPTER 6.4.3), but rather refer to CHAPTER 8 for a detailed description of the monitoring programme that will scientifically accompany the collector test. Detailed analyses and input of data into models, also in terms of future risk assessment, will allow a much more comprehensive future assessment of the nature and extent of similar impacts, perhaps related to test mining, and the development of recommendations on how to avoid, remedy or mitigate such impacts.

### **6.1 Description of potential impact categories**

The major types of physico-chemical environmental impacts of nodule removal from the seafloor, that will or potentially might occur during the DEME-GSR collector vehicle test, are (1) habitat/nodule removal, (2) sediment disturbance and plume formation, (3) biogeochemical alteration of the sediment (i.e. change of habitat integrity), (4) potential release of toxic sediments and/or substances into the lower water column, (5) emissions to air, and (6) potential additional impacts from natural hazards such as hurricanes or benthic storms. Most of these impact categories will also affect the biological environment (see CHAPTER 7), as will potential noise and light pollution. These potential impact categories are described in more detail in CHAPTER 6.2 to CHAPTER 6.7 below.

### **6.2 Emissions to air**

The vessels that will be in use in this project strictly follow the IMO obligations and standards regarding safety and environmental practice at sea, including the International Convention for the Prevention of Pollution from Ships, 1973, as modified by the Protocol of 1978 relating thereto (MARPOL) and the Protocol of 1997 to MARPOL concerning the prevention of air pollution from ships. In this way, the IMO regulates emissions to air and forces anti-pollution measures that aim at minimising all effects of air and water pollution at sea.

### **6.3 Nodule removal**

Picking up the nodules and removing the associated fine-grained muds fundamentally disturbs the benthic habitat in the mining area, leading to degradation of seabed habitat (see CHAPTER 7.4.1), and entails the generation of sediment plumes near the seafloor (see CHAPTER 6.4). From a physical impact

perspective, removing nodules (and sediments) from the seafloor will also change the micro-topography or roughness of the mined area (less friction due to nodule removal; production of small furrows and ridges), which in turn could affect the hydrodynamic current regime close to the seabed as well as processes of sedimentation/resedimentation. Preliminary experiments with a racetrack flume carried out at JUB (Bremen, Germany) have shown that the hydrodynamics between nodules is complex and vortices, erosion and accumulation zones can be determined. Bedload transport is more pronounced in areas of lower nodule abundance, suggesting that bedload transport will increase when nodules are removed.

In the case of the collector vehicle test planned here, the directly impacted area where nodules are removed will have a maximum size of only 0.1 km<sup>2</sup> and lies in the middle of a flat abyssal plain without any topographic constraints in the direct vicinity (FIGURE 3.4). We thus assume that, on a more regional scale, the removal of nodules in the test area will have an insignificant effect on the physico-chemical regime of the area.

## 6.4 Sediment disturbance and plume formation over time

Environmental concerns associated with the sediment discharge (the “sediment plume”) in the course of deep-sea mining include (a) artificial rapid redeposition of sediments from the resettling plume and bottom blanketing in the vicinity of the mine site (“near field”), burying benthic organisms and clogging the respiratory surfaces of filter feeders, (b) oxygen depletion in the blanketed seabed and the water body inside the plume through reactive constituents (e.g. labile organic matter or reduced metals), and (c) the release and deposition of toxic metals (see CHAPTER 6.6), which can lead to bioaccumulation of contaminants as is a well-known problem for the release of oil and gas drill cuttings (e.g., Rye et al., 2007). These processes will affect deep-sea ecosystem structure and functioning to a certain, presently unknown extent. To date only very few studies have focussed on analysing and modelling the scale of this impact at various environmentally relevant temporal and spatial scales, which is dependent on multiple local and regional factors such as the physical and chemical properties of the bottom sediments, the nature of the hydrodynamic regime (near field and far field), bottom topography, the type of mining equipment being used, and mining rate, amongst others. At the moment, the amount of sediment deposition from a mining-induced plume that could either be tolerable or lethal for any of the faunal groups of the deep sea is completely unknown.

### 6.4.1 ASSESSMENTS FROM BENTHIC IMPACT EXPERIMENTS

To date, only few publications have dealt with the possible behaviour of the sediment plume in abyssal manganese nodule exploration areas, these being mainly restricted to the results of mining tests carried out in the 1970s by Ocean Mining Inc. (OMI) and Ocean Mining Associates (OMA) (e.g. Lavelle et al., 1981) and to the results of benthic impact experiments and modelling activities carried out in the 1990s by Germany (DISCOL/ATESEPP; Peru Basin), Japan (JET; Japanese CCZ claim area) and Russia/USA (NOAA-BIE; former American CCZ claim area). These focused primarily on determining the impact of the resettled sediment plume on benthic fauna (for a detailed description of these experiments, see Jones et al., 2017). In these experiments, the extent of redeposited sediment in the surroundings of the impacted sites was inferred from seabed imagery (Yamazaki et al., 1997) and from numerical simulations forced by time-series measurements of ocean bottom currents and imposed static particle sizes and settling velocities (e.g., Nakata et al., 1997, Jankowski and Zielke, 2001, Rolinski et al., 2001). Deep-sea observational technology at the time of those experiments did not allow for comprehensive monitoring of

the actual sediment plumes as they were spreading laterally and vertically away from the source site, nor could differential particle aggregation processes which critically determine the redeposition of sediments from the plume be assessed.

In the JET experiment, a Deep Sea Sediment Resuspension System (DSSRS) was towed 19 times along two parallel 2000-m-long tow zones throughout a time period of ca. 1 month, ejecting a total of 352 tonnes of sediment slurry with at a rate of ca. 30 g/l and 60 l/s at a height approximately 5 m above the seafloor (Fukushima, 1995). Sediment trap analyses and modelling exercises showed that resedimentation or blanketing reached a maximum thickness of 2.6 mm close to the source (Barnett and Suzuki, 1997). Furthermore, empirical and modelling data of the JET and the technically very similar NOAA-BIE experiments showed that 90% of the suspended particles created by artificial disturbance of the sea floor had settled within a radius of 2 km from the impact area (Fukushima, 1995; Nakata et al., 1997). The residence time of a plume created by a single collector with an assumed pilot-scale production of 10 kg/s (about 5 times the output of the DSSRS) in a relatively small area (ca. 1500 m path length) was estimated by Jankowski et al. (1996) to be 1.5 to 6 days. As a comparison, the collector vehicle test that is planned for April 2019 in the framework of the MiningImpact 2 project will discharge sediments at least at a rate of ~135 t/h, = 37.5 kg/s. Although the coarser fraction was apparently deposited shortly after release, Segsneider and Sündermann (1998) and Rolinski et al. (2001) developed a far-field model with finite differences specifically for the south-eastern Pacific (Peru Basin) which showed that resettling of 90-95% of the total mass of relatively fine-grained sediments may take 3 to 14 years, and of 100% of the total mass 9 to 17 years, depending on the water depth of release. In all cases, adequate validation of the models used was hampered by incomplete and sparse current measurement data, these deriving from a handful of point current sensors at fixed water depths only (in contrast to present-day ADCPs that continuously measure over a whole range of water depths), and poor bathymetric data. Furthermore, the experiments and modelling exercises carried out focussed more strongly on blanketing, bottom destruction and faunal recovery than they did on plume dispersion in the water column, and they represent relatively small-scale single dose discharges, which probably cannot be extrapolated to a (sub-)industrial scale, continuous production level.

During the MiningImpact 1 project, several small-scale sediment dispersal experiments using an epibenthic sled (EBS) and a remotely operated vehicle (ROV) were conducted to suspend surface sediment. An attempt was made to track the plume using upward and downward-looking Acoustic Doppler Current Meters (ADCPs) mounted on benthic landers, light-backscatter sensors and HD cameras. While both experiments were not set up for quantitative analyses, some qualitative statements could be made: the sediment plumes did not rise more than 10 m above the seafloor, and the lateral spread varied largely in conformity with changing current velocity and direction during the experiment as well as seafloor topography.

Particulate elemental concentration was measured in a small-scale experimental plume that was produced by the ROV Kiel 6000 in the Peru Basin (cruise SO-242/2). DOC concentration was initially very high (immediately after production of the plume by the ROV), i.e. 57.28 mg/L after 1 minute, but strongly decreased to 0.63 mg/L after 4 minutes, and subsequently fluctuated only slightly between 0.79 and 0.57 mg/L within the 50 minutes of measurement. Background bottom water DOC values were in the range of 1.5-4 mg/L.

AUV mapping of the resettled sediment of one of the time series EBS tows in the Eastern German license area (PA1-West) (FIGURE 6.1 top) indicates that the major mass fraction of the suspended sediment covered nodules (and epifauna) up to 100 m to the south and up to 25 m to the north of the track (Peukert et al., *subm.*). The blanketing pattern was controlled by the predominantly southward current flow direction during the experiment. The small distance of sediment blanketing is corroborated by controlled laboratory



experiments documenting the importance of rapid particle aggregation for scavenging of the fine fraction (see CHAPTER 4.2.4.2). It must be stated, though, that the amount of sediment suspended by a towed EBS is unlikely to be comparable with that of the collector vehicle planned here (135 – 337 t/h, depending on driving speed, see CHAPTER 3.4). Upscaling of small-scale experiments is very challenging in this respect and therefore, larger-scale experiments with realistic gear such as planned in the project presented here are needed to reduce current uncertainties with respect to the fate, dynamics and impact of the suspended sediment plume.

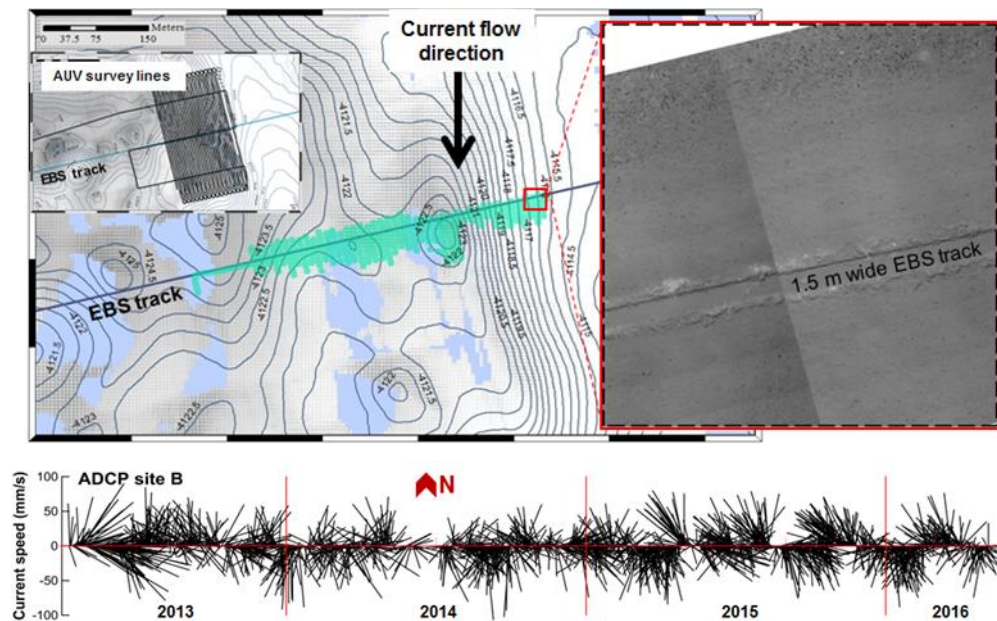


**Figure 6.1:** **Top left:** Map of an EBS sediment plume experiment in PA1-West (Eastern German license area). The resettled sediment was mapped (green area) by an AUV photo mosaic. **Top right:** Zoom into the assembled photo mosaic showing the 1.5-m wide EBS track and the resettled sediment blanketing the nodules (and epifauna) on the adjacent seafloor. **Bottom:** 3 years of current data (April 2013 to May 2016; 600 kHz ADCP data 12-16 m above the seafloor) obtained at close proximity to the EBS track site (see FIGURE 4.3). Current velocities are typically < 5 cm/s and directions are highly variable. Figure from Peukert et al. (submitted).

#### 6.4.2 PREVIOUS HYDRODYNAMIC PLUME MODELLING EXERCISES

With the currently available high-quality and high-resolution spatial and temporal hydrographic and sedimentological data, high-resolution bathymetric data and with modern computational power it is now possible to numerically simulate the initial (near field) and long-term (far field) stages of mining-related plume formation close to the seafloor. Particle aggregation processes (CHAPTER 4.2.4.2), not taken into account in previous modelling exercises of mining-induced plumes (e.g. Nakata et al., 1997; Aleynik et al., 2017), can now be specifically implemented into regional ocean circulation-sediment transport models to simulate the likely fate of the sediment plume produced by industrial-scale mining using different discharge scenarios.

The results of all available hydrographic analyses of CTD, MAPR, ADCP and OBM deployments from the eastern German license area and its vicinity (CHAPTER 4.2.3) have been used for the initialisation, calibration and verification of existing and specifically adapted ocean circulation and sediment transport models focussing especially on the conditions in PA1-West of the German license area as case study area. Such modelling work has been carried out in the framework of the EU FP7 project MIDAS by the Scottish Association of Marine Sciences (SAMS) and published in Aleynik et al. (2017), and more intensively during the first phase of the MiningImpact project (Purkiani et al., in prep.). These models provide more

insight into the likely near-field fate of the sediment plume produced by industrial-scale mining under varying discharge scenarios in comparison to the modelling efforts which took place in the framework of the Benthic Impact Experiments in the CCZ in the 1990s.

Deep ocean bottom boundary flows are often highly complex, dynamic and turbulent (Dale and Inall, 2015). On the abyssal plains, bottom flows reflect large-scale ocean circulation, as well as tides, transient eddies, fronts, and near-inertial waves originating at the ocean surface. In topographically complex regions, mixing-driven residual flows also become important. Stratification is typically weak, which means that even the relatively slow flows of the deep ocean (a few cm/s) can create turbulent disturbances which originate from the bottom boundary and may penetrate a hundred metres or more vertically. The complexity of near bed flows means that, for detailed predictions of plume structure, behaviour and dispersion, local numerical modelling is required at very high resolution (of order 100 m), and in three dimensions (MIDAS Report D2.2).

For deep ocean flow speeds ( $\sim 5$  cm/s), features of hundreds of metres or less in extent produce non-hydrostatic flow responses. Other phenomena with small-scale structure, such as internal waves and tides interacting with slopes also display non-hydrostatic dynamics. The deep ocean is rich in structure on these scales, and, for this reason, a non-hydrostatic modelling approach is essential when considering plume behaviour on these scales. The Massachusetts Institute of Technology general circulation model (MITgcm) is the most developed finite-volume, non-hydrostatic ocean modelling tool and is ideally suited to modelling deep ocean boundary layer flow (Marshall et al., 1997). Both MIDAS (SAMS) and JPI-O MiningImpact (University of Bremen) conclude that MITgcm model results for PA1-West, including predicted distributions of water temperature, salinity and current velocities at different depths, fit well to the observational data in this region.

The MITgcm model solves the Boussinesq and hydrostatic form of the Navier-Stokes equations for an incompressible fluid on a three-dimensional grid (Marshall et al., 1997). The present MIDAS model configuration (Aleynik et al., 2017) covers a small rectangular Cartesian domain with a grid of  $192 \times 192 \times 90$  cells in a box of approximately  $45 \times 45$  km in the horizontal (PA1-West) and 4000 m in the vertical (FIGURE 6.2). Vertical resolution is 20 m and horizontal resolution is 200 m in the majority (85%) of the model domain, i.e. centring on the ADCP mooring sites, but increases telescopically to 1 km towards the lateral open boundary to reduce the influence of reflection of internal waves back into the model domain. Tidal potential was computed with 8 major tidal harmonics using an inverse tidal solution, and daily-averaged, de-tided residual flow was added at the model open boundaries in addition to tidal forcing, which was extracted for the model domain using the TPX07.2 and OSU model (Egbert and Erofeeva, 2002). A nodal correction and tide origin time were adjusted to exactly match the model tidal phase with the observed one on duration of runs, which was restricted to five weeks in spring 2013. Horizontal eddy viscosity and diffusivity coefficients were set at  $0.1 \text{ m}^2/\text{s}$ . This estimate is comparable to the values of numerical diffusion for similar fine-scale horizontal grids.

Hydrodynamic model assessment and performance skill estimates for the MIDAS plume model were based on the comparison (regression analysis) of model results with measured velocity measurements in the deepest ocean layer at all three mooring sites. Observed and modelled 1-hourly sub-sampled and residual (de-tided; 12-hourly averaged) zonal and meridional velocities were at least in *very good* (0.72) agreement, corresponding to the Wilmott index. The difference between modelled and observed currents does not exceed 28% (see FIGURE 6.3C), which is substantially better than that published for other deep-sea simulations (Alford et al., 2015). The model demonstrates better performance skills at moorings sites A and B than at site C, which is topographically sheltered for northward flow. The model is thus successful in qualitatively reproducing the general trend of observed bottom current action.

The presence of locally (topographically) generated nonlinear internal waves could lead to strong velocity shear and mixing. The presence of internal waves in the area was detected from full-depth profiles of CTD casts that were obtained from the eastern German license area in June 2015 (SO-240 cruise). The fine temperature-salinity structure below 3 km depth remained very similar during two days of tow-yo measurement, not being destroyed but vertically displaced by 10-15 m. The thick, quasi-homogeneous bottom boundary layer (BBL) here is composed of Lower Circumpolar Water (a mixture of North Atlantic Deep and Antarctic Bottom Water) and extends as high as 300 m above the seafloor (3800–4100 m depth) with a narrow range of potential temperature  $\theta_4 = 1.465\text{--}1.483^\circ\text{C}$ , salinity  $S = 34.670\text{--}34.682$  and a very low buoyancy frequency  $N = 0.24$  cph ( $6.7 \cdot 10^{-5} \text{ s}^{-1}$ ). Bathymetry near the mooring sites reveals a mostly flat landscape with irregularities of the order of several hundred meters in the vertical and a few kilometres in the horizontal directions. To enable the model to resolve internal wave features, the Pacanowski-Philander vertical mixing scheme was applied (Pacanowski and Philander, 1981) with Richardson number dependant parameterisation for turbulent closure of vertical viscosity and diffusivity. Different experiments with energy dissipation computed with a closure scheme (Klymak and Legg, 2010) based on sorting of the vertical density profile demonstrated similar but more apparent internal waves dynamics (FIGURE 6.2).

The model-calculated internal wave field was generally weak except at steep slopes of scattered hills, where the slope angle is close to or exceeds the internal tide propagation angle, the critical value for increasing tidal energy conversion into turbulence. Model currents kinetic energy flux calculations indicate a ten-fold increase ( $\sim 20 \text{ J/m}^3$ ) over the hills in the north-western segment of the modelled domain ( $50 \times 50 \text{ km}$ ) in comparison to background values over the relatively flat seafloor. These topographic slopes are steep enough to emanate tidal energy flux, which concentrates along the beams, reflected from seabed at angles  $10\text{--}15^\circ$  (upward and downward). In the horizontal plane, the leading edge of the internal waves radiates slowly from the slopes and over relatively short distances (in the order of several kilometres), thus hardly reaching the nearest mooring site 1 which is located more than 15 km away. Vertical diffusivity averaged over a month in the deepest model layers shows locations of mixing *hotspots* (FIGURE 6.2b).

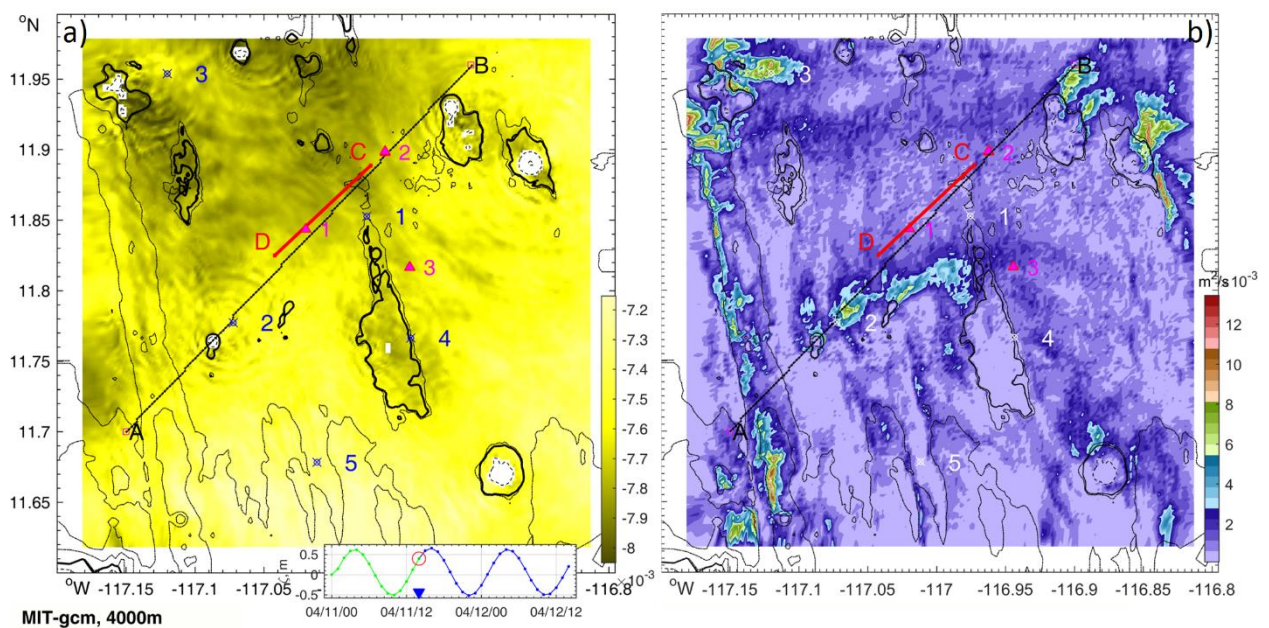


**Figure 6.2:** **a)** Modelling of the non-hydrostatic pressure potential ( $P_{NH}/p$ ,  $\text{m}^2/\text{s}^2$ , shadow) in PA1-West indicates radiation of Internal Waves from topography. **b)** Mixing hotspots are shown by the vertical diffusivity ( $10^{-3} \text{ m}^2/\text{s}$ ) in layer 100 mab averaged over a month. Pink triangles show the positions of the three mooring sites. Positions 1 to 5 reflect the positions of dissolved tracer plume experiments (see FIGURE 6.3). Figure from Aleynik et al. (2017).



### 6.4.2.1 Dissolved tracer plume modelling

A neutrally buoyant tracer plume model was configured by SAMS (Aleynik et al., 2017) and designed in a similar way to a dye release experiment over a shelf sea environment. The plume spreading simulation in this numerical experiment involved application of dissolved, neutrally-buoyant tracers and was constructed by applying constant tracer injections at a rate of 1 unit/s into the lowest model layers at 5 different locations in PA1-West for one hour and then tracing the dispersion of the plume in 12 h periods over the period 02-05 May 2013, i.e. during the time after eddy I passage through PA1-West. The release sites are shown in FIGURE 6.2 (sites 1,4,5 were chosen far from hotspots, and sites 2,3 near to hotspots). Near the topographically-enhanced mixing zone and in the downstream flow, a higher plume core dilution rate was noticed (FIGURE 6.3B). Maximum dissolved tracer concentrations reduce significantly immediately after plumes 2 and 3 trespass over mixing hotspots, while in plumes 1,4,5 travelling over calm and less energetic sites, concentrations remain higher for a longer period of time. Dilution was sufficient enough to disperse material up to 100-120 m into the mixed BBL within only a day. The experiment reveals that tracer dispersion is controlled by vertical diapycnal mixing in combination with horizontally and vertically sheared currents.

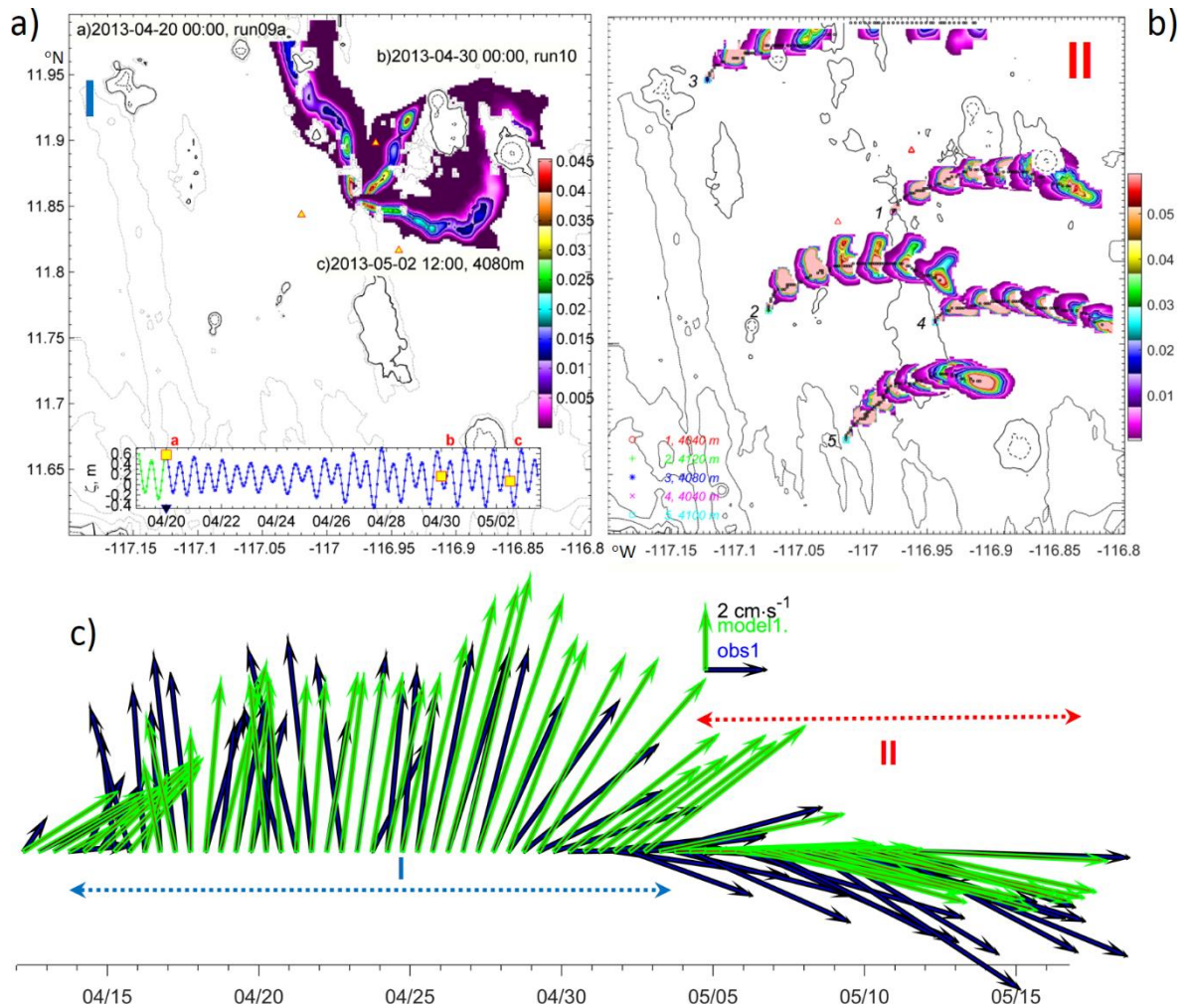


**Figure 6.3:** **a)** Dissolved matter plume core tracks (colours, concentration in parts per unit), formed by neutral tracers released in eddy period I (April 2013) at three different dates marked on inset surface elevation ( $\zeta$ , m) graph. Mooring sites are marked by the triangles. **b)** Plume core tracks formed by neutral tracers released in period II from 'calm' sources (1,4,5) and two more energetic sites (2,3) adjacent to 'hotspots' (shown in 12-hour intervals). **c)** Observed (blue) and modelled (green) residual current vectors averaged over 12 hours at 20 mab at mooring site A. Figure from Aleynik et al. (2017).

### 6.4.2.2 Particle-based plume modelling

In this numerical experiment, also carried out by SAMS (Aleynik et al., 2017), a suspended particulate matter (SPM) plume burden was simulated by tracking the transport of 0.57M discrete particles, representative of an experimental collector test scenario according to MIDAS criteria. The scenario involves the removal of the upper 15 cm of the sediment layer, of which 90% is exhausted and suspended near the seafloor by a single nodule prototype 'collector' that mines in a 'lawn-mowing' pattern at a speed of 0.3 m/s (along a spiral track). Natural sediment grain sizes were split into 44 discrete classes with fractions ranging from  $1.15 \div 2 \cdot 10^3 \mu\text{m}$  based on the analysis of sediment samples recently obtained from the UK claim area (Jones et al., 2015). The dry weight and bulk sediment densities were assumed to be 2.65 and 0.8 g/cm<sup>3</sup>, respectively. Sinking and settling speeds were determined via a Reynolds number-based approach (Fredse and Deigaard, 1992; Cheng, 1997). Every minute (SPM model time step), particles of randomly selected size fractions mimicking a discharge rate of 278 kg/s were suspended at 10 m above the seabed. During 10 days and working 57% of the time, such a single collector would suspend altogether 240,000 tons of sediments.

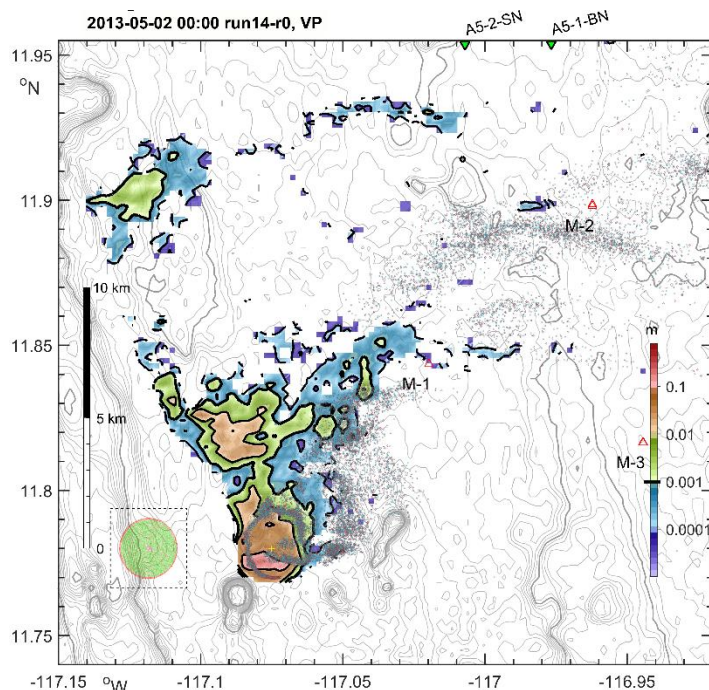


**Figure 6.4:** Modelled particulate plume on the 10<sup>th</sup> day after the start of release (at the end of eddy passing period I, 01.05.2013) containing 0.57M individual particles suspended in water (grey dots) and settled on the seabed (colours). The area with substantial accumulated sediment layer thickness (m) is shown over bathymetry (grey lines, 50 m). Points along the nodule collector tracks were aligned with an equally-spaced Archimedes spiral, and shown on the dashed inset to indicate the scale of the harvested zone during the last day (red) and since the beginning of the experiment (green). Figure from Aleynik et al. (2017).

The particulate plume consists of over half a million individual suspended particles and was traced for a duration of several weeks. Within 10 days, more than a half of the particles had settled within several km from the 'harvesting' vehicle, and the rest remained suspended or had left the model boundary (FIGURE 6.4). Both the shape of the SPM plume and its sedimentation (blanketing) footprint on the seafloor well match the background circulation pattern that was affected by the veering eddy transition during this experiment. After 10 days the area in which the re-deposited sediment thickness exceeded 10 cm did not stretch further than 1.25 km from the impact zone, while the isolines 1 and 0.1 cm were found at respectively 2 km and 5 km away from the source in the direction of dominant flow (FIGURE 6.4), which is



not dissimilar to previous observations (Trueblood, 1993). Within these deposition isolines, the natural background sedimentation rate in the Central Pacific reached in a thousand years (1-6 mm/kyr) (CHAPTER 4.2.4.4) is reached within just 10 days. The redeposition of plume SPM at this scale thus has a huge impact on the generally non-resilient deep ocean ecosystem, which could be prone to irreversible changes under such enormous pressure.

The SPM model was found to be robust in a series of sensitivity tests with varying horizontal and vertical mixing coefficients (particles diffusion) by three order of magnitude. The model produced very similar spreading patterns of suspended particles and its seabed footprint ("sediment blanketing") under the given flow regime and only marginally smoothed contours in experiments with higher diffusivity. However, in sensitivity tests with varying ambient flow speed, differences were detected in the settled particles size distributions. With greater current speeds, the sorting of particle size was enhanced and larger particles were able to reach mid-range distances (5-10 km), while near- and far-field particles sizes distribution generally remained nearly unchanged both in relatively low and high seabed speed tests.

Scalable comparison and model validation is difficult but possible with the data obtained from the centre of the CCZ in similar environments during the NOAA/Russian Benthic Impact Experiment (BIE) (Trueblood, 1993). During 19 days, almost 1427 tonnes of sediments were dispersed at a rate of 4 kg/s by a 6-m-wide "benthic disturber" that was towed in 49 parallel rows inside a 3000 m x 150 m polygon. Post-impact observations and analyses of 18 sediment traps (Jankowski and Zielke, 2001) revealed that the mean distribution of sediments collected in traps increased over 2 order of magnitude (0.03-1 mm) and was proportional to the distance from the source. Immediately near the tow zone, nodules were buried under 2 cm of fresh sediments. This is similar to the blanketing thickness at the same distance from the source calculated in this MIDAS model of the eastern CCZ German licence area (FIGURE 6.4). Ultimately, though, any serious validation of model results involves actual testing of equipment and synchronous monitoring of plume dispersal and sediment deposition as is planned in the MiningImpact 2 project that is the subject of this EIA.

One of the great shortcomings of the above-mentioned near-field hydrodynamic model for plume spreading and dispersion is that it does not take into account the cohesive properties and aggregation of fine-grained sediments, which are assumed to reduce both the horizontal extent and the height of vertical spreading of the plume (e.g. Jankowski and Zielke, 2001). The modelling work that is currently being carried out in the framework of the JPI-O MiningImpact 1 project (University of Bremen, Germany) integrates sediment-transport algorithms into a MITgcm plume model and is described in CHAPTER 6.4.2.3 below.

#### **6.4.2.3 Integration of a sediment transport model to account for aggregation**

A preliminary sediment particle analysis of sediment samples deriving from the German license area was performed at the Jacobs University in Bremen (see CHAPTER 4.2.4.2) and has shown that cohesive sediments form the main component of the top sediments at the seafloor, and that the mineral plume aggregates of the German license area settle considerably slower than sediments of similar size, thus deviating greatly from Stokes Law. Therefore, the inter-particle cohesion forces that lead to flocculation cannot be neglected when modelling the dispersion of a sediment plume. The integration of sediment-transport algorithms into a MITgcm plume model thus allows a more realistic modelling of the vertical sinking and lateral dispersion of fine-grained particles by ocean currents. The model needs to be fed with appropriate values for sediment parameters deriving from the case study area (e.g. sediment settling velocities, concentration-dependent flocculation potential, suspended particle matter size distributions, aggregation potential, erosion and resuspension potential). These have been derived from laboratory

analyses and experiments on sediments from the German license area by the Jacobs University in Bremen (see CHAPTER 4.2.4.2), and/or from physical equations for sediment transport that are integrated into the 3D hydrodynamic model.

The modelling work that was carried out at the University of Bremen in the framework of the first phase of the JPI-O MiningImpact project had a strong focus on integrating sediment transport algorithms into the MITgcm hydrodynamic plume model at an early stage of the model development process. A flocculation model presented by Winterwerp (1998) was implemented to account for cohesive sediment transport. Some major developments applied in the model are as follows:

- implementing cohesive sediment transport including the flocculation process;
- adding dynamic floc properties such as floc size, density and sinking velocity;
- reformulating the sediment-transport equation with a variable source term;
- developing a seafloor sediment deposition algorithm.

In contrast to the MIDAS plume modelling scenario in which the settling velocity is assumed to be constant, the flocculation model integrated here is able to calculate the dynamic floc sinking velocity at any depth. The most prominent parameter that controls the flocculation process (aggregation and break-up of particles) in this implementation are the shear rate  $G$  and the suspended sediment concentration. The initial values of horizontal and vertical diffusivity of every tracers are set to 0.1 and  $10^{-4} \text{ m}^2\text{s}^{-1}$ . However, the model uses the parameterisation method of Klymak and Legg (2010) to obtain the suitable content of eddy viscosity and turbulence dissipation values. The suspended sediment concentration is calculated by a coupled sediment-transport model that solves the passive tracer equation with additional settling velocity and sediment source and sink for different, predefined sediment size classes.

A multiple one-way nesting approach has been successfully applied in this investigation. The large-scale model that covers a rectangular  $2 \times 2^\circ$  domain in the eastern Pacific Ocean has a resolution of 3.6 km. It is laterally forced by temperature, salinity, meridional and zonal velocities throughout the entire water column obtained from the Hybrid Coordinate Ocean Model (HYCOM). An intermediate resolution (1 km) model for an area covering a smaller region of  $1 \times 1^\circ$  is nested into the coarser model. The finest resolution model (300 m) is generated for the area in which the current moorings were deployed (PA1-West). Vertical resolution was set to 20 m. The contribution of tidal currents in the total energy oscillation in the deep ocean is considered by applying the major tidal components in the equation of motions using the Tidal Model Driver (TMD) toolbox (Padman and Erofeeva, 2005). The model results are validated with the observed current velocities measured with bottom moored ADCPs. The simulated seawater properties such as temperature and salinity of the entire water column are compared with the vertical CTD profiles. These comparisons show that the model is able to reconstruct the general trend of current velocities as well as the temporal variation of seawater properties with a good agreement with the observations.

A moving sediment source with different discharge scenarios at pilot and industrial mining scales with an average discharge rate of 100 t/h and 1000 t/h, respectively, has been applied for a total duration of 17 days. A manuscript on these modelling processes and results, including all model inputs, assumptions and calibrations, is currently in preparation and should be ready for submission soon (K. Purkiani et al., in prep.).

MITgcm hydrodynamic modelling in a  $1 \times 1^\circ$  grid ( $11\text{--}12^\circ\text{N}$ ;  $116.5\text{--}117.5^\circ\text{W}$ ) with a moving collector producing a total sediment discharge of 1000 t/h (high-end industrial-scale value) for a total duration of 17 days shows noticeable differences in the total thickness of sediment deposition (“sediment blanketing”) caused by the plume when flocculation processes are included (FIGURE 6.5A) or excluded (FIGURE 6.5B). As the models predict that about 30% more particles remain in suspension to remote distances way beyond

the modelled area when neglecting flocculation, especially the fine-grained particles, the total amount of sediment blanketing is lower in the no-flocculation scenario (FIGURE 6.5B). The scenario with flocculation processes included is, however, much more realistic and shows a greater capability of the sediment (a) to resettle, and (b) to redeposit closer to the source.

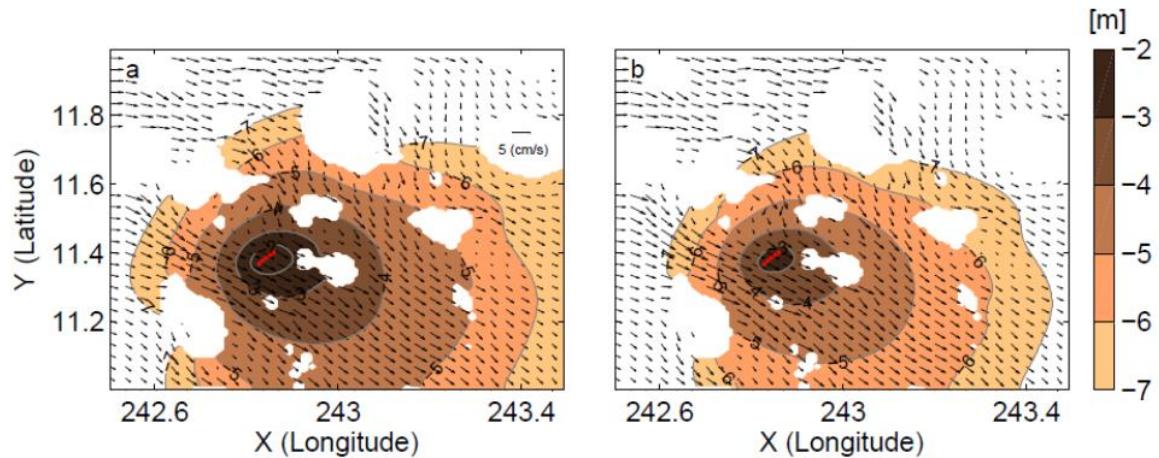


**Figure 6.5:** Modelled sediment plume deposition (sediment blanketing) caused by a moving collector (depicted by the red dots) that produces an industrial-scale sediment discharge of 1000 t/h close to the seafloor after 17 days of mining. The modelled area is a  $1 \times 1^\circ$  grid within the eastern German license area ( $11-12^\circ\text{N}$ ;  $116.5-117.5^\circ\text{W}$ ) with an approximate size of  $100 \times 100$  km. White patches represent topographic highs/seamounts. Arrows represent averaged current speeds and directions. Sediment blanketing is shown for (a) a model including processes of flocculation (see Figure 6.6: for more detail), and (b) a model neglecting flocculation.

FIGURE 6.6 shows the total sediment plume deposition/blanketing with processes of flocculation included in greater detail. After only 17 days of mining, sediment blanketing of  $>1$  mm occurs up to a distance of ca. 6 km upstream and ca. 12 km downstream of the source. Sediment blanketing of  $>0.1$  mm occurs up to a distance of ca. 26 km away from the source in this very short time frame.

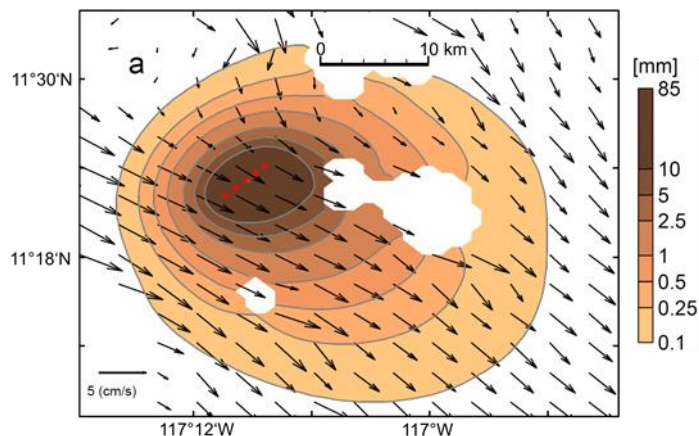


**Figure 6.6:** Close-up of FIGURE 6.5A showing modelled sediment plume deposition (sediment blanketing) between 0.1 mm and  $> 85$  mm caused by a moving collector (depicted by the red dots) that produces an industrial-scale sediment discharge of 1000 t/h close to the seafloor after 17 days of mining. The total modelled area is a  $1 \times 1^\circ$  grid within the eastern German license area ( $11-12^\circ\text{N}$ ;  $116.5-117.5^\circ\text{W}$ ) with an approximate size of  $100 \times 100$  km (FIGURE 6.5). White patches represent topographic highs/seamounts. Arrows represent averaged current speeds and directions.

Further analysis indicates a spatial variation of floc properties downstream along the dominant current, i.e. the deposition pattern of all flocs independent of their size is controlled by the dominant southeast current during the model run. This effect is enhanced for smaller floc sizes. As expected, larger particles

are deposited close to the source whereas smaller particles settle at lower speeds and either reach greater distances from the source, or remain in suspension to areas beyond the modelled domain.

As a total collector discharge of 1000 t/h may be considered as a high-end value, similar simulations were carried out with a discharge of 100 t/h. The observed patterns are similar for both scenarios, although, as expected, the spatial extent of blanketing is reduced in the latter scenario. The model, though not yet validated with experimental test mining plume observations, shows that sediment discharges of this dimension caused by 16-m-wide hydraulic collectors removing the topmost 15 cm of sediment and moving at a speed of 0.3 to 0.5 m/s will have a huge impact on the environment through sediment suspension and redeposition over tens of kilometres away from the source.

### 6.4.3 HYDRODYNAMIC PLUME MODELLING OF THE COLLECTOR TEST

Using an adapted, higher-resolution version of the JPI-O integrated 3D hydrodynamic and sediment transport model developed by the University of Bremen and described in CHAPTER 6.4.2.3 above, in combination with sediment input parameters from the German license area (CHAPTER 4.2.4.2) as determined by the Jacobs University Bremen, and using sediment discharge parameters and harvesting characteristics of the collector vehicle test as described in CHAPTER 3.4, the possible dispersion and blanketing ranges of the sediment plume that will be produced during 4 days of collector testing have been modelled for (a) “normal” background current conditions, and (b) a time in which a mesoscale eddy passes through the region, enhancing current speeds above the seafloor (see CHAPTER 4.2.3.5). The latter is modelled as current moorings between 2013 and 2016 have shown that it is not untypical to have such eddies passing by in the month of April, which is the month in which the test in the German area will occur. Furthermore, satellite-derived sea surface height anomaly data / eddy kinetic energy data between 2006 and 2017 show that the month of April was free of eddy activity over the mooring sites in PA1-West *only* in the La Niña years 2009 and 2010. All other years show eddy influence during this month.

The 3D hydrodynamic model described in CHAPTER 6.4.2.3 above was adapted to a horizontal resolution of 150 m and a vertical resolution of 5 m to better model the collector test scenario over a time period of 4 days in the northern part of area PA1-West (blue rectangular area in FIGURE 4.3). Discharge rates of the collector vehicle will vary between 135 and 337 t/h, depending on the speed of the vehicle (0.2 to 0.5 m/s, respectively). Due to the lawn-mower pattern of nodule uptake, in which the collector will drive for 3-7 minutes (depending on its speed) and then dump the nodules and turn around for a time period of ca. 15 minutes (see CHAPTER 3.4 and TABLE 3.4 for details), the collector will have an average discharge rate of  $3/18 \times 337$  t/h for the 0.5 m/s scenario and  $7/18 \times 135$  t/h for the 0.2 m/s scenario = 56 and 52.5 t/h, respectively. These values are very close to each other and thus show that variability in collector vehicle speed will not have a great effect on sediment discharge rate behind the collector. A worst-case continuous discharge of 60 t/h throughout the 4-day test period and at a height of 5 m above a flat seabed has thus been assumed for the plume modelling exercises here.

Experimental sedimentological parameters used as input for plume modelling were obtained by the Jacobs University (Bremen) from sediments deriving from the German license area (see CHAPTER 4.2.4.2) and are summarised in TABLE 6.1 for 3 different modelled scenarios: (1) a collector discharge / starting sediment concentration of 500 mg/l and a “normal” seafloor current regime with a mean current velocity of 3.8 cm/s and with a predominantly eastward current flow (turbulence  $G = 0$ ); (2) a collector discharge / starting sediment concentration of 500 mg/l and an “eddy” seafloor current regime with speeds of 10 cm/s and with a predominantly north-eastward current flow (see FIGURE 6.3) ( $G = 2.4$ ); and (3) a sediment concentration of only 105 mg/l and an “eddy” seafloor current regime with speeds of 10 cm/s and with a predominantly north-eastward current flow. Scenario (3) was introduced to analyse the path of the very

fine particle fraction under  $G = 2.4$  that does not aggregate at a low sediment concentration of 105 mg/l (TABLE 6.1) and probably stays in suspension for a longer period of time.

**Table. 6.1:** Experimental sedimentological parameters on aggregate size distribution and settling velocities of particles at different starting concentrations and shear rates. Blue colours indicate very low settling velocities of the very small particles that do not aggregate under a shear rate of 2.4.

Experimental parameters						
Starting sediment concentration (mg/l dry weight)	500		500		105	
Shear rate ( $s^{-1}$ )	0		2.4		2.4	
Experimental time of aggregation (min)	45		10		50	
Aggregate size distribution ( $\mu m$ )	d25	492	d25	9	d25	6
	d50	965	d50	815	d50	11
	d75	1351	d75	1351	d75	21
Settling velocity (m/d)	d25	102	d25	1.0	d25	1.0
	d50	164	d50	210	d50	1.8
	d75	171	d75	213	d75	3.4
$u^*$ critical for bedload transport (cm/s)	0.3 – 0.4		0.3 – 0.4		0.3 – 0.4	
$u^*$ critical for suspended load transport (cm/s)	0.5		0.5		0.5	

The concentration of sediment in the plume at a height of 10 m above the seafloor for each of the three particle size classes d25, d50 and d75 after the 4 days of collector testing, i.e. directly after test stop, is shown in FIGURE 6.7. Under “normal” flow, high plume concentrations of  $> 1$  g/l reach to maximally 1 km from the test site (source). The plume dilutes to zero concentration within maximally 3 km from the source. Under enhanced current speeds associated with eddy passage, the d50 and d75 coarse fractions appear to settle very quickly and hardly stay in suspension (maximum dispersal distance also 3 km), but the very low settling speeds of the fine fraction d25 mean that these particles are suspended over longer distances up to maximally 6 km from the source. This is shown nicely by the dispersion ranges of fine particles shown by scenario (3) when no aggregates are formed.



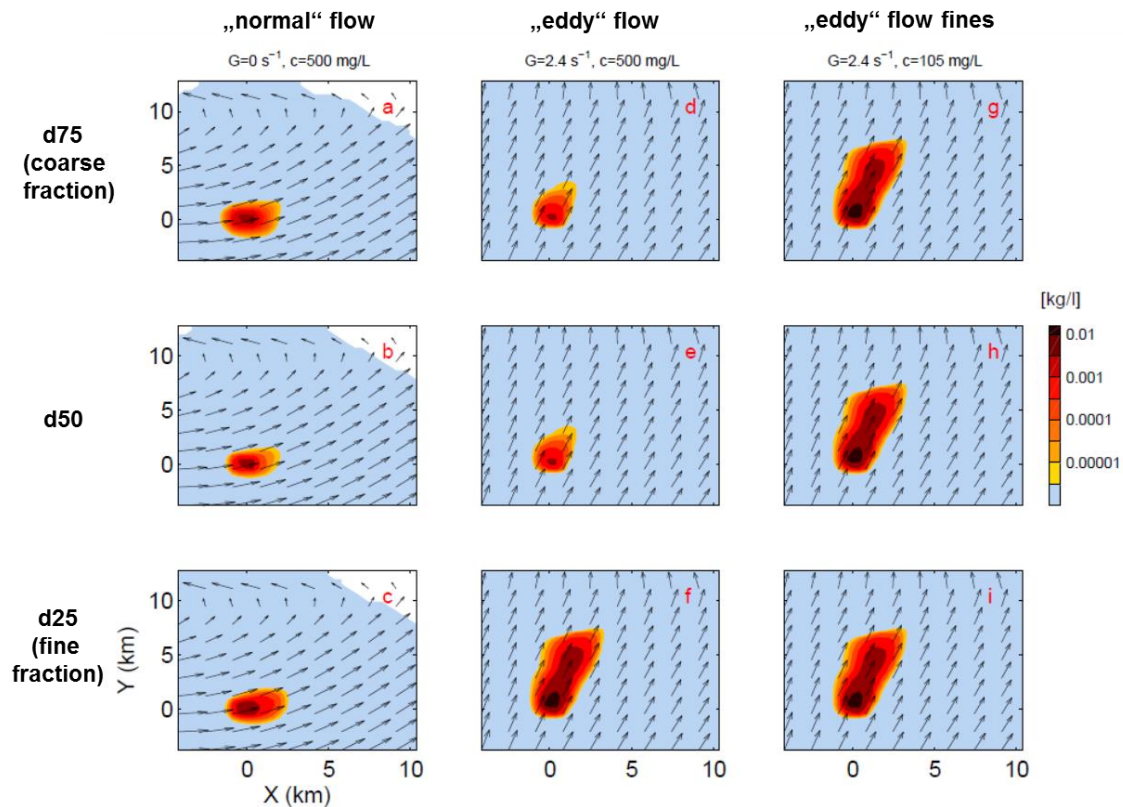


**Figure 6.7:** Suspension of plume particles at a height of 10 m above the seafloor (in kg/l) after 4 days of continuous sediment discharge at a rate of 60 t/h and a height of 5 m above the seafloor at position  $X, Y = 0$  (i.e. at the time of test stop). Concentrations are shown for three particle size classes (d25, d50, d75) and three different current regime conditions as summarised in TABLE 6.1.

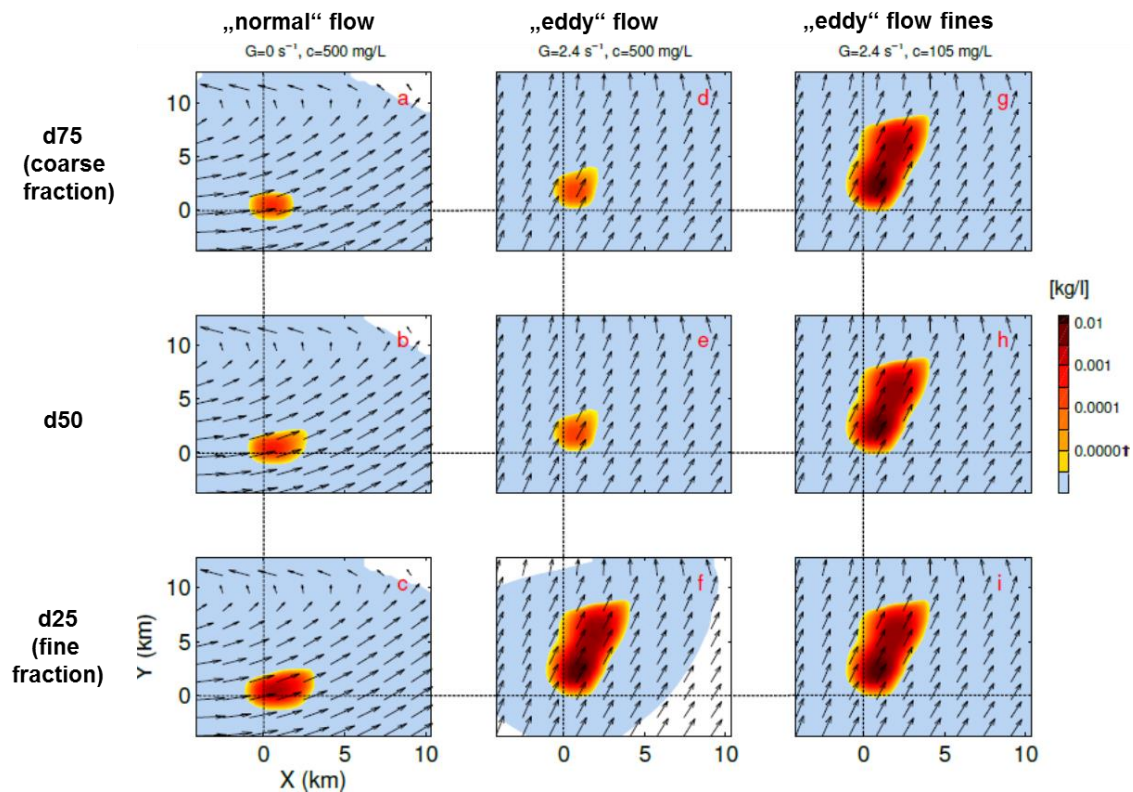


**Figure 6.8:** Suspension of plume particles at a height of 10 m above the seafloor (in kg/l) 1 day after test stop (i.e. 1 day after FIGURE 6.7). Dashed lines reflect the source position ( $X, Y = 0$ ). Concentrations are shown for three particle size classes (d25, d50, d75) and three different current regime conditions as summarised in TABLE 6.1.

The suspension shift one day after the test stop is shown in FIGURE 6.8. Under “normal” flow, concentrations in the plume have dropped to below 1 g/l and especially the larger particle size fractions have settled out of the water column. The same counts for the larger particle size fractions in the eddy situation, whereas the fine particles have hardly settled out of the water column and have been shifted by bottom currents by about 1.5 km in the direction of predominant flow.

According to the model, the plume does not reach a height of more than 30 m above the seafloor under “normal” flow conditions (FIGURE 6.9). However, should the very fine fraction not aggregate, e.g. in an eddy passage scenario, these very fine particles could reach up to a height of 300 m above the seafloor.

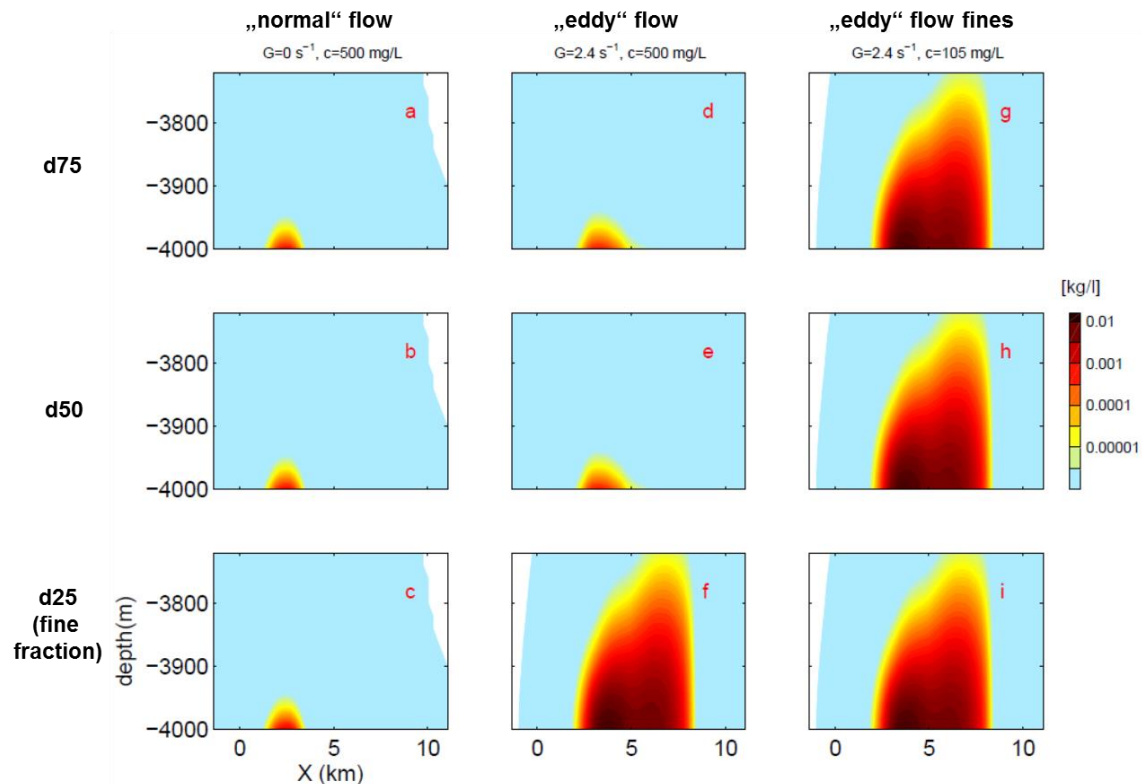


**Figure 6.9:** Vertical extent of suspension of plume particles above the seafloor (in kg/l) directly after test stop (compare with FIGURE 6.7). Concentrations are shown for three particle size classes (d25, d50, d75) and three different current regime conditions as summarised in TABLE 6.1. The X-axis represents a transect through the area of highest plume concentration, thus also showing the shift of the plume from the source (0) in 4 days' time.

The amount of sediment deposition/blanketing from the plume for each of the three particle size classes d25, d50 and d75 after the 4 days of collector testing, i.e. directly after test stop, is shown in FIGURE 6.10. Under “normal” flow, plume deposition of  $> 0.1 \text{ mm}$ , which may be thought to have a significant effect on faunal communities, reaches to maximally 2 km from the test site (source). The remaining minimal blanketing thins out to zero within maximally 3.5 km from the source. Under enhanced current speeds associated with eddy passage, the d50 and d75 coarse fractions settle even more quickly and the  $> 0.1 \text{ mm}$  depositional range is similar to that of the “normal” scenario (max. 2 km). Due to the greater current speeds, however, and the slow settling speeds of fine particles, blanketing thins out to zero at about 8 km from the source.

Some additional blanketing from plume sediments that are still in suspension directly after the test stop is expected to occur, but this is unlikely to influence the maximal ranges up to zero deposition (3.5 vs. 8 km). Thus, these latter values have been taken as maximal ranges for the development of an Environmental Monitoring Plan for the collector vehicle test (see CHAPTER 8.2).

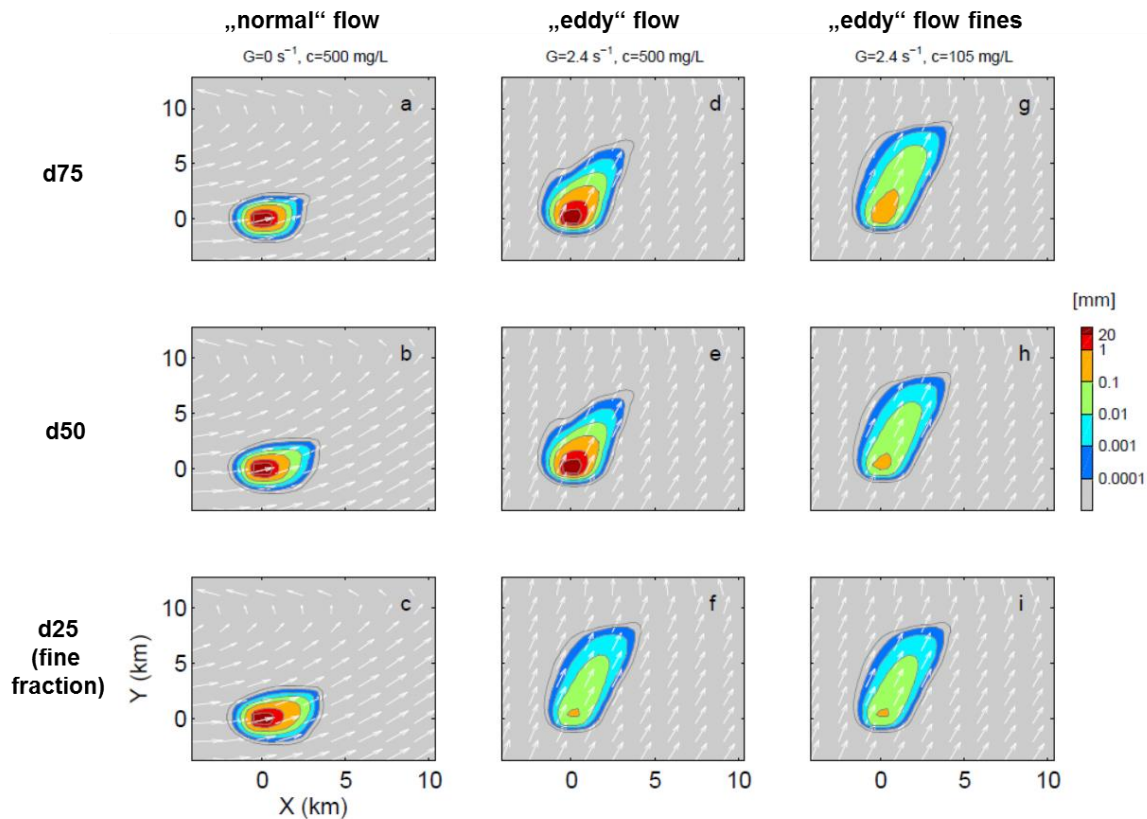


**Figure 6.10:** Sediment deposition/blanketing on the seafloor of plume particles (in mm) after 4 days of continuous sediment discharge at a rate of 60 t/h and a height of 5 m above the seafloor at position  $X, Y = 0$  (i.e. at the time of test stop). Sediment deposition is shown for three particle size classes (d25, d50, d75) and three different current regime conditions as summarised in TABLE 6.1.

The model results shown here were developed to inform the Environmental monitoring Plan and will be improved as time progresses towards the actual collector vehicle testing time in April 2019. A higher resolution model with a horizontal resolution of 50 m is planned once super-computer capacity becomes available (applications are running). Furthermore, more detailed experiments on the behaviour of sediments deriving directly from the test area are planned during and after the SO-262 BGR baseline study in April/May 2018, and hydrographic data deriving from the test site will deliver even better inputs to the hydrodynamic model, which can then be adapted and improved on a case-by-case basis.

Through observations of weather patterns off the coast of Mexico and using satellite imagery (sea surface heights, eddy kinetic energy), it should be possible to determine what the probability of eddy influence on bottom current dynamics will be well in advance of the test activity. According to such observations, the potential range of the plume and subsequently the design of the monitoring array / set-up can be determined shortly before the test starts in March 2019.

The modelling results above suggest that “normal” flow above the seafloor is preferable to allow relatively fast deposition of particles out of the suspension plume and to restrict blanketing to a relatively small fall-out area. However, the advantage of an “eddy” flow situation would be that, according to what we have seen in mooring data between 2013 and 2016, current directions are much more consistent – which would greatly facilitate physical monitoring of the plume. Whatever the case, one very important aspect of the monitoring of plume dispersal will be to validate the model(s) that have been and will be developed further in the near future. Validation and/or adaptation of these model(s) to better reflect reality will be an essential step for upgrading towards industrial-scale mining scenarios.

## 6.5 Biogeochemical alterations

Biogeochemical processes in deep-sea sediments are nowadays recognised as key functions of abyssal ecosystems playing a significant role in large-scale element fluxes with consequences for, e.g., the productivity of the seas (via nutrient regeneration) and for the global carbon dioxide budget (via organic matter remineralisation and burial) (e.g. Sweetman et al., 2017). The sediment biogeochemistry of undisturbed ecosystems is shaped by complex interactions of chemical and microbially-controlled processes and benthic food webs. This, in turn makes organic matter fluxes from the overlying water available to benthic communities, sustaining their biomass and unprecedented biodiversity.

Most Benthic Impact Experiments addressing environmental impacts of deep-sea mining were carried out several decades ago (e.g., see CHAPTER 6.4.1 and CHAPTER 7.4.2) and missed out on the effects on biogeochemical processes. First field investigations on biogeochemical alterations did not start before the late 1990s, i.e. several years after the disturbances were created (e.g., Haeckel et al., 2001a). Modern instrumentation (e.g., ROV-targeted sampling and *in situ* sensors) needed for precise characterisation of the nature and intensity of impacts and fully controlled investigations and sampling to address their biogeochemical consequences were not available at that time. Other recent methodological advances, e.g. molecular tools for the characterisation of microbial communities (e.g., DeLong, 2005), pulse-chase experiments to quantify transfer of energy and matter in benthic food webs (e.g., Witte et al., 2003), and advanced technologies for *in situ* measurements of benthic fluxes (e.g., Boetius and Wenzhöfer, 2009) have added further important tools for studying deep-sea biogeochemistry.

Investigations carried out in the first project phase, particularly in the DISCOL Experimental Area in the Peru Basin, successfully addressed disturbance effects on benthic biogeochemistry with a comprehensive suite of state-of-the-art technologies (Boetius, 2015; Martínez-Arbizu and Haeckel, 2015). For the first time, these investigations could provide direct evidence for impacts on seafloor biogeochemical processes several decades after the disturbances were created (Vonnahme et al., in prep). Investigations have shown that even a few decades after disturbance, the geochemical composition and redox-layering of surface sediments in disturbed areas is still strongly altered, whereas pore waters seem to equilibrate much faster. Pore water profiles do not show major differences in concentrations of the major and trace elements between undisturbed and disturbed sites from 26 years ago (Paul et al., subm.). At the same time, many geochemical and biogeochemical parameters showed an unexpectedly high degree of spatial variability (see also CHAPTER 4.2.4.3), suggesting the need for thorough characterisation of baseline conditions in order to identify mining-related effects and to assess their significance in relation to naturally-occurring temporal and spatial variations in the BBL (Mewes et al., 2014, Mogollón et al., 2016; Volz et al., submitted; Vonnahme et al., in prep). This also includes the distribution of trace metals between different physical and chemical species and the role of colloids and nanoparticles in transporting trace metals in the water column (CHAPTER 6.6.1 below). In this respect, detailed geochemical baseline investigations of the collector vehicle test area and the reference areas around it are planned for the upcoming BGR exploration cruise to the area in April/May 2018, as well as for the preparatory cruise of the MiningImpact 2 project in March 2019. Investigations have also documented that biogeochemical impacts are specific to the particular nature and intensity of the physical impact, with strongest effects observed in regions where the surface reactive layer of sediment with labile organic matter was lost and deeper sediment layers were exposed at the surface. Such a situation could be comparable to the impact that the collector vehicle will have in removing the topmost 10-12 cm of sediment. The remaining, deeper, stiffer sediment layer will be covered by a few centimetres of plume fallout sediment. Furthermore, sediment compaction caused by the collector tracks will squeeze out pore waters. In both cases, such stiffer and less porous sediments appear to be more difficult to recolonise by



bioturbating organisms that mix in fresh organic matter, and thus are unfavourable for re-establishing stable biogeochemical conditions and processes. There is a strong focus on the analysis of biogeochemical impacts of the test in the MiningImpact 2 project (see CHAPTER 8.2.1.3).

## 6.6 Toxic discharges

### 6.6.1 METAL RELEASE FROM THE SEDIMENT

The activity of the test collector over a period of 4 days will lead to the complete removal of nodules, disturbance of the top 10–12 cm of sediment with subsequent formation of an operational plume of suspended particles and sediment re-deposition, and to sediment compaction. These impacts may lead to increased concentrations of dissolved and particle-bound (toxic) metals in the benthic boundary layer (BBL), which comprises the near-bottom layer of water, the sediment-water interface, and the top layer of sediment that is directly influenced by the overlying water. Impacts related to increased toxic metal load in bottom waters may occur directly at the test site (100 x 900 m), but also in the plume sediments that drift away from the test site. Possible processes leading to increased metal concentrations in bottom waters involve (FIGURE 6.11):

- Expulsion of pore waters enriched in dissolved metals into overlying bottom water,
- Trace metal mobilisation from suspended particulate material in the sediment plume and from reworked sediments due to mineral dissolution and desorption,
- Trace metal mobilisation related to remineralization of organic matter,
- Trace metal accumulation on Fe and Mn-rich (nano)particles.

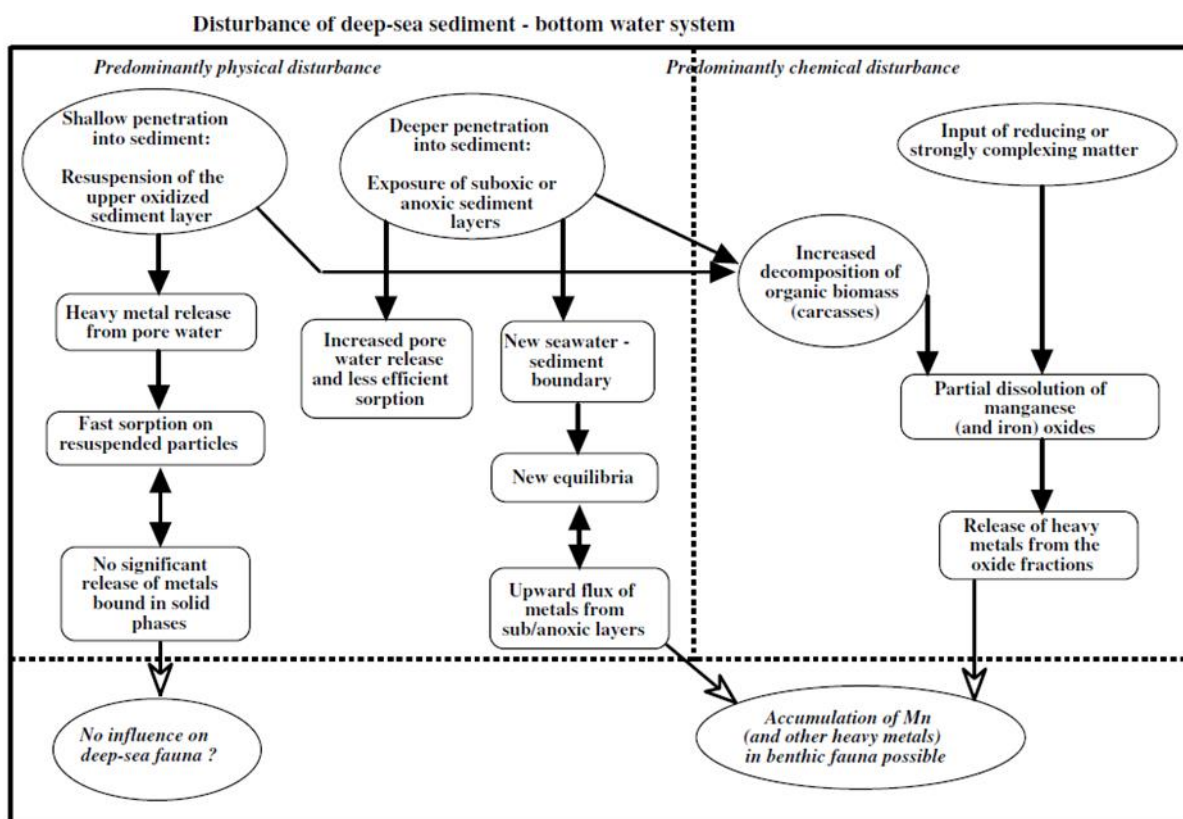


**Figure 6.11:** Summary of possible disturbances of surface sediment at the deep seafloor with different intensities – effects on the heavy metal cycle (from Koschinsky et al., 2003b).



The operational plume generated at the collector vehicle test site will consist of fine clay to silt-sized sedimentary material containing higher amounts of authigenic Mn-oxides. In oxic environments like the CCZ (CHAPTER 4.2.4.3), a reduction of these oxic mineral phases with a release of metals is not expected. Mobilisation of trace metals from suspended sediment particles will be controlled by the solubility of the minerals present (i.e., mineralogy), particle concentration, and size. Similarly, adsorption of dissolved metals on suspended particles strongly depends on the type of minerals present, with Mn and Fe oxides being strong scavengers. These minerals are relatively abundant in CCZ surface sediments and will also be whirled up by nodule mining.

In the Eastern German license area, the bottom water is oxic and the oxygen penetration depth into the sediments is about 2-3 meters (CHAPTER 4.2.4.3). Oxic pore waters generally have lower metal concentrations compared to suboxic pore waters, and measured pore water concentrations of Mn, Fe, Co, Ni, Cd, As in the upper 20-30 cm of sediment in the German license area are similar to bottom water (unpublished data, AWI and JUB). Even in an extreme case with the release of high concentrations of dissolved metals from anoxic pore waters, such metals are expected to be immediately immobilised due to scavenging to mineral particle surfaces in the oxic bottom water. From previous laboratory experiments it appears that increased particle load and an increasing surface area of oxide particles will lead to increased sorption of particle-reactive elements from the water column. Especially the resuspension of the Mn oxide-rich surface sediment layer may lead to a strong sorption of trace metals, and release of dissolved metals at oxic conditions is rather unlikely for most metals (Koschinsky et al., 2001, 2003a,b). Heavy metals that are slightly to moderately enriched in oxic pore water compared to ambient bottom water would be released into the bottom suspension, but would be re-immobilised by rapid sorption on the suspended particles. An essential precondition is that the geochemical milieu remains unchanged. Rapid scavenging in the suspension after the disturbance was observed for cationic particle-reactive metals like Mn, Co, Ni, Zn, Cu, Cd, Pb, and Fe, while anionic metal species like Mo, V, and U showed neither strong release nor sorption. Based on this current knowledge, we do not expect strong increases in truly dissolved concentrations of toxic metals. However, an increased colloidal/nanoparticulate pool with high concentrations of trace metals (from crushed Mn nodule material, or authigenic Fe and Mn oxides from the sediments scavenging metals from bottom water) could be potentially harmful (e.g., sorption of metals on Fe (oxyhydr)oxide nanoparticles), as they could be taken up by filter feeders, with potentially toxic effects.

Experimental *in situ* measurements of particulate metal concentrations in plumes in the CCZ are restricted to one small-scale experiment that was carried out in the German license area during the cruise SO-239 in 2015. Water samples collected from directly above the seafloor and from an experimental plume that was produced by epibenthic sled (EBS) in PA1 (see CHAPTER 6.4.1 above) were filtered (0.2 µm), and the filters with particles were acid digested and subsequently analysed with ICP-OES for major elements and ICP-MS for trace elements. Elemental concentrations in undisturbed bottom water were almost all below the detection limit for the measured elements. A plume experiment was carried out with the EBS and samples were taken afterwards with the CTD, which worked quite well. Some elements had elevated concentrations after the disturbance as compared to before, e.g. Al, Co, Fe, Mn, whereas Ca, Cu, Ni, Sr, Zn concentrations were lower afterwards. Based on these data it is difficult to make clear statements about the element release through the plume, showing that more detailed sampling strategies and analyses around the collector test will be necessary to register possible concentration changes of metals bound to sediment particles and to interpret results in terms of potential toxic impact.

Further laboratory experiments are currently being conducted on PA1 sediments and nodules at the BGR and will provide further information on trace element mobility in man-made sediment plumes (Fe, Mn, Co, Ni, Zn, Cd, V, Mo), fractionation between colloidal and truly dissolved pools over time, and the impact of

increased Mn oxide particles in suspension. Time-series experiments are being conducted with different size fractions of deep-sea sediments (i.e., different mineralogy) and using Pacific deep water, and are still in progress.

*In situ* experiments are necessary to measure real changes in the physico-chemical environment of the deep seafloor over periods of days and weeks, including the presence of organic ligands (as the solubility of Fe, and other trace metals such as Cu, in deep ocean water is controlled by complexation with natural organic ligands and colloids). Furthermore, nothing is currently known about the potential role of microbial interactions within plume particles and redeposited sediments that may affect the mobility and flux of metals, changes in oxidation states of metal ions and organic-metal complexation. Such analyses are planned in the framework of the MiningImpact 2 project (see CHAPTER 8.2.1.3).

## **6.6.2 POTENTIAL TOXICITY DUE TO HYDRAULIC OIL DISCHARGE, CHEMICAL CONTAMINATION**

Accidental events (see CHAPTER 6.8) could potentially lead to the release of hydraulic oil into the water column. For the unlikely event that system failure leads to oil leakage, a non-toxic, readily biodegradable oil (according to OECD criteria) is being used, of type Panolin Atlantis 5, 15 or 22 (manufactured by Panolin AG, Madetswil, Switzerland). Material Safety Data Sheets (MSDS) can be obtained from the manufacturer at [info@panolin.com](mailto:info@panolin.com).

Fluorescent particle tracers (EcoTrace Fluorescent Tracer) will be added to the sediment plume generated by the nodule collector. These environmentally-friendly tracers are anticipated to disperse with the sediment plume and can be detected using particle tracer cameras. The EcoTrace Fluorescent Tracer is manufactured by c/o Environmental Tracing, Helensburgh, Argyll, UK and is a solid, non-soluble solution of fluorescent dye in a natural mineral and thermoplastic polymer base. It does not contain any substances presenting a health hazard within the meaning of Article 27 of the Dangerous Substance Directive 67/548/EEC as amended by the Seventh Amendment 92/32/EEC. The MSDS can be obtained from the manufacturer at [jon.marsh@environmentaltracing.com](mailto:jon.marsh@environmentaltracing.com).

Tests were conducted on low specific gravity ETS EcoTrace particles with a particle size of ca. 5 microns in conjunction with a UK Government Research Laboratory (Centre for Environment, Fisheries and Aquaculture Science) to assess any impact on Pacific shellfish areas including oyster beds. The oysters were exposed to extremely high concentrations of EcoTrace particles and the rate of uptake and concentration held within the oyster, as well as rate of elimination, was measured over time. Results show that particles were not preferentially selected or rejected by the oysters during any of the tests as a result of tracer particle uptake. The full report is available upon request.

## **6.7 Natural hazards**

Based on BGR's experiences during exploration cruises and long-term analyses of meteorological conditions at the test site, weather conditions are generally favourable for exploration work in the months between March and May (CHAPTER 4.2.2). Meteorological hazards are only to be expected from tropical storms or hurricanes and could potentially endanger the two vessels used for the collector vehicle test. However, for the time period between March and May, the occurrence of such storm events is highly unlikely as the storm season only starts in mid-May (FIGURE 4.10). Moreover, continuous observation of the weather forecast by the ship's command would allow to leave the storm area early enough and to sail to a safe place.

Further natural hazards that could impact the environment and also the effectivity of the collector vehicle test in the Eastern German license area include volcanism, seismic activity, sediment slumping and the occurrence of benthic storms on the seafloor. There has been no submarine volcanic activity in the license area for at least the last 10 Million years, suggesting that such an impact is highly unlikely during the lifetime of the project. As there is no information on recent seismic activity in the area, potential impacts are impossible to decipher. Sediment slumping may occur close to seamounts (i.e. in areas with great slopes) once in a while. Evidence of such events has been found in long sediment cores taken from the immediate proximities of seamounts in the north-western part of the German license area (Kuhn et al., 2015). However, these are relatively localised events with a radius of several kilometres at the most and the abyssal plains such as area PA1-West will most likely remain untouched by such natural disasters.

There is also little information on the potential impact of natural benthic storms on the seafloor, which are known from other oceanic regions to cause major erosion/depositional events on the seafloor. Even during times of mesoscale eddy passage, which induce a two to three-fold increase of bottom current speeds up to maximally 20 cm/s in the Eastern German license area (see CHAPTER 4.2.3.5), turbidity measurements have not given evidence for the resuspension of bottom sediments and ADCP backscatter data also have shown no change in SPM concentration in the water column. The term "benthic storm" in the CCZ has been used deceptively in the past. The myth of "benthic storms" resuspending sediment in the CCZ was initiated by Kontar and Sokov (1994), who used the term "benthic storm" to describe moderate enhancement of currents (to 13 cm/s) at 6 m above the seafloor, apparently also by mesoscales eddies passing by. They did not measure any sediment resuspension, nor would you expect it based on other studies (e.g., Gardner et al., 1984) that show that flows of 13 cm/s do not cause sediment erosion in the CCZ. Detailed photographic analyses of vast seafloor areas of the CCZ indicate extremely clear bottom waters and no sediment deposition on the nodules, which would be expected if natural resuspension events were common. Current speeds of maximally 20 cm/s could lie around or above anticipated thresholds for natural resuspension of deep-sea muds according to McCave and Hall (2006) – but we have no evidence for it. Laboratory experiments with deep-sea sediments from the Eastern German license area (using Gust-Erosion chambers) have shown that the speed required for resuspension of CCZ particle aggregates is indeed 17-20 cm/s (JUB, unpubl. data). BGRs current mooring data over three consecutive years show that these speeds are hardly ever reached: the average speed during the largest mesoscale eddy transition was 12 cm/s. Although April/May is a time in which the probability of a mesoscale eddy passing through the test area is high (see also CHAPTER 6.4.3), we thus assume that the likelihood of a natural benthic storm occurring on the seafloor simultaneously is extremely low to negligible.

## 6.8 Accidental events

The company GSR, as subsidiary of the group DEME, has a long experience of working in the marine environment. Safety and environment are two of the core values, through its Quality, Health and Safety, Environmental, Sustainability and Security (QHSE-S) charters. Therefore, GSR works according to a management system complying with various standards:

- OHSAS 18001 "Occupational Health & Safety Management System - Requirements";
- SCC\*\* "Safety, Health & Environment Checklist Contractors" (VCA\*\* two stars);
- ISO 9001 "Quality Management Systems - Requirements";
- ISO 14001 "Environmental Management Systems - Requirements";
- ISO 14064 "Greenhouse gasses - Part 1: Specification with guidance at the organization level for quantification and reporting of greenhouse gas emissions and removals";

- ISM "International Safety Management Code";
- ISPS "International Ship & Port Facility Security Code".

Subsequently, everything is done to avoid any adverse and irremediable consequences, and the best available practices are promoted. Nevertheless, working in sometimes remote and hostile environments often presents specific challenges and risks. It is important to anticipate all the potential accidental events knowing that the study area is located at three sailing days away from the coast in case of emergency. System failures can be mitigated for according to the procedures set out in CHAPTER 6.8.1 below.

### 6.8.1 SYSTEM FAILURES AND MITIGATION MEASURES

During the operational deployment of Patania I it took some effort to reach to the seabed. Component equipment failures were encountered, however never leading to an accidental event as equipment loss or unwanted releases into the marine environment. The previous campaign has allowed for the technical team to gain experience to mitigate equipment failure and resolve unexpected breakdowns. Furthermore, a buffer period of 21 days is considered in the planning if equipment failure occurs and a return to San Diego is unavoidable.

The Patania II system is electrically powered. The electrical power provided by the ship's generators and delivered to the Patania II is transferred to hydraulic power by a subsea Hydraulic Power Unit (HPU). HPU's are responsible for driving the hydraulic pump motors, hydraulic track drives and actuating the cylinders. Accidental discharge of hydraulic oil could occur only in the case of mechanical or hydraulic failure on the vehicle.

The hydraulic system and gearboxes are filled with hydraulic oil. The complete system will be pressure-tested and checked for any leakages before entering the water. Pre-dive check-listing is part of the operational management program and executed prior to launching. The large oil volumes on the vehicle are constantly monitored in the control cabin during descent/ascent/operation on the seafloor. If a leakage occurs, the system will detect this and the vehicle can be recovered onboard for repair. Furthermore, on the vehicle, hydraulic hoses are used which can withstand a nominal system pressure of 320 bar. The vehicle is limited to 250 bar system pressure, so some safety margins are included. The burst pressure of the hydraulic hoses is far beyond the 320 bar.

### 6.8.2 EMERGENCY RECOVERY

#### Patania II Hydraulic / Electrical Failure. Dead Sub Recovery

In the event of a total failure of the Patania II while in operation on the seabed, the procedure for recovery would be as follows:

- Position vessel over Patania II using the navigation equipment on the Patania II and the vessel to give a vertical lift from seabed.
- Simultaneously with the above, pull in on the umbilical winch to maintain correct catenary and protect the umbilical cable.
- When the vessel is over the Patania II, confirmed by the navigation equipment, lift Patania II to 10m clear off the seabed and hold until system seems stabilized.
- Commence recovery of the Patania II.
- Lift the Patania II, using the umbilical winch to a depth of 20 meters under the docking head using the vessel to achieve this position.
- Recover as per standard launch and recovery procedures.

### A-Frame Failure

The wide angle A-Frame comprises a fabricated steel portal frame pivoted at the bottom of the two legs. The gantry is moved back and forth by the action of two hydraulic cylinders which are mounted on two base sections, positioned one on each side of the gantry.

A lift beam or cursor system that is docked onto the top part of the vehicle is used for deployment and recovery through the splash zone to a clear distance (approx. 20 m) from the keel of the vessel. The cursor system provides added mass, unloads the umbilical during air lifting and correctly orientates the vehicle during recovery. Two separate lifting winches mounted on the A-Frame top beam will lower and hoist the cursor system–vehicle assembly through the splash zone.

A docking cone on the cursor system provides a lead in for the vehicle bullet and a smooth-running surface for the umbilical. The 360 degree latches on the cursor are completely failsafe meaning that even in the event of a failure in the lift beam controls or hydraulics, the vehicle can always be latched. Indicators are provided to confirm when the vehicle is latched.

In the event of a failure of the A-Frame whilst in the inboard position, the first action would be to replace the failed part. If this was found to be impossible then the hoses would be removed and the A-Frame would be manually jacked out. A vessel's winch and / or crane would be used as a hold back to control the speed of deployment of the A-frame.

If the A-Frame failed in the outboard position, recovery would be by using the vessel's winch and/or crane. Actions: (1) Release all hoses, (2) Open valves to release ram pressures, (3) Attach the vessel's winch and/or crane to the A-Frame and slowly pull A-Frame to inboard position.

### Lift Wire Winch Failure

If the Lift wire winch fails then the first course of action would be to repair the broken parts. Failure of a drive motor can be overcome by disconnecting the hydraulic lines to the faulty motor, so it is free to rotate and operate the lift winches with the one remaining motor. The hydraulic lines would require capping.

Up to moderate depth only, if it is impossible to repair the winch(es) before recovering the Patania II it will be necessary to use temporary rigging to choke and pull on-board the lift wires in stages, until such time as the cursor can be recovered and secured to the docking head. Recovery of Patania II could then be carried out as per 1.1.5 Cursor System Failure.

### Umbilical Winch Failure

The primary purpose of the umbilical winch is to store the umbilical and allow launching and recovery of Patania II to depth along with communication and control of the vehicle via the slip-ring. If the umbilical winch fails then the first course of action would be to repair the broken parts.

The winch assembly consists of a single drum supported by a drive end (DE) and non-drive end NDE0 pedestal. The winch is driven several (assumed 3 to 4) hydraulic motor/gearbox units with an option for redundancy included for one motor, i.e. if failure of one drive unit occurs then the winch is still capable of functioning on the remaining two operational drives. Failure of a drive motor can be overcome by disconnecting the hydraulic lines to the faulty motor, so it is free to rotate and operate the winch with the other (assumed 2 to 3) motors. The hydraulic lines would require capping.

Up to moderate depth only, in the unlikely event that it is impossible to repair the winch before recovering the Patania II, it will be necessary to use temporary rigging to choke and pull on-board the umbilical in



stages, until such time as the Patania II is 20 meters below surface / under the A frame to allow the cursor to be deployed and recovery of Patania II to be completed.

#### Cursor System Failure

If the cursor system fails then the first course of action would be to repair the broken parts. If this was found to be impossible then the option to recover the vehicle using the umbilical could be implemented, but this in turn may compromise the umbilical and could possibly lead to internal conductor failure. As the Patania II will not be securely locked in to the cursor, then this option would require good umbilical management during the operation of in-boarding the A Frame.

Depending on availability, a possible option to temporarily rig a recovery wire and with the use of the ships crane in tandem with a work class ROV to connect the wire to Patania II could be implemented. This option would depend on the vessel, vessel crane and available deck space in which to safely land out the Patania II and would require to be risk assessed prior to any recovery taking place.

#### Umbilical Cable Internal Failure

In the event of umbilical cable internal failure, the Patania II will be recovered in the same manner as used in Patania II Hydraulic / Electrical Failure: Dead Sub Recovery.

#### Severing of the Umbilical

The umbilical monitoring remains complex, since no to limited visuals are available along the water column once the collector is driving on the seafloor. A safety margin of three regarding the minimum breaking strength of the umbilical was taken into account: submerged vehicle weight, including the lift umbilical at 5000 m of water depth, is estimated at 250 kN while the umbilical is designed to attain a minimum breaking load of 700 kN.

If the umbilical breaks or is cut when the Patania II is on the seabed, then unlike most ROV's, there is no possibility that Patania II will, due to its inherent buoyancy, float to the surface where it can be tracked using the fitted radio beacon. The Patania II should will stationary on the seabed in the same location that the umbilical parted. In the unlikely case of a collector loss on the seafloor, the PPV is equipped with a battery driven beacon. Subsequently, the vessels USBL system should be able to locate the vehicle.

Once tracking and visual sighting with 3rd party ROV has been confirmed, an on-board decision between the Patania II superintendent, GSR management and the vessel's representative can be made to proceed with the safe recovery of Patania II. A mechanical lifting point is installed on top of the vehicle. By means of a work-class ROV, a lifting wire or a plasma line can be hooked up to recover the Collector. It can be recovered up to the splash zone, from where it should be connected to the cursor frame to retract it inboard.

This option would depend on the vessel in use, the vessel crane and available deck space in which to safely land the Patania II and would require to be risk-assessed prior to any attempted recovery taking place.

#### Surface Equipment Hydraulic Power Unit (HPU) Failure

The HPU is used when launching and recovering the Patania II, it has no direct contact with the Patania II and therefore failure should cause no immediate danger to the Patania II. If failure does occur, the

vessel and Patania II will hold station until repairs are implemented / completed. If repairs prove to be impossible, the A-frame and Umbilical winch can be operated and the Patania II recovered in same the manner as used in A-Frame failure and Umbilical winch failure.

## **7. Description of impacts on the biological environment**

This section provides an overview of potential impacts that the collector vehicle test will have on the biological environment, in a descriptive form that is based on the best scientific information that is available at this time. The aim of the MiningImpact 2 project is to assess the immediate, short-term and intermediate-term (2 year) physical and chemical impacts of the collector vehicle test on the seafloor and its overlying waters, as well as the response of benthic organisms to the impact, which in turn is crucial for the recovery of benthic standing stocks and biodiversity and for the maintenance of associated ecosystem functions. We thus refrain from providing detailed assessments or prognoses on the extent of impacts here, but rather refer to CHAPTER 8 for a detailed description of the monitoring programme that will scientifically accompany the collector test. Detailed analyses and input of data into models, also in terms of future risk assessment, will allow a much more comprehensive future assessment of the nature and extent of similar impacts and the development of recommendations on how to avoid, remedy or mitigate such impacts.

### **7.1 Description of potential impact categories**

The major types of impacts that will or potentially might affect biological communities during the DME-GSR collector vehicle test are (1) habitat/nodule removal, (2) sediment disturbance and plume deposition, (3) increased concentrations of plume particles in the water column directly above the seafloor, (4) biogeochemical alterations of the sediment (i.e. change of habitat integrity), (5) potential release of toxic sediments and/or substances into the lower water column, and (6) noise and light pollution. These potential impact categories are described in more detail in CHAPTER 7.2 to CHAPTER 7.4 below.

### **7.2 Biological impacts at the surface**

Potential biological impacts at the surface could be due to (1) accidental discharges (hydrocarbon contamination, hydraulic oil) or waste discharges from the surface vessels (RV SONNE and the ship of opportunity chartered for the deployment of the test collector), (2) noise caused by the vessels themselves or by ship-based, hull-mounted acoustic systems, and (3) light from the vessel itself. As no nodules will be brought up to the surface, there will be no discharge of excess sediments or nodule abrasion at the sea surface.

The vessels that will be in use in this project strictly follow the IMO obligations and standards regarding safety and environmental practice at sea, including the International Convention for the Prevention of Pollution from Ships, 1973, as modified by the Protocol of 1978 relating thereto (MARPOL). In this way, the IMO regulates anti-pollution measures, whether the introduction of polluting substances into the sea is the result of an accident involving a ship or from the operational discharges from vessels. Such regulations aim at minimising all effects of air and water pollution at sea. We do not expect any discharges from normal operations except standard vessel discharges. The vessel operational deck areas will have directly accessible oil spill detainment kits in order to prevent accidental discharge of fluids into the seawater. Emergency response procedures will be on board the vessel to assist in minimising the impact of any accidents that may lead to spills with potential to affect the marine environment. In addition, a

shipboard marine pollution Emergency Response Plan will be implemented to combat any accidental spills or non-routine discharges of pollutants.

The noise caused by the vessels themselves do not exceed standard levels acceptable for shipping. The RV SONNE is equipped with modern, hull-mounted acoustic systems which are designed to reduce pollution effects to the environment as much as is physically possible. No dedicated, ship-based bathymetric surveys (EM122 multibeam) will be carried out during the cruises, but the system will run in between stations. The acoustic systems make use of low energy, medium frequency signals (12 kHz) that lie within the same range as those used for communication by many large marine mammals living in the area. Fish hearing is mostly reduced to sounds < 1 kHz, so that these should not be impacted directly by the acoustic system. The exact impacts of acoustic systems on the behaviour of larger animals are largely unknown. Depending on the distance of the animal from the source, impacts range from detection, the masking of communication calls, behavioural response (e.g. disorientation) to injury and hearing loss in close proximity of the source. However, no whales or larger sea mammals have been sighted in the German license area during any of BGR's exploration cruises, six of which have also taken place in spring (April/May). We thus assume that sporadic use of the EM122 multibeam within a small test area will have no direct impact on larger animals that can also move away from the source in all directions should the noise levels be unfavourable. Deployment of the AUV (autonomous deep multibeam system) a few tens of meters to a few meters above the seafloor has the advantage that it has no potential impacts on mammals, as these are not found at the abyssal depths of the license area.

Light pollution refers to the introduction of light to an environment where there are no natural light sources or any occurring light is much weaker and/or irregular. Light pollution can have an impact at the surface, due to light emanating from the support vessel that attracts insects, birds, and marine mammals (DNV.GL, 2016). This impact will only be temporary for the time period that the vessels are in the test area. Attention will be paid that there is no or limited direct light shining into the water column. During night work, deck light will be avoided as much as possible, whilst still maintaining safe operations.

### **7.3 Biological impacts at midwater depths**

Due to the fact that no instrumentation or technology is deployed in midwaters, no biological impacts in excess to those described for the surface waters in CHAPTER 7.2 above are expected for the entire water column up to a height of ca. 250 m above the seafloor, which is the maximal height of modelled operational plume dispersion and is described as seafloor impact in CHAPTER 7.4.3.

### **7.4 Biological impacts at the seafloor**

The magnitude of impacts on benthic deep-sea fauna varies widely with the scale and intensity of disturbances (Jones et al., 2017; Gollner et al., 2017). The species' potential to recover after major disturbances depends on substrate availability (loss or alteration of its composition) and substantial shifts in community structure do occur, with a wide variation in recovery rates among taxa, size and mobility of fauna. While densities and diversities of some taxa can recover to or even exceed pre-disturbance levels, community composition remains affected after decades (Miljutin et al., 2011; Vanreusel et al., 2016; Jones et al., 2017). The various types of seafloor impact are described in detailed in CHAPTER 7.4.1 to CHAPTER 7.4.6 below.

### 7.4.1 NODULE REMOVAL AND EFFECTS ON THE EPIFAUNA

Picking up nodules and removing the associated fine-grained muds fundamentally disturbs the benthic habitat in the mining area, leading to degradation of seabed habitat. In the framework of the JPI-O MiningImpact 1 project, several year-old to decade-old disturbance tracks in ISA license areas in the CCZ we re-visited in 2015. These disturbance tracks typically consisted of a single or a few multiple tracks, a couple of meters wide and up to ~2 nm long, created by a benthic disturber, epi-benthic sleds or dredges. Visual and hydroacoustic inspection of the disturbances by AUV, ROV and OFOBS identified prominent marks on the seafloor that are clearly visible even several decades after the tracks were created (e.g., 20 years for the IOM-BIE, 37 years for the OMCO track), irrespective of their size. For the purpose of the collector vehicle test that is planned here, the area and duration of impact is quite comparable to that of the benthic impact experiments (BIEs) in the 1990s.

Results of biological and geochemical investigations at the disturbance sites are in line with previous studies that covered shorter time scales of only 5-7 years after the impact (e.g. in the DISCOL area in the Peru Basin: Thiel and Schriever, 1990, Thiel et al., 2001). In general, epifaunal abundances, sessile fauna attached to the nodules (e.g., sponges, hydrozoa) and also mobile fauna associated to the nodule hard substrate (e.g., ophiuroids, isopods), are reduced in the CCZ tracks even decades after the impact was created (FIGURE 5.26; Vanreusel et al., 2016). A similar picture could also be seen at the DISCOL site, where a shift of the epifaunal community structure from dominantly filter feeders (decreasing from 76% to 42%) to detritivores/predators (increasing from 20% to 49%) was observed after 26 years (Marcon and Purser, unpubl. data). In the area of impact of the collector test described here, which will have an approximate size of 0.1 km<sup>2</sup> and will be left mostly barren of nodules, we assume that a similar process of shifting in epifaunal/megafaunal community structure will occur. This is, however, unlikely to influence gene flow or connectivity of species due to the sheer small size of the disturbed area.

### 7.4.2 FAUNAL ABUNDANCE CHANGES RELATED TO SEDIMENT DISTURBANCE AND PLUME DEPOSITION (BLANKETING)

The hydraulic collector vehicle will suck in large amounts of bottom sediment along with the nodules (up to maximally 865 m<sup>3</sup>/h, assuming a sediment layer thickness intake of 12 mm), and with that, many of the organisms that live in and on the topmost sediments – leading to the crushing of larger animals and mortality that depends on the original densities and size distributions of the organisms inhabiting the test area (to be determined in baseline studies prior to the test).

The removal of topmost sediments in the direct test area and the redeposition of these sediments after discharge and dispersion to more remote areas will furthermore lead to the smothering of organisms, the clogging of respiratory or filter-feeding organs of particular organisms and/or the release of potentially toxic or oxygen-consuming substances. Processes of nutrient cycling and organic matter remineralisation will also be affected. In the CCZ, abundance and biomass of all faunal size classes (meio, macro- and megafauna) typically decrease along the productivity gradient from eutrophic (eastern) to oligotrophic (western) environments (Martínez-Arbizu and Haeckel, 2015). This underlines the importance of nutrient supply and benthic-pelagic coupling for the determination of ecosystem structure and the potential negative effect on the benthos when (1) the topmost 10 to 12 cm of bottom sediment are sucked up, suspended in a particulate plume and consequently redeposited with very low average organic carbon content and in altered grain-size distributions, in turn leading to a change in organic matter remineralisation processes, and (2) naturally occurring phytoplankton and detritus arriving at the seafloor during times of plume dispersion aggregate and alter the nutrient dispersal pattern (Pabortsava et al., 2011; Purser and Thomsen, 2012). These processes effect all faunal classes from microorganisms to the



megafauna. Other modifications to the habitat will be caused by significant sediment compaction and pore water expulsion due to the weight of the collector (only in the collector tracks), which alter the biogeochemistry of the remaining sediment and are assumed to hinder processes of bioturbation and recolonization (see also CHAPTER 7.4.4 below).

Environmental impact assessment of the deep-water oil and gas exploitation industry indicates that both increased sedimentation and toxicant exposure have significant ecological effects that can extend to more than 5 km from the point source (Cordes et al., 2016). However, impacts depend on both the magnitude and composition of the released material, which differs significantly both within and between the deep-sea oil and gas industry and the deep-sea mineral industry, preventing direct inferences of resistance to deep-sea mining impacts. Seafloor coverage by a 3 mm thick layer of drill cuttings can significantly affect infaunal communities (Schaaning et al., 2008). However, significant quantitative impacts on meiofaunal abundance and community composition have also been observed beyond the extent of observable drill cuttings deposition (Netto et al., 2009). Resistance of species to enhanced particle loads and sedimentation generated by mineral extraction processes is likely low as natural sedimentation rates are in the order of only 1-6 mm/kyr (CHAPTER 4.2.4.4), but will vary based on the ecology of individual species, for example depending on whether taxa are epifaunal or infaunal, errant or sessile, suspension feeders, filter feeders, deposit feeders, or necrophages (Cordes et al., 2016 and references cited therein). Unfortunately, we know little about the specific effects of ecological drivers in deep-sea ecosystems, especially in these areas with extremely low sedimentation rates.

Since 1970, 11 small-scale disturbance experiments have been conducted in different parts of the world oceans (CCZ, Peru Basin, Central Indian Ocean Basin) to study the potential effects of nodule mining on the benthos (reviewed by Jones et al., 2017; see also CHAPTER 6.4.1). The results of meta-analyses performed on population density and diversity recovery after these disturbances have been published in Jones et al. (2017) and Gollner et al. (2017). Despite the fact that different methodologies were used, putting limitations on the quality and comparability of the data (for details see Jones et al., 2017), several general conclusions could be made. At seven sites in the Pacific, multiple surveys assessed recovery in fauna over periods of up to 26 years. Impacts are often severe immediately after mining, with major negative changes in density and diversity of most groups occurring (FIGURE 7.1). Of all the faunal groups studied, 64% of the faunal classes, in addition to bulk meiofauna and megafauna, showed negative impacts in faunal density relative to the controls <1 year after disturbance. Reductions in density were also observed for polychaetes (INDEX, DISCOL), crustaceans (JET) and total macrofauna (INDEX, DISCOL). The greatest standardised reduction in density following initial disturbance from mining simulations was for polychaete macrofauna at the JET site (CCZ). However, there are also some exceptions to the general pattern of reductions in density after simulated mining disturbance. At the BIE II site (NOAA BIE) there are two macrofaunal groups that show an increase in density: polychaetes and isopods, which lead to associated increases in the total crustaceans.

When the time series of biological effects of disturbance experiments are considered, there is evidence of minor recovery of density in some groups in some experiments (FIGURE 7.1). In some cases, the mobile fauna and very small-sized fauna experienced less negative impacts over the longer term, i.e. almost all studies show some recovery in faunal density and diversity for meiofauna and mobile megafauna, often within one year. On the other hand, some faunal groups showed no evidence of recovery (FIGURE 7.1). The only study of sessile fauna specifically was DISCOL, and sessile megafauna did not show any evidence of recovery. Also, very few faunal groups return to baseline or control conditions after two decades, and so the effects of polymetallic nodule mining are likely to be long term.

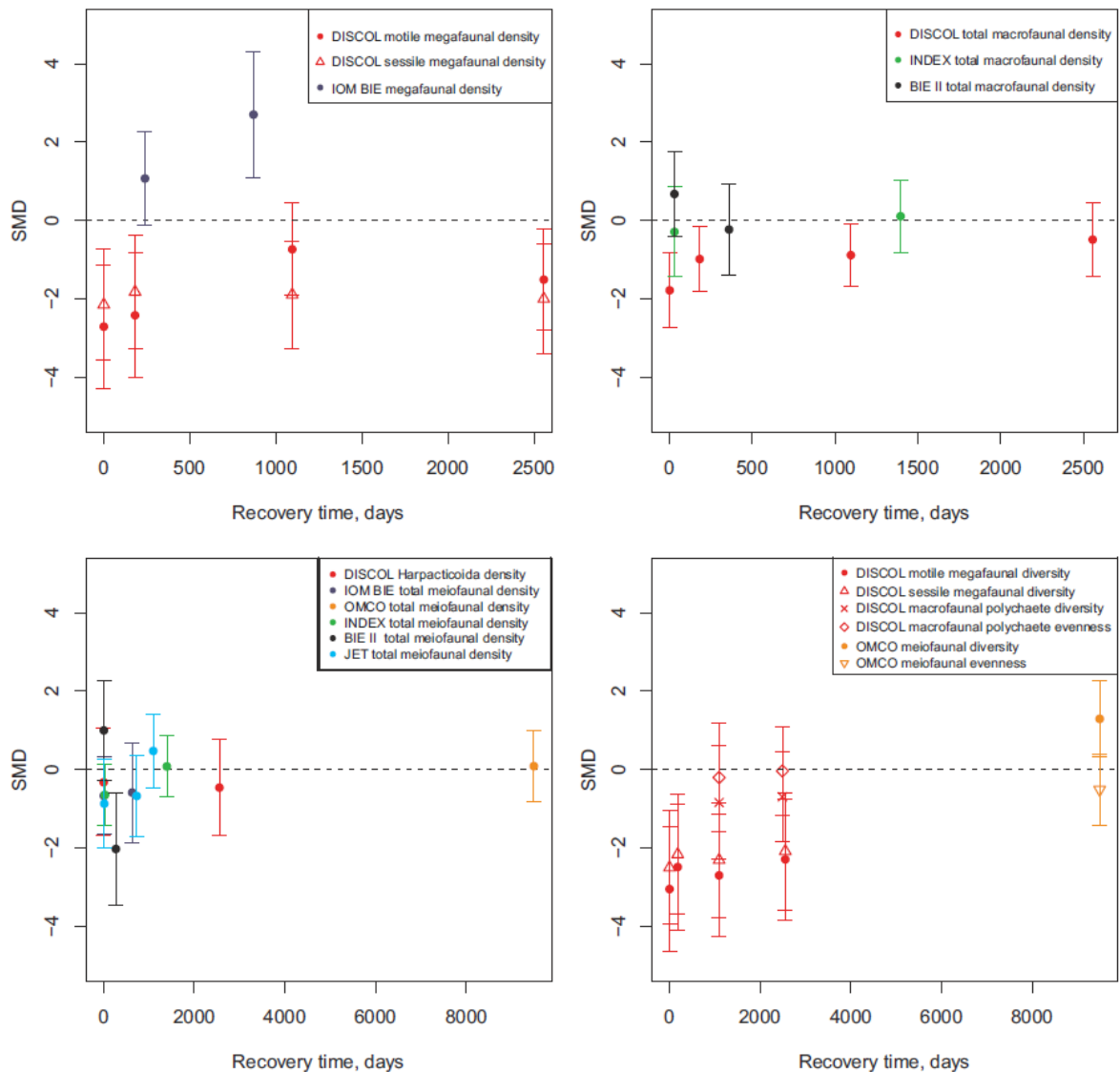


**Figure 7.1:** Changes in effects of mining activities over time on faunal density and diversity (from Jones et al., 2017). Changes shown for megafaunal density (top left), macrofaunal density (top right) and meiofaunal density (bottom left) and diversity (including evenness) of megafauna and meiofauna (bottom right). If totals were not available, the value for the most abundant taxon was plotted and indicated in the legend. Values represent standardised mean differences (SMD) between faunal densities or diversities at impacted sites and control sites and 95% confidence intervals. Diversity was reported as Shannon-Wiener diversity and evenness was Pielou evenness index in the studies used.

The data presented in Jones et al. (2017) suggest that some signs of recovery were able to be observed, i.e. there is a general reversion, mainly in density, towards control levels over time, most obvious for meiofauna. However, although species richness and biomass of, for example, harpacticoid copepods recover after 26 years (DISCOL site), differences in community composition remain obvious. This could be validated for the German, French, Belgian and IOM license areas even after 37 years. Thus, it can be concluded that a total recovery process of meiofauna after anthropogenic impact would take at least several decades.

Species diversity is often more sensitive to change than density and appears to be more significantly impacted (Jones et al., 2017). Recolonisation of benthic communities has long been thought to be slow in the deep sea, although recolonisation of deep-sea soft sediment by macrofauna and meiofauna can take place relatively rapidly (months to years). As the experiments removed nodules, this could lead to slower recolonisation rates, although almost all of the experiments (with the exception of megafaunal

evaluations) focussed on the soft sediment fauna and not the fauna associated with nodules. The latter would be unlikely to recover for millennia owing to lack of nodule habitat to recolonise, as the growth rate of new nodules is only a few millimetres per million years.

The first study to address mining-related impacts on microbial communities, conducted in the Peru Basin during the MiningImpact 1 project, indicated that, surprisingly, even the microbial communities do not seem to be capable of adapting to the seafloor disturbances within several decades, which is expressed, for example, in reduced metabolic activity and reduced oxygen consumption in the surface sediments (Vonnahme, 2016; Vonnahme et al., in prep). Whilst the removal of the active surface layer of sediment and/or the nature of the remnant compacted sediment may affect these communities, the effects of small-scale disturbances in plough tracks are not easy to discriminate from natural variability (Janssen et al., 2017). This calls for an extension of the suite of molecular tools and for studies in more realistic mining scenarios as planned in the context of the MiningImpact 2 project.

All in all, insufficient information is currently available to generalise the observed biological effects to the scale of the DEME collector vehicle test that is being planned in the framework of the MiningImpact 2 project, nor on longer terms, larger scales, and greater disturbance intensities expected to result from full-scale mining activities. In the case of the collector test proposed here, it appears to be essential to accurately and precisely quantify baseline conditions of the abyssal ecosystem that is going to be impacted, particularly with regard to ecosystem processes and functions. The systematic monitoring of the nature and extent of impacts at high resolution over relevant temporal and spatial scales (see CHAPTER 8) will be an essential element to increase the knowledge of mining impacts beyond what has been analysed before.

### 7.4.3 EFFECTS OF PLUMES ON EPIFAUNA, DEMERSAL SCAVENGERS AND FISH

While the impact of blanketing on the benthic ecosystem by resettling sediment particles has been addressed in some of the BIEs (e.g., Radziejewska et al., 2001a,b; Radziejewska, 2002) or by natural analogue studies (e.g., volcanic ash fallouts: Hess and Kuhnt, 1996; Haeckel et al., 2001b), we lack information on whether and to what extent resuspended high particle concentrations and prolonged life-times of the plumes harm the deep-sea fauna by e.g., smothering of organisms, clogging the respiratory or filter-feeding organs or releasing potentially toxic or oxygen-consuming substances. Our current understanding of the impact of mining plumes on the deep-sea environment is thus not based on direct observation, but inferred from ecological status assessments before and after impact experiments (see CHAPTER 7.4.2 above), *ex situ* sediment exposure and ecotoxicological experiments conducted with model species from shallow water depths, and observations made in shallow-water settings.

In the framework of the MIDAS and MiningImpact 1 projects, different responses of deep-water corals and sponges exposed to various types of particulate matter were tested and observed: (1) high survival and minor sub-lethal effects in the scleractinian coral *Lophelia pertusa* (Larsson et al., 2013); (2) reduction in metabolic rates, deteriorating tissue condition, tissue necrosis and death in the octocoral *Dentomuricea meteor*; and (3) high tolerance to sedimentation with reduced metabolic activity in the sponge *Geodia baretii* (Kutti et al., 2015). Similar tests and experiments will be carried out to test the effects of the plume (particulates and enhanced dissolved metal concentrations) on sessile and mobile epifaunal organisms (e.g. Anthozoans, Holothurians) (see CHAPTER 8.2.1.2).

For the short temporal and low spatial scale of the collector vehicle test activity, we assume that larger mobile epifaunal organisms and demersal scavengers and fish will readily move out of the area of impact

under the influence of light, noise, vibration and enhanced particle concentrations in the lowermost water layers.

#### **7.4.4 BIOGEOCHEMICAL ALTERATIONS, BENTHIC ECOSYSTEM PROCESSES AND MICROBIAL ACTIVITIES**

Biogeochemical impacts are specific to the particular nature and intensity of the physical impact, with strongest effects observed in regions where the surface reactive layer of sediment with labile organic matter is lost and deeper sediment layers are exposed at the surface. Such stiffer and less porous sediments may be more difficult to recolonise by bioturbating organisms that mix in fresh organic matter and created favourable conditions for re-establishing stable geochemical conditions and biogeochemical processes. Potential impacts of nodule mining activities on biogeochemical processes from a physico-chemical perspective are described in CHAPTER 6.5.

Mining activities may alter the trophic conditions of deep-sea ecosystems and this can have important consequences for the functioning of benthic food webs and biogeochemical processes over long time scales (i.e. years). CoNISMa has analysed the potential impact of mining activities on organic matter composition and key ecological processes such as degradation rates in the CCZ during the SO-239 cruise. In the German license area, the topmost sediments deriving from 6 control sites and 2 impacted sites (EBS tracks that were sampled 3 years after impact) were analysed for their biochemical composition (phytopigment, protein, carbohydrate, lipid and biopolymeric C concentrations), as well as for prokaryotic abundance and extracellular aminopeptidase activity as a proxy for protein turnover rate. No significant differences between impacted and non-impacted areas were found in phytopigment concentration or in the biogeochemical classes of compounds, but biopolymeric C showed that less trophic resources are available in impacted sediments. However, there appears to be a progressive recovery of trophic conditions in surface sediments over time (comparing all analysed disturbed sites of the CCZ), perhaps due to the supply of fresh organic matter from photosynthesis above, although at 3-5 cm depth recovery is much less pronounced. These results suggest that benthic ecosystems receiving greater amounts of organic matter from the water column (i.e. in higher productivity areas such as the Eastern German license area; with higher sedimentation rates) are potentially more resilient. Surprisingly, however, concentrations of benthic deep-sea microbes, which are expected to be highly resilient, were found to be significantly lower after disturbance, even after 37 yrs (French area). Reductions in microbial activity in the DISCOL experimental area 26 years after disturbance have also been reported (see section below). Aminopeptidase activity was also significantly lower at all impacted sites. Deep-sea mining could thus lead to a significant decrease in the efficiency of microbially-controlled degradation and reduced turnover rates of N-rich organic compounds (i.e. proteins), with potential cascade effects on biomass production and N cycling.

Analyses of benthic processes and fluxes measured *in situ* as a function of disturbance intensity and nodule coverage in the DISCOL area (Peru Basin) confirm that oxygen uptake rates are reduced in all disturbed habitats as compared to rates observed in the reference areas (Vonnahme, 2016). Reductions are particularly prominent in the fresh disturbance tracks created with an EBS tow approx. 5 weeks before (FIGURE 7.2).

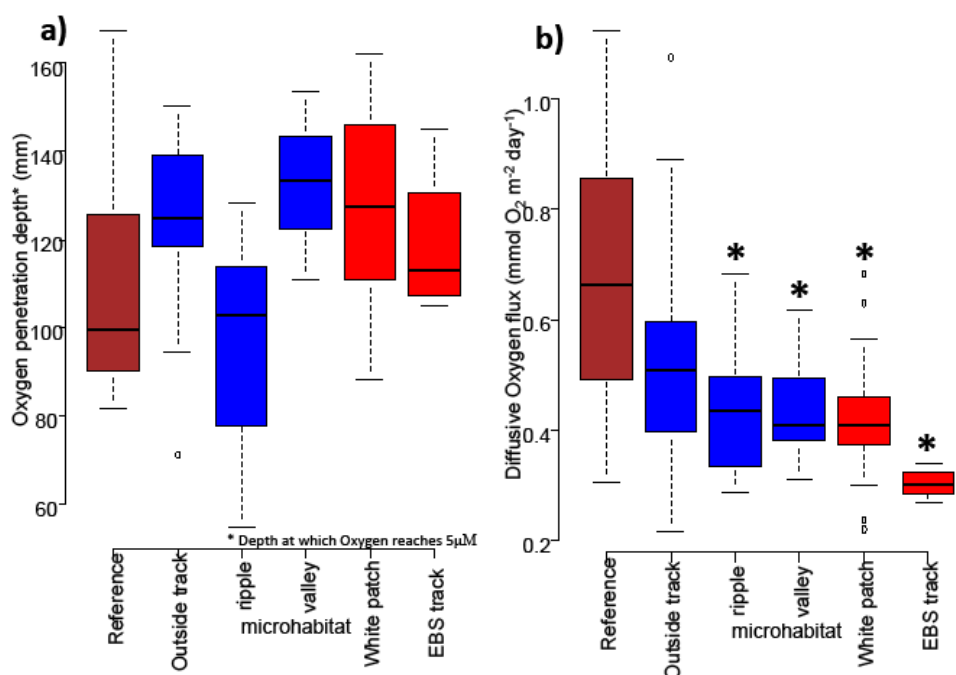


**Figure 7.2:** Oxygen penetration depth and diffusive oxygen flux in sediments from the DISCOL experimental area (Peru Basin) 26 years after the disturbance and in a 5-week-old EBS track. **a)** Depth at which oxygen reaches concentrations below 5  $\mu\text{M}$  for the different microhabitats of the disturbance, **b)** Diffusive oxygen flux from the bottom water into the surface sediment (Figure from Vonnahme, 2016).

Reduced rates of microbial activity based on radiotracer incubations were also observed at the disturbed sites, particularly where surface sediments were lost or covered upon disturbance, i.e., in the EBS track and within the historical ploughmarks. In addition, DIC and leucine uptake rates were also reduced in ripples where sediments have been piled up by ploughing 26 years ago. The disturbance of the sediments clearly reduced microbial community metabolism even after 26 years, with largest effects observed for DIC uptake and for potential activities of glucosidase, esterase, and chitinase.

Activities of organic-matter degrading enzymes, oxygen consumption rates, organic matter quality, porosity, and radio-isotopes constraining bioturbation activity prove to be very effective monitoring variables for assessing the overall status of benthic biogeochemical functions (Vonnahme et al., in prep). However, in order to conduct comprehensive numerical simulations of effects on biogeochemical functions and food webs, including prognostic modelling of their expected recovery, an even more comprehensive suite of biogeochemical variables is required. This will be a strong aim of the monitoring work that is planned in the framework of the MiningImpact 2 project (see CHAPTER 8.2.1.3).

#### 7.4.5 EFFECTS OF TOXIC DISCHARGES ON FAUNAL ORGANISMS

In the EU MIDAS project, considerable research capacity was invested to assess the lethal and sub-lethal sensitivity of different megafaunal (shallow water) species to single metal toxicants such as copper or combinations of different metals and potential by-products of mining as a function of temperature and pressure. Interactions were found to be extremely complex and species-dependent (e.g. MIDAS, 2016).

In the CCZ, if there is a release of metals from the sediments and potentially crushed nodules at all (see CHAPTER 6.6), there will be a low-level metal exposure through the dispersal of the sediment plume created by the mining tool at the seafloor or through the discharge of contaminated water or tailings during processing. We presently lack detailed information on how re-suspended, high (nano) particle

concentrations harm the deep-sea fauna by e.g. releasing potentially toxic or oxygen-consuming substances.

During the MiningImpact 1 cruise to the DISCOL experimental area in the Peru Basin in 2015, *in situ* effects of metal exposure on bioaccumulation and gene transcription in megafauna and meiofauna community structure were analysed by the University of Southampton (UK), University of Gent (Belgium) and the Institute of Marine Research (IMAR, Portugal).

Enclosure corals (40 cm height, 40\*40 cm top and 30\*30 cm bottom dimensions) were used to isolate meiofauna and assigned to the following treatments: Control without sediment addition (NS), Control with uncontaminated sediment (UnC) and four treatments with copper-spiked sediment of 4 concentrations (1, 5, 10 and 20 ppm Cu<sup>2+</sup>, C1-4). After ca. 96 h bottom incubation time, three push cores were taken from each corral and analysed. Total meiofauna densities ranged between 101 ind. 10 cm<sup>-2</sup> in the highest copper treatment (C4) and 334 ind. 10 cm<sup>-2</sup> in the control without added substrate (NS). Although a decreasing trend with copper concentration could be observed, total meiofauna densities did not significantly differ between the different treatments and the controls (FIGURE 7.3A). Interestingly, a large proportion of the meiofauna migrated into the added substrate. While about  $35.1 \pm 3.2$  % of nematodes migrated into the artificial sediment, this proportion was significantly higher (ANOVA,  $p < 0.001$ ) for copepods and nauplii ( $61.67 \pm 2.65$  % and  $66.42 \pm 2.91$  %, respectively) (FIGURE 7.3B).

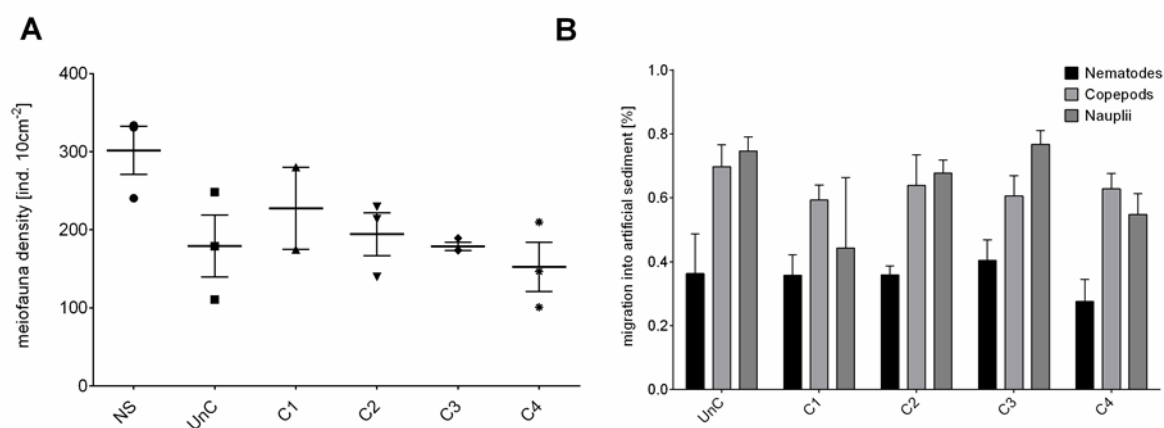


**Figure 7.3: A)** Meiofauna densities per core expressed in ind. 10 cm<sup>-2</sup>. The line and error bars indicate mean and standard error, all data points are shown. **B)** Proportion of nematodes, copepods and nauplii that migrated into the added substrate. NS = no sediment addition, UnC = addition of uncontaminated sediment, C1-C4 = addition of sediment spiked with 1, 5, 10 and 20 ppm Cu.

Burial with sediment apparently alters vertical meiofauna community structure, but copper toxicity did not affect total meiofauna densities. However, further analyses on the tissue copper concentrations of nematodes in different treatments, by means of X-ray imaging, will provide more information on their mortality and the actual impact of copper-contaminated sediment. A similar migratory response especially of copepods and nauplii was found during *in situ* experiments in which bottom sediments were covered by 2 cm of (1) crushed nodule material, and (2) bottom sediment, for a few days.

The behavioural and physiological (antioxidant enzyme activity) response of a deep-sea holothurian (*Amperima* sp.) and a shallow-water proxy holothurian (*Holothuria forskali*) to copper-spiked artificial sediments were analysed *in situ* in the Peru Basin and in the laboratory, respectively. Interestingly, these studies demonstrated that holothurians are sensitive to contaminated sediments and exhibit consistent avoidance responses, which appear to reduce the oxidative stress imposed on this biological group. No



antioxidant response was observed in either species, which was interpreted to be the consequence of avoiding copper exposure (Brown et al., 2017).

To better assess the potential impacts of mining activity with respect to the release of toxic metals, several *in situ* and *ex situ* experiments are planned within the framework of the MiningImpact 2 project (see CHAPTER 8.2.1.2). In addition to investigating the possible physical damage inflicted by suspended sediment particles on fauna living on or close to the seafloor (sediment clogging, thus impairing filter-feeding and suspension-feeding megabenthos such as corals and sponges, see CHAPTER 7.4.3), the MiningImpact 2 project also aims at investigating ecotoxicological effects due to metal-containing particles and dissolved metals.

#### 7.4.6 LIGHT AND NOISE POLLUTION

The response of species to light and sound/vibration/electromagnetic radiation produced by mining operations is poorly understood. Shallow-water marine mammals, fish, and invertebrates are physiologically sensitive to acoustic disturbance (Aguilar de Soto and Kight, 2016), with potential for ecological effects such as alteration in natural behaviour, reduction in communication ranges, reduction in foraging ability, prevention of predator avoidance, complete habitat avoidance, and death (Stanley and Jeffs, 2016; Burritt and Lamare, 2016). However, causal effects of these potential stressors on deep-sea fauna are poorly constrained and data on sound/vibration and/or electromagnetic radiation impact at nodule fields are few and uninformative in a deep-sea mining context.

The collector test will occur at a depth of 4100 m below the surface, in the middle of the Pacific Ocean. It is well established that there is very little natural light below 1000 m below sea surface (NOAA, 1984). Thus, many deep-sea organisms have developed bioluminescent capabilities for counter illumination camouflage, attraction, defense, warning, communication or mimicry. Most deep-sea organisms have developed “super-eyes” to detect dim light of bioluminescence. Therefore, the artificial white light of the collector, as also of ROV/AUV, could potentially induce temporary or long-term blindness, or obscure or even completely block the function of bioluminescence. No background records of light are available for this specific area of interest. Nevertheless, during the lowering of DEME-GSRs TSTD Patania in 2017 through the water column, three distinct organism behavioural patterns could be observed: (1) attraction towards the artificial light source; (2) fleeing of nekton; (3) complete indifference. From literature review, it appears to be species-dependent (Ortega, 2014 and references therein).

From a technical perspective, light and noise pollution are unavoidable around the collector. Cameras associated with the lightening will be aiming at the vehicle itself, to monitor the vehicle, the tracks, the hoses, potential hydraulic leakage, hydraulic and electric connectors. Light will aimed directly at the surrounding environment will be limited as this is not used for steering. There are a total of eight lamps installed on the current design of the vehicle. The lamps are all independently dimmable from zero up to 100%, with a max of 3200 lumens per lamp. However, there is no light source in the water column (except while the collector is lowered).

Limited information is available at this stage regarding the noise level of the test collector vehicle. It is envisaged to place a hydrophone will on the collector that will record the evolution of noise. It will then be compared with the dive logbook, to link artificial noise and the vehicle activity. The main components of the collector responsible for generating noise are the HPU hydro-power-unit, pumps and the nodule transport itself. The HPU and pumps used in the pre-prototype were noise-reduction designed. Hydraulic pumps design features having to do with noise emission, like hydrostatic bearing, commutation, canalling interfaces and housing shape have been optimised with regard to pulsation and noise transmission. A

general assumption is that mining activities at the seabed and in the water column will create general background noise of up to 50 dBA (DNV.GL, 2016).

## 7.5 Cumulative impacts

Polymetallic nodule mining will increase the pressure on abyssal ecosystems, which may lead to the loss of genetic and species diversity, the fragmentation of natural habitats and the degradation of ecosystem functions (Jones et al., 2017; Gollner et al., 2017). Future mining therefore requires a clear and strong policy that will regulate activities and their pressures on the environment in order to minimise their effect and impact. Unfortunately, little is known on causal activity-pressure-effect relations of the targeted ecosystem and its components (i.e. species populations and communities, habitats and ecosystem functions), and the cumulative pressures that mining activities will exert on ecosystems or their components (Tamis et al., 2017). In particular in the CCZ, more data are needed to quantify the impact of mining activities and to identify specific pressures and their cumulative effects on the vulnerability and recovery potential of the ecosystem. FIGURE 7.4 illustrates potential relations between activities and pressures on different ecosystem components. Although a few studies have documented the individual effects of different mining pressures on species and ecosystems (Auguste et al., 2016; Mevenkamp et al., 2017), research on cumulative and interactive impacts of multiple stressors from nodule mining in the abyss is still completely lacking. One major aim of the monitoring study proposed here is to use the results of the different individual impact studies around the collector vehicle test to collectively and statistically analyse possible scales and ranges of cumulative impacts (see CHAPTER 8.2.1.5).

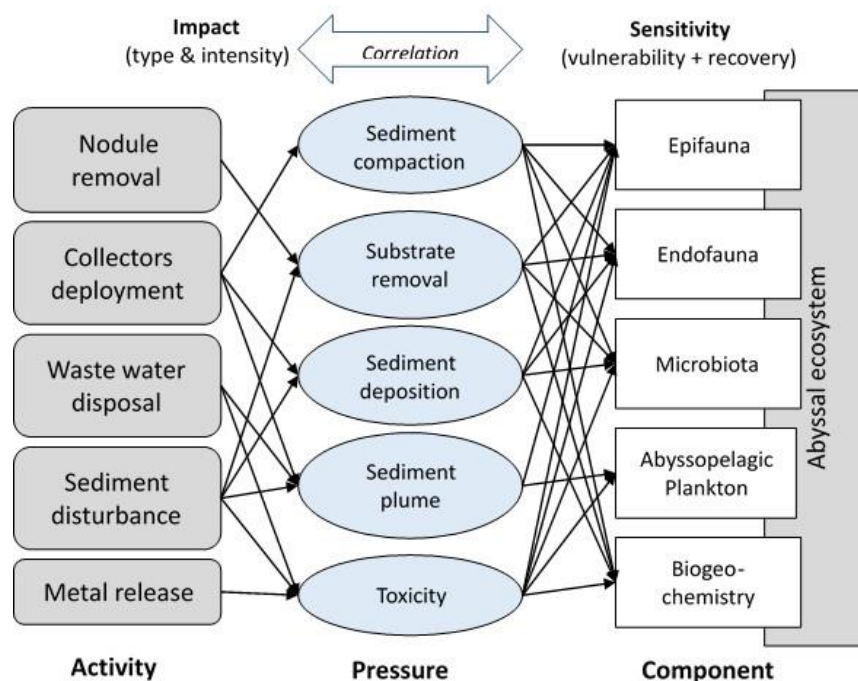


**Figure 7.4:** Generic outline for cumulative effect assessment of potential future mining-related activities that may generate pressures on different ecosystem components. The conceptual scheme visualizes potential relationships between impact intensity and sensitivity that need to be assessed (modified after Tamis et al., 2017).

## 8. Environmental management, monitoring and reporting

### 8.1 Organisational structure and responsibilities

The organisational structure of the JPI-O MiningImpact 2 project is outlined in CHAPTER 1.3 and consists of 5 different work packages (WP) and 3 cross-cutting themes (CCT) (FIGURE 1.2). A high degree of coordination between the WPs and CCTs is required in order to achieve a good all-round baseline sampling strategy, an efficient monitoring of the collector vehicle test that simultaneously allows implementation of all monitoring objectives, the setting up of a coordinated monitoring programme, and an efficient data management, reporting and dissemination programme. These highly interconnected tasks necessitate a comprehensive project governance structure (FIGURE 8.1) that allows collaborative decision making and consultation within the JPI Oceans framework. To assist in evaluating the project's progress, an advisory board consisting of representatives of NGOs, the mining industry, policymakers, and regulators is envisioned for the second phase of the project. A list of suitable advisors will be determined at the kick-off meeting by all participants (General Assembly, FIGURE 8.1).

Responsibilities in terms of project dissemination, data and sample management as well as outreach and reporting are elaborated on in chapter 8.3 below.

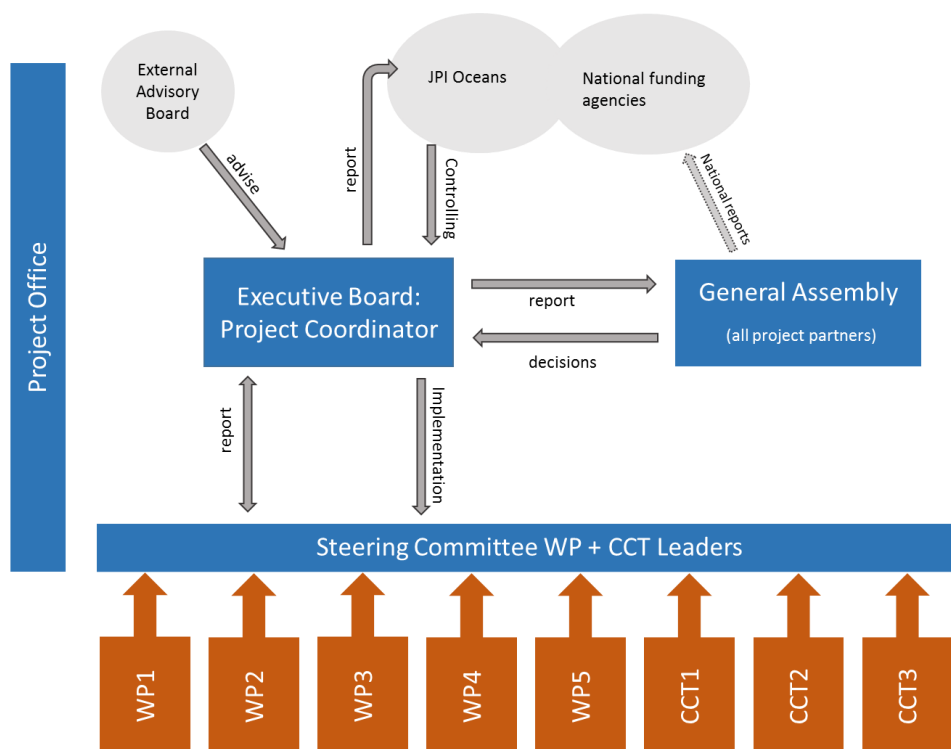


**Figure 8.1:** Outline of the JPI-O MiningImpact 2 project structure.

## 8.2 Environmental Monitoring Plan

The Environmental Monitoring Plan (EMP) will focus on the immediate, short-term and intermediate-term (2 year) physical and chemical impacts of the collector vehicle test on the seafloor and its overlying waters, as well as on the response of benthic organisms that is crucial for the recovery of benthic standing stocks and biodiversity and for the maintenance of associated ecosystem functions. An assessment of plume impacts on longer time scales (i.e., more than 2 years after the test) is desirable but dependent on ship availability and funding. Discussions are ongoing with respect to such further monitoring cruises that would then take place towards the end of the MiningImpact 2 project.

The EMP involves several different phases of activity which can also be seen as clear objectives of the project:

1. planning of the EMP layout around the collector test;
2. cruise station time planning;
3. onsite pre-impact physical, chemical and biological assessment (BGR baseline data, BGR exploration cruise 2018, JPI-O cruise 2019);
4. *in situ* and *ex situ* plume experimentation before the collector vehicle test takes place;
5. near real-time modelling to predict plume fallout areas directly before the collector test;
6. comprehensive *in situ* monitoring survey of the collector test itself;
7. validation of plume modelling;
8. onsite post-impact physical, chemical and biological assessment;
9. evaluation of the effectiveness of the EMP workflow and used monitoring technologies;
10. recolonization/restoration experiments (ecosystem engineering);
11. evaluation of mining-related pressures and effects on ecosystem components;
12. development of tools for integrated (cumulative) environmental impact assessment.

A schematic presentation of the spatial and temporal coverage of pre- and post-impact assessment and the restoration experiments is given in [FIGURE 8.2](#). Details of the monitoring approach and programme are described in [CHAPTER 8.2.1](#) and [CHAPTER 8.2.2](#) below. The test plan and monitoring programme includes, to the maximum extent possible at this moment in time, a detailed description of the aims and designs of the surveys, but will be adapted and/or refined prior to testing and at other appropriate times, if refinement is necessary (e.g. due to the collection of new baseline data shortly before the test takes place).

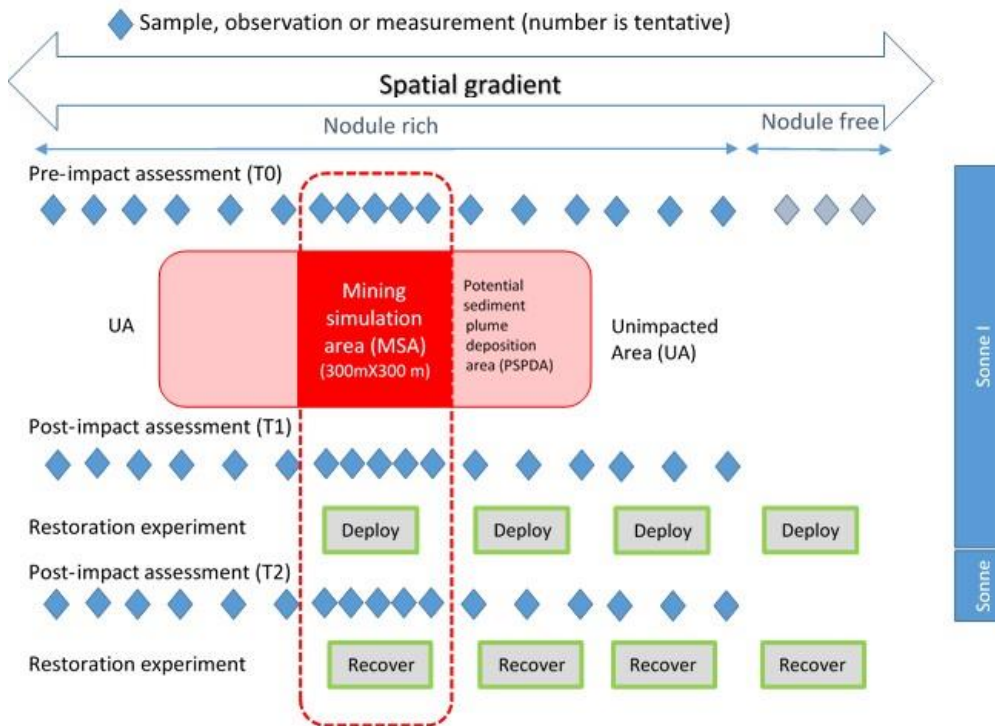


**Figure 8.2:** Schematic presentation of the spatial and temporal coverage of pre- and post-impact assessment, and the restoration experiment.

The geographical scale / sampling scale of the monitoring survey is very much dependent on the predicted size of the impact, which is mostly determined by the modelled dispersion distance of the sediment plume, and the results of seafloor classification and habitat mapping efforts using ship- and AUV-based bathymetric and optical information as well as geological and biological sediment sampling data (baseline data). Spatial design involves defining the Impact Zone and the gradients of impact within that zone, as well as defining one or more control reference sites (potentially reflecting different habitats) against which any changes in the biodiversity of the marine environment can be assessed. The Impact Reference Zone (IRZ) of the collector vehicle test can be defined as the area that is directly impacted by the test (i.e. in which the nodules are removed). The total Impact Zone, however, is much larger due to the development and spreading of a particulate operational plume, and theoretically extends to a distance where the impact of the plume can no longer be detected. We refer to this area as the Plume Impact Reference Zone (PIRZ). Depending on the bottom current dynamics at the time of testing ("normal" conditions vs. current conditions during the passage of an eddy in the area), the distance that the plume is likely to spread varies between maximally 3.5 and 8 km, respectively (see CHAPTER 6.4.3 and FIGURE 8.3).

Based on the results of baseline studies that are planned to take place before the test, one or more control reference sites will be established around the test IRZ. One already fixed reference site will be the area in which time-series analyses have been carried out throughout the last few years, which lies approximately 8 km to the SE of the test IRZ and so will not be affected by the testing activities, including the effects from the discharge plume (FIGURE 8.3). Such reference sites should ideally have a species composition that is comparable to that of the test area.

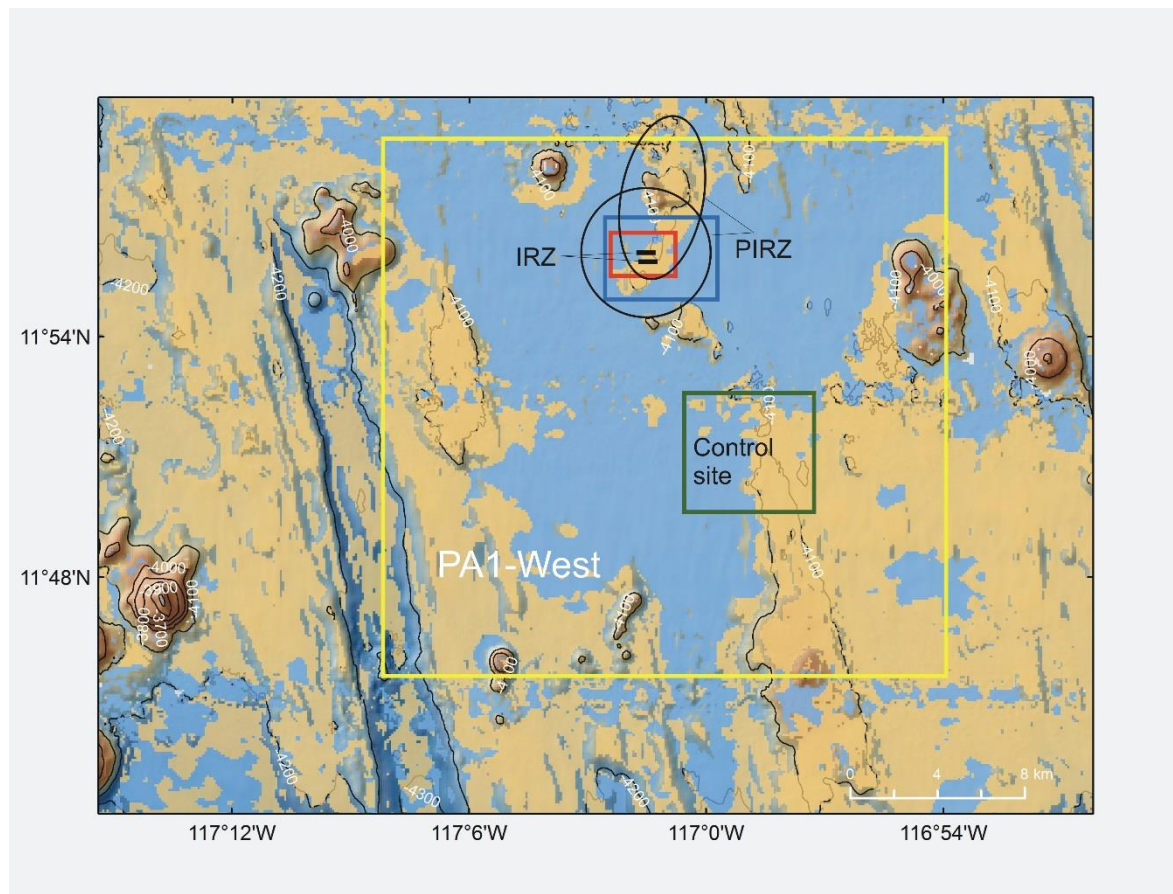


**Figure 8.3:** Environmental monitoring plan for the collector vehicle test. The collector vehicle test (small black rectangle; IRZ) will take place within the 2x3 km<sup>2</sup> red rectangular area in the northern part of PA1-West (see FIGURE 8.4 for a more detailed map of a potential monitoring array in this area). The black circle represents the maximum extent of plume dispersal during “normal” background seafloor current conditions; the black ellipse represents the maximum extent of the plume during eddy conditions (PIRZ). The green rectangular area represents an area of intensive previous analysis that will be used as a control reference site for the test. Areas are mapped onto a combined map of nodule size clipped with seafloor slope (>3°) in PA1-West. The blue colour refers to areas covered with predominantly large nodules (> 4 cm diameter), whereas the yellow colour refers to areas covered with predominantly small nodules (< 4 cm diameter).

These sites are not to be confused with the much larger Preservation Reference Zone (PRZ) that was established by the BGR in 2013 and lies approximately 60 km to the west of the test area (see FIGURE 3.1), and conforms to the ISA recommendations for environmental assessment during exploration (ISBA/19/LTC/8, Para. 26(d)). Due to the small spatial and temporal scale of the project, it is not applicable to define closed areas or preservation areas for the purpose of conservation and the maintenance of biodiversity and ecosystem structure and function in this context. Neither are spatial management tools required to minimise the amount of damage exerted – rather, the results of this project will be used to inform the development of best-practice management and monitoring tools for future (test)mining activities.

The exact survey monitoring design of the collector vehicle test will include spatial and temporal sampling schedules / transects with indications of sample sizes and numbers. Such a design, e.g. for the monitoring of the sediment plume as it disperses laterally away from the test site, can only be substantiated shortly before the test takes place in a flexible and adaptive way so as to take account of all local conditions at and around the seafloor at the time of testing (e.g. dominant current speeds and directions, possible effects of eddies; see also CHAPTER 8.2.2 and FIGURE 8.4). At this stage of survey planning, one year in advance of the test activity, a detailed, interactive monitoring approach and a more generalised monitoring programme can be presented as shown in the chapters below.



## 8.2.1 MONITORING APPROACH

### 8.2.1.1 Biodiversity, connectivity, resilience (WP1)

WP1 will focus on taxonomic and functional biodiversity, connectivity and resilience of benthic communities and will address both natural variability and the effects of impacts connected to the nodule collector test. Studies on benthic assemblages (microbiome, meiofauna, macrofauna and megafauna) will follow a Before-After Control Impact (BACI) design with replication conducted during both the baseline study and the impact study at stations located in the areas defined in the general environmental impact monitoring plan (EMP). The exact location of impacted sites for faunal sampling (using e.g. boxcorer, multicorer, EBS, ROV, faunal traps), combined optical and hydroacoustic surveys (with e.g. ROV, AUV, OFOBS), and time-lapse camera deployments will be identified based on plume impact monitoring carried out during and immediately after the collector test (WP2, CCT1). Both image-based and acoustic surveys to assess habitat structure and megafauna community structure have been conducted in polymetallic nodule areas previously, but have seldomly been used to monitor a disturbance event (Bluhm, 2001; Greinert, 2015; Boetius, 2015; Purser et al., 2016; Vanreusel et al., 2016). In this project a range of innovative acoustic and imaging static, towed and autonomous free swimming devices will be used to map at high resolution habitat features and faunal distributions across the surveyed region prior, during and post disturbance. Data collected will be processed using workflows developed during MiningImpact 1 (Marcon and Purser, 2017; Dreutter, 2017; Purser et al., in press).

Results obtained on changes in presence, activity and functions of specific groups of faunal and microbial communities and any impact indicator taxa that can be identified will feed into the analysis of disturbance effects (CCT2). Particular emphasis will be on the analysis of similarities in the response of different faunal components (meio- macro and megafauna) and microbial communities to specific impact types and intensities and to effects on biogeochemical processes. This knowledge will help to assess the suitability of biodiversity and community structure analyses of the different faunal compartments and microbial assemblages for future impact monitoring and feed into risk assessment and recommendations (CCT3).

WP1 focusses on four main tasks:

- (1) Megafaunal communities and their connection to physical habitat characteristics addressing natural variabilities, disturbance effects, and their temporal evolution

At each station, detailed seafloor imaging and acoustic data will be collected using AUV, ROV and the towed camera platform OFOBS to characterise habitat features and the megafauna communities present at the time of the survey. Each station will be visited prior to and after the collector test to allow any changes in megafauna community structure to be identified. Where possible, time-lapse camera units will be deployed on the seafloor prior to the collector test to observe any visual responses of epifauna to the disturbance.

ROV transects will be conducted at each station before and after the nodule collector test to collect image data which can be used to assess the plume impact on detritivores, suspension feeders and filter feeders. Once the plume has settled, one transect is to be carried out along the direction of the created plume. A second and a third transect will be carried out at different angles from the same starting point, to analyse different degrees of disturbance regime and to evaluate possible fleeing movements of mobile fauna. These transects will be repeated several times following the collector test, allowing both temporal and spatial responses to be gauged. From the ROV image data, a selection of three key representative megafaunal taxa (a suspension feeder, a detritivore and a filter feeder) will be chosen for direct physical

sampling. The ROV will then be used to collect representatives of the three taxa to assess their ecophysiology.

(2) Meio- and macrofaunal assemblages and their connection to physical habitat characteristics addressing natural variabilities, disturbance effects, and their temporal evolution

This task aims to decipher the spatio-temporal dynamics of the meiofauna and macrofauna from quantitative samples obtained according to the plan described above. On-board sampling of faunal specimens for taxonomic work (morphological and molecular) will follow Glover et al. (2015) methodology. A combined morphological and molecular approach will be used whenever possible allowing accurate taxonomic identifications, the detection of cryptic diversity and description of new faunal species. Typically, invertebrate markers such as cytochrome oxidase I mitochondrial gene (COI), 16S mitochondrial ribosomal RNA coding genes and 18S or 28S nuclear genes will be targeted. This work will contribute to and improve existing datasets and will be crucial for further assessments of biodiversity and connectivity.

Taxonomic and trophic diversity and community structure (e.g. alpha and beta-diversity) will be analysed in each faunal compartment and compared between faunal compartments. Functional and trophic relationships within meiofauna and macrofauna assemblages will be explored (e.g. by stable isotope analysis). A metagenomic approach will be used for biodiversity assessments and comparative analyses of selected taxa (e.g. nematode, polychaete and amphipod assemblages). Spatial and temporal patterns of faunal assemblages will be analysed (e.g. using multivariate analyses) in relation to comparable data obtained during MiningImpact 1 and to available abiotic and biotic environmental parameters, and will allow to establish criteria for the definition of “good environmental status”. Sensitive versus persistent species to mining plumes will be identified and listed.

The sponge *Plenaster craigi* is one of the common filter feeders on nodules and is likely susceptible to increased turbidity and nodule removal (Lim et al., 2017), so that it has been chosen as a potential indicator species for monitoring the impact of a mining plume. The mapping of *Plenaster craigi* abundance will be carried out using data from box cores and high-resolution *in situ* photography, and the impact from exposure to experimental sediment plumes will be subsequently assessed.

Short-term impacts of the collector vehicle test on connectivity will be investigated by assessing the dispersal of larvae and resuspended benthos by the sediment plume (e.g. via resuspended sediment, passive dispersal via currents).

Newly obtained molecular data will be used to complement previous and/or ongoing analyses of data from MiningImpact 1 and other projects (Glover et al., 2016b; Dahlgren et al., 2016; Wiklund et al., in press) and detect shared species at a regional scale within the CCZ. Novel Next-Generation RAD-seq techniques (Burford-Reiskind et al., 2016) will be applied to investigate the population genomics of amphipod species and provide data on population histories and connectivity at high resolution and statistical confidence. Genetic connectivity of mobile and sessile species will be analysed and related to their recovery potential in the disturbed area and on restoration substrates (CCT2). Population genomics can allow the detection of Single Nucleotide Polymorphisms (SNP) under selection, which can consequently be used to unravel species-specific adaptations to deep-sea environments and obtain new data on their resilience.

### (3) Effects of sediment disturbance on microbial and micro-eukaryote communities

Molecular approaches will be applied to sediment samples collected with ROV push-cores prior to and after the collector test to characterise the microbial and micro-eukaryote communities within undisturbed, directly mined and plume-exposed seafloor areas.

Microbial community composition and diversity (via 16S rRNA gene Tag sequencing), functional diversity (via metagenomes), and dominant active microbial taxa (via 16S rRNA/cDNA Tag sequencing and metatranscriptomes) will be identified. Analyses will address microbial biodiversity at taxonomic levels ranging from phyla to individual 'species' (i.e. operational taxonomic units), as well as links of key-ecosystem functions to specific groups. Investigations of sediments from undisturbed sites will assess regional variability of microbial biodiversity and spatial connectivity, while samples obtained after the test will focus on mining-related effects on communities and functions. Manganese nodule material will be analysed in order to investigate the contribution of communities of the outer nodule layer to the overall taxonomic diversity found in the area.

Following the same sampling strategy used for microbial assemblages, changes in benthic micro-eukaryote biodiversity (i.e. protists and fungi) will be investigated through a metagenomic approach applied on extracellular DNA. The extracellular DNA will be selectively extracted from the sediments using a combination of physical and chemical procedures (Corinaldesi et al., 2005; Danovaro, 2010), which allow excluding the contamination by the DNA of any biological component, including viruses. Once extracted the extracellular DNA will be amplified by using primer sets targeting 18S rRNA genes and ITS (internal transcribed spacer) of eukaryotes and the amplicons analysed by high-throughput sequencing platforms (e.g. Illumina MiSeq).

### (4) Development of molecular methods and protocols for rapid biodiversity assessments and environmental monitoring

Methodological improvements have provided evidence that the large majority of DNA pools in benthic ecosystems is not associated directly with living biomass, but rather to extracellular DNA (eDNA) (Dell'Anno and Danovaro, 2005) containing amplifiable prokaryotic and eukaryotic gene sequences suitable for assessing biodiversity at different spatial and temporal scales (Corinaldesi et al., 2008, 2011). Other molecular methods increasingly used in biodiversity assessments are the metabarcoding and the Maldi-TOF proteome approach (Bik et al., 2012; Laakmann et al., 2013). These three molecular methods will be tested and compared to determine their suitability and/or complementarity as tools for rapid assessments of biodiversity and monitoring of the impact of mining activities on deep-sea microbial and faunal assemblages.

The reference databases built up during MiningImpact 1 enable a wide application of metabarcoding and eDNA techniques, revolutionising our ability to undertake biodiversity and connectivity analyses. The new droplet digital PCR (ddPCR) technology (Doi et al., 2015) will be used to develop molecular identification assays for a set of REM taxa, and evaluate their presence and abundance across the CCZ. A set of ddPCR assays will be developed to target REM (Rare, nodule-Endemic and Megafauna) indicator species based on the existent reference dataset (Glover et al., 2016b; Dahlgren et al., 2016; Wiklund et al., in press). eDNA samples of mud and bottom water will be collected at different stations and extracted on-board (Lekang et al., 2015). Initial assay feasibility tests will be carried out on CCZ samples that are readily available and optimal standardised method protocols for use of eDNA and ddPCR in environmental monitoring will be developed.

Sediments will be sampled and fixed for molecular studies prior and after disturbance in the areas influenced by plume deposition as well as non-impacted reference areas, and three different molecular methods for rapid biodiversity assessment will be applied. Ground truthing will be performed by comparing with results generated in WP2. Changes in the pristine abyssal eDNA signature will be investigated following the nodule collector test and subsequent recovery through time. For the metabarcoding approach, organisms will be extracted from the sediment first and the DNA will be extracted from the whole community without further sorting. Different gene fragments (COI-mini, 18s V1-V2, V4 and V9 regions) will be amplified and sequenced in parallel using Illumina NGS technology and compared to a genetic library for the assignment of taxonomic entities. The suitability of the different gene regions to capture abyssal meiofauna diversity and structure will be examined. For the proteome approach, the whole proteome from single specimens will be measured using Maldi-ToF (matrix-assisted laser-desorption/ionization time-of-flight) mass spectrometry that generates a species-specific fingerprint of the proteins' mass. The aim of this study is to test the efficiency and sensitivity of the three different molecular approaches to detect and monitor changes produced by mining impacts and recovery through time of the standing stocks and community structure in micro, meio and macrofaunal communities.

#### 8.2.1.2 Fate and toxicity of the sediment plume (WP2)

WP2 focuses on assessing the fate and impact of the sediment plume generated by the nodule collector test. The work will involve monitoring of the dispersal of suspended sediment and sediment redeposition in space and time, assessment of the evolution of physical (e.g., particle concentration, size, and aggregation) and chemical (e.g., trace metals) characteristics of the plume as it is drifting away from the site of its origin, and assessment of the impact of the sediment plume on seafloor sediment and biota.

Field observations and experimental work will generally follow the EMP-based strategy developed in CCT1 (see CHAPTER 8.2.1.4 and CHAPTER 8.2.2). Baseline investigations of bottom water, surface sediments, nodules, and biota will be collected before the test occurs from sites where the major plume impact is expected to occur (PIRZ), as well as from unimpacted reference sites. A 3D array of optical and acoustic turbidity sensors and particle cameras on static and mobile platforms will be deployed along the anticipated main direction of plume dispersal prior to the onset of the nodule collector test to monitor the dispersal of the sediment plume in space and time. Plume modelling efforts will be supported by *in situ* observation and *ex situ* experiments addressing turbulence-induced particle aggregation in the bottom boundary layer as well as scavenging of particles by seasonal phytodetritus falls. Plume monitoring data and experimental results will be used for calibration and validation of near-field and far-field sediment transport models which are an important tool for predicting the areal extent of sediment dispersal resulting from industrial mining operations.

Results from *in situ* and *ex situ* geochemical and biological experiments will be integrated with diagenetic and food web modelling carried out in WP3 to improve predictions of mining impacts on the deep-sea ecosystem. Potential mobilization of trace metals in sediment plumes and redeposited sediments will be addressed by geochemical analysis of bottom water and surface sediment samples, shipboard and laboratory experiments, and numerical modelling of trace metal reactions. The different impacts that mining plumes may have on deep-sea biota will also be investigated, such as translocation of benthic microbial communities and small meiobenthos from the mined area where the plume is generated to the area of redeposition of plume material, physical damage inflicted by suspended sediment particles on meroplankton and zooplankton living in the near-bottom water, impaired feeding and respiration in filter-feeding and suspension-feeding megabenthos like corals and sponges due to sediment clogging, and ecotoxicological effects due to metal-containing particles and dissolved metal. Much of this work will be

conducted for the first time, not only for this part of the Pacific Ocean but for this water depth in general and will be complemented by *in situ* and *ex situ* sediment exposure studies.

The environmental hazard by the plume will be evaluated by means of the quantitative weight of evidence (WOE) model, in which impact on biota and ecosystem functioning is assessed with information from the chemistry (in the different environmental matrices) and from the ecotoxicological impact. Knowledge obtained on the suitability of instruments and methods for monitoring and evaluating mining impact will feed into the development of policy recommendations.

The work of WP2 is organised in three interconnected tasks:

(1) Plume dispersal and sediment deposition

This task addresses the dispersal of suspended material in the sediment plume in space and time and the spatial extent and amount of sediment redeposition from the plume. Following the experimental design of the EMP, a 3D sensor array of moorings and landers will be geared up and deployed across the area designated for the nodule collector field test. Apart from standard oceanographic sensors, the array will include a large number of acoustic and optical turbidity sensors with different sensitivity and measuring range, as well as particle cameras, to monitor the lateral and vertical dispersal of the plume and evolution of its physical characteristics as it drifts away from its site of origin. A focus will be on the determination of long-term (seasonal) variability of currents and rates of sediment deposition, and to that end current profilers and sediment trap moorings will already be deployed in April 2018. During the collector test, the traps will be redeployed close to the seafloor at a proximal and a more distal position downstream of the mining test site, in concert with traps deployed on landers in order to record particle fluxes settling from the plume within certain proximities to the test site. Another focus is on particle aggregation in the bottom boundary layer, assessed *in situ* by particle cameras, in relation to suspended particulate matter concentration determined by different types of turbidity sensors and turbulence determined from high-frequency ADV current measurements.

In addition to the static sensor array, AUV and ROV will be deployed for dynamic monitoring of the plume. Next to optical turbidity sensors, multibeam WCI technology and ADCP-backscatter on the ROV will be used to track the sediment plume in real-time allowing for an adaptive monitoring (real time data access via the ROV). Likewise, the AUV will be used to record turbidity along predefined vertical and lateral transects through the plume, using standard optical turbidity sensors as well as haze analysis of photos taken with HD camera along the transects. Data processing will be conducted directly on board to adapt the monitoring scheme if necessary and to support targeted sampling for sedimentological, geochemical and biological studies. To assess net deposition of sediment from the plume (blanketing), automated image analysis of photomosaics collected by AUV prior, during and after the disturbance experiment will be carried out, as well as advanced AUV-based multibeam backscatter analysis to quantify extent and thickness of sediment blanketing. Resettled sediment thickness will also be constrained by placing checker boards with ruler sticks in the anticipated impact area to be photographed by ROV and AUV. These image-based analyses will be compared with results from sediment physical and radionuclide analyses of sediment cores.

Fluorescent tracer material will be added to the sediment plume generated by the nodule collector by means of a diffusor. These environmentally-friendly tracers are anticipated to disperse with the sediment plume and care will be taken to fabricate tracer particles that closely mimic the plume particle properties with respect to sinking velocity and hydrodynamics. Experiments in this regard will be conducted prior to the collector test. The tracer itself can be detected up to several years after deployment and thus also

allows tracing of secondary suspension and redeposition. A rapid evaluation can already be carried out on-board using fluorescence microscopy.

Modifying numerical models developed for shallow-water dredging plumes, and using turbidity sensor data from the direct vicinity of the collector test area for validation and calibration, model simulations of the initial stages of the plume in the near-field of the nodule collector will be performed. Results from the comprehensive plume monitoring program and from experiments addressing sediment particle properties and ensuing evolution of sediment concentration and sediment deposition will enable project partners to calibrate and test the new flocculation module integrated in the numerical regional ocean circulation-sediment transport model which was developed during the MiningImpact1 phase. The complete set of *in situ* / *ex situ* experiments will allow an adaptation of the flocculation model of Winterwerp (1998) to the deep-sea environment and provide a suitable flocculation parameterisation applicable to other deep-ocean environments.

## (2) Evolution of physical and chemical characteristics of the plume

This task will address the physical and chemical characteristics of the plume as well as the temporal and spatial evolution thereof.

Laboratory experiments, if possible on-board, focusing on aggregation and hydrodynamic behaviour of particles in the plume will be carried out. Experiments will be conducted under *in situ* temperature and salinity conditions with sediments from the test site, using shear tanks, roller tanks and benthic resuspension chambers. Using different particle concentrations and turbulence regimes, optimal conditions for aggregate formation and thereby enhanced redeposition of plume particles will be determined. This may provide guidance for engineering solutions and operational practices that help to reduce plumes formed in the wake of mining operations. In addition, the effect of seasonal phytodetritus falls on the removal and redeposition of fine-grained suspended sediment from the plume will be determined using isolated microalgae from the test area cultivated on-board, and with particle concentrations of 175-2000 mg L<sup>-1</sup> (as also used for discharge models of drill cuttings in the oil & gas industry by Norwegian authorities).

Potential mobilisation of trace metals in the plume and their bioavailability will be addressed. Plume samples (particles and surrounding water) will be collected using CTD/Niskin bottles and ROV in spatial and temporal gradients during and after the collector test. The samples will be analysed for major and trace element composition as well as natural radionuclide concentrations. Laboratory experiments will be set up to study the sorption-desorption and dissolution-precipitation equilibria between plume particles and bottom water under defined conditions, e.g. under variable redox conditions, particle density, type and size of suspended particles. Of particular interest is the role of microbial interactions with plume particles on trace metal reactions, e.g. the role of heavy-metal resistant bacteria, the role of particle aggregation in the plume on the trace metal distributions, and the distribution of trace metals between different physical and chemical species and the role of colloids in transporting trace metals in the water column. A numerical model of trace metal reaction kinetics will be developed, using published data on reaction kinetics and integrating empirical results from the particle aggregation experiments described above. On the basis of the model, potentially toxic metal fluxes induced by mining activities may be predicted.



### (3) Ecological impact of the plume

This task assesses the impact of the sediment plume and sediment deposition on biota, and integrates all impact data into a weight-of-evidence (WOE) model to classify environmental hazard.

Toxicity bioassays will focus on different endpoints (e.g. survival, reproduction, larval development) with different organisms (Bebianno et al., 2015; Simpson et al., 2016) such as *V. fischeri* bacteria, amphipods and/or bivalves. Results will be compared with those previously obtained from sediments and nodules from PA1, thus providing an overview of natural toxicity levels of the region. Collected specimens of representative faunal groups will be analysed for metal contents and for baseline biomarker levels indicative of oxidative stress, metal exposure, biotransformation, oxidative damage, and neurotoxicity (Mestre et al., 2017). In addition, the bioconcentration factor of legacy contaminants (PCBs, PBDEs, organochlorine pesticides; extendable to PAHs and non-targeted screening) in the sediment plume and in amphipods (Lysianassidae), using techniques outlined in Jamieson et al. (2017), will be analysed. Metal contents, changes in molecular signaling pathways, epigenetic regulation and gene expression will be evaluated before as well as during plume generation.

Collected Anthozoans from areas exposed to the plume will be analysed to assess the response of the coral host to sedimentation. Anatomy and changes in the gonadal tissue within the mesoglea will be investigated by optical and electron microscopy (Waller and Baco, 2007; Hall-Spencer et al., 2007). In addition, the microbiome response to increased sedimentation will be assessed, using high-throughput 16S rRNA gene next-generation sequencing and transcriptomics (Hall-Spencer et al., 2007; Lawler et al., 2016) in order to describe (a) taxonomically or functionally conserved bacterial associates of the selected species, and (b) shifts in anthozoan microbiome composition and function in response to increased sediment load. Collected corals will also be subjected to condition index analyses, energy budget analysis (proteins, lipids, carbohydrates), and biomass measurements. *Ex situ* controlled aquarium experiments will be carried out to test the impact of different concentrations of CCZ sediments with and without POC using cold-water corals from the Azores region. Eco-physiological responses in aquaria will be compared with *in situ* octocoral responses to better understand the interaction between sediments and POC and determine sediment concentration thresholds on the physiology of these organisms.

A WHOI SyPRID plankton sampler (Billings et al., 2017) adapted to the ROV will be deployed to collect meroplankton (e.g. larvae) and zooplankton (e.g. copepods) inside and outside of the plume. SyPRID is a novel sampling equipment that allows obtaining paired, large-volume plankton samples of well-preserved specimens at specified depths. Optical and electron microscopic analyses will allow assessment of physical damage of body parts, entanglement of particles on swimming structures, inclusion of particles in stomach contents, damage of feeding structures (mouth parts) and organs. These results in combination with those obtained in WP1 will represent the first data on larvae of CCZ communities. Provided enough material is collected, the metal accumulation and biomarker levels will also be assessed. The SyPRID samples will also be used to assess the presence of resuspended benthic meiofauna in the plume. Changes in microbial community composition, functions and metabolic activities that occur when sediments are translocated within the plume will also be studied. The primary interest of these investigations is to follow the fate of resuspended organisms and the functions that they provide from source to sink, but data may also allow addressing effects of the resuspended matter and contaminants on the native microbial communities in bottom waters.

Short-term effects of exposure to sediment plumes will be investigated in deposit-feeding megafauna (e.g., holothurians), using benthic corrals (Brown et al., 2017) that will be deployed *in situ* over targeted specimens by ROV. Filter/deposit-feeder organisms and other components of the benthic community (prokaryotes, meio- and macrofauna) will be sampled close to the corral deployment locations before

disturbance and within corals after disturbance for analysis of bioaccumulation, biomarkers and guided *de novo* transcriptomes. In another *in situ* experiment, physiological responses of filter feeders exposed to sediment plumes will be investigated within CUBE benthic incubation chambers (slightly modified from Stratmann et al., in prep). The CUBEs will be placed by ROV over specimens of common filter-feeding species before and after the test, followed by respiration measurements and water sampled at pre-set time steps to detect changes in nutrient fluxes – from which changes in uptake or excretion by the organism can be assessed.

The environmental hazard at each sample location, including sites exposed to the plume, will be analysed using a quantitative weight-of-evidence (WOE) model (e.g. Bebianno et al., 2015; Mestre et al., 2017) that integrates data from different levels-of-evidence (LOE), such as sediment/plume chemistry, bioaccumulation/bioavailability, sub-lethal effects/biomarkers, bio-assay results. The WOE model will be applied to different sampling times, i.e. before impact, shortly after impact, and if additional ship-time can be made available, also 1-2 years after the impact, in order to provide insight into the temporal evolution of plume impact hazards.

### 8.2.1.3 Biogeochemistry and ecosystem functioning (WP3)

WP3 aims at assessing mining impacts on seafloor ecosystems with a focus on sediment physical characteristics (e.g., shear strength, porosity, diffusivity) and their respective effects on sediment biogeochemical characteristics, processes and fluxes (e.g., oxygen, nutrients, organic matter, metals) as well as ecosystem functions (e.g., organic matter remineralisation, food webs). Natural heterogeneity as well as effects of direct (e.g., compaction, sediment and nodule removal) and indirect disturbance (sediment blanketing) will be addressed.

Baseline investigations, particularly to fill the gaps in the existing data of the test area, will be carried out prior to the test. Effects of the impacts created by the collector will be studied directly after the disturbance to assess severity and spatial extent of immediate effects and to establish a starting point for investigations of longer-term changes (secondary effects and recovery) during anticipated post-impact expeditions. *Ex situ* analyses, shipboard incubations and land-based experiments using sediment samples obtained from ROV pushcores and deployments of the video-guided multicorer, gravity corer and boxcorer will be combined with *in situ* measurements and dedicated experiments performed directly at the seafloor.

Studies on the natural heterogeneity and on the effects of different impact types and intensities on biogeochemical processes and overall benthic ecosystem functions will be captured and harmonised with investigations carried out in WP1 and 2. In order to conduct comprehensive numerical simulations of the effects of the physical impact on biogeochemical functions / process rates and food webs, including prognostic modelling of their expected recovery, a comprehensive suite of biogeochemical variables is required, e.g., *in situ* studies of sediment geomechanical properties and benthic fluxes, radionuclide and stable isotope studies, food web experiments directly at the seafloor, and investigations of microbial and viral productivity and functions. As investigations will address freshly created impacts by a heavy collector system that probably involves significant sediment compaction and pore water expulsion, investigation will allow addressing effects that occur on shorter temporal scales and better represent realistic scenarios compared to studies in decade-old disturbances created with relatively small and lightweight gear. Furthermore, the collector test will, for the first time, allow for representative investigations of secondary disturbance effects (i.e., sediment blanketing by resettling plume material) while precluding apparent recovery of biogeochemical conditions by lateral processes (e.g., diffusion and recolonisation) from areas in the direct vicinity of the disturbance tracks.

Knowledge obtained on the applicability of state-of-the-art instruments and methods and the relevance of the obtained data for assessing mining effects on seafloor ecosystems will feed into a set of recommendations for monitoring and assessment (CCT3).

The work of WP3 is organised into five interconnected tasks:

(1) Compaction effects on sediment physical properties and pore water expulsion

This task assesses the physical impact associated with the collector test and its effect on key sediment properties such as shear strength, compaction/porosity and diffusivity.

To investigate the mechanical response of the sediment to a collector vehicle with caterpillar propulsion in terms of compaction and pore water expulsion, geomechanical properties of the surface sediments will be determined before and after the collector test using a 'GraviProbe', an innovative geotechnical device provided by DEME-GSR for *in situ* analyses of the top 4 m of sediment. Using a combination of accelerometer with pressure sensor, natural variability and changes in static bearing strength of the sediments will be determined and compared to shear strength measurements performed in GEOMAR's high-pressure experiment lab (Deusner et al., 2016). Furthermore, effects on porosity and the effect of the reduced pore space on diffusion and sorption/desorption properties will be determined. Investigations will focus on trace metal behaviour and will include measurements of porosity and trace metal distribution in multicores and push cores as well as experiments on trace metal diffusion in sediment slides of different porosity. Natural radium, thorium and actinium radioisotopes will be measured in samples obtained with bottom water samplers and *in situ* pumps to quantify the loss of pore water from the sediments during the collector test.

(2) Assessment of sedimentation and bioturbation dynamics

This task addresses sedimentation rates and bioturbation characteristics (depth, rate) as key factors of natural sediment deposition and reworking and key input parameters for diagenetic modelling (Task 3). Natural variabilities as well as impact effects will be addressed to quantify changes and to serve as a starting point for subsequent assessments of recovery.

Vertical distributions of natural and anthropogenic radionuclides in sediments will be analysed using multicores and push cores to assess rates of sediment accumulation and bioturbation as well as the depth of the bioturbated layer. In cores directly from the test site, this will further allow to quantify the layers of sediment lost by disturbance or deposited from settling plumes. Studies focusing on different radionuclides in sediment solids and pore waters with different chemical properties and half-lives ( $^{226}\text{Ra}$ ,  $^{210}\text{Pb}$ ,  $^{137}\text{Cs}$ , ratios of  $^{230}\text{Th}/^{231}\text{Pa}$ ,  $^{234}\text{U}/^{238}\text{U}$ ) will be combined to address processes associated with different sediment compounds and different time scales. The studies will be complemented by high resolution 3D X-ray imaging (Computed Tomography, CT) of intact cores sampled nearby. This will allow to visualise and quantify structures indicative of disturbance effects (exposed dense subsurface sediments, blanketing with unconsolidated plume sediments, cracks, buried nodule debris) and biogenic activity (macrofaunal burrows). CT analyses will be compared to geochemical and radionuclide data of and validated with radionuclide analyses performed on samples from specific structures in selected cores.

### (3) Effects on sediment biogeochemistry (redox zonation, diagenetic fluxes, biogeochemical processes)

This task quantifies the degree of change in sediment biogeochemical characteristics and diagenetic processes and fluxes and their footprints in comparison to natural variability observed at undisturbed sites. Investigations will be based on a comprehensive dataset of biogeochemical process variables comprised of dissolved pore water and solid phase constituents and key isotopic signatures measured in sediment core samples collected by means of multicores, push cores, and gravity cores and will be complemented by *in situ* respiration measurements.

Extensive geochemical analyses of pore waters and solids including nutrients, the carbonate system, dissolved metals, major cations, sulphate and total sulphur, and isotopic ratios (e.g., of C, H, O, Sr and Li) will be carried out. One focus will be on the effects of sediment and nodule removal on pore water distributions of oxygen and nutrients, and on different Fe and Mn mineral phases. Fe and Mn reactivity will be addressed by sequential extraction and analyses of stable Fe isotopes. Analyses of the effects of sediment compaction on the redox zonation and the distribution of elements, with special emphasis on trace metals, and their dynamic biogeochemical reactions will be investigated. This also includes investigation of N-isotopes and organic compounds (DOC, amino acids) indicative of organic matter degradation processes. Spectrophotometric/fluorometric methods will be applied to quantify organic compounds (e.g., phytopigments, proteins, carbohydrates, lipids, extracellular DNA concentrations), assess their bioavailability and contribution to phosphorous cycling as well as respective changes in response to the collector impact. HPLC-based characterisation of phytopigments and fluorometric quantification of Chl  $\alpha$  and phaeopigments will also be carried out in selected cores. Data on sediment biogeochemistry changes will inform experiments and feed into biogeochemical model simulations.

Sample-based investigations will be complemented by *in situ* quantifications of diffusive and total benthic solute fluxes (primarily oxygen) to assess respiration rates as a proxy for microbial activity and organic matter remineralisation, using automated micro-profilers and benthic chambers deployed with autonomous lander platforms or as self-contained modules manipulated by ROV.

State-of-the-art numerical diagenetic modelling will help to quantify processes and fluxes in order to identify key effects on biogeochemical ecosystem function and to predict the time scales required for the environment to return into a steady state. Subsequently, the geochemical data collected at discrete sites and corresponding model-derived rates and fluxes will be correlated with spatial information obtained from habitat and plume mapping procedures to estimate the overall impact induced by the collector test.

### (4) Effects on microbial ecology and functions

This task assesses ecosystem functions of microbial communities as key components of benthic ecosystems in terms of biomass and their contribution to biogeochemical processes. Using a combination of molecular and microscopic methods with shipboard tracer incubations, key functions of microbial communities and viruses can be identified and quantified, and compared to the data obtained on biogeochemical processes (Task 3 above).

Microbial activity and biomass production will be determined using  $^3\text{H}$ -labelled leucine and  $^{14}\text{C}$  bicarbonate in both undisturbed and impacted sediments. Additional measurements in ground nodule material will address the activity of nodule-specific microbial communities. Microbial activities will further be quantified (in terms of radiotracer incorporation and extracellular enzymatic activity) in samples taken from the sediment plume to investigate the effects on functions of microorganisms relocated from pristine surface sediments as well as of natural bathypelagic microbial communities. Rate measurements in

sediments will be accompanied by microscopic quantifications of microbial abundance and biomass. In addition, molecular techniques for the quantification of microorganisms will be combined with measurements of radiotracer uptake into microbial cells to assess the contribution of specific functional groups to overall microbial biomass production. Furthermore, shipboard incubations with fluorescent analogues of organic substrates will be carried out to determine potential activities of the main extracellular enzymes as a proxy for the degradation potential of organic matter by prokaryotes. Effects on virus productivity and virus-induced prokaryotic mortality (using epifluorescence and transmission electron microscopy) will also be assessed.

#### (5) Effects on ecosystem functioning

This task assesses the scale of the impact on benthic ecosystem functioning at the abyssal seafloor through *in situ* experiments and food web modelling with a focus on effects of the settling and re-suspension of plume material on organic matter processing. Experimental work will be carried out directly at the seafloor using open 'corrals' and sealed benthic enclosures ('CUBES') that are deployed by ROV. All experiments follow the pulse-chase approach, during which labelled particulate organic material ( $^{13}\text{C}$  and  $^{15}\text{N}$  algae 'POM') or dissolved organic material ( $^{13}\text{C}$  labelled and  $^{15}\text{N}$  'DOM') is added to the enclosures. In this way, the transfer of matter and energy in benthic food webs can be assessed in taxa of all size classes with special emphasis on surface deposit and filter-feeding megafauna that are expected to be particularly affected by sediment blanketing and suspended matter loads. The analysis of the samples also involves ecotoxicological / transcriptome studies. Natural C and N stable isotope signatures of all the benthic assemblages will be quantified by means of isotope ratio mass spectrometry in undisturbed samples taken close to the impact site. In addition, the freshness of sedimentary organic matter will be determined at the experimental sites.

Corrals will be deployed before the collector test along the predicted gradient of settling plume material to investigate immediate effects of mining-induced sedimentation on organic matter utilisation in benthic food webs, with a focus on holothurians as key deposit-feeding megafaunal organisms. The uptake of  $^{13}\text{C}$  and  $^{15}\text{N}$ -labelled POM added to the corrals will be quantified in holothurians and all other benthic organisms collected from the corrals. After the collector test, CUBEs will be deployed over sessile encrusting or stalked sponges and in control areas without sponges that have been exposed to different amounts of resettled plume material.  $^{13}\text{C}$  and  $^{15}\text{N}$ -labelled DOM will be added to address the effects on the uptake of DOM and the metabolic activity of sponges and other members of the benthic community. In addition to quantifications of uptake of labelled DOM by the microbial, meio-, macro- and megafaunal assemblages, total oxygen uptake will be determined by continuous oxygen monitoring in the overlaying water and discrete samples for the determination of nutrient fluxes will be taken throughout the deployment. Additional deployments of CUBEs over sponges and sponge-free control areas that were subjected to thick plume sediment blanketing will be used to assess the effect of resuspended plume material on the physiology of sponges. Clouds of suspended sediment will be artificially created in the CUBEs by means of intense stirring or sediment injection. Changes in oxygen and nutrient fluxes will be determined throughout the incubation. Remineralisation of added labelled DOM and the alteration of its composition will be determined by  $^{13}\text{C}$ -DIC measurements and fluorometric FDOM-scanning in water samples. Additionally, the uptake of labelled DOM will be quantified in sponges and all other benthic organisms collected from the CUBEs.

Results from the experiments described above will be combined with benthic biomass estimates (input from WP1) and assessments of organic matter freshness and biogeochemical process rates (Task 3) in order to carry out model-based food web analyses. Linear inverse food web models that proved

successful to assess disturbance effects in the DISCOL disturbance area during the first project phase (Stratmann et al., in prep) will be utilised with a focus on the effects of difference in nodule coverage and organic matter availability.

#### 8.2.1.4 Plume monitoring and habitat/disturbance characterisation (CCT1)

Operational monitoring of deep-sea mining activities and of environmental impacts requires an integrated approach. The overall aim is to avoid (or at least minimise) damages to the abyssal ecosystem, particularly sensitive or rare fauna, outside the mined area. Real-time sensor-based monitoring which can be tied closely to monitoring operations is mainly performed with landers, ROVs, and increasingly with AUVs. MiningImpact 2 will apply these technologies as part of its environmental monitoring program around the pre-prototype nodule collector test to provide more realistic information on the environmental footprints and consequences. This is a critical step forward, because upscaling of the “small-scaled” experiments as they have been undertaken in the past, such as the Benthic Impact Experiment II (Brockett and Richards, 1994; Tsurusaki, 1997), the Japan Deep-Sea Impact Experiment (Barnett and Suzuki, 1997), and the IOM-BIE (Kotlinski and Stoyanova, 1998; Radziejewska, 2002), is very difficult if not impossible.

The methodologies used so far in impact studies are often based on traditional sampling strategies, where data are collected with various sampling platforms (moorings, landers) and sensors giving substantial temporal and spatial gaps. Little emphasis has been given on integration of information between time periods of investigation, thus limiting the possibility to separate the impacts from overall natural variation in an area. Thus, a primary goal of CCT1 is to provide a guidance document on how monitoring of the seabed around mining operations should be performed. However, lack of standardisation of monitoring techniques in accordance with present knowledge and latest advances in technologies precludes comparison of the situation before mining, during mining, and post mining, creating comparable challenges as pertains to deep-water drilling (Purser and Thomsen, 2012). This further demonstrates the need for systematic and scientifically acceptable approaches, the utilisation of adequate sampling and observation technologies and the design of monitoring strategies. In addition to using cost-efficient technologies for real-time monitoring of plume dispersion and sediment resettling, the main bathymetric and oceanographic features of the (test)mining site have to be implemented in a predictive dispersion model that is based on local current information of high temporal resolution (minimum of 12 data points per day) over a prolonged time period (~1 year) from the vicinity of mining operations (see also CHAPTER 6.4.2). These dispersion models enable evaluating the likely transport pathways of sediments, thereby allowing for a much better positioning of monitoring gear. Particle aggregation processes, not taken into account in previous modelling exercises of mining-induced plumes, should be implemented in updated regional and near-field ocean circulation and sediment transport models (see also CHAPTER 4.2.4.2). This will be supported by *in situ* observation and *ex situ* experiments addressing turbulence-induced particle aggregation in the bottom boundary layer as well as scavenging of particles by seasonal phytodetritus falls (Thomsen and McCave, 2000; Pabortsava et al., 2011).

The project will investigate the dispersal of the test-related mining plume in great detail, complemented by *in situ* and *ex situ* sediment exposure studies. All field data from both *in situ* sensors and *ex situ* experiments will be transferred onshore to the physical oceanography partners to be fed into a near-field plume model which will be used for both ground-truthing of model results and to predict the plume dispersal under varying hydrodynamic conditions, which is a requirement for adaptive monitoring. Details of the monitoring programme that has been developed by CCT1 and will be further developed before the collector vehicle test takes place in April 2019 as more information becomes available (e.g., through the



collection of further baseline environmental data during the BGR exploration cruise to the test area in April/May 2018 and the first leg of the SONNE cruise in March 2019) are provided in CHAPTER 8.2.2 below.

#### **8.2.1.5 Disturbance effects in time and space (CCT2)**

Polymetallic nodule mining will increase the pressure on abyssal ecosystems, which may lead to the loss of genetic and species diversity, the fragmentation of natural habitats and the degradation of ecosystem functions (Jones et al., 2017; Gollner et al., 2017). For the development of (i) a clear and effective policy to minimise impacts of future mining (e.g. by the ISA), and (ii) a sound environmental management plan for regions of interest in the Area, more insight is needed on causal activity-pressure-effect relations of the targeted ecosystem and its components (i.e. species populations and communities, habitats and ecosystem functions), and the cumulative pressures that mining activities will exert on ecosystems or their components (Tamis et al., 2017). In particular in the CCZ, more data are needed to quantify the impact of mining activities and to identify specific pressures and their cumulative effects on the vulnerability and recovery potential of the ecosystem (see FIGURE 7.4).

The proposed monitoring of the nodule collector test will allow identification of the cumulative impact of different pressures resulting from mining activities on various ecosystem characteristics and identifying the sensitivity of different ecosystem components. A range of variables to identify the intensity of the impact will be assessed (pre- and post-disturbance) and correlated to different variables for ecosystem structure and function. For these purposes, a detailed analysis and integration of spatial and temporal variability in (bio)geochemistry, element fluxes, bioturbation, and sediment and pore water characteristics will be carried out, and the intensity of the observed changes after disturbance will be related to specific (combinations of) pressures compared to the observed variability in baseline environmental conditions. Similarly, a detailed analysis and integration of spatial and temporal variability in benthic communities (microorganisms, meio-, macro-, and megafauna) with respect to biodiversity, abundances and biomass will be carried out, and the intensity of the observed changes after disturbance will be related to specific (combinations of) pressures compared to the observed variability in baseline benthic faunal conditions. Last but not least, the spatial and temporal variability in benthic ecosystem functions (e.g., organic matter processing, microbial growth, food web) will be analysed in the same way. The integration of results obtained from the different work packages (WP1, 2 and 3) and CCT1 will be organised in different steps starting from a qualitative and semi-quantitative presentation and scoring of pressures and responses of all ecosystem components. This initial step is a first broad scale, low-detailed assessment based on the available information and/or expert judgement and classification schemes (Tamis et al., 2017). The criteria for such assessment form an important part of this process and will be adapted from existing procedures from other marine ecosystems (Halpern et al., 2007; Knight et al., 2015). In a second step, a quantitative assessment of intensities of pressures and responses of ecosystem components will be undertaken. This step is required for a focused, high-detailed assessment based on functional relationships. This approach will generate measures of sensitivity based on both empirical data (evidence-based) and expert judgement (Stelzenmüller et al., 2015).

An environmental management plan for the CCZ requires that pressures caused by mining activities on the marine ecosystem are kept within acceptable minimum levels. To identify these pressure levels a multitude of environmental assessment (EA) approaches are possible, but given the size of the area and the different stakeholders (concession holders), there is a need for a harmonised and integrated EA approach: one that considers cumulative impacts and at the same time is sufficiently evidence-based. Given the interactions of multiple stressors and pressures, an integrated assessment is required by combining multiple Lines of Evidence (LOE) that reflect different biological, chemical and physical data (Bebianno et al., 2015; Caeiro et al., 2017; Mestre et al., 2017). The integration of LOE through Weight of

Evidence (WOE) approaches is one of the tools developed for informed decision-making (Weed, 2005). Overall, a WOE approach is the process of considering strengths and weaknesses of different types of information or evidence in order to make a decision among competing alternatives.

It is important to carry out an assessment of the scale of analysis (sampling units, surface covered, distance of transects, etc.) and replication necessary to reveal ecologically significant patterns. Perceptions of deep-sea diversity and community composition are observed to change with the scale analysed. At the temporal scale, ecotoxicological parameters can also identify sub-lethal effects in deep-sea fauna from hours of exposure to months or years (e.g. Mestre et al., 2017). Hence, a multiple-scale analysis is proposed in which the importance of the observation scale (both spatial and temporal) is put forward. The possibility of making predictions and extrapolations based on small observation windows for similar ecosystems and distances from the impact will be put to the test.

Identification of thresholds and indicators is important for effective environmental management and monitoring of deep-water mining projects. Both ensure that consistent and representative environmental measurements are being obtained in monitoring programmes. There is little consensus on the appropriate indicators for deep-sea mining. Thus, the outcomes of experimental assessment here will be used to identify suitable indicators and to assess how they change in response to the impact.

#### Recolonization experiments

Potential mitigation mechanisms will be investigated by initiating restoration experiments (McKenney and Kiesecker, 2010) in which the feasibility of different substrates for recovery of nodule-specific biota will be tested. Artificial settlement substrates will be deployed after the impact at the site directly disturbed during the collector test (IRZ), in the area of indirect impact (PIRZ), and in a no-impact area with and without nodules. Per location and time different substrates will be deployed. A video-guided 'nodule dropper' will be used to deploy individual colonization structures/artificial nodules remotely-triggered directly at the seafloor for later visual inspection and sampling by ROV. In addition INDEEP frames (<http://www.indeep-project.org>) may be deployed to compare the biota that settles in the CCZ with those from different locations around the world. Recovery is planned after one to two years. To account for the expected slow growth of sessile fauna, substrates will also be deployed that may be recovered after several more years. To study the function of ecosystem engineers in nodule fields, artificial stalked sponges will be mounted on concrete blocks to simulate natural sponges which are known to host a diverse community of fauna. To our knowledge, this approach is unique in its field and will provide substantial information on the usefulness of substrates as mitigation action, as well as on the function of hard substrates for biodiversity in nodule fields. Faunal data from settlement substrates will be compared to the biodiversity data from the impact assessment (pre-impact vs. post-impact) to unravel the role of potential diversity enrichment of substrates after the test-mining event. Genetic connectivity studies (WP 1) will be used to unravel the role of connectivity on recovery processes.

Biofilms from the recovered substrates will be sampled for 16S rRNA gene tag sequencing to assess the microbial communities colonizing the surfaces and to analyse how they differ depending on the nature of the substrate. Furthermore, the relationship between substrate type, faunal/microbial recolonization and the geochemistry of the surrounding and underlying (disturbed) surface sediment will be determined. In particular, the influence of the different substrates on regeneration of the impacted surface sediments with respect to redox zonation and biogeochemical processes will be investigated.

## 8.2.2 MONITORING PROGRAMME

### (1) Planning of the EMP layout around the collector test (outlined in CCT1)

Based on the information from numerical oceanographic and sediment plume modelling exercises as outlined in CHAPTER 6.4.2, the layout of the sampling and monitoring array in and around the collector vehicle test area can be planned in advance. However, it will be susceptible to adaptation and change (e.g., due to integration of further baseline environmental data that will be collected during the BGR exploration cruise to the test area in April/May 2018 and the first leg of the SONNE cruise in March 2019; through improvement and adaptation of the numerical plume models as time until the start of the project progresses). In general the array will consist of 2 stationary landers (DOS and BoBo: equipped with CTDs, cameras, ADCPs, sediment traps) and short moorings with ADCP and CTDs as well as bottom stations consisting of e.g. sediment traps, upward-looking ADCPs, CTDs with optical sensors, particle cameras and ruler-boards (i.e. chess-boards with an upward-directed stick with centimeter marks, see WP2). Depending on availability, a total of 13 to 16 monitoring stations will be prepared and distributed over a ~2 km<sup>2</sup> large monitoring array (FIGURE 8.4). Based on the results of pre-impact studies and the bottom current conditions at the time of the collector trial, the EMP layout will be adjusted during the cruise, if necessary.

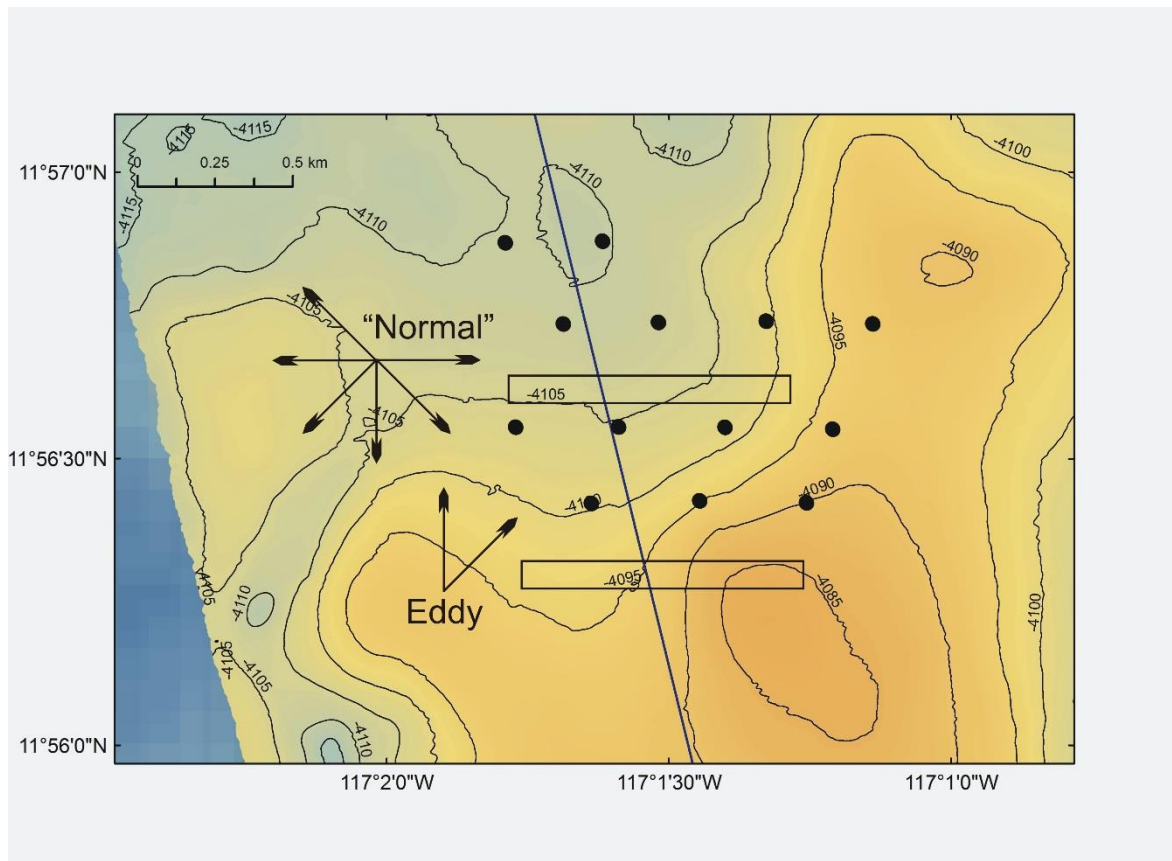


**Figure 8.4:** Schematic layout of a possible monitoring array in relation to two potential collector test sites within an area of 2x3 km<sup>2</sup> (red rectangle in FIGURE 8.3). The two alternative test sites indicate the strategy to adapt to changing bottom current directions during the time of the collector test. Since placing the monitoring array is very time-consuming, the area of the collector test will be shifted, if necessary, to ensure effective monitoring of the sediment plume. The southern test site can be used during an eddy situation with predominantly northward current flow, whereas the northern test site would be more suitable for “normal”, variable seafloor current conditions. Hence, both areas will be sampled and surveyed prior to and after the plume experiment as IRZ and PIRZ in the EMP. Wider AUV surveys are planned to cover the entire PIRZ (see CHAPTER 6.4.3).

(2) Cruise station time planning (outlined in CCT1)

In dialogue with all partners of the project and based on the results and recommendations that come out of point (1) above, a detailed cruise plan will be developed that accounts for AUV and ROV survey times, biological, geological and biogeochemical field work as well as deployment times for moorings. Technical pre-conditions of the collector system and safety issues for the two-vessel operation as well as real-time communication will be prepared in dialogue with DEME. Monitoring technologies as outlined in CHAPTER 8.2.1.4 and described in CHAPTER 8.2.1.2 need to be prepared and large amounts of monitoring equipment and moored sensors need to be precisely deployed and inter-calibrated at suitable facilities of partner institutions prior to the test.

(3) Onsite pre-impact assessment (outlined in WP1, 2, 3)

A coordinated approach of the pre-impact assessment within the designated zones is required. This will include sediment sampling for the determination of baseline sedimentological, geochemical and biological conditions as well as improved habitat characterisation using statistical methods to make biological/optical sampling more effective with regards to habitat distribution.

Pre-impact assessment of the collector test area (the Impact Zone [IRZ/PIRZ] and one or two control reference sites) will start in April/May 2018 during a BGR exploration cruise to the Eastern license area. This pre-impact assessment especially involves taking multicores for biological and geochemical analyses, video-surveying the seafloor, epibenthic sled and multicore deployment to the south of the test area to compliment the BGR biological time series analyses that started in 2013, and the deployment of 2 ADCP/RCM moorings and a sediment trap that will measure background current conditions close to the seafloor directly in the test area and background particle fluxes in the water column, respectively, between April 2018 and March 2019 so as to deliver local information on the hydrodynamic conditions and particle fluxes in the area to better feed into predictive models for the dispersion of the sediment plume.

Further pre-impact assessment will be a priority of the first JPI-O MiningImpact 2 SONNE cruise to the test area in March 2019 and will focus on collecting baseline data according to the approaches for monitoring that have been described in detail in CHAPTER 8.2.1 above.

(4) Small-scale *in situ* experiments related to plume behaviour (outlined in WP2 and 3)

A coordinated approach of *in situ* experiments and observations of the behaviour of small plumes produced by the ROV on the seafloor will help to determine changes in aggregation behaviour, including the effects of the injection of phytodetritus (local species cultivated on-board), and plume dispersion of plumes of different sediment densities. Such information will also be important to ground-truth particle camera data.

(5) *Ex situ* experiments related to plume behaviour (outlined in WP2 and 3)

Laboratory-based experiments using a LISST, roller tanks and erosion chambers will provide site-specific data for sediment transport modelling using local sediment samples from the topmost 10 cm of sediment. Data on particle size distribution before and after subsequent particle aggregation under conditions of low and moderate turbulence will be provided and resulting  $w_s$ ,  $d_i$ ,  $u^*_{cri}$ ,  $u^*_{dep}$  characteristics under commonly found flow conditions (low flow and eddy induced flow) will feed into the particle transport models of point (6) below.

(6) Near real-time modelling to predict fallout areas (outlined in WP2)

During the cruise and in preparation of the collector test, regular updates of the plume dispersion model will allow for an adaptive monitoring effort. At the same time models can be verified by newly-obtained field data and observations.

(7) In situ monitoring of the plume produced by the collector test (outlined in WP1, 2, 3)

A coordinated monitoring design for the quantification of plume dilution and dispersion will be developed that involves all previously mentioned technologies. Modelled plume behaviour will be ground-truthed and validated using stationary and mobile observations with ADCPs, OBS, cameras, particle cameras, tracer particle cameras. Important will be the use of a water column-imaging multibeam echo-sounder and parallel downward-looking ADCP on the ROV to actively map the distribution of the plume from 30 to 50 m above the seafloor. Varying the plume dispersal by changing the release conditions (volume flow, diffuser array, turbulence, sediment concentration) from the collector will be an important experiment in which ROV observations will play an important role.

(8) On-site post-impact assessment (outlined in WP1, 2, 3)

After the collector test, all monitoring activities of the pre-impact assessment will be repeated to determine the extent of the fallout area and the thickness of sediment blanketing as well as the impact on fauna, microbial activity and biogeochemical conditions/processes. This will include the determination of blanketing effect/layer thickness by AUV-based imagery, possible changes in multi-beam backscatter intensity, measurement by ROV, and the observation of ruler-boards deployed before the experiment. In addition the resuspension and aggregation behaviour of freshly-deposited plume particles including introduced fluorescent particle tracers will be investigated.

(9) Evaluation of the effectiveness of the EMP workflow and used monitoring technologies (outlined in CCT1)

An evaluation of the workflow outlined above for the planning and execution of a plume/impact monitoring campaign will be carried out to assess its effectivity in covering all important aspects and processes. The performance of the deployed sensors and platforms will be analysed with respect to e.g., detection ranges of particle concentrations and determining the footprint and thickness of the deposited sediment blanket. A best practice guidance document on monitoring technology, layout scheme and workflow will be produced by the consortium in order to inform monitoring activities accompanying future mining tests.

(10) Colonisation experiment (outlined in CCT2)

The feasibility of artificial hard substrates for restoration action through time and space will be tested and the role of substrate type for settlement success of biota explored, including early formation of microbial biofilms, and impact on sediment biogeochemistry.

(11) Evaluation of mining-related pressures and effects on ecosystem components (outlined in CCT2)

A detailed analysis and integration of spatial and temporal variability in (i) (bio)geochemistry, element fluxes, bioturbation, and sediment and pore water characteristics, (ii) benthic communities, biodiversities,

abundance and biomass, and (iii) benthic ecosystem functions such as organic matter processing, microbial growth and food web structure will be carried out, and the intensity of the observed changes after disturbance will be related to specific (combinations of) pressures compared to the observed variability in baseline environmental conditions. a quantitative assessment of intensities of pressures and responses of ecosystem components will be done. The aim is to carry out a focused, high-detailed assessment of ecosystem components based on functional relationships, which will generate measures of sensitivity based on both empirical data (evidence-based) and expert judgement.

(12) Development of tools for integrated (cumulative) environmental impact assessment (outlined in CCT2)

Robust approaches for ecological impact/risk assessment will be identified (e.g. Weight of Evidence approach [WOE]; Environmental Hazard and Impact Identification [ENVID]). A multiple-scale analysis to test the importance of the scale of sampling and observation (both spatial and temporal) for impact assessment will be performed. The types of impacts (compaction, nodule and/or surface sediment removal, blanketing, particle concentration and shape in the water column, toxicity, etc.) that have the largest effects on benthic communities and functions and determine the relevant 'intensity thresholds' (thickness of surface sediment mixed or lost, thickness of blanketing layer, etc.) will be identified. 'Indicator species' / 'indicator groups' / 'indicator functions' as a proxy for effects on specific parts of the benthic ecosystem (e.g., distinct taxonomic or functional groups, size classes, or distinct functions like organic matter remineralisation, bioturbation, element and energy transfer in food webs) or the ecosystem in general (i.e. 'seafloor integrity') will be sought for. All developed tools will feed into proposing methodologies for mining-related risk assessment and for developing concepts for minimising harmful impacts on the environment (i.e. developing environmental management tools).

### **8.3 Data management, reporting and dissemination**

The project is committed to organising, facilitating and effectively managing the archival of generated data and samples in databases with established structures and capabilities, such as PANGAEA and European museum collections, based on established protocols and best practices for research expeditions, the specific code of conduct for marine sciences, and the EU principles of data and knowledge sharing. Work package workshops and annual meetings will ensure the exchange of knowledge between project partners. Consortium members of the JPI-O MiningImpact 2 project make a commitment to publish their results in peer-reviewed scientific publications, and data and outcomes will be made publicly available in an appropriate time frame.

#### **8.3.1 DATA MANAGEMENT**

The project will generate huge volumes of data across all work packages and scientific disciplines. These comprise a large variety of different data types, such as acoustic data from e.g. multibeam and side-scan sonars and ADCPs, photo and video images from AUV, ROV and towed camera surveys, comprehensive datasets of a multitude of chemical compound concentrations in the water column and the sediment, faunal diversity and abundances, genetic information and microbial parameters.

The entire life cycle of data management from recording, processing, standardisation, consistency and technical quality assessment, to archiving of data needs to be covered. Tools, working plans, deployments and the ship's handling will be checked and controlled for potential environmental imprint on a regular



daily basis; protocols of every deployment comprise notes on bottom time, sampling, biodiversity, geological setting, and oceanographic measurements and will be summarised in the cruise reports. Directly after the SONNE cruises, the ship's station list and all metadata from sampling and observations as well as raw and processed hydroacoustic data will be stored in the MaNIDA database, which is also accessible via the EMODnet data portals. GEOMAR will facilitate the long-term storage of the project data in the information system PANGAEA at the World Data Center for Marine Environmental Sciences (WDC-MARE) through its Ocean Science Information System (OSIS-Kiel). OSIS-Kiel will also be used for the sharing of datasets among project partners. PANGAEA is operated on a long-term basis by AWI and MARUM. All data will be geo- and time-referenced and deposited with a Digital Object Identifier (DOI) to make them citable and retrievable by library catalogues or Google Scholar. Data published within PANGAEA are provided through harvesting techniques for global distribution. These techniques include standard metadata exchange formats such as ISO19115, Dublin-Core and OAI-PMH. Two further features of PANGAEA are geo-referencing of data and establishing best-practice guidelines to allow efficient browsing in spatially and temporally organised data.

A project data policy will be generated to specify time schedules from data creation to internal project availability and final publication (time periods will be adjusted according to the scientific disciplines) in PANGAEA as well as general data use agreements. These data sharing modalities will achieve a stable research support environment for all project partners and will guarantee the availability of the project data to the scientific community beyond the project's life time.

All molecular data concerning fauna will be deposited in GenBank (overseen by SGN). All sequencing data with the appropriate sets of metadata will be uploaded via GFBio to the European Nucleotide Archive (ENA) and PANGAEA. MPI will further upload all image and hydroacoustic OFOBS survey data to PANGAEA. Video data collected with OFOBS as well as other video-footage provided by project partners will be uploaded to the video annotation platform vidlib (<http://vidlib.marum.de>) for joint analysis by project members. This may be extended to other video-footage provided by project partners if needed, e.g. for comparison with the video annotation functionality added to BIIGLE 2.0 (see CHAPTER 8.3.3).

### **8.3.2 SAMPLE MANAGEMENT**

The distribution of samples taken for faunal analyses and the standardisation of sampling and processing techniques will be coordinated by the German Center for Marine Biodiversity Research (DZMB at SGN). After the life time of the project, participants will be asked to return any non-needed samples and biological material to SGN for long-term storage. Holotypes of new species will be deposited in an appropriate collection of a European natural history museum (e.g. Natural History Museum in London, Muséum National D'Histoire Naturelle in Paris, Senckenberg in Frankfurt) and information on the fate of samples and specimens will be made available to SGN. Storage of microbial samples will take place at MPI. Sediment and pore water samples from collected cores will be stored in the GEOMAR core repository.

### **8.3.3 DATA IMAGE ANALYSIS AND ARCHIVING**

A main objective of the project is to further develop the functionalities of the BIIGLE 2.0 image annotation software (Benthic Image Indexing, Graphical Labelling and Exploration) of the University of Bielefeld in order to cater for the increasing demand for sharing of knowledge and image data between partners (e.g., morphotype catalogues, annotation of videos, and integration of geospatial information or maps with annotation results such as species abundances).

The field of computational marine image analysis is rather novel. The ultimate aim of developing a fully generalizable, automated marine image annotation system appear unrealistic at this stage due to the strong variation in imaging conditions, huge species' diversity and low per-species density. To make manual annotation through visual inspection by experts more efficient, different tools have been proposed in the last years, such as SQUIDLE, CATAMI, PAPARAZZI, ECOTAXA and BIIGLE. Although these systems provide valuable support for the annotation process, the integration of all the data (annotation, taxonomic catalogues, etc) across many institutes has not been addressed enough so far.

Only very few annotation systems have been proposed for video annotation (e.g. VIDLIB, Adelie), even though the analysis of video data collected with ROV is one standard procedure in marine biology, environmental sciences or underwater infrastructure inspection. One special problem seems to be the lack of a clear general problem specification, like a definition of a labelling protocol and how to avoid a time consuming labelling of objects in multiple consecutive frames. This task could benefit from an integration of algorithmic solutions like machine learning to make video annotation more efficient.

In the first phase of the MiningImpact project, the focus was put on the development of DIAS, a first alpha-version of a mobile software for the annotation of marine image collections recorded with different platforms such as AUV, ROV or OFOBS during the expeditions with RV SONNE in 2015. After the cruises the DIAS system was merged with the already existing BIIGLE database to form a new online annotation database system BIIGLE 2.0 (Langenkämper et al., 2017) and used for annotation in the acquired image data.

In the proposed project MiningImpact 2, the aim is to address image analysis issues in a practical mining monitoring context and to develop methods to deal with problems related to temporal mining impact monitoring and posterior observation. The algorithmic basics and software structures for an advanced marine image analysis toolbox BIIGLE 2.0 will be developed by the University of Bielefeld. In all phases of mining we can expect that images with a variety of platforms such as OFOBS, AUV and ROV will be collected, but in the context of this project video data will play a role of greater significance as well as the evaluation of (time lapse) image sequences from camera-equipped underwater observatories (FUO) or landers. These large amounts of accumulating image and video data (with some images covering a visual footprint of approx. 400 m<sup>2</sup> per image) need to be evaluated and assessed, e.g. sediment plume patterns, habitat information (nodule abundance; associated fauna). The University of Bielefeld will develop new video annotation capabilities for the BIIGLE 2.0 tool (Langenkämper et al., 2017), which is currently limited to still images only. To develop the video annotation tool, a number of studies with experienced users from marine biology will be carried out to carefully render the specifications for the tool. This includes data specification (e.g. volumes, codecs, etc.) as well as usability issues. In addition to the software development itself, general guidelines for video annotation will be set up, similar to those outlined for still images in the first project phase. A large part of this image and video evaluation is still done by human observers who shall jointly annotate regions of interest with pre-defined semantic categories, morphologies or taxonomies and integrate the annotation results with geospatial information.

In addition to the BIIGLE 2.0 system that is installed at partner institutes GEOMAR, SGN and the University of Bielefeld, the *mobile* BIIGLE 2.0 system will be used during cruises at sea. To support a flexible use not only of the image data but also of derived data, such as label trees and morphotype catalogues, all of these data need to be hosted by a global data server together with user ID and user information. It should be noted that such a server is not intended to become a new data repository itself (as these already exist, e.g. PANGAEA). The aim is to support collaboration and standardisation in annotation and to avoid redundancies at the local BIIGLE spots.

During mining operations the annotations and statistics of the objects and events in the images and videos must be analysed in a geospatial and temporal context. Thus, new interfaces and routines will be implemented that support a data fusion in the geospatial and/or temporal domain. These new integrated datasets enable users to browse and analyse the data from different perspectives, which is necessary to work on different scales in time (short/long-term impact) or space.

To link the annotation results to geographical information, a more sophisticated tool for geospatial visualisation, browsing and filtering will be implemented. Currently, BIIGLE 2.0 visualises the locations of the images using *OpenStreetmap*. Users can visualise images (e.g. selected according to a species abundance filter) at a geographical location or select images according to their geographical location for a detailed visualised inspection. The new module shall support users to plot this information on imported bathymetric maps or other kinds of maps. If video data is provided with geospatial information, geospatial gating or filtering through the map will also be supported.

### 8.3.4 DISSEMINATION

In order to achieve effective dissemination of the project outcomes, an audience analysis will be performed by GRID-Arendal that will lead to an updated compilation of the existing stakeholder database. Dissemination and outreach will be carried out both in a passive (making information available) and an active (targeted events) way. Part of the outreach efforts will be devoted to disseminate to a high-level audience (e.g. decision-makers).

The ISA, as a partner in the MiningImpact 2 project, will organise targeted workshops on specific topics, such as spatial management, risk assessment, monitoring plans and technology, and environmental impacts. These are aimed at discussing and exchanging knowledge with ISA's contractors, policymakers, NGOs, the interested deep-sea mining industry, as well as countries planning offshore mining activities in their exclusive economic zones (EEZ). In addition, at least one Side Event at an ISA Annual Meeting in Jamaica is planned to present the project's results and policy recommendations to the ISA Council, LTC, contractors, mining industries, and NGOs. International conferences, such as UMC, OMS, EGU, AGU and Goldschmidt, are good opportunities to inform the science community, but also industry and the general public about the project results. Special sessions at several conferences will be organised during the project's life time.

Outreach products are planned that explain deep-sea mining impacts on the environment to both a non-specialised and a specialised audience, such as policy stakeholders, who are interested in specific aspects of deep-sea mining. The content of these outreach products will be carefully selected so that they match the different purposes and audiences for which they will be produced. As part of this task, GRID-Arendal will develop a number of policy briefs in order to highlight the major research findings obtained through the project, explore policy options if suitable and provide recommendations on the best options. Supporting science to policy outreach and dissemination could also be served by innovative geospatial products like Story Maps. This will be determined as part of the audience analysis mentioned above.

The existing project website, consisting of public and secure internal areas, will be used for external, but also internal communication. The secure internal project website will be used as a vehicle to enhance communication between project partners and facilitate data management by providing entrance to PANGAEA and the OSIS-Kiel data portal. GRID-Arendal and GEOMAR will be responsible for updating and maintaining the website. These activities include publication of a project newsletter, press releases, and social media feeds running throughout the project's life-cycle. Updated information on project progress and developments in research, policy and industry related to deep-sea mining will be further

disseminated, including social media activities. A project benchmarking system will be developed by GRID-Arendal at the onset of the project and this will be included in the internal protected area of the website to allow for internal monitoring and evaluation of progress (quality, time/cost) in the achievement of the project goals.

The project coordination at GEOMAR will organise annual meetings for all participants to present their results and discuss further joint data analyses and interpretation. As in the first project phase, interested stakeholders and policymakers will be invited to these meetings to foster knowledge exchange, but also help the project to focus on relevant issues, e.g. towards policy regulations. Individual WP workshops will be organised by the respective WP leaders. In addition, the coordination will organise joint project reporting to JPI-Oceans and at the SONNE status seminar. Finally, a special issue publication of the main project results is envisioned in an internationally reviewed scientific journal, ideally with open-access policy, such as Biogeosciences.

## 9. Glossary and abbreviations

AAIW	Antarctic Intermediate Water
ADCP	Acoustic Doppler Current Profiler
ADV	Acoustic Doppler Velocimeter
AGU	American Geophysical Union
Al	aluminium
AMOVA	Analysis of Molecular Variance
AMS	Accelerator Mass Spectrometry
ANOSIM	pairwise one-way analysis of similarities test
ANOVA	Analysis of Variance
APEI	Area of Particular Environmental Interest
AUV	Autonomous Underwater Vehicle
AVISO	Satellite-derived sea-surface dynamic topography (altimetry)
AWI	Alfred Wegener Institut, Bremerhaven
BACI	Before-After-Control-Impact design
BBL	Bottom Boundary Layer
Be	beryllium
BGR	Bundesanstalt für Geowissenschaften und Rohstoffe, Hannover, Germany
BIE	Benthic Impact Experiment
BIIGLE	Bio-Image Indexing and Graphical Labelling Environment; a web-based software for automated species identification on underwater images developed by the Biodata Mining Group, University of Bielefeld, Germany
BIONOD	Joint Franco-German cruise with RV L'ATALANTE to the French and German license areas in 2012
Blue Atlantis	EU project "Innovative Mining of Marine Mineral Resources – A European Pilot Mining Test in the Atlantic on Tools, Facilities, Operations and Concepts" (European Innovation Partnership on Raw Materials)
Blue Mining	EU FP7-project to develop breakthrough solutions for sustainable deep-sea mining (2014 – 2018)
Blue Nodules	EU Horizon 2020 research and innovation project to develop a deep-sea mining system for the harvesting of polymetallic nodules from the sea floor with minimum environmental impact (2016 – 2020)
BMF	German Federal Ministry of Education and Research
BMWi	German Federal Ministry of Economics and Energy)
BoBo lander	Bottom Boundary lander; belongs to NIOZ and is equipped with ADCPs, OBSs, CTD, sediment trap
BOLD	Barcode of Life Data System: genetic data retrieval database
C	carbon
Ca	calcium

CBD	Convention on Biological Diversity
CCT	Cross-cutting theme
CCZ	Clarion-Clipperton Zone
Cd	cadmium
Co	cobalt
COI	mitochondrial cytochrome c oxidase subunit I
CoNISMa	Inter-University Consortium for Marine Science, Italy
Cs	cesium
CT	Computed Tomography
CTD	Conductivity-Temperature-Depth Sensor
CTW	Coastally-trapped waves
Cu	Copper
CUBE	benthic incubation chamber
DBD	Dry Bulk Density
ddPCR	droplet digital polymerase chain reaction
DEME	Belgian Dredge company and manganese nodule contractor in the CCZ
DIC	Dissolved Inorganic Carbon
DISCOL	German-funded research project “DISturbance and ReCOLonisation Experiment”, in which a disturbance experiment was carried out in a manganese nodule area in the SE Pacific (Peru Basin) in 1989
DOM	Dissolved Organic Matter
DOMES	US American / NOAA project “Deep Ocean Mining Environmental Study”, 1975-1976
DOS lander	Deep-Sea Observatory lander; belongs to GEOMAR and is equipped with ADCPs, CTD, camera, sediment trap
DSSRS	Deep Sea Sediment Resuspension System
DVL	Doppler Velocity Log
DW	Deep Water
DZMB	German Center for Marine Biodiversity Research, Senckenberg am Meer, Wilhelmshaven, Germany
EA	Environmental Assessment
EBS	Epibenthic sled
EEZ	Exclusive Economic Zone
EGU	European Geosciences Union
EIA	Environmental Impact Assessment
EKE	Eddy Kinetic Energy
EM 120/122	Kongsberg 12 kHz multibeam echosounder system
EMODnet	European Marine Observation and Data Network
EMP	Environmental Monitoring Plan
ENA	European Nucleotide Archive
ENSO	El Niño/Southern Oscillation
ENVID	Environmental Hazard and Impact Identification



EU	European Union
Fe	Iron
FP7	7 <sup>th</sup> Framework Programme of the European Union
G	shear rate (s <sup>-1</sup> ) (hydrodynamic) / genus richness (biological)
GDMB	Gesellschaft der Metallurgen und Bergleute e.V.
GenBank	National Center for Biotechnology Information genetic sequence database
GEOMAR	Helmholz Centre for Ocean Research Kiel, Germany
GIS	Geographical Information System
GmbH	Gesellschaft mit beschränkter Haftung / private limited company (Ltd.)
GSR	Global Sea mineral Resources NV, Oostende, Belgium
JET	Japan Deep-Sea Impact Experiment
JPI-O	Joint Programming Initiative – Oceans
H	hydrogen
H'	Shannon Index of diversity
HD	High Definition
HOMESIDE	BGR-owned deep-towed multibeam echosounder system
HPU	Hydraulic Power Unit
HYCOM	Hybrid Coordinate Ocean Model
IA	Implementing Agreement
ICP-MS	Inductively Coupled Plasma-Mass Spectrometry
ICP-OES	Inductively Coupled Plasma-Optical Emission Spectrometry
IMAR	Institute of Marine Research, Azores, Portugal
IMO	International Maritime Organization
INDEEP	International network for scientific investigation of deep-sea ecosystems
INDEX	Indian Deep-sea Environment Experiment
INS	Inertial Navigation System
IOM	Interoceanmetal; manganese nodule contractor in the CCZ, existing of a consortium of representatives from Bulgaria, Cuba, Czech Republic, Poland, Russia, Slovakia
IRZ	Impact Reference Zone
ISA	International Seabed Authority, Kingston, Jamaica
ITCZ	Intertropical Convergence Zone
JORC	Joint Ore Reserves Committee
JUB	Jacobs University, Bremen, Germany
LBEG	German State Authority for Mining, Energy and Geology, Clausthal-Zellerfeld, Germany
LCPW	Lower Circumpolar Water
Li	Lithium
LISST-100X	Laser In-Situ Scattering and Transmissometry Analysor
LOE	Level of Evidence
LOSC	Law of the Sea Convention (Synonym to UNCLOS)
LTC	Legal and Technical Commission (of the ISA)

mab	meters above bottom
MAPR	Miniature Autonomous Plume Recorder
MARPOL	International Convention for the Prevention of Pollution from Ships
MARUM	Center for Marine Environmental Sciences, University of Bremen, Germany
MBergG	Meeresbodenbergbaugesetz (German legislation for marine mineral exploration)
MIDAS	EU FP7-project „Managing Impacts of Deep-Sea Resource Exploitation” (2013 – 2016)
MiningImpact	JPI-O Project “Ecological aspects of deep-sea mining”, 2015-2017
MITgcm	Massachusetts Institute of Technology general circulation model
Mn	Manganese
Mo	Molybdenum
MOTU	Molecular Operational Taxonomic Unit
MPI	Max-Planck-Institute for Marine Microbiology, Bremen, Germany
MSDS	Material Safety Data Sheet
MUC	Multicorer
N	nitrogen
NGO	Non-Governmental Organisation
NGS	next generation sequencing
Ni	Nickel
NIOZ	Royal Netherlands Institute for Sea Research, Texel, the Netherlands
nMDS	non-metric, multi-dimensional scaling plot
NOAA	National Oceanic and Atmospheric Administration, USA
NPDW	North Pacific Deep Water
NPIW	North Pacific Intermediate Water
NTNU	Norwegian University of Science and Technology, Norway
O	oxygen
OBM	Ocean Bottom Mooring
OBS	Optical Backscatter Sensor
OECD	Organisation for Economic Cooperation and Development
OFOBS	Ocean Floor Observation System
OMA	Ocean mining Associates
OMCO	Ocean Minerals Company (Exploration Company of the 70ties)
OMI	Ocean Mining Inc.
OMS	Ocean Mining Symposium
OMZ	Oxygen Minimum Zone
OSIS	Ocean Science Information System
Pa	protactinium
PA1	Prospective Area #1 in the Eastern German license area
PA2	Prospective Area #2 in the Eastern German license area
PANGAEA	Data Publisher for Earth & Environmental Science, Bremen
Pb	lead
PCR	polymerase chain reaction

PIRZ	Plume Impact Reference Zone
PMA	Synonym for PA2
POC	Particulate Organic Carbon
POM	Particulate Organic Matter
PRZ	Preservation Reference Zone
Ra	radium
RAD	with relative abundance
RBINS	Royal Belgian Institute of Natural Sciences, Oostende, Belgium
RCM	Recording Current Meter
REY	rare earth elements and yttrium
ROV	Remotely Operated Vehicle
RV SONNE	Research Vessel SONNE
SAMS	Scottish Association of Marine Science
SEM	Scanning Electron Microscopy
SGN	Senckenberg am Meer, Frankfurt, Germany
SMD	standardised mean difference
SOG	speed over ground
SOI	Southern Oscillation Index
SPM	Suspended Particulate Matter
Sr	strontium
SSH	Sea surface height
SST	Sea surface temperature
STSW	Subtropical Surface Water
SyPRID	A large-volume, high-resolution, autonomous, deep-ocean precision plankton sampling system
TC	Thermistor chain
Th	thorium
TOC	Total Organic Carbon
TRI	Topographic Ruggedness Index
TSTD	Track Soil Testing Device
TSW	Tropical Surface Water
TU Delft	Delft University of Technology, the Netherlands
U	uranium
UAlgrave	CIMA, Universidade do Algarve, Portugal
UBA	German Environment Agency, Dessau, Germany
UMC	Underwater Mining Conference
UNCLOS	United Nations Convention of the Law of the Sea (synonym to LOSC)
USBL	Ultra-Short Base Line acoustic technology
V	vanadium
WDC-MARE	World Data Center for Marine Environmental Sciences
WHOI	Woods Hole Oceanographic Institution, Massachusetts, USA
WOE	Weight of Evidence

WP	Work package
XRG	X-ray granulometry
XRF	X-ray fluorescence spectroscopy
Zn	zinc

## 10. Study team

This EIA has been compiled by the BGR, Hannover, Germany (Department of Marine Resource Exploration) based on data that have either been obtained by the BGR as part of its exploration activities or by scientific projects such as MIDAS and JPI-O MiningImpact 1. Sources of data are mentioned where appropriate and references are listed for published data.

As this EIA describes the planned assessment of impacts produced by the testing of a collector vehicle in the framework of the European JPI-O MiningImpact 2 project, much input to this EIA was delivered by the proposal for the project to the JPI-O head office in Brussels, which was submitted by the coordinator of the project, Dr. Matthias Haeckel (GEOMAR, Germany) on 01. November 2017. A list of the 31 partners of the MiningImpact 2 project is provided in [APPENDIX 1](#).

Technical information on the collector vehicle was provided by the Belgian company and contractor DEME-GSR. Several sections of this EIA were written together or in consensus with DEME-GSR, who will be submitting a separate EIA for testing within their own license area in the framework of the same MiningImpact 2 project.

## References

- Adams, D.K., McGillicuddy, D.J., Zamudio, L., Thurnherr, A.M., Liang, X., Rouxel, O., et al. (2011). Surface-Generated Mesoscale Eddies: Transport Deep-Sea Products from Hydrothermal Vents. *Science* 332 (6029), 580-583.
- Aguilar de Soto, N., Kight, C. (2016). Physiological effects of noise on aquatic animals. In: Solan, M., Whiteley, N.M. (Eds.), *Stressors in the Marine Environment*. Oxford University Press, Oxford, 135-158.
- Akin, H., Siemens, H. (1988). *Praktische Geostatistik*. Springer, Berlin-Heidelberg-New York, 304 pp.
- Aleynik, D., Inall, A., Dale, A., Vink, A. (2017). Impact of remotely generated eddies on plume dispersion at abyssal mining sites in the Pacific. *Scientific Reports* 7, 16959. DOI: 10.1038/s41598-017-16912-2.
- Alford, M.H., Peacock, T., MacKinnon, J.A., Nash, J.D., Buijsman, M.C., Centuroni, L.R., et al. (2015). The formation and fate of internal waves in the South China Sea. *Nature* 521 (7550), 65-69.
- Auguste, M., Mestre, N.C., Rocha, T.L., Cardoso, C., Cambon-Bonavita, M.A., Cueff-Gauchard, V., Le Bloa, S., Ravaux, J., Shillito, B., Zbinden, M., Bebianno, M.J. (2016). Development of an ecotoxicological protocol for the deep-sea fauna using the hydrothermal vent shrimp *Rimicaris exoculata*. *Aq. Tox.* 175:277-285.
- Bailey, R.C., Kennedy, M.G., Dervish, M.Z., Taylor, R.M. (1998). Biological assessment of freshwater ecosystems using a reference condition approach: comparing predicted and actual benthic invertebrate communities in Yukon streams. *Freshwater Biology* 39, 765-774.
- Baker, A.N. (2016). An illustrated catalogue of type specimens of the bathyal brittlestar genera *Ophiomusium* Lyman and *Ophiosphalma* H.L. Clark (Echinodermata: Ophiuroidea). *Zootaxa* 4097 (1), 1-40.
- Barckhausen, U., Bagge, M., Wilson, D.S. (2013). Seafloor spreading anomalies and crustal ages of the Clarion-Clipperton Zone: *Marine Geophysical Research* 34, 79–88.
- Barnett, B., T. Suzuki (1997). The use of kriging to estimate resedimentation in the JET experiment. *Proceedings, international symposium on environmental studies for deep-sea mining*.
- Bebianno, M.J., Pereira, C.G., Rey, F., Cravo, A., Duarte, D., D'Errico, G., Regoli, F. (2015). Integrated approach to assess ecosystem health in harbor areas. *Sci. Total Env.* 514, 92-107.
- Belz, H. (2015). Physical sediment properties and particle sizes of deep-sea siliceous oozes in the Clarion-Clipperton Fracture Zone, North-East Pacific. Master Thesis, University of Tübingen, 114 pp.
- Benndorf, J. (2015). Vorratsklassifikation nach internationalen Standards – Anforderungen und Modellansätze in der Lagerstättenbearbeitung. *Markscheidewesen* 122(2-3), 6-14.



- Bik, H.M., Porazinska, D.L., Creer, S., Caporaso, J.G., Knight, R., Thomas, W.K. (2012). Sequencing our way towards understanding global eukaryotic biodiversity. *Trends in Ecology & Evolution* 27, 233-243.
- Billings, A., Kaiser, C., Young, C.M., et al. (2017). SyPRID sampler: A large-volume, high-resolution, autonomous, deep-ocean precision plankton sampling system. *Deep-Sea Res II* 137, 297-306.
- Blöthe, M., Wegorzewski, A.V., Müller, C., Simon, F., Kuhn, T., Schippers, A. (2015). Manganese-Cycling Microbial Communities inside Deep-Sea Manganese Nodules. *Environmental Science & Technology* 49, 7692-7700.
- Bluhm, H. (2001). Re-establishment of an abyssal megabenthic community after experimental physical disturbance of the seafloor. *Deep-Sea Research II*, 48, 3841-3868.
- Boetius A. (ed.) (2015). RV SONNE Cruise Report SO242-2: JPI OCEANS Ecological Aspects of Deep-Sea Mining, DISCOL Revisited. GEOMAR Report 27, 552 pp.
- Boetius, A., Wenzhöfer, F. (2009). In Situ Technologies for Studying Deep-Sea Hotspot Ecosystems. *Oceanography* 22, 177.
- Borowski, C., Thiel, H. (1998). Deep-sea macrofaunal impacts of a large-scale physical disturbance experiment in the Southeast Pacific. *Deep Sea Research Part II, Topical Studies in Oceanography* 45, 55-81.
- Brockett, T., Richards, C.Z. (1994). Deep-sea mining simulator for environmental impact studies. *Sea Technology* 35 (8), 77-82.
- Brown, A., Wright, R., Mevenkamp, L., Hauton, C. (2017). A comparative experimental approach to ecotoxicology in shallow-water and deep-sea holothurians suggests similar behavioural responses. *Aquatic Toxicology*. doi:10.1016/j.aquatox.2017.06.028.
- Burford-Reiskind, M. O., Coyle, K., Daniels, H. V., Labadie, P., Reiskind, M. H., Roberts, N. B., Roberts, R. B., Schaff, J., Vargo, E.L. (2016). Development of a universal double-digest RAD sequencing approach for a group of nonmodel, ecologically and economically important insect and fish taxa. *Mol. Ecol. Resour.* 16, 1303-1314.
- Burritt, D.J., Lamare, M.D. (2016). The cellular responses of marine algae and invertebrates to ultraviolet radiation, alone and in combination with other common abiotic stressors. In: Solan, M., Whiteley, N.M. (Eds.), *Stressors in the Marine Environment*. Oxford University Press, Oxford, pp. 117e134.
- Caeiro, S., Vaz-Fernandes, P., Martinho, A.P., Costa, P.M., Silva M.J., Lavinha J., et al. (2017). Environmental risk assessment in a contaminated estuary: an integrated weight of evidence approach as a decision support tool. *Ocean & Coast. Manag.* 143, 51-62.
- Carman, K.R., Sherman, K.M., Thistle, D. (1987). Evidence that sediment type influences the horizontal and vertical distribution of nematodes at a deep-sea site. *Deep-Sea Research* 34 (1), 45-53.
- Canals, M., Pawlak, G., MacCready, P. (2009). Tilted Baroclinic Tidal Vortices. *Journal of Physical Oceanography* 39 (2), 333-350.
- Chelton, D.B., Freilich, M.H., Esbensen, S.K. (2000). Satellite Observations of the Wind Jets off the Pacific Coast of Central America. Part II: Regional Relationships and Dynamical Considerations. *Monthly Weather Review* 128 (7), 2019-2043.

- Cheng, N.S. (1997). Simplified Settling Velocity Formula for Sediment Particle. *Journal of Hydraulic Engineering* 123 (2), 149-152.
- Clark, M.R., Rouse, H.L., Lamarche, G., Ellis, J.I., Hickey, C.W. (2017). Preparation of Environmental Impact Assessments: General guidelines for offshore mining and drilling with particular reference to New Zealand. NIWA Science and Technology Series 81, 103 pp.
- Cordes, E.E., Jones, D.O., Schlacher, T.A., Amon, D.J., Bernardino, A.F., Brooke, S., Carney, R., DeLeo, D.M., Dunlop, K.M., Escobar-Briones, E.G., Gates, A.R., Genio, L., Gobin, J., Henry, L.-A., Herrera, S., Hoyt, S., Joye, S., Kark, S., Mestre, N.C., Metaxas, A., Pfeifer, S., Sink, K., Sweetman, A.K., Witte, U.F. (2016). Environmental impacts of the deep-water oil and gas industry: a review to guide management strategies. *Front. Environ. Sci.* 4, 58.
- Corinaldesi C., Danovaro R., Dell'Anno A. (2005). Simultaneous recovery of extracellular and intracellular DNA suitable for molecular studies from marine sediments. *Applied and Environmental Microbiology* 71, 46-50.
- Corinaldesi C., Beolchini F., Dell'Anno A. (2008). Damage and degradation rates of extracellular DNA in marine sediments: implications for the preservation of gene sequences. *Molecular Ecology* 17, 3939-3951.
- Corinaldesi C., Barucca M., Luna G.M., Dell'Anno A. (2011). Preservation, origin and genetic imprint of extracellular DNA in permanently anoxic deep-sea sediments. *Molecular Ecology* 20, 642-654.
- Craig, J.D. (1979). The relationship between bathymetry and ferromanganese deposits in the north equatorial Pacific. *Marine Geology* 29, 165-186.
- Creasey, S.S., Rogers, A.D. (1999). Population Genetics of Bathyal and Abyssal Organisms. *Advances in Marine Biology* 35, 1-151.
- Dahl, P.H. et al. (2007). Underwater ambient noise. *Acoustics Today* 3.1, 23-33.
- Dahlgren, T.G., Wiklund, H., Rabone, M., Amon, D.J., Ikebe, C., Watling, L., Smith, C.R., Glover, A.G. (2016). Abyssal fauna of the UK-1 polymetallic nodule exploration claim, Clarion-Clipperton Zone, central Pacific Ocean: Cnidaria. *Biodiversity Data Journal* 4, e9277.
- Dale, A.C., Inall, M.E. (2015). Tidal mixing processes amid small-scale, deep-ocean topography. *Geophysical Research Letters* 42, doi:10.1002/2014GL062755.
- Danovaro R. (2010). *Methods for the Study of Deep-Sea Sediments, Their Functioning and Biodiversity*. CRC Press, Taylor & Francis Group.
- Danovaro, R., Gambi, C., Della Croce, N. (2002). Meiofauna hotspot in the Atacama Trench, eastern South Pacific Ocean. *Deep-Sea Research I* 49, 843-857.
- Dee, D., and co-authors (2011). The ERA-Interim reanalysis: Configuration and performance of the data assimilation system. *Quarterly Journal of the Royal Meteorological Society* 137 (656), 553–597.
- Dell'Anno A., Danovaro R. (2005). Extracellular DNA plays a key role in deep-sea ecosystem functioning. *Science* 309, 2179.
- DeLong, E.F. (2005). Microbial community genomics in the ocean, *Nature Reviews Microbiology* 3 (6), 459-469.
- Demidova, T.A., Kontar, E.A., Sokov, A.V., Belyaev, A.M. (1993). The bottom currents in the area of abyssal hills in the north-east tropical Pacific Ocean. *Physical Oceanography* 4(1), 53-61.

- Deusner C., Kossel E., Bigalke N., Haeckel M., Gupta S., Freise M., Anbergen H., Wille T. (2016). The role of high-pressure flow-through experiments for evaluating the mechanical behaviour of gas hydrate-bearing soils. In: Wuttke, Bauer, Sanchez (eds.) *Energy Geotechnics*. CRC Press, 437-443.
- DNV.GL (2016). Recommended Practice. Managing environmental aspects and impacts of seabed mining. DNV GL-RP-O601 Edition September 2016.
- Doi, H., Takahara, T., Minamoto, T., Matsushashi, S., Uchii, K., Yamanaka, H. (2015). Droplet digital polymerase chain reaction (PCR) outperforms real-time PCR in the detection of environmental DNA from an invasive fish species. *Environmental Science & Technology* 49 (9), 5601-5608.
- Dreiseitl, I., Bednarek, R., Seul, C. (2013). Grain Size of the Seabed Sediments Underlying Polymetallic Nodules in the Exploration Area of InterOceanMetal. *Proc. of the tenth (2013) ISOP Ocean Mining Symposium*, Szczecin, 5 pp.
- Dreutter, S. (2017). Multisensor microbathymetric habitat mapping with a deep-towed ocean floor observation and bathymetry system (OFOBS). Master Thesis, HafenCity University Hamburg.
- Egbert, G.D., Erofeeva, S.Y. (2002). Efficient Inverse Modelling of Barotropic Ocean Tides. *Journal of Atmospheric and Oceanic Technology* 19 (2), 183-204.
- El-Syed, S.Z., Taguchi, S. (1979). Phytoplankton standing crop and primary productivity in the Tropical Pacific. In: Bischoff J.L., Piper D.Z. (eds) *Marine Geology and Oceanography of the Pacific Manganese Nodule Province*. Marine Science 9, Springer, Boston, MA, 241-286.
- European Commission (2008). Directive 2008/56/EC of the EU Parliament and Council on establishing a framework for community action in the field of marine environmental policy (Marine Strategy Framework Directive). <http://eur-lex.europa.eu/legal-content/EN/TXT/?uri=celex:32008L0056>.
- Ferguson, R., Church, M. (2004). A simple universal equation for grain settling velocity. *Journal of Sedimentary Research* 74, 933-937.
- Fiedler, P.C., Talley, L.D. (2006). Hydrography of the eastern tropical Pacific: A review. *Progress in Oceanography* 69, 143-180.
- Fitzsimmons, J.N., Carrasco, G.G., Wu, J., Roshan, S., Hatta, M., Measures, C.I., Conway, T.M., John, S.G., Boyle, E.A. (2015). Partitioning of dissolved iron and iron isotopes into soluble and colloidal phases along the GA03 GEOTRACES North Atlantic Transect. *Deep. Res. Part II Top. Stud. Oceanogr.* 116, 130-151.
- Foell, E.J., Pawson, D.L. (1986). Photographs of invertebrate megafauna from abyssal depths of the north-eastern equatorial Pacific Ocean. *Ohio Journal of Science* 86 (3), 60-68.
- Fredsøe, J., Deigaard, R. (1992). *Mechanics of coastal sediment transport*, vol. 3. World scientific, 1992.
- Fryxell, G.A., Taguchi, S., El-Sayed, S.Z. (1979). Vertical distribution of diverse phytoplankton communities in the Central Pacific. In: Bischoff J.L., Piper D.Z. (eds) *Marine Geology and Oceanography of the Pacific Manganese Nodule Province*. Marine Science 9, Springer, Boston, MA, 203-239.
- Fukushima, T. (1995). Overview: Japan deep-sea impact experiment = JET. *Proceedings of the first ISOP Ocean Mining Symposium*, Tsukuba, Japan, 47-53.

- Galéron, J., Sibuet, M., Mahaut, M.L., Dinét, A. (2000). Variation in structure and biomass of the benthic communities at three contrasting sites in the tropical Northeast Atlantic. *Marine Ecology Progress Series* 197, 121-137.
- Garcia, H.E., Locarnini, R.A., Boyer, T.P., Antonov, J.I., Baranova, O.K., Zweng, M.M., Reagan, J.R., Johnson, D.R. (2013). *World Ocean Atlas 2013, Volume 4: Dissolved Inorganic Nutrients (phosphate, nitrate, silicate)*. NOAA Atlas NESDIS 76 4, 27 pp.
- Gardner, W.D., Sullivan, L.S., Thorndike, E.M. (1984). Long-term photographic, current, and nephelometer observations of manganese nodule environments in the Pacific. *Earth and Planetary Science Letters* 70 (1), 95-109.
- Gardner, W.D., Tucholke, B.E., Richardson, M.J., Biscaye, P.E. (2017). Benthic storms, nepheloid layers, and linkage with upper ocean dynamics in the western North Atlantic. *Mar. Geol.* 385, 304–327.
- Giere, O. (2009). *Meiobenthology; The microscopic motile fauna of aquatic sediments*. 2<sup>nd</sup> edition, Springer Verlag, Berlin, Heidelberg.
- Glover, A.G., Smith, C.R. (2003). The deep-sea floor ecosystem: current status and prospects of anthropogenic change by the year 2015. *Environmental Conservation* 30 (3), 219-241.
- Glover, A., Paterson, G., Bett, B., Gage, J., Myriam, S., Sheader, M., Hawkins, L. (2001). Patterns in polychaete abundance and diversity from the Madeira Abyssal Plain, northeast Atlantic. *Deep Sea Research Part I: Oceanographic Research Papers* 48, 217-236.
- Glover, A.G., Smith, C.R., Paterson, G.L.J., Wilson, G.D.F., Hawkins, L., et al. (2002). Polychaete species diversity in the Central Pacific abyss: local and regional patterns, and relationships with productivity. *Mar. Ecol. Prog. Ser.* 240, 157-170.
- Glover, A., Dahlgren, T.G., Wiklund, H., Mohrbeck, I., Smith, C.R. (2015). An End-to-End DNA Taxonomy Methodology for Benthic Biodiversity Survey in the Clarion-Clipperton Zone, Central Pacific Abyss. *Journal of Marine Science and Engineering* 4 (1), 2.
- Glover, A., Dahlgren, T., Taboada, S., Paterson, G., Wiklund, H., Waeschenbach, A., et al. (2016a). The London Workshop on the Biogeography and Connectivity of the Clarion-Clipperton Zone. *Research Ideas and Outcomes* 2, e10528–47.
- Glover, A., Wiklund, H., Rabone, M., Amon, D., Smith, C., O'Hara, T., Mah, C.L., Dahlgren, T.G. (2016b). Abyssal fauna of the UK-1 polymetallic nodule exploration claim, Clarion-Clipperton Zone, central Pacific Ocean: Echinodermata. *Biodiversity Data Journal* 4: e7251–48.
- Gollner, S., Kaiser, S., Menzel, L., Jones, D.O.B., Brown, A., Mestre, N.C., van Oevelen, D., Menot, L., Colaco, A., Canals, M., Cuvelier, D., Durden, J.M., Gebruk, A., Egho, G.A., Haeckel, M., Marcon, Y., Mevenkamp, L., Morato, T., Pham, C.K., Purser, A., Sanchez-Vidal, A., Vanreusel, A., Vink, A., Martinez Arbizu, P. (2017). Resilience of benthic deep-sea fauna to mining activities. *Marine Environmental Research* 129, 76-101.
- Gonella, J. (1972). A rotary-component method for analysing meteorological and oceanographic vector time series. *Deep Sea Research and Oceanographic Abstracts* 19 (12), 833-846.
- Greinert J. (ed.) (2015). *RV SONNE Cruise Report SO242-1: JPI OCEANS Ecological Aspects of Deep-Sea Mining, DISCOL Revisited*. GEOMAR Report 26, 290 pp.

- Guidi-Guilvard, L.D., Thistle, D., Khripounoff, A., Gasparini, S. (2009). Dynamics of benthic copepods and other meiofauna in the benthic boundary layer of the deep NW Mediterranean Sea. *Marine Ecology Progress Series* 396, 181-195.
- Haeckel, M., König I., Riech V., Weber M. E., Suess E. (2001a). Pore water profiles and numerical modelling of biogeochemical processes in Peru Basin deep-sea sediments. *Deep-Sea Research II* 48 (17–18), 3713-3736.
- Haeckel, M., van Beusekom, J., Wiesner, M., König, I. (2001b). The impact of the 1991 Mount Pinatubo tephra fallout on the geochemical environment of the deep-sea sediments in the South China Sea. *Earth and Planetary Science Letters* 193, 153-168.
- Haley, B.A., Du, J., Abbott, A.N., McManus, J. (2017). The Impact of Benthic Processes on Rare Earth Element and Neodymium Isotope Distributions in the Oceans. *Front. Mar. Sci.* 4, 426.
- Hall-Spencer, J.M., Pike, J., Munn, C.B. (2007). Diseases affect cold-water corals too: *Eunicella verrucosa* (Cnidaria: Gorgonacea) necrosis in SW England. *Diseases of aquatic organisms* 76 (2), 87-97.
- Halpern, B.S., Selkoe, K.A., Micheli, F., Kappel, C.V. (2007). Evaluating and ranking the vulnerability of global marine ecosystems to anthropogenic threats. *Conserv Biol* 21, 1301-1315.
- Hanawa, K., Talley, L.D. (2001). Mode waters. In: Siedler, G., Church, J., Gould, J. (Eds.), *Ocean Circulation and Climate: Observing and Modeling the Global Ocean*. Academic Press, New York, pp. 373-386.
- Hannides, A.K., Smith, C.R. (2003). The northeastern Pacific abyssal plain. In: Black, K.D., Shimmiel, G.B. (eds.) *Biogeochemistry of marine systems*. Balckwell Publishing, Oxford.
- Hansbo, S. (1957). A new approach to the determination of shear strength of clay by the fall-cone test, *Proc. Royal Swed. Geotech. Inst.* 14, 5-47.
- Hess, S., Kuhnt, W. (1996). Deep-sea benthic foraminiferal recolonization of the 1991 Mt. Pinatubo ash layer in the South China Sea. *Marine Micropaleontology* 28, 171-197.
- Hill, P.S., Newgard, J.P., Law, B.A., Milligan, T.G. (2013). Flocculation on a Muddy Intertidal Flat in Willapa Bay. Washington. Part II: Observations of Suspended Particle Size in a Secondary Channel and Adjacent Flat. *Continental Shelf Research*.
- Homoky, W.B., Weber, T., Berelson, W.M., Conway, T.M., Henderson, G.M., van Hulten, M., Jeandel, C., Severmann, S., Tagliabue, A. (2016). Quantifying trace element and isotope fluxes at the ocean–sediment boundary: a review. *Philos. Trans. R. Soc. A Math. Phys. Eng. Sci.* 374.
- Hoppe, M. (2015). Geochemical and mineralogical investigations of sediments and ferromanganese nodules from the equatorial East Pacific. Master Thesis, Technical University of Freiberg, 86 pp.
- Houlsby, G.T. (1982). Theoretical analysis of the fall cone test, *Géotechnique* 32, 111-119.
- Hughes, S.J.M., Ruhl, H.A., Hawkins, L.E., Hauton, C., Boorman, B., Billett, D.S.M. (2011). Deep-sea echinoderm oxygen consumption rates and an interclass comparison of metabolic rates in Asteroidea, Crinoidea, Echinoidea, Holothuroidea and Ophiuroidea. *The Journal of Experimental Biology* 214, 2512-2521.
- Hurlbut, C.J. (1991). Larval substratum selection and postsettlement mortality as determinants of distribution of two bryozoans. *Journal of Experimental Marine Biology and Ecology* 147, 103-119.

- International Seabed Authority (2010). A geological model of polymetallic nodule deposits in the Clarion-Clipperton Fracture Zone. In: International Seabed Authority, Development of geological models for the Clarion-Clipperton Zone polymetallic nodule deposits. ISA, Technical Study No. 6, Kingston, Jamaica, pp. 14-96.
- International Seabed Authority (2012). Environmental Management Needs for Exploration and Exploitation of Deep Sea Minerals. Report of a workshop held by The International Seabed Authority in collaboration with the Government of Fiji and the SOPAC Division of the Secretariat of the Pacific Community (SPC) in Nadi, Fiji, from 29 November to 2 December 2011. ISA, Technical Study No. 10, Kingston, 47 pp.
- International Seabed Authority (2017). Environmental assessment and management for exploitation of minerals in the Area. ISA, Technical Study No. 16, Kingston, 66 pp.
- Jamieson, A. J., Malkocs, T., Piertney, S. B., Fujii, T., Zhang, Z. (2017). Bioaccumulation of persistent organic pollutants in the deepest ocean fauna. *Nature Ecology and Evolution* 1, 1-4.
- Jankowski, J., Zielke, W. (2001). The mesoscale sediment transport due to technical activities in the deep sea. *Deep Sea Research Part II: Topical Studies in Oceanography* 48 (17), 3487-3521.
- Janssen, A., Kaiser, S., Meißner, K., Brenke, N., Menot, L., Martínez-Arbizu, P. (2015). A Reverse Taxonomic Approach to Assess Macrofaunal Distribution Patterns in Abyssal Pacific Polymetallic Nodule Fields. *PLoS ONE* 10(2), e0117790. doi:10.1371/journal.pone.0117790.
- Janssen, A., Miljutin, D., Rühlemann, C., Martínez-Arbizu, P. (submitted). Metazoan meiofauna communities from deep-sea fields of polymetallic nodules (Clarion-Clipperton Zone, Pacific) and their dependence on abiotic parameters at local and regional scale. *Deep Sea Research I*.
- Janssen, F., Vonnahme, T., Molari, M., Wenzhöfer, F., Haeckel, M., Boetius, A. (2017). Effects of experimental polymetallic nodule mining on deep-sea microbial communities and functions (DISCOL experimental area, tropical SE Pacific), Goldschmidt Conference, Paris, 14-18.8.2017.
- Jones, D.O.B. et al. (2015). RRS James Cook Cruise JC120 15 Apr-19 May 2015: Manzanillo to Manzanillo, Mexico. Managing Impacts of Deep-sea resource exploitation (MIDAS): Clarion-Clipperton Zone, North Eastern Area of Particular Environmental Interest. Southampton, 2015.
- Jones, D.O.B., Kaiser, S., Sweetman, A.K., Smith, C.R., Menot, L., Vink, A., Trueblood, D., Greinert, J., Billett, D.S.M., Arbizu, P.M., Radziejewska, T., Singh, R., Ingole, B., Stratmann, T., Simon-Lledó, E., Durden, J.M., Clark, M.R. (2017). Biological responses to disturbance from simulated deep-sea polymetallic nodule mining. *PloS One* 12 (2), e0171750, 10.1371/journal.pone.0171750.
- JORC (2012). The JORC Code. Australasian Code for Reporting of Exploration Results, Mineral Resources and Ore Reserves. 2012 ed. Carlton: AusIMM, (2012): Retrieved 31.01.2016 from [http://www.jorc.org/docs/jorc\\_code2012.pdf](http://www.jorc.org/docs/jorc_code2012.pdf).
- Kessler, W.S. (1990). Observations of long Rossby waves in the northern tropical Pacific. *Journal of Geophysical Research* 95, 5183-5217.
- Klymak, J., Legg, S. (2010). A simple mixing scheme for models that resolve breaking internal waves. *Ocean Modelling* 33 (3), 224-234.
- Knight, A.M., Piet, G.J., Jongbloed, R.H., Tamis, J.E., White, L., Akoglu, E., Boicenco, L., Churilova, T., Kryvenko, O., Fleming-Lehtinen, V. et al. (2015). An exposure-effect approach for evaluating



- ecosystem-wide risks from human activities. ICES J. Mar. Sci. Available from: DOI: 10.1093/icesjms/fsu245.
- Knobloch, A., Kuhn, T., Rühlemann, C., Hertweg, T., Zeissler, K.-O., Noack, S. (2017). Predictive mapping of the nodule abundance and mineral resource estimation in the Clarion-Clipperton Zone using artificial neural networks and classical geostatistical methods. In: R. Sharma (Ed.): Deep Sea Mining. Springer Verlag, Heidelberg.
- Knowlton, N. (2000). Molecular genetic analyses of species boundaries in the sea. *Hydrobiologia* 420, 73-90.
- Kofoed, C.A., Skogsberg, T. (1928). The Dinoflagellata: the Dinophysoidae. Memoirs of the Museum of Comparative Zoology at Harvard College, Cambridge, USA: Printed for the Museum.
- Kontar, E.A., Sokov, A.V. (1994). A benthic storm in the northeastern tropical Pacific over the fields of manganese nodules. *Deep Sea Research Part I: Oceanographic Research Papers* 41 (7), 1069-1089.
- Koschinsky, A., Gaye-Haake, B., Arndt, C., Maue, G., Spitzzy, A., Winkler, A., Halbach P. (2001). Experiments on the influence of sediment disturbances on the biogeochemistry of the deep-sea environment. *Deep. Res. Part II Top. Stud. Oceanogr.* 48, 3629–3651.
- Koschinsky, A., Winkler, A., Fritsche, U. (2003a). Importance of different types of marine particles for the scavenging of heavy metals in the deep-sea. *Applied Geochemistry* 18, 693-710.
- Koschinsky, A., Borowski, C., Halbach, P. (2003b). Reactions of the heavy metal cycle to industrial activities influence on heavy metal cycle in the deep sea. *Internat. Rev. Hydrobiol.* 88, 102-127.
- Kotlinski, R., Stoyanova, V. (1998). Physical, Chemical, and Geological Changes of Marine Environment Caused By the Benthic Impact Experiment At the 10M BIE Site. The 8th International Offshore and Polar Engineering Conference, International Society of Offshore and Polar Engineers.
- Kuhn, T. and Shipboard Scientific Party (2015). Low-temperature fluid circulation at seamounts and hydrothermal pits: heat flow regime, impact on biogeochemical processes and its potential influence on the occurrence and composition of manganese nodules in the NE Pacific. Cruise Report of R/V SONNE Cruise SO240/FLUM. Hannover, 185 pp. [http://dx.doi.org/10.2312/cr\\_so240](http://dx.doi.org/10.2312/cr_so240).
- Kuhn, T., Wegorzewski, A., Rühlemann, C., Vink, A. (2017a). Composition, formation, and occurrence of polymetallic nodules. In: Sharma, R., (Ed.). Deep-Sea Mining. Springer International, Cham, pp. 23-63.
- Kuhn T., Versteegh G.J.M., Villinger H., Dohrmann I., Heller C., Koschinsky A., Kaul N., Ritter S., Wegorzewski A.V. and Kasten S. (2017b). Widespread seawater circulation in 18–22 Ma oceanic crust: Impact on heat flow and sediment geochemistry. *Geology* 45 (9), 799-802. doi: <https://doi.org/10.1130/G39091.1>.
- Kutti, T., Bannister, R.J., Foss, J., Krogness, C.M., Tjensvoll, I., Søvik, G. (2015). Metabolic responses of the deep-water sponge *Geodia barretti* to suspended bottom sediment, simulated mine tailings and drill cuttings. *Journal of Experimental Marine Biology and Ecology* 473, 64-72.
- Laakmann, S., Gerds, G., Erler, R., Kneibelsberger, T., Martínez-Arbizu, P., Raupach, M.J. (2013). Comparison of molecular species identification for North Sea calanoid copepods (Crustacea) using proteome fingerprints and DNA sequences. *Molecular Ecology Resources* 13, 862-876.

- Lambshead, P.J.D., Boucher, G. (2003). Marine nematode deep-sea biodiversity – hyperdiverse or hype? *Journal of Biogeography*, doi: 10.1046/j.1365-2699.2003.00843.x.
- Lambshead, P.J.D., Brown, C.J., Ferrero, T.J., Hawkins, L.E., Smith, C.R., Mitchell, N.J. (2003). Biodiversity of nematode assemblages from the region of the Clarion-Clipperton Fracture Zone, an area of commercial mining interest. *BMC Ecology* 3 (1), <http://www.biomedcentral.com/1472-6785/3/1>.
- Langenkämper D., Zurowietz M., Schoening T., Nattkemper T.W. (2017). BIIGLE 2.0 - browsing and annotating large marine image collections. *Frontiers in Marine Science* 4, 83.
- Larsson, A.I., van Oevelen, D., Purser, A., Thomsen, L. (2013). Tolerance to long-term exposure of suspended benthic sediments and drill cuttings in the cold-water coral *Lophelia pertusa*. *Marine Pollution Bulletin* 70 (1-2), 176-188.
- Lavelle, J., Ozturgut, E., Swift, S., Ericson, B. (1981). Dispersal and resedimentation of the benthic plume from deep-sea mining operations: a model with calibration. *Marine Mining* 3 (1/2), 59-93.
- Lawler, S. N., Kellogg, C. A., France, S. C., Clostio, R. W., Brooke, S. D., Ross, S. W. (2016). Coral-Associated Bacterial Diversity Is Conserved across Two Deep-Sea Anthothela Species. *Frontiers in Microbiology* 7 (14), doi:10.3389/fmicb.2016.00458.
- Lekang, K., Thompson, E. M., Troedsson, C. (2015). A comparison of DNA extraction methods for biodiversity studies of eukaryotes in marine sediments. *Aquatic Microbial Ecology* 75 (1), 15-25.
- Levin, L.A., Thomas, C.L. (1989). The influence of hydrodynamic regime on infaunal assemblages inhabiting carbonate sediments on central Pacific seamounts. *Deep-Sea Research* 36 (12), 1897-1915.
- Lim, S.C., Wiklund, H., Glover, A.G., Dahlgren, T.G., Tan, K.S. (2017). A new genus and species of abyssal sponge commonly encrusting polymetallic nodules in the Clarion-Clipperton Zone, East Pacific Ocean. *Systematics and Biodiversity*, 1-13.
- Lins, L., da Silva, M.C., Neres, Esteves, A.M., Vanreusel, A. (2016). Testing deep-sea biodiversity paradigms on abyssal nematode genera and *Acantholaimus* species. *Deep Sea Research Part II: Tropical Studies in Oceanography*, doi: 10.1016/j.dsr2.2016.12.005.
- Lutz, M.J., Caldeira, K., Dunbar, R.B., Behrenfeld, M.J. (2007). Seasonal rhythms of net primary production and particulate organic carbon flux to depth describe the efficiency of biological pump in the global ocean. *Journal of Geophysical Research* 112, doi: 10.1029/2006JC003706.
- Marcon, Y., Purser, A. (2017). PAPARA(ZZ)I: An open-source software interface for annotating photo-graphs of the deep sea. *SoftwareX* 6, 69-80.
- Marshall, J., Adcroft, A., Hill, C., Perelman, L., Heisey, C. (1997). A finite-volume, incompressible Navier-Stokes model for studies of the ocean on parallel computers. *Journal of Geophysical Research* 102 (C3), 5753-5766.
- Martínez-Arbizu P., Haeckel M. (2015). RV SONNE Cruise Report SO239: EcoResponse Assessing the Ecology, Connectivity and Resilience of Polymetallic Nodule Field Systems. *GEOMAR Report* 25, 204 pp.
- McCave, I.N., Hall, I.R. (2006). Size sorting in marine muds: Processes, pitfalls, and prospects for paleoflow-speed proxies. *Geochemistry, Geophysics, Geosystems*, doi: 10.1029/2006GC001284.

- McKenna, M.F., et al. (2012). Underwater radiated noise from modern commercial ships. *The Journal of the Acoustical Society of America* 131 (1), 92-103.
- McKenney, B.A., Kiesecker, J.M. (2010). Policy Development for Biodiversity Offsets: A Review of Offset Frameworks. *Environmental Management* 45,165-176.
- Mestre, N.C., Rocha, T.L., Canals, M., Cardoso, C., Danovaro, R., Dell'Anno, A., Gambi, C., Regoli, F., Sánchez-Vidal, A., Bebianno, M.J. (2017). Environmental hazard assessment of a marine mine tailings deposit site and potential implications for deep-sea mining. *Environ. Poll.* 228,169-178.
- Mevenkamp, L., Stratmann, T., Guilini, K., Moodley, L., Van Oevelen, D., Vanreusel, A., Westerlund, S., Sweetman, A.K. (2017). Impaired short-term functioning of a benthic community from a deep Norwegian Fjord following deposition of mine tailings and sediments. *Frontiers in Marine Science*, <https://doi.org/10.3389/fmars.2017.00169>.
- Mewes, K., Mogollón, J. M., Picard, A., Rühlemann, C., Kuhn, T., Nöthen, K., Kasten, S. (2014). Impact of depositional and biogeochemical processes on small scale variations in nodule abundance in the Clarion-Clipperton Fracture Zone, *Deep-Sea Research I* 91, 125-141.
- Mewes, K., Mogollón, J.M., Picard, A., Rühlemann, C., Eisenhauer, A., Kuhn, T., Ziebis, W., Kasten, S. (2016). Diffusive transfer of oxygen from seamount basaltic crust into overlying sediments: An example from the Clarion-Clipperton Fracture Zone. *Earth and Planetary Science Letters* 433, 215-225.
- MIDAS Report D2.2 (2015). Near-field hydrodynamic modelling of two case study sites. 21 pp.
- MIDAS Report D3.5 (2016). Validation report on the response of biological indices to toxicant exposure in macro- and megafauna from exposures to contaminant complexes collected, including field exposures, to feed into WP7 and WP8. 75 pp.
- Middag, R., van Hulten, M.M.P., Van Aken, H.M., Rijkenberg, M.J.A., Gerringa, L.J.A., Laan, P., de Baar H.J.W. (2015). Dissolved aluminium in the ocean conveyor of the West Atlantic Ocean: Effects of the biological cycle, scavenging, sediment resuspension and hydrography. *Mar. Chem.* 177, 69–86.
- Mikkelsen, O., Hill, P.S., Milligan, T., Chant, R. (2005). In situ particle size distributions and volume concentrations from a LISST-100 laser particle sizer and a digital floc camera. *Continental Shelf Research* 25, 1959-1978.
- Miljutin, D.M., Miljutina, M.A., Martinez-Arbizu, P., Galéron, J. (2011). Deep-sea nematode assemblage has not recovered 26 years after experimental mining of polymetallic nodules (Clarion-Clipperton Fracture Zone, Tropical Eastern Pacific). *Deep Sea Research Part I: Oceanographic Research Papers* 58 (8), 885-897.
- Miljutina, M., Miljutin, D., Mahatma, R., Galéron, J. (2010). Deep-sea nematode assemblages of the Clarion-Clipperton Nodule Province (Tropical North-Eastern Pacific). *Marine Biodiversity* 40, 1-15.
- Mogollon J.M., Mewes K., Kasten S. (2016). Quantifying manganese and nitrogen cycle coupling in manganese-rich, organic carbon-starved marine sediments: Examples from the Clarion-Clipperton fracture zone. *Geophysical Research Letters* 43, 7114-7123.

- Mohrbeck, I., Janssen, A., Kaiser, S., Brenke, N., Borges, V.A., Albers, L., Raschka, U., Martínez-Arbizu, P. (2015). Isopod distribution patterns in polymetallic nodule fields: German vs. UK license area. 14th Deep Sea Biology Symposium, Aveiro, Portugal, 31.08.-04.09.2015.
- Morris, K.J., Bett, B.J., Durden, J.M., Benoist, N.M.A., Huvenne, V.A.I., Jones, D.O.B., Robert, K., Ichino, M.C., Wolff, G.A., Ruhl, H.A. (2016). Landscape-scale spatial heterogeneity in phytodetrital cover and megafauna biomass in the abyss links to modest topographic variation. *Scientific Reports* 6, 34080.
- Mullineaux, L.S. (1987). Organisms living on manganese nodules and crusts: distribution and abundance at three North Pacific sites. *Deep-Sea Research* 34 (2), 165-184.
- Nakata, K., Kubota, M., Aoki, S., Taguchi, K. (1997). Dispersion of resuspended sediment by ocean mining activity – modelling study. *Proceedings of the first International Symposium on Environmental Studies for Deep-Sea Mining*, Tokyo, Japan, 169-186.
- Naumann, C.L. (2008). The ANTARES Collaboration 2008. *J. Phys., Conf. Ser.* 136, 042064.
- Netto, S.A., Gallucci, F., Fonseca, G. (2009). Deep-sea meiofauna response to synthetic-based drilling mud discharge off SE Brazil. *Deep-Sea Res. II* 56, 41e49.
- NOAA (1984). Deep Seabed Mining: Draft environmental impact statement on issuing an exploration license to Ocean Mining Associates. Office of Ocean and Coastal Resource Management, Ocean Minerals and Energy Division, Washington.
- Ortega, A. (ed.) (2014). Towards Zero Impact of Deep Sea Offshore Projects – An assessment framework for future environmental studies of deep-sea and offshore mining projects. Report IHC Merwede.
- Ostmann, A., Schnurr, S., Martinez Arbizu, P. (2014). Marine environment around Iceland: hydrography, sediments and first predictive models of Icelandic deep-sea sediment characteristics. *Polish Polar Research* 35 (2), 151-176.
- Pabortsava, K., Purser, A., Wagner, H., Thomsen, L. (2011). The influence of drill cuttings on the physical characteristics of phytodetritus. *Marine Pollution Bulletin* 62, 2170-2180.
- Pacanowski, R.C., Philander, S.G.H. (1981). Parameterisation of Vertical Mixing in Numerical Models of Tropical Oceans. *Journal of Physical Oceanography* 11, 1443-1451.
- Padman, L., Erofeeva, S. (2005). Tide Model Driver (TMD) Manual. Earth and Space Research Institute, Seattle.
- Palacios, D.M., Bograd, S.J. (2005). A census of Tehuantepec and Papagayo eddies in the northeastern tropical Pacific. *Geophysical Research Letters* 32 (23).
- Paterson, G.L.J., Wilson, G.D.F., Cosson, N., Lamont, P.A. (1998). Hessler and Jumars (1974) revisited: abyssal polychaete assemblages from the Atlantic and Pacific. *Deep Sea Research Part II: Topical Studies in Oceanography* 45, 225-251.
- Paul, S. A. L., Gaye, B., Haeckel, M., Kasten, S., Koschinsky, A. (submitted). Biogeochemical regeneration of a nodule mining disturbance site: trace metals, DOC and amino acids in deep-sea sediments and pore waters. *Frontiers in Marine Science*.
- Pennington, J.T., Mahoney, K.L., Kuwahara, V.S., Kolber, D.D., Calienes, R., Chavez, F.P. (2006). Primary production in the eastern tropical Pacific: A review. *Progress in Oceanography* 69, 285-317.

- Peukert, A., Schoening, T., Alevizos, E., Köser, K., Kwasnitschka, T., Greinert, J. (submitted). Understanding Mn-nodule distribution and related deep-sea mining impacts using AUV-based hydroacoustic sensing and visual observations. *Biogeosciences*.
- Picard, A., Ferdelman, T. (2011). Linking microbial heterotrophic activity and sediment lithology in oxic, oligotrophic sub-seafloor sediments of the North Atlantic Ocean. *Frontiers in Microbiology* 2, 1-10.
- Purkiani, K., Paul, A., Gillard, B., Schulz, M. (in prep). The effect of low turbulence-induced flocculation on deep sea sediment transport in Pacific Ocean. To be submitted to *Deep-Sea Research Part II*.
- Purser, A., Thomsen, L. (2012). Monitoring strategies for drill cutting discharge in the vicinity of cold-water coral ecosystems. *Marine Pollution Bulletin* 64 (11), 2309-2316.
- Purser, A., Marcon, Y., Hoving, H.-J., Piatowski, U., Eason, D., Vecchione, M., Boetius, A. (2016). Recent observations of deep sea incirrate octopi from three manganese-rich locations in the Pacific Ocean. *Current Biology* 26 (24), R1268-R1269.
- Purser, A., Marcon, Y., Dreutter, S., Hoge, U., Sablotny, B., Hehemann, L., Lemburg, J., Dorschel, B., Biebow, H., Boetius, A (in press). OFOBS - Ocean Floor Observation and Bathymetry System: A new towed camera / sonar system for deep-sea habitat surveys. *IEEE Journal of Oceanic Engineering*.
- Radziejewska, T. (2002). Responses of deep-sea meiobenthic communities to sediment disturbance simulating effects of polymetallic nodule mining. *International Reviews Hydrobiology* 87, 457-477.
- Radziejewska, T., Drzycimski, I., Galtsova, V.V., Kulangieva, L.V., Stoyanova, V. (2001a). Changes in genus-level diversity of meiobenthic free-living nematodes (Nematoda) and harpacticoids (Copepoda Harpacticoida) at an abyssal site following experimental sediment disturbance. *Proceedings of the Fourth Ocean Mining Symposium, Szczecin, Poland*, 38-43.
- Radziejewska, T., Rokicka-Praxmayer, J., Stoyanova, V. (2001b). IOM BIE revisited: meiobenthos at the IOM BIE site 5 years after the experimental disturbance. *Proceedings of the Fourth Ocean Mining Symposium, Szczecin, Poland*, 63-68.
- Raiswell, R., Canfield, D.E. (2012). The Iron Biogeochemical Cycle Past and Present. *Geochemical Perspect.* 1, 222 pp.
- Ramirez-Llodra, E.Z., Brandt, A., Danovaro, R., De Mol, B., Escobar, E., German, C.R., Levin, L.A., Martinez Arbizu, P., Menot, L., Buhl-Mortensen, P., Narayanaswamy, B.E., Smith, C.R., Tittensor, D.P., Tyler, P.A., Vanreusel, A., Vecchione, M. (2010). Deep, diverse and definitely different: unique attributes of the world's largest ecosystem. *Biogeosciences* 7 (9), 2851-2899.
- Raschka, U. (2014). Distribution of selected macrobenthic taxa (Isopoda, Polychaeta) within the German manganese nodule license area: Prospective area vs. Reference area. Master Thesis, Carl von Ossietzky University of Oldenburg, 73 pp.
- Reiss, H., Birchenough, S., Borja, A., Buhl-Mortensen, L., Craeymeersch, J., Dannheim, J., Darr, A., Galparsoro, I., Gogina, M., Neumann, H., Populus, J., Rengstorf, A.M., Valle, M., van Hoey, G., Zettler, M.L., Degraer, S. (2015). Benthos distribution modelling and its relevance for marine ecosystem management. *ICES Journal of Marine Science* 72 (2), 297-315.

- Rex, M.A., Etter, R.J., Morris, J.S., Crouse, J., McClain, C.R., Johnson, N.A., Stuart, C.T., Deming, J.W., Thies, R., Avery, R. (2006). Global bathymetric patterns of standing stock and body size in the deep-sea benthos. *Marine Ecology Progress Series* 317, 1-8.
- Richardson, W.J., Wursig, B., Greene, C.R. Jnr. (1990). Reactions of bowhead whales (*Balaena mysticetus*) to drilling and dredging noise in the Canadian Beaufort Sea. *Marine Environmental Research* 29, 135-160.
- Rolinski, S., Segschneider, J., Sündermann, J. (2001). Long-term propagation of tailings from deep-sea mining under variable conditions by means of numerical simulations. *Deep-Sea Research II* 48, 3469–3485.
- Ruhl, H.A. (2007). Abundance and size distribution of abyssal epibenthic megafauna in the Northeast Pacific. *Ecology* 88 (5), 1250-1262.
- Rühlemann, C. and Shipboard Scientific Party (2010). Microbiology, Paleoceanography and Biodiversity in the Manganese Nodule Belt of the Equatorial NE Pacific. Cruise Report of R/V SONNE Cruise SO-205, BGR, Hannover, 86 pp.
- Rühlemann, C., Kuhn, T., Wiedicke, M., Kasten, S., Mewes, K., Picard, A. (2011). Current status of manganese nodules exploration in the German license area. Proc. Ninth ISOPE Ocean Mining symposium, International Society of Offshore and Polar Engineers (ISOPE), Maui, pp. 168-173.
- Rühlemann, C. and Shipboard Scientific Party (2012). Biodiversity, Geology, and Geochemistry of the German and French License Areas for the Exploration of Polymetallic Nodules in the Equatorial NE Pacific. Cruise Report of R/V L'Atalante Cruise BIONOD, BGR, Hannover, 302 pp.
- Rühlemann, C. and Shipboard Scientific Party (2014). Geology and Biodiversity of the German license area for the exploration of polymetallic nodules in the equatorial NE Pacific. Cruise Report of R/V KILO MOANA Cruise MANGAN 2013, BGR, Hannover, 355 pp.
- Rühlemann, C. and Shipboard Scientific Party (2015). Geology, Biodiversity and Environment of the German license area for the exploration of polymetallic nodules in the equatorial NE Pacific. Cruise Report of R/V KILO MOANA Cruise MANGAN 2014, BGR, Hannover, 349 pp.
- Rühlemann, C. and Shipboard Scientific Party (2017). Geology, Biodiversity and Environment of the German license area for the exploration of polymetallic nodules in the equatorial NE Pacific. Cruise Report of R/V KILO MOANA Cruise MANGAN 2016, BGR, Hannover, 299 pp.
- Rye, H., Reed, M., Frost, T.K., Smit, M.G.D., Durgut, I., Johansen, Ø., Ditlevsen, M.K. (2007). Development of a numerical model for calculating exposure to toxic and non-toxic stressors in the water column and sediment from drilling discharge. *Integr. Environ. Assess. Manage.* 4 (2), 194-203.
- Schaaning, M.T., Trannum, H.C., Øxnevad, S., Carroll, J., Blake, T. (2008). Effects of drill cuttings on biogeochemical fluxes and macrobenthos of marine sediments. *J. Exp. Mar. Biol. Ecol.* 361, 49e57.
- Segschneider, J., Sündermann, J. (1998). Simulating large scale transport of suspended matter. *Journal of Marine Systems* 14, 81–97.
- Semina, H.J. (1974). *Pacific Phytoplankton*. Publishing House Nauka, Moscow.
- Simpson, S.L., Campana, O., Ho, K.T. (2016). Sediment toxicity testing. In: Blasco J., Campana O., Chapman P., Hampel M. (Eds.), *Marine Ecotoxicology: Current Knowledge and Future Issues*, 197-235.



- Singh, R. (2015). Biodiversity of deep-sea nematode communities from commercially important manganese nodules areas. PhD Thesis, Carl von Ossietzky University of Oldenburg, 171 pp.
- Singh, R., Miljutin, D.M., Vanreusel, A., Radziejewska, T., Miljutina, M.M., Tchesunov, A., Bussan, C., Galtsova, V., Martínez-Arbizu, P. (2016). Nematode communities inhabiting the soft deep-sea sediment in polymetallic nodule fields: do they differ from those in the nodule-free abyssal areas? *Marine Biology Research*, DOI:10.1080/17451000.2016.1148822.
- Smith, C.R., Berelson, W., Demaster, D.J., Dobbs, F.C., Hammond, D., Hoover, D.J., Pope, R.H., Stephens, M. (1997). Latitudinal variation in benthic processes in the abyssal equatorial Pacific: control by biogenic particle flux. *Deep-Sea Research II* 44 (9-10), 2295-2317.
- Stanley, J.A., Jeffs, A.G. (2016). Ecological impacts of anthropogenic underwater noise. In: Solan, M., Whiteley, N.M. (Eds.), *Stressors in the Marine Environment*. Oxford University Press, Oxford, pp. 282e297.
- Stelzenmüller, V., Fock, H.O., Gimpel, A., Rambo, H., Diekmann, R., Probst, W.N., Callies, U., Bockelmann, F., Neumann, H., Kroncke, I. (2015). Quantitative environmental risk assessments in the context of marine spatial management: Current approaches and some perspectives. *ICES J. Mar. Sci.* 72, 1022-1042.
- Stratmann, T., Lins, L., Purser, A., Marcon, Y., Rodrigues, C., Ravara, A., Cunha, M.R., van Oevelen, D. (in prep.). Carbon flows in deep-sea food webs need more than twenty-six years to recover from an experimental disturbance in the Peru Basin.
- Suckow, A., Treppke, U., Wiedicke, M.H., Weber, M.E. (2001). Bioturbation coefficients of deep-sea sediments from the Peru Basin determined by gamma spectrometry of  $^{210}\text{Pb}_{\text{exc}}$ . *Deep-Sea Research II* 48, 3569-3592.
- Sweetman, A.K., Thurber, A.R., Smith, C.R., Levin, L.A., Mora, C., Wei, C.-L., Gooday, A.J., Jones, D.O.B., Rex, M., Yasuhara, M., Ingels, J., Ruhl, H.A., Frieder, C.A., Danovaro, R., Würzberg, L., Baco, A.R., Grupe, B.M., Pasulka, A., Meyer, K.S., Dunlop, K.M., Henry, L.-A., Roberts, J.M., (2017). Major impacts of climate change on deep-sea benthic ecosystems. *Elementa Science of the Anthropocene* 5 (4), doi: 10.1525/elementa.203.
- Taboada, S., Kenny, N.J., Riesgo, A., Wiklund, H., Paterson, G.L.J., Dahlgren, T.G., Glover, A.G. (in press). Mitochondrial genome and polymorphic microsatellite markers from the abyssal sponge *Plenaster craigi*: tools for understanding the impact of deep-sea mining. *Marine Biodiversity*.
- Tamis, J.E., de Vries, P., Jongbloed, R., Lagerveld, S., Karman, C., Tjalling J., Van der Wal, J., Slijkerman, D.M.E., Klok, C. (2017). Toward a Harmonized Approach for Environmental Assessment of Human Activities in the Marine Environment. *Integr. Environ. Assess. Manag.* 12, 2016.
- Taylor, M.L., Roterman, C.N. (2017). Invertebrate population genetics across Earth's largest habitat: The deep-sea floor. *Molecular Ecology*, doi: 10.1111/mec.14237.
- Thiel, H., Schriever, G. (1990). Deep-Sea Mining, Environmental Impact and the DISCOL Project, *Ambio* 19 (5), 245-250.
- Thiel, H., Schriever, G., Bussaut, C., Borowski, C. (1993). Manganese nodule crevice fauna. *Deep-Sea Research Part I*: 40 (2), 419-423.

- Thiel, H., Schriever, G., Ahnert, A., Bluhm, H., Borowski, C., Vopel, K. (2001). The large-scale environmental impact experiment DISCOL: reflection and foresight. *Deep-Sea Research II* 48, 3869-3882.
- Thomsen, L., Gust, G. (2000). Sediment erosion thresholds and characteristics of resuspended aggregates on the western European margin. *Deep Sea Research Part I: Oceanographic Research Papers* 47, 1881-1897.
- Thomsen, L., McCave, I.N. (2000). Aggregation processes in the benthic boundary layer at the Celtic Sea continental margin. *Deep-Sea Research I* 47, 1389-1404.
- Thomsen, L., van Weering, T., Gust, G. (2002). Processes in the benthic boundary layer at the Iberian continental margin and their implication for carbon mineralization. *Progress in Oceanography* 52, 315-329. doi:10.1016/S0079-6611(02)00013-7.
- Trueblood, D.D. (1993). US Cruise Report for BIE II. NOAA Technical Memorandum NOS OCRM 4, National Ocean Service, 1993.
- Tsurusaki, K. (1997). Concept and Basic Design of the Plume Discharge. Proceedings, international symposium on environmental studies for deep-sea mining Tokyo, Japan.
- van de Flierdt, T., Griffiths, A.M., Lambelet, M., Little, S.H., Stichel, T., Wilson, D.J. (2016). Neodymium in the oceans: a global database, a regional comparison and implications for palaeoceanographic research. *Philos. Trans. R. Soc. A Math. Phys. Eng. Sci.* 374.
- Vanreusel, A., Hilario, A., Ribeiro, P.A., Menot, L., Martinez-Arbizu, P. (2016). Threatened by mining, polymetallic nodules are required to preserve abyssal epifauna. *Scientific Reports* 6, 26908.
- van Soosten, C., Schmidt, H., Westheide, W. (1998). Genetic variability and relationship among geographically widely separated populations of *Petitia amphophtalma* (Polychaeta: Syllidae). Results from RAPD-PCR investigations. *Marine Biology* 131, 659-669.
- Volz, J., Mogollón, J., Geibert, W., Martínez Arbizu, P., Koschinsky, A., Kasten, S. (submitted). Natural variability of geochemical conditions, biogeochemical processes and element fluxes in sediments of the eastern Clarion-Clipperton Zone, Pacific Ocean.
- Vonnahme, T.R. (2016). Microbial diversity and function of deep-sea manganese nodule ecosystems. Master Thesis, Max-Planck Institute for Marine Microbiology, Bremen, 145 pp.
- Vonnahme, T.R., Molari, M., Janssen, F., Wenzhöfer, F., Haeckel, M., Titschack, J., Boetius, A. (in prep.). Effects of simulated deep-sea mining impacts on microbial communities and functions in the DISCOL experimental area after 26 years.
- Waller, R.G., Baco, A.R. (2007). Reproductive morphology of three species of deep-water precious corals from the Hawaiian archipelago: *Gerardia* sp., *Corallium secundum*, and *Corallium lauuense*. *Bulletin of Marine Science*, 533-542.
- Ward, R.D., Holmes, B.H., O'Hara, T.D. (2008). DNA barcoding discriminates echinoderm species. *Molecular Ecology Resources* 8, 1202-1211.
- Webb, S.C. (1992). The equilibrium oceanic microseism spectrum. *J. Acoust. Soc. Am.* 92, 2141-2158.
- Wedding, L.M., Friedlander, A.M., Kittinger, J.N., Watling, L., Gaines, S.D., Bennett, M., Hardy, S.M., Smith, C.R. (2013). From principles to practice: a spatial approach to systematic conservation planning in the deep sea. *Proceedings of the Royal Society B: Biological Sciences* 280 (1773).

- Widmann, P. (2014). Enrichment of mobilizable manganese in relation to manganese nodules abundance. Master thesis at the Eberhard Karls Universität Tübingen and the Federal Institute for Geoscience and Resources (BGR), Hannover, 182 pp.
- Wiedicke-Hombach, M. and Shipboard Scientific Party (2009). RV Kilo Moana campaign to the German Contract Area for polymetallic nodule exploration. Cruise Report MANGAN 2008, BGR, Hannover, 89 pp.
- Wiedicke-Hombach, M. and Shipboard Scientific Party (2010). RV Kilo Moana campaign to the German Contract Area for polymetallic nodule exploration. Cruise Report MANGAN 2009, BGR, Hannover, 64 pp.
- Wiklund, H., Taylor, J.D., Dahlgren, T.G., Todt, C., Ikebe, C., Rabone, M., Glover, A.G. (in press). Abyssal fauna of the UK-1 polymetallic nodule exploration area, Clarion-Clipperton Zone, central Pacific Ocean: Mollusca. *Zootaxa*.
- Willett, C.S., Leben, R.R., Lavín, M.F. (2006). Eddies and Tropical Instability Waves in the eastern tropical Pacific: A review. *Progress in Oceanography* 69 (2-4), 218-238.
- Wilson, G.D.F. (2016). Macrofauna abundance, species diversity and turnover at three sites in the Clipperton-Clarion Fracture Zone. *Marine Biodiversity*, DOI 10.1007/s12526-016-0609-8.
- Winterwerp, J.C. (1998). A simple model for turbulence induced flocculation of cohesive sediment. *Journal of Hydraulic Research* 36 (3), 309-326.
- Witte, U., Wenzhöfer, F., Sommer, S., Boetius, A., Heinz, P., Aberle, N., Sand, M., Cremer, A., Abraham, W.-R., Jørgensen, B. B., Pfannkuche, O. (2003). In situ experimental evidence of the fate of a phytodetritus pulse at the abyssal sea floor. *Nature* 424, 763-766.
- Yamazaki, T., Barnett, B.G., Suzuki, T. (1997). Optical determination of the JET deep sea sediment disturbance. *Proceedings of the International Symposium on Environmental Studies for Deep-Sea Mining*, Tokyo, Japan, 153-167.
- You, Y. (2003). The pathway and circulation of North Pacific Intermediate Water. *Geophys. Res. Lett.* 30, 2291. doi:10.1029/2003GL018561.
- Zeppilli, D., Bongiorno, L., Santos, R.S., Vanreusel, A. (2014). Changes in nematode communities in different physiographic sites of the Condor Seamount (North-East Atlantic Ocean) and adjacent sediments. *PloS ONE* 9 (12), e115601. doi:10.1371/journal.pone.0115601.
- Zhang, Y., Liu, Z., Zhao, Y., Wang, W., Li, J., Xu, J. (2014). Mesoscale eddies transport deep-sea sediments. *Scientific Reports* 4, 5937.
- Zhang, Z., Tian, J., Qiu, B., Zhao, W., Chang, P., Wu, D., et al. (2016). Observed 3D Structure, Generation, and Dissipation of Oceanic Mesoscale Eddies in the South China Sea. *Scientific Reports* 6, 24349.
- Zheng, X.-Y., Plancherel, Y., Saito, M.A., Scott, P.M., Henderson, G.M. (2016). Rare earth elements (REEs) in the tropical South Atlantic and quantitative deconvolution of their non-conservative behavior. *Geochim. Cosmochim. Acta* 177, 217-237.
- Zinßmeister, C., Wilke, T., Hoppenrath, M. (2016). Species diversity of dinophysoid dinoflagellates in the Clarion-Clipperton Fracture Zone, eastern Pacific. *Marine Biodiversity*, DOI: 10.1007/s12526-016-0607-x.

## A Appendix 1

<i>List of partners in the JPI-O MiningImpact 2 project</i>			
No	Partner	Acronym	Country
1	GEOMAR Helmholtz Centre for Ocean Research Kiel	GEOMAR	Germany
2	Max Planck Institute for Marine Microbiology	MPI	Germany
3	Senckenberg Gesellschaft für Naturforschung	SGN	Germany
4	Bielefeld University	UBielefeld	Germany
5	Alfred Wegener Institute Helmholtz Centre for Polar & Marine Research	AWI	Germany
6	Jacobs University Bremen gGmbH	JUB	Germany
7	Federal Institute for Geosciences and Natural Resources	BGR	Germany
8	MARUM - Center for Marine Environmental Science, University Bremen	MARUM	Germany
9	Walther Schücking Institute for International Law, Kiel University	UKiel	Germany
10	NIOZ – Royal Netherlands Institute for Sea Research	NIOZ	The Netherlands
11	Utrecht University	UUtrecht	The Netherlands
12	Delft University of Technology	TUDelft	The Netherlands
13	Ghent University	UGent	Belgium
14	Royal Belgian Institute of Natural Sciences	RBINS	Belgium
15	DNVGL	DNVGL	Norway
16	Norwegian Institute for Water Research	NIVA	Norway
17	Uni Research	URearch	Norway
18	GRID-Arendal	GRIDA	Norway
19	Norwegian University of Science and Technology	NTNU	Norway
20	Universidade de Aveiro (CESAM)	UAveiro	Portugal
21	CIIMAR LA - Interdisciplinary Centre of Marine & Environmental Research	CIIMAR	Portugal
22	CIMA, Universidade do Algarve	UAlgarve	Portugal
23	IPMA - Instituto Português do Mar e da Atmosfera	IPMA	Portugal
24	IMAR (Institute of Marine Research)	IMAR	Portugal
25	Ifremer	Ifremer	France
26	Polytechnic University of Marche	UniVPM	Italy
27	Natural History Museum	NHM	U.K.
28	University of Southampton	USou	U.K.
29	University of Łódź	ULodz	Poland
30	International Seabed Authority	ISA	Jamaica
31	Centre for applied research at NHH	SNF	Norway

